A FRACTURE MECHANICS BASED APPROACH TO ULTRASONIC TESTING OF FRETTING FATIGUE CRACKS

by

Ioannis C. Tsironis, Dipl. Eng.

Thesis Submitted for the Degree of
Doctor of Philosophy

Department of Mechanical Engineering
UNIVERSITY COLLEGE LONDON

November 1993

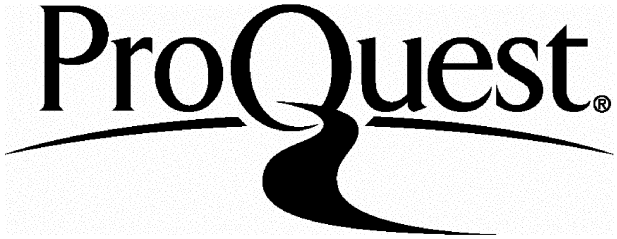

To my mother

and the memory of my father

ACKNOWLEDGEMENTS

I would like to thank my supervisors Dr L.J. Bond and Dr N. Saffari for all their help and guidance during this work. My gratitude is due to Dr L.P. Pook of UCL and Dr David Bruce of RAE Farnborough who drew my attention to significant points of this work and helped me with their remarks. Many thanks also go to my colleagues in the Ultrasonics group of UCL: P. Albach, A. Som, J. Yang and M. Deschampes. I also appreciate the helpful discussions with Prof. G. Tsamasfyros of the National Technical University of Athens and with Dr. D.A. Hills and Dr. D. Nowell of the Department of Engineering Science, Oxford University.

I gratefully acknowledge the financial support from the Greek State Scholarship Foundation (IKY). I also thank the people from the Structures Department of RAE, Farnborough, who provided the fretting specimen and the motivation for this work.

Finally, I would like to thank the Hellenic Air Force Academy and all my colleagues there, especially Prof. I. Koullias. My leave of absence for so long time would not have been possible without their support.

I. Tsironis

October 1993

ABSTRACT

This thesis reports a study with the aim of compiling a complete non-destructive evaluation scheme for characterising the early stages of fretting fatigue cracks on the surface of a thick aluminium plate. The size and orientation of the cracks is sought for use in fatigue life analyses.

A stress and fracture mechanics analysis is first conducted in order to provide information about the parameters that affect the cracks shape. The mathematical model of the contact and crack problems was formulated and discussed. A technique making use of the distributed edge dislocations was developed and implemented for the easy determination of mode-I and mode-II stress intensity factors and the new results were evaluated against known data from the literature. Very good precision was achieved with less computing time than other numerical methods. The present model can also take into regard material and traction distribution effects, the implications of which are included in the investigation. The shape of the fretting fatigue cracks was determined to be a kinked one, starting at an angle to the surface and developing perpendicularly to it. The conclusion is that fretting fatigue can adequately be described by a stress and fracture mechanics analysis which provides the distribution of the tractions and the fracture parameters.

The non-destructive testing work concentrates on the use of ultrasonics techniques for the crack shape and length determination. After a general background study, an ultrasonics spectroscopy method was developed and the Rayleigh wave scattering by different kinked surface slots was experimentally investigated. Different ranges of ratios d/λ, which express the relation between the defect size and the wavelength, were considered and the reflected signals were analysed in both the time and the frequency domain. A spectral ray study provided data for the anticipated magnitudes of the signals from every feature of the crack. The implications for the inverse nondestructive characterisation of fretting fatigue cracks are discussed and it is found that the selection of the transducer wavelength in relation to the first angled part of the crack is of paramount importance for the crack characterisation.

CONTENTS

LIST OF TABLES

LIST OF FIGURES

NOTATION

When symbols appear only once, they are defined in the respective Sections

A = Specimen cross sectional area

A_f = pad foot area

a,d = overall crack length

a_c = critical crack length for fatigue crack propagation

b_x,b_y = Burger's vectors of dislocation

B_x,B_y = Burger's vector densities

B = contact width

c = crack semi-surface length, half-width of stick zone

c_L = longitudinal waves velocity

c_T = shear waves velocity

c_R = Rayleigh waves velocity

C = crack shape correction factor

d = crack length

d_1 = angled part length of a kinked crack

d_2 = normal part length of a kinked crack

da/dn = crack growth rate per cycle

E_p = Young's modulus of pad material

E = Young's modulus of the specimen

F_n,F_t = normal and frictional tangential force per fretting pad foot

G = shear modulus of the specimen

G_p = shear modulus of pad material

k = wavenumber

K_i = Stress Intensity Factor (SIF) (i=I for mode-I and II for mode-II)

K_{mean} = total mean SIF

K_{me} = mean SIF due to externally applied fatigue stresses

K_{mc} = mean SIF due to contact loading

K_t,K_{tn} = total and normalised SIF due to frictional tangential

loading

K_n, K_{nn} = total and normalised SIF due to normal contact loading

L = contact half-length

n = fatigue stress cycles, number of elements in integration

p_0 = maximum normal traction under contact

$p(x)$ = normal traction under contact

P = normal force acting on the pad foot

$q(x)$ = shear traction under contact

Q = tangential force acting on the pad foot

R = stress ratio, ratio of maximum to minimum SIF, reflection coefficient

T = transmission coefficient

t, W = speciment thickness

ΔF_t = frictional force range per pad foot

ΔK_a = total applied SIF range

ΔK_{ax} = SIF range due to externally applied fatigue stresses

ΔK_{fr} = SIF range due to fluctuating frictional tangential force

ΔK_r = (negative) SIF range component due to load redistribution

Δ_0 = threshold SIF range

θ = inital crack angle

λ = wavelength

μ = coefficient of friction

ν = Poisson's ratio

$\sigma_a(\Delta\sigma)$ = applied fatigue stress amplitude (range)

σ = tensile stress

σ_m = mean fatigue (bulk) stress

$\sigma_{ys}(\sigma_{yc})$ = yield strength (cyclic yield strength in fatigue)

ϕ_x, ϕ_y = bounded part of B_x, B_y

1. INTRODUCTION

1.1 Statement of the problem and motivation

1.1.1 Fracture Mechanics and NDE

Over the past several decades, the field of fracture mechanics has been developed in response to the need to provide quantitative answers to specific problems concerning cracks in structures. The object of fracture mechanics is the assessment of the resistance to failure of components which contain initial defects or discontinuities that may develop fatigue cracks (Frost *et al* (1973), Rolfe and Barsom (1977), Edwards and Wanhill (1988)). Fundamental to the fracture mechanics approach to evaluating structural integrity and to predicting crack propagation life is the concept of Stress Intensity Factor (SIF) K, which provides a measure of the magnitude of the concentrated stress field in the vicinity of the crack tip. If there are no regions in the component where significant plastic straining occurs or if the crack itself is large enough with respect to microstructural features, such as grain size, then linear elastic fracture mechanics (LEFM) may be applied for evaluating structural integrity (Knott (1973).

The calculation of the SIF K is accomplished through a basic equation *(ibid)*:

$$K = Y \sigma \sqrt{\pi a} \qquad (1.1)$$

where:

K = stress intensity factor (SIF)

σ = stress

a = crack length

Y = dimensionless SIF modification coefficient which accounts for geometry, stress distribution and possible superposition of loads.

The critical SIF may be considered as a material property (even though it depends on temperature and loading rate), which tends to decrease with increasing thickness reaching a minimum value, termed fracture toughness for plane strain K_{IC}. The critical crack size for unstable crack growth can be computed by substituting the value of the critical SIF for plane stress (K_c) or plane strain (K_{IC}) into Equation 1.1 and the greatest value of stress in a loading history for σ, and then solving for a. Approximate knowledge of the critical crack size for fracture may be used to supplement the traditional strength evaluations which do not assume the presence of flaws.

Apparently, full advantage can only be made from this analysis, if the presence of the existing cracks in a component and their population, location, type and dimensions are all accurately determined. For this purpose, there is a need for improved NDE (Non-destructive Evaluation) techniques which can be employed for the characterisation of the defects. Once the defects are sized by some non-destructive method and the load environment is established, engineering calculations can establish the suitability of continued service and any appropriate inspection interval.

An alternative approach allows the determination of the stress value above which crack growth occurs. This may be obtained by rearranging Equation 1.1 for critical conditions and solving for the critical stress σ_c:

$$\sigma_c = K_{IC} / \sqrt{\pi a} \qquad (1.2)$$

In this equation, the critical crack size 'a' is a function of the NDE system capability. Thus, the availability of a NDE system capable of characterising small

cracks allows a design at higher stress levels with a resulting saving in the amount of the required material.

From the preceding discussion it can be inferred that fracture mechanics serves as an integrator of material properties, design stress and flaw detectability (Bray and Stanley (1989)). The present thesis provides an NDE method for the characterisation of the cracks that can be encountered in fretting fatigue situations. Their type and size can eventually be employed for failure prevention based on fracture mechanics.

1.1.2 Fretting fatigue and NDE

When two metal components are pressed together by a normal load with simultaneous transverse cyclic stress applied to one of them, wear of these mating surfaces occurs (Waterhouse (1981)). If the magnitude of the tangential displacement between these adjacent metal surfaces at their point of contact is small, the resulting structural degradation is termed fretting. When fretting occurs in conjunction with a bulk stress in the body of the component, the phenomenon is known as fretting fatigue. The fatigue strength of a fretted specimen is expected to be less than that of a plain one, because fretting not only damages the surface of a component but also causes local stress concentrations, which in turn may promote the growth of what are known as fretting fatigue cracks. These cracks generally appear as surface microcracks in sites near the contact edge on the fretted surface, and usually grow inside the zone of the relative slip between the two surfaces (Figure 1.1) (Hills *et al* (1988)).

The main feature of the fretting fatigue situation is that the influence of the fretting is local. Especially for the case where the fretting loads are introduced by a pressing pad in contact with a flat surface, the crack propagation is assumed to

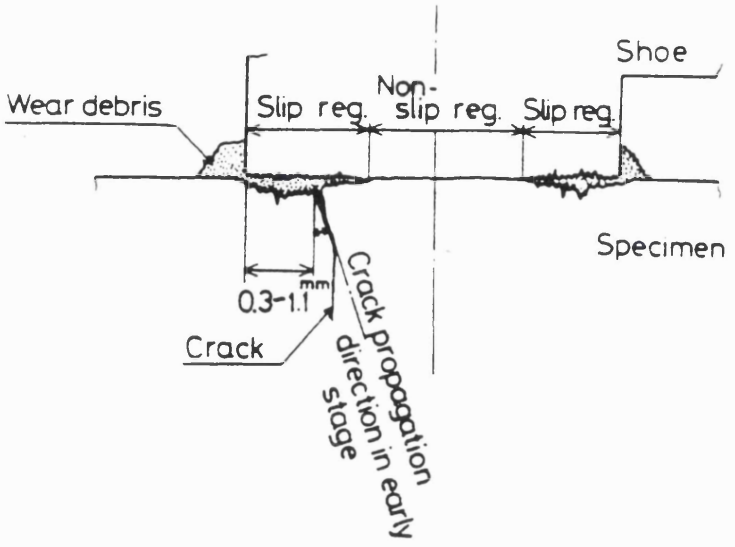

Figure 1.1 Schematic illustration of fretting fatigue damage

consist of two stages. In its first stage, the crack grows inclined to the surface (at about 45°) but, after some time, the influence of the fretting pad has disappeared, and then the crack grows normal to the surface and perpendicular to the principal axis of the repeated stress (the direction of the specimen axis) (Figure 1.2) (Endo and Goto (1976), Tanaka *et al* (1985)). The exact crack propagation path cannot be accurately determined with the present state-of-the-art calculations. This is due to the fact that extraneous factors govern to some extent the slip plane on which the extrusion bands develop (Frost *et al* (1974)). Depending on the surface conditions, crystallography and the environment, a distinct knee at the point where the crack changes direction may not always be evident, but for fracture mechanics modelling purposes the crack can be assumed to be a kinked one (Endo and Goto (1976), Li Yingzhi and Hills (1990)).

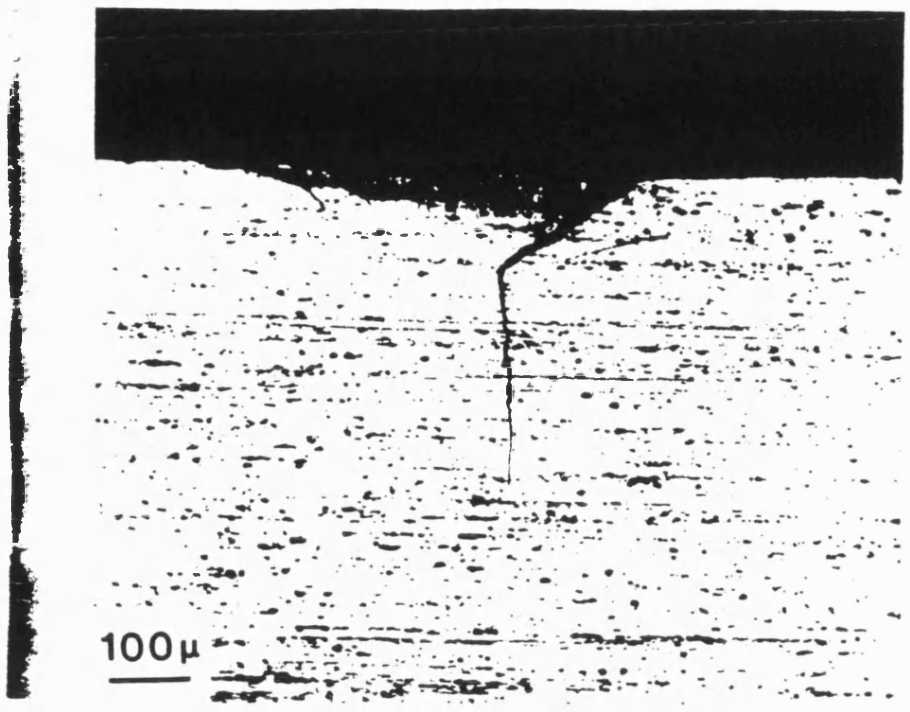

Figure 1.2 Fretting fatigue in surface of Al-4Cu alloy (from Waterhouse (1981))

Although fretting can been considered as a wear process and assessed by measuring the relative slip range between the two mating surfaces (ESDU data item 67012 (1967)), a fretting fatigue model based on fracture mechanics can often be easier applied. For example, the actual relative slip range between a turbine disc and rotor shaft is very difficult to evaluate accurately (Nix and Lindley (1988)). Also, assessment methods based on the quantity of debris produced, cannot always give satisfactory results. In terms of the fatigue strength, the fretting conditions which give a high rate of surface damage, as the large slip amplitudes and high contact pressures, are not necessarily the most detrimental for the specimen (Frost *et al* (1974)). For all these reasons, many researchers have resorted to fracture mechanics calculations, provided the cracks have grown enough to become surface macrocracks of such size that can be studied by the application of the fracture mechanics

principles (Endo and Goto (1976), Edwards *et al* (1977), Nix and Lindley (1985), Tanaka *et al* (1985), Sato *et al* (1986), Sato (1988), Hills *et al* (1988), Hattori *et al* (1988), Mutoh *et al* (1989)).

If an assessment based on fracture mechanics is to be undertaken, a technique of accurately sizing the fretting fatigue cracks is necessary. The initial aim of the present work was the determination of the crack length in a fretting fatigue experiment. This experiment was carried out in the Materials and Structures Department of RAE Farnborough, in the context of a series of materials evaluation programmes based on the fracture mechanics assessment of fretting fatigue. The results from the NDE could provide the crack size data to complement the fracture mechanics and fatigue calculations without interrupting the experiments and breaking open the small fatigue cracks that appear.

Because fretting fatigue involves mainly slanted cracks, it was soon realised that this angled shape of the fretting fatigue cracks posed an interesting problem. There were neither any published data for the propagation of angled fretting fatigue cracks, nor any NDE model for determining the topography of any kinked crack-like surface features. Although most researchers acknowledge that the fretting fatigue cracks initially grow at an angle to the surface (LiYingzhi and Hills (1990)). they do not take into account the angled effects. These effects are the main property of the fretting fatigue cracks, as the cracks are marked by an abrupt change in their propagation angle, once the fretting pads are removed, and become perpendicular to the surface thereafter (Nix and Linley (1988). It was thus decided to examine angled and kinked cracks from both the fracture mechanics and the NDE perspective, because a thorough study of the initial stages of fretting fatigue is clearly necessary to understand what happens in each regime of the crack propagation. For this reason the parameters that affect the shape of angled cracks were first studied with the aid of fracture mechanics and it was investigated how they could complement each other in a complete evaluation scheme. Two parameters, namely the stress field beneath

the contact and the SIFs are explicitly investigated, due to their significance for the fretting fatigue assessment (Nix and Lindley (1988), Hattori *et al* (1988), Hills *et al* (1988)). Basic to this assessment is also the determination of a third parameter, namely the crack length, which is carried out in the second part of the thesis.

An NDE method is then applied in order to find the geometry of cracks, so that accurate failure predictions can be made. Of the many ways of characterising the geometry of surface defects, the fruitful family of techniques making use of the Rayleigh waves scattering from surface features was chosen for obtaining depth-related information (Viktorov (1967)). The problem addressed is the investigation of the scattering mechanism when pulsed elastic waves are launched at the feature. The scattered field is analyzed for amplitude and time-of-flight information and the data are then interpreted to predict the defect's characteristics.

The fretting fatigue cracks are modelled for the NDE as angled and kinked cracks with the constraints that they remain open during the examination and that only the surface containing the defect is accessible. It is also presumed that the crack is accessible from only one side, that is the one that is not occupied by the pressing pad. This configuration alleviates the need for complete disassembly of the two contacting components. It also facilitates the testing when the space occupied by the pad, once this is removed, is too small to accommodate the coupling of a transducer, as it happens for the configuration examined in this study. Of the many choices of initial crack angles, one of 135°, namely slanted at 45° under the pressing pads, was chosen for explicit theoretical and experimental investigation. This seems a reasonable assumption, considering that the crack in its initial stage of propagation continues to grow along the direction of the Stage I embryo cracks or microcracks (Forsyth (1969)). These microcracks are initiated under maximum repeated shearing stress and are inclined at roughly 45° under the pads. However, some aspects of the examination from the other side of the crack are also considered, along with the implications for the NDE when different initial angles are involved.

1.2 Outline of the thesis

The fretting fatigue model considered in this thesis is that of an elastic half-space, subjected to loading by normal and tangential tractions over a given length of its surface. The tractions are introduced by a contacting rectangular pad, which presses onto the surface of the half-space and a crack is situated just under the apex of the pad.

After an introduction to the problem, an insight into the fretting fatigue from the fracture mechanics viewpoint is given in Chapter 2, in order to provide a theoretical basis for the study of the crack shapes that occur in the first stages of crack propagation. A review of previous investigations is first presented, along with a stress analysis of the contacting bodies. As mentioned, it is necessary to have a knowledge of the stress field beneath the contact, in order to investigate how the fretting properties are governed by the stresses in the fretting system.

In Chapter 3 an integral equation formulation, making use of the method of the continuous dislocations is introduced. The method is subsequently used as a means of determining the SIFs of edge cracks in fretting fatigue. The numerical problem is solved and after a check on its accuracy, new SIFs results are presented in Chapter 4 for angled cracks in terms of the pad foot length and the friction coefficient. The critical crack length is determined through a fatigue analysis and the theoretical model is compared with known experimental results. Factors which influence fretting fatigue cracks are estimated by comparing the SIFs ranges with the threshold SIF range of the material. The conclusions of the investigation indicate that fretting fatigue may adequately be assessed by a fracture mechanics model.

The following Chapters form the second part of the study and examine an NDE technique for evaluating fretting fatigue cracks. For this purpose, a quantitative description of the interaction of Rayleigh waves with modelled fretting fatigue cracks

is presented. Chapter 4 deals with the background for the ultrasonics study, reviewing the theoretical and experimental models for the scattering from both normal and angled features. Chapter 5 presents the experimental study for the Rayleigh waves interaction with slots which simulate fretting fatigue cracks, along with comments on the complex scattering events. Then in Chapter 6 interpretation of the inverse characterisation problem is sought by combining the findings of the different approaches to the kinked crack problem. A critical assessment of the implications of the results for a NDE technique based on Rayleigh waves is also reported.

Chapter 7 brings together the main conclusions from the numerical fracture mechanics model and from the Rayleigh wave scattering results. Suggestions for further improvements and extensions of the present work conclude the main part of this thesis.

The Appendix contains detailed derivations of the numerical expressions for the stress field due to dislocations.

1.3 Claim of contribution

The originality of this work lies in the fact that it supplements a fracture mechanics study with the crack length and shape determination through an NDE method based on ultrasonics. The crack characterisation is of paramount importance to a fracture mechanics approach to fretting fatigue, because it allows the determination of the crack growth stage (angled or normal to the surface). Other parameters that affect fretting fatigue, such as stress field, material and angled effects are also explicitly examined. It is to be noted that to-date most of the existing theoretical models for the fretting fatigue modelling make use of the Rooke and Jones's (1977) solutions for SIFs. These refer to elementary stress distributions for

components made of the same material, without any regard to angled cracks. Moreover, the present model is more easily applied for the fretting fatigue assessment than the models which relate fretting fatigue strength simply to relative slip range and it is also scientifically closer to reality. Indeed, in many cases of the practice, the crack length is a more tangible parameter than the true value of slip range, provided that a suitable NDE method is available.

In particular, the original contributions reported in this study can be summarised as:

1. The development of a loading configuration, in which the pressing pad is a rectangular stamp or punch. The new model is more representative of the stress field in the specimen than the existing models. The influence of stress field beneath the contact, which plays a paramount role in fretting fatigue and the limitations in the application of simpler stress distributions are thus investigated. An analysis of the mathematical contact model and of the parameters that affect its application is also carried out to help clarify some important aspects of fretting fatigue.

2. The contact-crack model has been examined from both the mechanical and mathematical points of view and the corresponding equations have been derived. For their solution, the simple numerical method of the continuous dislocations, which is more efficient than the finite element method, has been extended to cover the case of fretting fatigue. An investigation into the stability and accuracy of the method is carried out and validated against a series of known results.

3. The numerical model allowed the application of different stress distributions due to the pressing punch and not only uniform ones. A series of new results for SIFs in the case of fretting fatigue is compiled in graphical form in terms of the angle, the depth and the coefficient of friction. Note that slant edge cracks occur widely in wear and rolling contact problems (Nowell and Hills (1987)), and the determination of the SIFs could be useful in these cases, too.

4. The new numerical model is further extended by taking into account the influence of the materials of the mating surfaces. Such investigation is not possible at all with

the conventional methods and offers new insights into the examination of fretting fatigue, when different materials are involved. Also, the new model is compared with the conventional models and, being more accurate of them, allows the limits of their application to be determined. The influence of stress ratio and crack closure is also investigated.

5. Ultrasonic measurements for angled and kinked cracks are carried out and an interpretation for the scattered field is given. The focus has been the development of experimental techniques which can make accurate and reproducible measurements of the scattered field. For this purpose, all the returning echoes, even from backwall reflections in a plate, were considered, and their contribution was analyzed in both the time and frequency domains.

6. New results for the reflection coefficients of kinked cracks are presented. It was shown that their structure displays a large number of remarkable features that can be employed for the inverse characterisation of a fretting fatigue crack. Different methods of analysis are used to elucidate the scattering mechanism, providing new quantitative descriptions of the interactions.

7. Lastly, the findings of the fatigue model and the ultrasonics analysis were incorporated in proposals for a suitable method of fretting fatigue assessment using fracture mechanics. The improved NDE method allows not only the determination of the crack length without interrupting the experiment but also benefits the design for life improvement, by reducing the assumed size of the initial defect (Section 2.1.2).

2. STRESS ANALYSIS FOR THE FRETTING FATIGUE MODEL

2.1 Occurrence of fretting fatigue in practice

2.1.1 Fretting in structures

There are some common features in fretting fatigue (Forsyth (1981), which can be encountered in numerous engineering situations:

1. some degree of freedom for relative movement between surfaces in contact;
2. individual points of contact at asperities;
3. sufficient high stress at or near these points to cause cracking.

The relative movement, combined with the normal pressure which provides the contact between the bodies, leads to minute relative slip between the adjacent surfaces. The slip amplitude is typically less than 0.1mm and zones of slip and locking are formed on the contacting surfaces (Figure 1.1, also: Hills and Comninou (1985)). In the slip region, the asperities continually weld together and then break (Frost *et al* (1974), Waterhouse (1981)). Particles are detached from the mating materials leading to deterioration in surface finish, often exacerbated by the ingress of corrosive fluids. These small fragments of metal may also form oxide particles which are usually harder than the material itself and, becoming trapped between the contacting surfaces, cause abrasive wear and scoring. The simultaneous presence of

a bulk cyclic stress applied to one element can lead to a marked reduction in its fatigue life. The minimum number of fatigue cycles with fretting, which leads to the specimen's failure is defined as "fretting fatigue limit" or "fretting fatigue damage threshold" (Sato (1986)). The ratio of the fretting fatigue life, obtained from fatigue tests where the specimen is fretted to failure, to the fatigue life during plain fatigue, varies from 50% (*ibid)* to 10% (Nowell and Hills (1990)), depending, of course, on the conditions.

Some of the most common engineering applications which can suffer from fretting fatigue are the fastened joints, such as those used in aircrafts. These can be flanges, i.e. bolted or riveted flat surfaces under shear loads with a possible degree of slippage. They can also be loaded filled holes, with pins or fasteners bearing on the bores of holes and subjected to some interface sliding (for example, lugs loaded through push-fit pins) or shafts having pressed-on wheels. Forsyth (1981) distinguishes between these two cases, stating that in the flange case the tangential and normal stresses occur independently of each other, whereas in the filled holes case the stresses are interdependent. Some specific examples of fretting fatigue of flange faces are shown in Figures 2.1 and 2.2. From these figures it can be inferred that non-uniform contact, especially in thin-sheet construction, can be expected to result in the appearance of fretting scars. This lack of flatness may be introduced during manufacture (in the cutting and forming operations) or during assembly and consequently its degree may be difficult to estimate during design.

Fretting problems, belonging to the general case of the pin-hole combinations, can be encountered in the "shrunk-on" and dovetail fixing components of electrical generators and gas-turbines (Waterhouse (1981), Nix and Lindley (1988)). This category includes the assemblies of rotor blades and discs, discs and shafts and pole plates and rotors. In general, fretting occurs in virtually every assembly containing metal surfaces which are in contact. Examples of components where fretting has been a problem include the strands in wire ropes or cables in contact, spring washers, coil

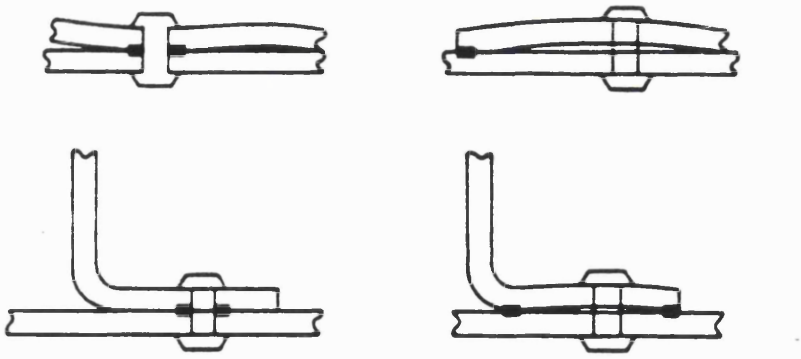

Schematic diagrams of thin sheet joints illustrating commonly occurring fretting points. Danger points indicated thus ■.

Figure 2.1 Fretting points in thin sheets (from Forsyth (1981))

Schematic diagram illustrating the positions of frequently observed fretting damage. Danger points indicated thus ■.

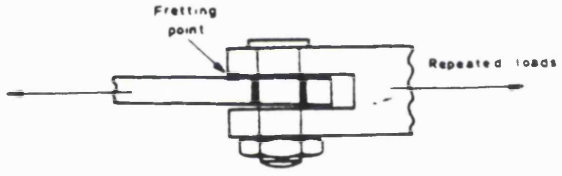

Schematic diagram illustrating how misalignment of a fork end fitting can cause fretting fatigue problems.

Figure 2.2 Fretting resulting from misalignment (from Forsyth (1981)

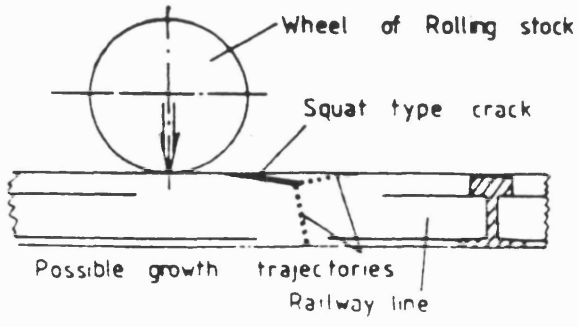

Figure 2.3 Fretting fatigue in railway lines (from Hills et al (1984))

and leaf springs etc (Forsyth (1981), Waterhouse (1981), Tanaka *et al* (1985)).

Last but not least a problem occurring in railway lines must be reported (Figure 2.3). It is rather a contact mechanics than a typical fretting fatigue problem, as the railway lines are not subjected to any alternating stress causing fatigue. Cracks, which occur due to the sliding force between wheel and rail, propagate obliquely to the surface and have an approximately elliptic boundary, so that a relatively small opening may hide a disproportionately large void. When such a crack has grown away from the surface, it usually turns. If it turns upwards, then a small portion of the railway line may be detached. This incident causes less trouble than the downwards propagation of the crack, which can lead to complete through-thickness fracture of the rail and possible derailment of the train (Hills *et al* (1984)). The problem is reported here because a similar numerical formulation, like that derived in this thesis for the determination of the SIFs for slant cracks under normal and tangential loading, can be used for its modelling. Note, however, that while fretting fatigue cracks ordinarily grow in an opening mode, cracks occurring in rolling contact may grow in a more complicated mixed mode (Hills *et al* (1988), Otsuka (1991)).

2.1.2 Design approaches to the lifing of components

The experimental work on materials evaluation in fretting fatigue can be classified in two broad categories, depending on the intended applications. The first generally involves fatigue cracks developed in structures, especially in airframes. In this case, crack growth models may be applied for fretting fatigue cracks and be used for design purposes (the "airframe structures" approach, for example Edwards *et al* (1977 etc), Tanaka *et al* (1985) etc). A typical crack growth "law" can usually be described by a relation in the form of the empirical Paris equation (Paris and Erdogan (1963)):

$$\frac{da}{dn} = C(\Delta K)^m \qquad (2.1)$$

where C and m are experimentally determined material constants for a given stress ratio R, n is the number of fatigue stress cycles and $\Delta K=K_{max}-K_{min}=Y\Delta\sigma\sqrt{\pi a}$ is the SIF range.

The remnant life of structures can in principle be evaluated when the flaw sizes involved are such that can be quantitatively characterised by a suitable NDE technique (Wanhill (1986)). Application of a crack growth analysis for a structure implies the existence of a NDE method, which should be able in practice to monitor the cracks with a reasonable margin of confidence and provide data for the crack growth analysis (Norris (1985)). In these component lifetime predictions the most critical parameter is the initial crack size. This deduction may be derived by considering the number of cycles Δn for propagation from the initial length a_i to a final critical one a_f, after integrating Equation (2.1) (Parker (1981)):

$$\Delta n = \frac{1}{CY^m\pi^{m/2}(\Delta\sigma)^m}\frac{a_i^{1-(m/2)}-a_f^{1-(m/2)}}{m/2-1} \qquad (2.2)$$

where it has been assumed that Y of Equation (1.1) is independent of a.

The nature of the final expression 2.2 is such that its value is strongly influenced by the assumed initial length. Therefore, one of the options available to the designer for life improvement is the improvement of the inspection technique and hence the reduction of the assumed size of the initial defect. From the discussion above, the vital role of NDE in the crack growth approach to the lifing of components becomes clear.

The second category of fretting fatigue research models involves crack growth in engine parts, which are subjected to high number of loading cycles during service. These are more liable to a SIF range threshold analysis, because once a crack starts

to grow the component will inevitably fail. Here, the loads usually occur in-phase and might be easier to define under normal conditions than the loads on an airframe structure, which depend on the stress histories, non-constant amplitude stresses etc. In general, cracks will not grow unless a threshold value of SIF range ΔK_0 is exceeded. Thus this design criterion dictates that the operational stress levels be such that ΔK is lower than ΔK_0, and $\Delta\sigma=\Delta\sigma_{max}-\Delta\sigma_{min}$ is lower than the fatigue limit $\Delta\sigma_f$. Alternatively, if a crack is detected by some NDE means, this should be smaller than the non-propagating crack that corresponds to the threshold SIF range ΔK_0. This approach for life evaluation finds application in the components of turbogenerators and electrical generators (the "energy industry" approach: Nix and Lindley (1985 etc) and Waterhouse (1981)).

A problem encountered in fretting fatigue considerations is the definition of the stages of propagation of a kinked crack. A source of misunderstanding is that some researchers define the fretting fatigue stage where the crack is still inclined to the surface as Stage I fretting fatigue (Sato *et al* (1986)). This term may cause confusion with the Forsyth's (1969) notation for the fatigue crack propagation (Figure 2.4: The three stages of crack propagation). In his Stage I notation, the short cracks (or microcracks) are influenced by the shear mode and they propagate in shear mode at an angle to the surface, but they are not readily modelled in terms of LEFM. In Forsyth's Stage II notation the cracks (or macrocracks) are long enough to be driven by the maximum principal applied stress growing perpendicular to it.

On the other hand, the angled fretting fatigue cracks may or may not be in Stage II of Forsyth's notation, depending on the scale of the problem. In addition to the physical length of the crack, another controlling parameter affecting the application of LEFM in fretting fatigue cracks is the plastic zone size at the crack tip in comparison with the overall crack length. There are numerous examples in the literature, where LEFM is applicable for 'short' cracks, provided the plastic zone is limited. For example, Endo (1981) quotes that even an oblique crack with less than

70μm length grows in tensile mode. In that particular experiment the crack grew in Stage II of the Forsyth's notation, namely perpendicular to the principal tensile stress, which is the combination of the repeated bulk fatigue stress and the surface tangential stress. An investigation into the influence of the short cracks effects on the LEFM application is carried out in Section 2.6.

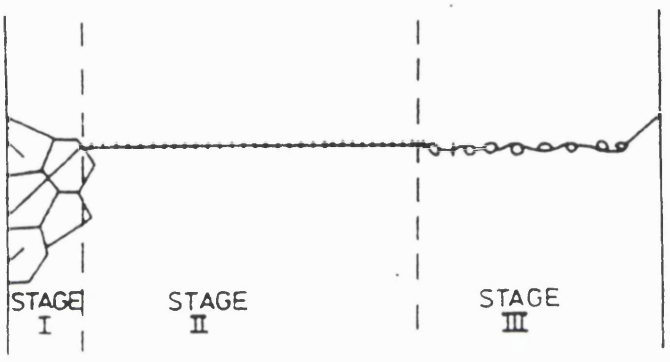

The three stages of fatigue crack propagation in a metal

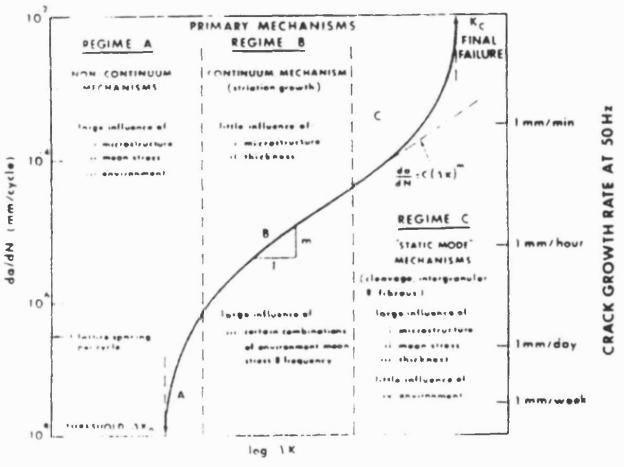

Figure 2.4 The three stages of fatigue crack propagation and the fatigue crack growth rate curve da/dn-ΔK (after Ewalds and Wanhill (1984))

In the following, the notation 'stage S_I and S_{II}' (which is common in the fretting fatigue nomenclature) will be used for angled and kinked fretting fatigue cracks respectively and the expressions "Stage I" and "Stage II" fatigue cracks will continue to apply for the usual Forsyth's notation.

2.2 The influence of the relative slip range

In this work fretting fatigue will be examined from a fracture mechanics viewpoint, but there are additional parameters that influence the wear and delamination induced by fretting. Except of the metallurgical properties of the contacting materials, an important controlling parameter of fretting is the relative slip range between the two bodies, measured on their surface (ESDU (1967)). The main objection to an assessment route based on an evaluation of the surface damage induced by the relative slip of the contacting bodies, is that the reduction of the fatigue strength due to fretting is not always increased in line with increasing slip range (Nix and Lindley (1988)). Although slip range does determine the rate of material removal from the surface, no correlation seems to exist between the quantity of debris produced and the loss of fatigue strength (Frost *et al* (1974)). Large slip amplitudes do increase the quantity of debris and promote wear, but, at the same time, they cause abrasive removal of superficial material, which may contain incipient cracks and hence mitigate the damage (Nix and Lindley (1988)).

Nevertheless, assessment methods based on relative slip range can still be of importance in some cases. If, for example, a surface treatment, or palliative layer, has been applied to the surface, then relative slip could result in degradation of the surface by material removal and thus enhancement of the initiation and propagation of cracks. Here, the operating fretting mechanism is in confliction with the previous case, when the removal of superficial material was rather beneficial. The surface treatment may be obtained through the use of anti-fretting agents, such as oils and

greases, which reduce metal-to-metal contact, absorb the fretting movement, spread the local severity of damage and exclude the corrosive action of the atmosphere (Frost *et al* (1974)). In this way, friction is kept as low as possible, when complete suppression of the slip is not feasible. However, these aspects of fretting fatigue are outside the scope of this work and need application of the principles of tribology for their study (Waterhouse (1981)).

It must be mentioned, too, that if prevention of slip is possible, then high friction is desirable. A means of achieving slip suppression is by applying a contact load which bears a sufficiently high ratio to the tangential load that is responsible for the fretting (Frost *et al* (1974)). The influence of the normal contact load, which may lead to a marked increase in the fatigue strength through the reduction of slip, is discussed later in Chapter 4.

2.3 Fretting Fatigue testing

Most researchers have used either square-ended or cylindrical pads in their fretting fatigue tests. As fretting is initially a contact mechanics problem, the stress field at the specimen due to the pads must first be determined using either analytical or numerical methods. The stress field itself depends on the geometry, the nature of the loads and the friction between the surfaces. In the case of cylindrical pads on a flat surface the contact stress field is well defined and the stresses in the specimen can be found relatively easy. The oscillating tension is applied in phase with the fretting force. Normal force P is applied onto the surface, through the pad, and the fatigue stress σ_m induces a simultaneous tangential force Q at the contact, which can be regulated through the use of springs. This kind of test specimen was used by Endo and his co-workers (Endo *et al* (1973,1974,1976)), Nishioka and Hirakawa (1969), Wharton *et al* (1973), Nowell and Hills (1987, 1988) among others.

Other experiments and theoretical work have been performed using square-edged pads, as it is schematically shown in Figure 2.5. The problem in this case is that the distribution of tractions induced by the frictional and normal loads are not known beforehand and assumptions must be made about their form, so that the stresses in the specimen can be calculated. Such configurations were used by the RAE Farnborough researchers (Edwards *et al* (1977 etc), Rooke and Edwards (1987)), as well as by Nix and Lindley (1985, 1988), Sato *et al* (1986), Hattori *et al* (1988) and by Wright and O'Connor (1973) for finite element calculations. In the present study, a test specimen was considered, which was identical to that used by the Materials and Structures Department of RAE Farnborough (Figures 2.6-7) ("dog-bone" shape) and similar to that considered by Nix and Lindley (1985).

It is well worth mentioning at this point that most of the researchers associated with fretting and fretting fatigue have contributed to two important publications which review the field, which are connected with the same person: the first is the book *"Fretting Fatigue"* edited by R.B. Waterhouse (1981) and the second is a series of papers in the journal *Wear* (Vol. 125, 1988), dedicated to R.B. Waterhouse on the occasion of his retirement.

2.4 The contact and crack models used in this work

As mentioned, an elastic stress analysis must first be performed in order to study the contact problem of a pad pressing onto the specimen surface. It can be assumed that the stresses in this region do not critically depend on the shape of the bodies distant from the contact region (Johnson (1985)), provided of course that the dimensions of the contacting bodies themselves are large compared with the dimensions of the contact area. In general, a specimen thicker than two contact widths can be idealised as an elastic half-space (Nowell and Hills (1990)). This idealisation is made almost universally in contact mechanics and facilitates the

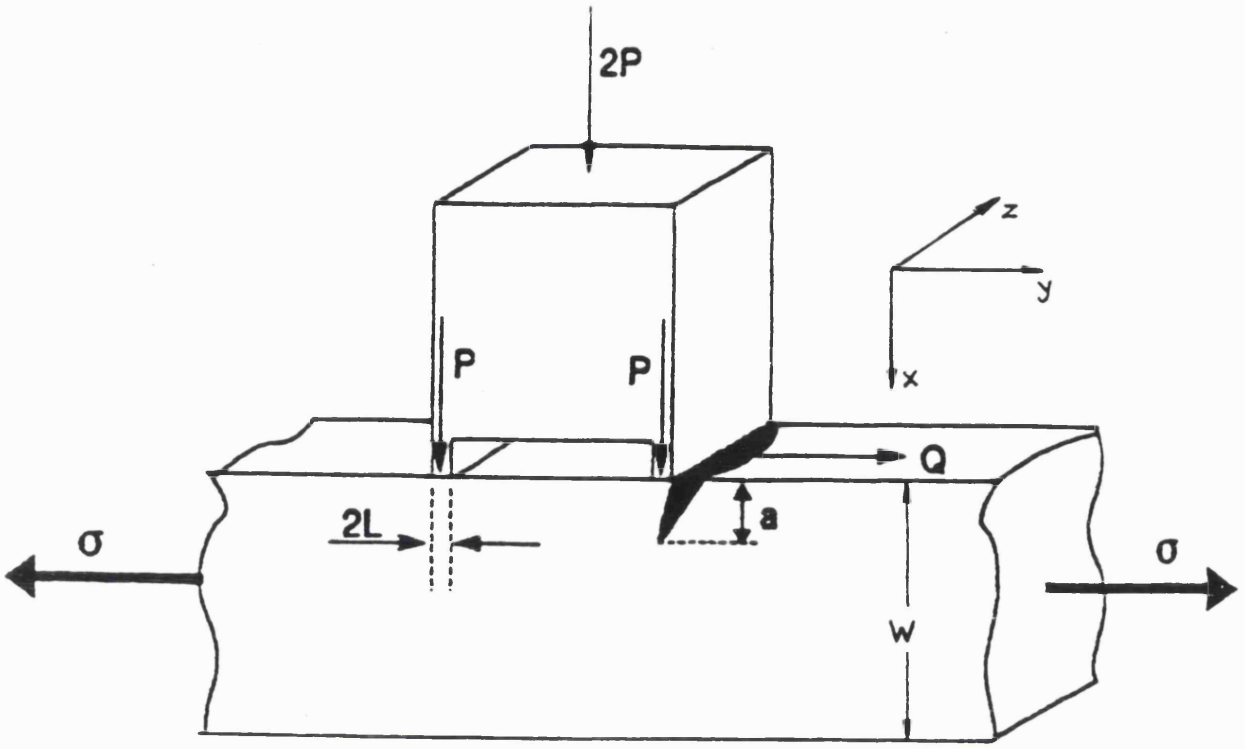

Figure 2.5 Schematic representation of fretting pad and specimen

investigation of the contact stresses by making available the vast body of theory that has been developed for the elastic half-space.

The stress analysis of an elastic body has been taken up by many investigators (Johnson (1985)). The parameters that have drawn more attention are the shape of the space (half-space, quarter-space and wedge of arbitrary angle), the loading (point or distributed, normal or tangential or both), the simultaneous presence of a crack etc (Hanson and Keer (1989)). In moving situations, the normal and tangential forces are of course assumed to move slowly enough for inertia effects to be neglected. The elastodynamic problem for the similar configuration, namely for a loaded quarter-space or wedge domain, has been studied by Eringen (1974) and by Gautessen (1985,1987) for the case of the scattering by a wedge of an incident Rayleigh wave. This case is further discussed in Chapters 5-7.

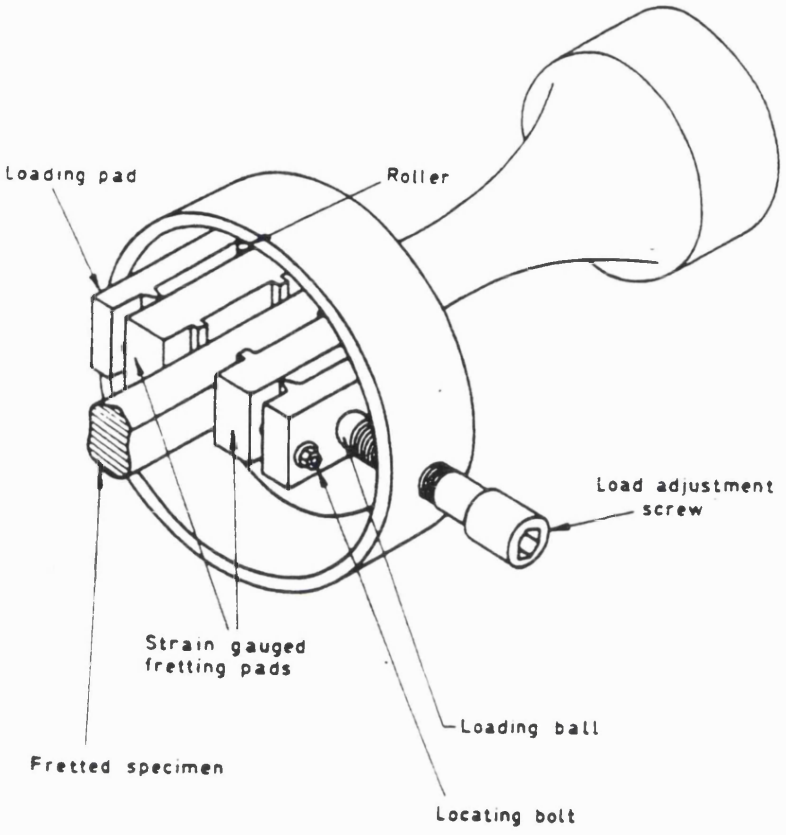

Figure 2.6 Fretting specimen assembly (from Edwards and Cook (1978b))

The contact problem has received less attention, due to its complexity especially when there is a simultaneous presence of a crack (see Wright and O'Connor (1971) for a flawless body with friction, Nied and Erdogan (1981) for a cracked body). Indeed, there are two aspects of the problem which require investigation: (1) the traction distribution between the contacting bodies must be computed; and (2) given the nominal stress field indicated by the first part of the solution, it is required to find the stresses as modified by a preexisting crack. The SIFs are of particular interest for the latter case.

The complexity stems from the fact that the two parts of the solution are coupled, since the presence of a crack affects the compliance of one of contacting bodies. Consequently, the distribution of the surface tractions is not known and is dependent on the crack geometry as well as on the geometry of the pressing stamp (Nied and Erdogan (1979). However, the present state of affairs is considerably simplified if the integral equation which describe the problem are uncoupled by first neglecting the influence of the tangential traction on the normal pressure (Johnson (1985) and then the influence of the contact on the crack problem (Edwards (1981). Although this simplified technique of superposing the contact and crack solutions is routinely used in the literature, its limitations must always be investigated, as it will be done later in this Chapter. Note that a static analysis of the stress state does not take into account the traction distribution history between the two bodies, which may include any zones of slip and locking (Wright and O'Connor (1971), nor the transmitted frictional forces between the crack faces in the case of partially closed cracks (Hills and Comninou (1985). Nevertheless, the results from a rather simplified static model are necessary for further investigation of the problem (Rooke and Edwards (1987)).

The first part of this study is devoted to the fracture and fatigue analysis of the standard fretting fatigue specimen shown in Figure 2.7. From the cases reported in the literature, it can be deduced that fretting fatigue cracks developed in materials evaluation tests are generally short (Section 2.6), due to the limited scale of the test rigs. Although LEFM fails for shallow cracks (Pook (1989) sets a 0.25 mm lower limit for the application of the SIF approach to the mixed mode fatigue), many researchers have shown that for defects down to 0.1 mm in depth, LEFM models do give good predictions for their particular test configurations. (Edwards and Cook (1978), Nix and Lindley (1985), Hills *et al* (1988), Hattori *et al* (1988)).

In the vicinity of the crack tip, the total stress field which is due to many different Mode-I (or -II or -III) loadings can be obtained in the elastic region, by superposition of the respective SIFs (Nix and Lindley (1985), Hattori *et al* (1988)).

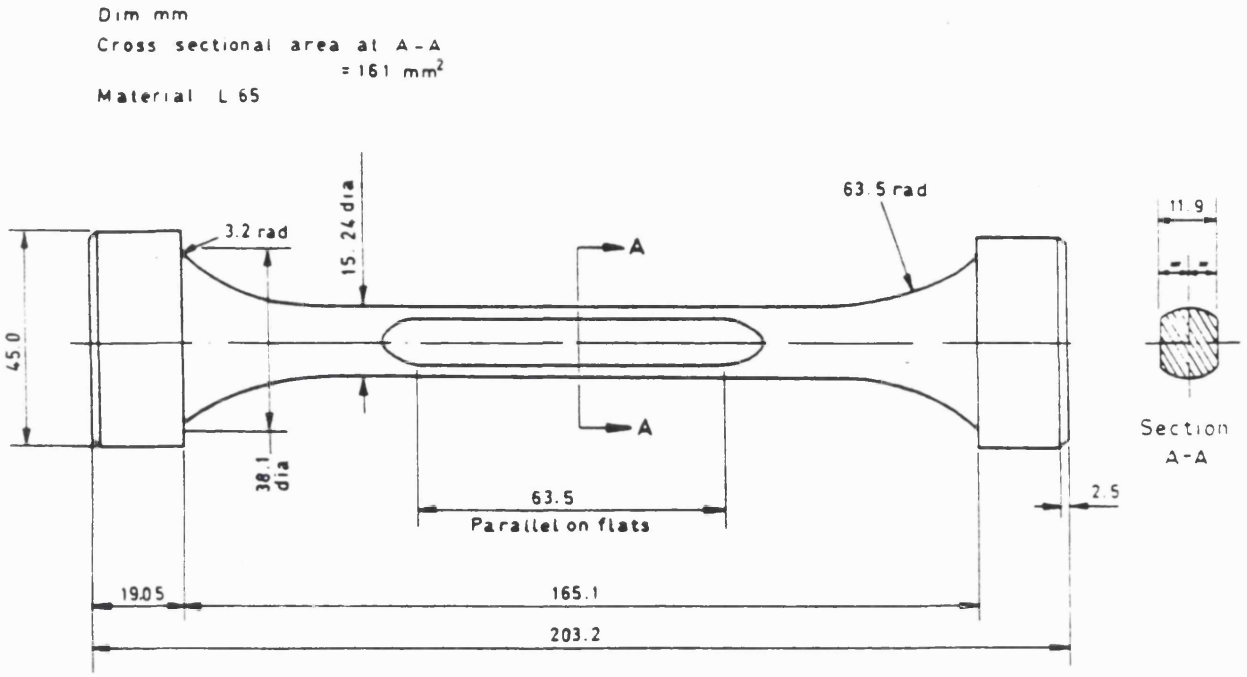

Figure 2.6a *Fretted specimen*

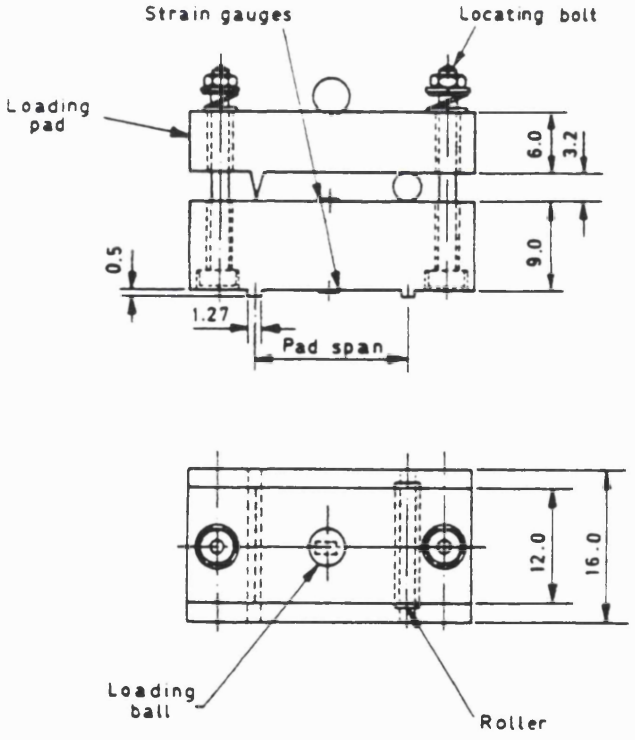

Figure 2.7 (a) Fretting specimen (b) strain gauged fretting pad (from Edwards and Cook (1978b))

For the case of an edge crack inclined to the cyclic tensile axis, which is considered here, there is a normal and tangential loading of the half-space and an additional tensile loading of the specimen, along its axis. Both situations occur simultaneously and give rise to different SIFs, which can be superposed as long as they are referred to the same mode of loading, i.e. we take the sum of all Mode-I and the sum of all Mode-II SIFs (*ibid*).

The basic assumptions made throughout the theoretical stress analysis and fracture mechanics study were:

1. The unloaded surface of the interface is perfectly flat and the contact is continuous. The axial fatigue stress in the specimen is uniform in regions remote from the fretting pads.

2. The crack is a Stage-II edge crack, growing first obliquely to the surface and then normally to it. The crack therefore resembles a kinked one. The assumption of a distinct knee at the point where the crack changes direction is of course an approximation. It is nevertheless a common conjecture in their modelling (Li Yingzhi and Hills (1990)), as it has been observed experimentally (Figure 1.2), depending of course on the material and testing conditions (Tanaka *et al* (1985), Sato *et al* (1986)).

3. The tangential and normal forces that act through the pad foot into the specimen surface have the same distribution. Most researchers make use of this assumption, which has also been observed experimentally (Johnson (1985), Hattori *et al* (1988))

4. The crack length is small when compared with the overall dimensions of the specimen and especially its thickness, so that the specimen can be considered as an elastic half-space. The stress state behaviour is investigated in the next Section.

5. The faces of the crack are always open and they are not pressed together, so that they don't suffer any Coulomb friction. However, the method used for the determination of the SIFs can easily be extended to the case where the crack faces are partially closed (Hills *et al* (1985a, 1985b,1989)). In this case the situation is dependent on the history of loading during the loading and unloading phases (Hills and Comninou (1985), Sheppard *et al* (1986)).

2.5 The state of stress in the crack tip region

Generally speaking, the application of the SIF approach is only appropriate if the plastic zone is concentrated in the vicinity of the crack tip. The plastic zone size affects the fatigue crack propagation threshold ΔK_0 as well as the fatigue crack growth rate curve, and this influence is different for each material (Tanaka *et al* (1981b)). The plastic zone size is smaller under plane strain conditions and yielding will not occur until the applied stress is much higher than the yield stress σ_{ys}. Pook (1989) suggests two checks: a global check to examine whether the nominal section stress is close to the general yield and a local check to ensure that the crack tip plastic zone is small compared with the overall crack length. Once the crack has developed and is governed by mode-I extension, the global check is supposed to be more discriminating. However, it is reasonable to perform both checks for fretting fatigue cracks, because it cannot be easily verified whether the crack grows in tensile mode or not; even small cracks may have reached the Stage-II of their propagation (Section 2.1.2).

When the size of the plane stress plastic zone, i.e. the diameter $2r_y$ in Irwin's analysis, is smaller than one-tenth of the specimen width (which in Figure 2.5 is assumed to be along the z-axis) we can expect predominantly plane strain conditions (Ewalds and Wanhill (1984)). The Irwin's diameter $2r_y$ for the monotonic plane stress plastic zone is given by: (*ibid*)

$$2r_y \approx \frac{1}{\pi} \left(\frac{K_I}{\sigma_{ys}}\right)^2 \qquad (2.3)$$

where σ_{ys} is the yield strength. We can take as K_I the plane strain fracture toughness and as σ_{ys} the 0.2% proof stress, which are readily available from tables. In this way an upper bound can be established for comparison with the 1/10 of the specimen width. In an analogous manner the empirical requirement for the plate thickness of the compact tension specimens can provide a general idea of the dimensions which ensure nominal plane strain behaviour:

$$W \geq 5.0 \left(\frac{K_{Ic}}{\sigma_{ys}}\right)^2 \qquad (2.4)$$

(The thickness W is implied along the x-axis in Figure 2.5)

In this study, the order of magnitude for the size of the plastic zone was estimated to be in the range of a millimetre for Al 2014A, whose mechanical properties can be found in Table 2.2. The specimen width is 12 mm (Figure 2.7a), namely more than 10 times bigger than the plane stress plastic zone size $2r_y$, thus ensuring plane strain conditions.

2.6 The influence of the short crack length

The problems associated with the behaviour of short cracks in fatigue must be also addressed, because the validity of LEFM for their study, beyond some length and stress limit is questionable.

The common property of the fretting fatigue cracks in the tests of the literature is that they are extremely "short"; either in terms of length or in terms of the high level of stress applied (according to the definition of the short cracks in the

review by Miller (1989)). A main characteristic of short cracks (≈0.1mm in steel) is that, for the same alternating SIF, they grow considerably faster than longer cracks (≈0.6mm) (Edwards *et al* (1977)). The threshold for short crack propagation is also considerably lower than that for longer cracks (*ibid*). Therefore, the present design procedures are in danger of being non-conservative, when it comes to the short cracks considerations.

However, it seems that in most cases in literature no short crack corrections have been taken into account for the study of fretting cracks. This may be due to the fact that short crack behaviour only recently has been extensively studied. One can find in the literature some absolute values for short crack lengths in various alloys which establish the lower bound for the applicability of conventional ("long crack") LEFM considerations (for example Lindley and Nix (1985): down to 100μm for medium strength steels; Blom *et al* (1986): 150μm for high strength Al-alloys). These values are sometimes conflicting, as they strongly depend on the parameters of the experiments and dictate different threshold values ΔK_0 than the corresponding "long" cracks in order to be valid (for example, see Miller (1989) and Vol.14 (1991) of the journal *Fatigue Fract. Engng Mater. Struct.* for a recent review on short cracks).

Miller (1989) postulates that most of the hypotheses which have been proposed to account for short crack behaviour can be divided into two main types: those based on microstructure, for which the grain size is important and those based on plasticity for which the appropriate parameter is the plastic zone size. According to Taylor (1986), for the LEFM to be valid the crack length should be at least 10 times longer than both a characteristic microstructural dimension 'd' (of typical extent 10μm) and the plastic zone size in fatigue r_p, the extent of which is estimated at:

$$r_p = 0.04 \left(\frac{\Delta K}{\sigma_{y,c}}\right)^2 \qquad (2.5)$$

where σ_{cy} is the cyclic yield strength.

Let's first examine the influence of microstructure. It is possible to talk in terms of homogeneous mechanical properties, such as elastic moduli, yield stress etc., if the local variations in polycrystalline solids are averaged out. The usual assumption that the material is both isotropic and homogeneous is thus an approximation for the small cracks region of fretting fatigue, where microstructural features may influence the behaviour (Atkins and Mai (1985)). Consequently, cracks less than some critical length show anomalous growth behaviour, which cannot be quantified by LEFM.

An early quantitative discussion of the problem can be found in Frost *et al* (1974), who referred to a length at which a crack developing in a plain specimen starts to grow as a macrocrack, namely in Stage II of Forsyth's (1969) notation, where the LEFM relations hold true. This changeover length varies from 0.007mm in aluminium alloys to 0.25mm in nickel and it can be considered as the maximum depth of surface scratch or flaw that can be tolerated without affecting the fatigue limit of a material. If a crack grows in its Stage I, namely before reaching its changeover length, and reaches a grain boundary it may be held up. However, if a crack has started growing as a macrocrack (Stage II) before reaching a grain boundary, the grain boundary will have little, if any, effect on its development. Therefore, for plain fatigue, a grain size-effect should be absent for cracks longer than the changeover length. Assuming that a crack must be 10 times longer than the grain size when this is taken equal to the changeover length should suffice to guarantee that, under most conditions, the crack has already reached its Stage II of propagation and is no more affected by the grain size. This criterion puts the calculations on the safe side in terms of LEFM validity. It would thus suggest that for cracks in aluminium alloys longer than 100μm (that is much longer than the changeover length), LEFM in fretting fatigue could be applicable, provided of course

that the specimen section is not close to general yielding. Indeed, most of the crack sizes of the experiments of the literature are longer than 100μm.

With regard now to the extent of crack tip plasticity, this must be limited compared to the crack length, if a LEFM analysis is to be undertaken. Crack closure phenomena render the phenomenon more complicated for fatigued specimens than for specimens subjected to monotonic loading. However, the criterion based on Equation 2.5 guarantees that the effective SIF values for small cracks do not differ more than 10% from those derived for longer cracks (Taylor (1986)). It also ensures that most of the crack front experiences plane strain conditions (*ibid*). Indeed, the plane stress field extends into the body for a distance approximately equal to the plastic zone size r_p (Knott (1973)). Therefore, a crack longer than $10r_p$ will have adequately penetrate some distance into the bulk of the body, away from the surface where plane stress conditions prevail. For these reasons and because the criterion is easy to apply too, it will be used in this work to test the assumption of small scale yielding conditions at the crack tip.

2.7 Properties of the specimen materials

The results of the theoretical study will be compared mainly with experimental data referring to samples made of aluminium alloys Al 2014A and Al 2024-T3 and of steel alloys 3.5 NiCrMoV and 1CrMo. Their chemical compositions and mechanical properties are given in Tables 2.1-2, which were compiled from the publications by Sato *et al* (1986), Nix and Lindley (1988) and Gdoutos (1984). These aluminium alloys belong to the general category of alloys known under the commercial name "duraluminium" and are the traditional materials for the aircraft structures. The steel alloys are mainly used for turbine blades.

Element	3.5NiCrMoV	1CrMo	Al 2014A	Al 2024-T3
C	0.21	0.42		
Si	0.25	0.30	0.5	0.14
Mn	0.30	0.59	0.5	0.54
S	0.006	0.022		
P	0.010	0.030		
Ni	3.43	0.29		
Cr	1.57	1.42		0.02
Mo	0.41	0.75		
V	0.12			
Fe			0.2	0.20
Cu			5.0	4.48
Mg			0.4	1.40
Zn				0.03
Ti plus Zr				0.03

Table 2.1 **Chemical composition of the specimen and fretting pad materials in weight per cent (Sato *et al* (1986), Nix and Lindley (1988) and Gdoutos (1984))**

Property	3.5NiCrMoV	1CrMo	Al 2014A	Al 2024-T3
0.2% proof $\sigma_{0.2}$	600 MPa	843 MPa	458 MPa	350 MPa
Tensile strength	733 MPa	999 MPa	504 MPa	495 MPa
Elongation δ (%)	25	21	9.8	15
Reduction ϕ in area (%)	70	59	-	24
Vickers hardness	222 (VPN)	340 (VPN)	155 (VPN)	339 (HV)
Poisson's ratio ν	0.25	0.25	0.33	0.33
Toughness K_{Ic} (MPa $m^{1/2}$)	-	-	27	27

Table 2.2 Mechanical properties of the specimens and the fretting pads. (Sato *et al* (1986), Nix and Lindley (1988) and Gdoutos (1984))

2.8 Stress analysis

2.8.1. Stresses in the half-space

The problem to which we shall turn our attention in this subsection, is the determination of the distribution of the tangential q(y) and normal p(y) surface tractions which are produced at the foot of the fretting pad, and are not beforehand known. The former result from friction between the pad and specimen, whereas the latter are due to the applied contact load. The task of defining the suitable form of the tractions due to fretting pads is fundamental to the early stages of any fretting fatigue study, because in real situations, there are almost as many loading distributions as applications.

To a first approximation the specimen can be considered as a half-space and this is expected to be the case for the configuration considered in this study under the conditions presented in the previous Sections 2.1.3-5. The analysis is mainly two-dimensional and consequently the distribution of tractions across the thickness of the fretting pads, i.e. from -L to L (Figure 2.8) will be only considered. This can be justified as follows: it has been found in similar experiments that straight through cracks, highly extended along the z axis of Figure 2.5, were common in the specimens (Edwards and Cook (1978a)). The aspect ratio of the cracks a/c (depth over semi-surface length 'c') is in all cases near zero (Nix and Lindley (1988)), implying very long cracks in the z-direction. Hence, the frictional and contact forces are actually applied uniformly over the entire contact width (which is implied along the z axis in Figure 2.5). However, no such assumption could be made about the distribution of the loads between the front and the back of the fretting pad feet (from -L to L) and this is the subject of the following analysis.

In general, contact problems belong to the category of "mixed boundary value" problems (Johnson (1985)), where a combination of displacements and surface

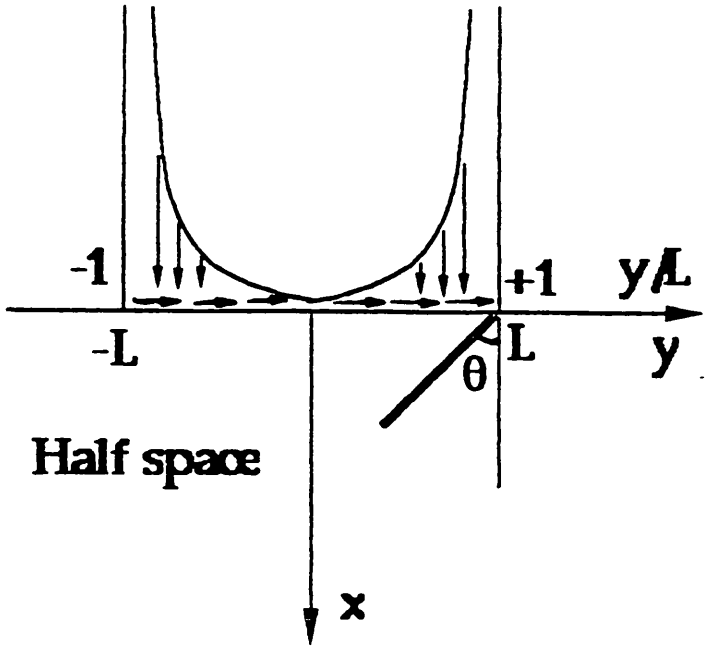

Figure 2.8 Modelling of the normal and tangential loading of a half-space

tractions are specified within the contact region, whilst outside the contact the surface tractions are specifically zero. The particular problem pertains to a class of boundary conditions where the normal displacement at the contact region is specified by the known profile of the pressing pad and the tractions can either be specified (for example, by $q(y)=0$; frictionless contact) or be related by $q(y)=\pm\mu p(y)$, where μ is an average coefficient of friction.

Most of the models of the literature make use of simplified distributions of tractions, taking no account of any displacement in the loaded region. The boundary conditions in these cases amount to specifying the distribution of tractions (uniform, triangular, parabolical etc) over the contact boundary of the half-space and the displacements follow from the solution of the stress-strain relationships. The models give rapid solutions to the uncoupled crack-contact problems with acceptable accuracy, when compared with experimental findings. The only shortcoming, from the engineering point of view, is that they do not account for the slip and friction between the mating surfaces, which significantly contribute to the fretting damage.

The mathematical model should therefore be investigated as regards the influence of these parameters to explore the limitations of the simplifications.

In terms of the stress field, consider first an uncracked elastic half-space (Figure 2.8), loaded over the strip y≤|L| by a normal pressure p(y) and tangential traction q(y). Suppose for a moment that the distribution of the tractions p(y) and q(y) is known and these are related by the above mentioned relation through the average coefficient of friction. Needless to say that the usual assumptions for isotropic and homogeneous materials have been taken into regard. The stress due to p(y) and q(y) at any point A in the half-space are given in Johnson (1985) for plane strain conditions as:

$$\sigma_{yy}=-\frac{2x}{\pi}\int_{-L}^{L}\frac{p(s)(y-s)^2ds}{[(y-s)^2+x^2]^2}-\frac{2}{\pi}\int_{-L}^{L}\frac{q(s)(y-s)^3ds}{[(y-s)^2+x^2]^2} \qquad (2.6)$$

$$\sigma_{xx}=-\frac{2x^3}{\pi}\int_{-L}^{L}\frac{p(s)ds}{[(y-s)^2+x^2]^2}-\frac{2x^2}{\pi}\int_{-L}^{L}\frac{q(s)(y-s)ds}{[(y-s)^2+x^2]^2} \qquad (2.7)$$

$$\tau_{yx}=-\frac{2x^2}{\pi}\int_{-L}^{L}\frac{p(s)(y-s)ds}{[(y-s)^2+x^2]^2}-\frac{2x}{\pi}\int_{-L}^{L}\frac{q(s)(y-s)^2ds}{[(y-s)^2+x^2]^2} \qquad (2.8)$$

These relations were derived by direct integration from -L to L of the standard solutions for the stresses induced in a half-plane by a concentrated normal and a concentrated tangential load. From these equations the resulting strains can be calculated by applying the Hooke's law under conditions of plane strain (Timoshenko and Goodier (1970)), although the integration in closed form is usually difficult:

$$\varepsilon_y = \frac{1}{E}\left[(1-\nu^2)\sigma_{yy} - \nu(1+\nu)\sigma_{xx} \right]$$

$$\varepsilon_x = \frac{1}{E}\left[(1-\nu^2)\sigma_{xx} - \nu(1+\nu)\sigma_{yy} \right] \qquad (2.9)$$

$$\gamma_{yx} = \frac{1}{G}\tau_{yx} = \frac{2(1+\nu)}{E}\tau_{yx}$$

(E is the elastic modulus and G the shear modulus), where the plane strain conditions are given by:

$$\varepsilon_z = 0, \qquad \sigma_{zz} = \nu(\sigma_{yy}+\sigma_{xx}) \qquad (2.10)$$

Since, the strains ε_y, ε_x and γ_{yx} are related to the displacements u_x and u_y by:

$$\varepsilon_y = \frac{\partial u_y}{\partial y}, \qquad \varepsilon_x = \frac{\partial u_x}{\partial x}, \qquad \gamma_{yx} = \frac{\partial u_y}{\partial x} + \frac{\partial u_x}{\partial y} \qquad (2.11)$$

one can find, by some straightforward manipulation, the displacement gradients u_x and u_y at the surface, where the pad presses onto the elastic half-space with Poisson's ratio ν: (Johnson (1985))

$$\frac{\partial \bar{u}_y}{\partial y} = -\frac{(1-2\nu)(1+\nu)}{E}p(y) - \frac{2(1-\nu^2)}{\pi E}\int_{-L}^{L}\frac{q(s)}{y-s}\,ds \qquad (2.12)$$

$$\frac{\partial \bar{u}_x}{\partial y} = \frac{(1-2\nu)(1+\nu)}{E}q(y) - \frac{2(1-\nu^2)}{\pi E}\int_{-L}^{L}\frac{p(s)}{y-s}\,ds \qquad (2.13)$$

2.8.2 The tractions distribution

a) The models used in the literature

From the testing point of view, the researchers tend to use two main forms of pads and, consequently, pressure distributions, as it was mentioned in Section 2.3. For the case of cylindrical pressing pads and assuming contact in the region -L to L, the distribution:

$$p(y)=p_0\sqrt{1-(\frac{y}{L})^2} \qquad |y|\leq L \tag{2.14}$$

is used for the so-called Midlin problem of two cylinders pressed together (Endo *et al* (1973,1974,1975), Nowell and Hills (1987b), Hills *et al* (1988)). This model does not require cumbersome estimates of the traction distributions, since the contact of the two solids can be adequately studied by the application of the Hertzian theory (Johnson (1985)). However the application of the Hertzian theory demands that the contact region of the two bodies be small. This requirement is obviously not fulfilled when the two solids are elastic rectangular blocks (Wright and O'Connor (1971)) and consequently many cases of the practice are not adequately represented by this model.

For the case of square-ended pads a uniform distribution of normal and tangential tractions is mainly used (Hills *et al* (1985a, 1985b), Edwards *et al* (1976 etc), Nix and Lindley (1985,1988)), although other forms of elementary distributions have also been considered (e.g. (negative or positive) triangular , parabolic etc). These distributions simplify considerably the problem, but a theoretical assessment of the rather complicated contact problem must first be made to explore the limits of their application. The following analysis will reveal the influence of slip, which is not been taken into account in most of the fracture mechanics models of the literature.

b) The contact problem

For the configuration considered in this study, it seems that the most suitable representation is that of a rigid flat punch pressing onto an elastic half-space. (Figures 2.5 and 2.8). The flat punch has a thickness 2L (from -L to L) and sharp square corners; it is long in the z direction, which is perpendicular to the plane of Figure 2.8, so that plane strain conditions can be assumed. In formulating the 2-D problem, it is assumed that there is no tilting of the punch and that the surface of the elastic solid in contact with the rigid punch remains flat. Therefore, the first boundary condition follows from the specification that the normal displacement u_x is constant.

The frictional conditions at the interface determine the second boundary conditions in the loaded region. Assuming first a frictionless contact (q(y)=0), the solution of the integral equations system of the Equations (2.12-13) yields: (Johnson (1985))

$$p(y)=p_0\,(L^2-y^2)^{-1/2} \tag{2.15}$$

The constant p_0 is given by:

$$p_0 = \frac{P}{\pi} \tag{2.16}$$

Now, substituting this value of p(y) in Equation (2.12), we can find the tangential displacement under the punch:

$$\bar{u}_y(y) = - \frac{(1-2\nu)(1+\nu)P}{\pi E} \sin^{-1}(y/L) \tag{2.17}$$

For a compressible material ($\nu<0.5$), this expression shows that some slip occurs, because points on the surface will move towards the centre of the punch. In practice, it is this slip motion that should be opposed by friction and, if possible, prevented altogether to avoid the detrimental action of slip that accelerates the

fretting mechanism (Section 2.2). For example, the prevention of slip by this means should lead to a considerable increase in the fatigue life of a pin joint, when the pin is made an interference fit in the hole in the lug.

Let's now release the condition that $q(y)=0$ and assume that there is no slip. In this case the integral Equations (2.12-13) are coupled. Nevertheless, if we uncouple the system by first assuming $q(y)=0$, solve the system for $p(y)$ and substitute this value to find a approximate solution for $q(y)$, we discover that the difference between this simplified solution and the actual one is not large (Johnson (1985)). This conclusion shows that the influence of the tangential traction on the normal pressure is generally small. Consequently the system of the integral Equations (2.12-13) can be uncoupled, without considerable loss of accuracy. In the rest of this work in the problems involving tangential traction, it will be assumed that the stresses due to the normal pressure and the tangential traction are independent of each other and that they can superposed to find the resultant stress. It should be mentioned that this assumption is strictly true only when the elastic constants of the two bodies in contact are the same. However, the technique of superposing the normal and tangential tractions is used almost universally in the literature (as in Rooke and Jones (1989)).

For this no-slip case, the general shape of the tractions is the same as in the previous no-friction case (Equation 2.15): a singularity arises at $y=\pm L$, leading to infinite stresses just under the pad edges. Theoretically, the material is expected to yield plastically close to the edges of the punch even at the lightest load. Apparently, the linear elastic theory is inadequate to handle the high strain gradients in the region of the singularity. This conclusion is not surprising when one recalls that the original assumption that there is no slip at the interface implies that the two bodies should effectively behave as one.

In real materials, the high tractions near the punch edge cannot be sustained,

since they would require an infinite coefficient of friction. Therefore, some micro-slip occurs at both edges of the contact strip. One could conclude that the original assumption that there was no slip, is not physically acceptable. A stick zone is expected, which is centrally placed from y=-c to y=+c, say, for the case of a purely normally load. In this no-slip zone $q(y)<\mu p(y)$, whilst in the slip zones $c\leq |y| \leq L$ it holds $q(y)=\pm\mu p(y)$. The extent of the no-slip zone is governed by the Poisson's ratio ν and the coefficient of friction μ. For constant normal load, micro-slip begins immediately at the two edges of the contact and spreads inward as the tangential load increases.

The problem becomes further complicated for oscillating tangential forces, because in this case the final state of contact stresses will depend on the history of loading and not solely on the final values of the normal and tangential stresses (Hills and Comninou (1985)). Nevertheless, the results from the linear elastic theory provide a useful tool for the understanding of the stress concentrations and the resulting plastic flow of the material.

The above simplified analysis reveals some important aspects of fretting fatigue: first that high stress concentrations and eventually slip should always be expected near the corners of the punch and secondly that increase of friction leads to suppression of slip and consequently improves the contact strength. According to what has been said in the discussion of fretting mechanism about the influence of slip on the crack initiation, the possible points of crack emergence should be located just under the fretting pad corners.

c) The coefficient of friction

A point that may cause confusion is the definition of the coefficient of friction. The mean or average coefficient of friction is the dimensionless ratio $\Delta F_t/P$

during sliding, where ΔF_t is the amplitude of the (tangential) frictional force per unit area of pad foot. This ratio is virtually a coefficient of the tangential force, as is more aptly termed by Endo and Goto (1976). On the other hand, the true local coefficient of friction is the ratio of the surface tractions q/p in the region of slip. This quantity varies from point to point as surface modification occurs due to the contacting asperities as well as with time.

In addition to the two types of coefficients, two types of slip also appear during fretting (Edwards and Cook (1978a), Tanaka *et al* (1985)). The first is termed "elastic slip", during which the fretting scars are relatively superficial and the frictional forces are being developed by elastic deformation of the contacting asperities. The second type of slip is termed "macroslip" and in this case the asperities slide over each other and the pads tend to wear away the specimen surface. This is explained by the accumulation of oxidized debris between the contact surfaces which accounts for the fretting damage. In this case, the frictional force has already reached a plateau value and a constant average coefficient of friction has been achieved at alternating stresses greater than a critical value (Nix and Lindley (1988). The coefficient value becomes high after several fatigue cycles and usually varies from 0.7 to 1 (Endo and Goto (1976), Tanaka *et al* (1985), Nix and Lindley (1985,1988)).

For the present case of a pressing pad onto a half-space, most of the references refer to the average coefficient of friction under steady state sliding. It will be assumed that the sliding friction law applies at each area of the interface, so that:

$$\frac{|\, q(y) \,|}{p(y)} = \frac{|\, Q \,|}{P} = \mu \qquad (2.18)$$

This condition corresponds to either sliding over the specimens surface or to conditions of incipient sliding of the two bodies. The assumption simplifies the

analysis and is certainly reasonable, because it has been found experimentally that the frictional force per foot rapidly achieves a limiting value almost equal to the contact force per foot, as it was mentioned above. In this case, the stick region shrinks to a line at y=0 around the centre of the punch, so that the bodies are on the point of sliding (Johnson (1985)) and the condition expressed by the Equation (2.18) holds true. Even with a relatively lower value of μ, for example μ=0.7, the stick zone has started to vanish as the slip zone spreads inwards from the punch corners, where first emerges.

d) The rigidity of the pressing punch

The choice of the "rigid-punch" configuration is corroborated by the experimental observation that the crack starts near the apex of the punch, as a consequence of the micro-slip that occurs there. The theoretical analysis above showed that the micro-slip is a result of the high stresses there, consequently a singularity exists in the stress field just under the pad edges. For more details, especially in the case where the pad is a wedge with an angle other than 90°, refer to Johnson (1985) and Gdoutos and Theocaris (1975) (for the influence of the friction on the stress concentration). The problem of the compression under axial loads of an elastic rectangle by two identical elastic half-spaces in plane strain has been also investigated by Khadem and O'Connor (1971), and Wright and O'Connor (1971) with the aid of the finite element method.

The "rigid-punch" assumption simplifies considerably the elastic problem, although the condition of the "rigidity" of the punch can only be rigorously approached when the elastic modulus of the half-space is much lower than that of the punch. It should therefore be examined whether this assumption alters the physical representation of the problem, when real elastic materials are involved. Because the assumed rigidity of the punch introduces a stress singularity under the pad edge, an investigation into whether this singularity arises in reality for the

particular materials combination is necessary.

According to Dundurs and Lee (1972) and Comninou (1976), the stress field becomes theoretically infinite under the pad corners, if the following inequality that measures the difference in "plane strain modulus" $\{(1-\nu^2)/E\}$ between the materials of the two bodies holds true:

$$\frac{[(1-\nu_1)/G_1]-[(1-\nu_2)/G_2]}{[(1-\nu_1)/G_1]+[(1-\nu_2)/G_2]} \geq \frac{\mu\pi-1}{\mu\pi+1} \qquad (2.15)$$

For the particular combination of aluminium alloy specimen-steel pad, the above expression is true irrespective of the value of coefficient of friction μ, indicating that a singularity invariably appears in the stress field. Therefore, even though the "rigid punch" hypothesis is an approximation, it does not misrepresent the physical model and the resulting stresses state for the particular materials. Strictly speaking, however, the above criterion simply dictates that the stresses are not finite close to the apex of the punch and does not reveal anything about the strength of the singularity, which is outside the scope of this study.

2.9 Results and discussion for the uncracked body case

Having examined the distribution of surface traction, we are now able to proceed to the calculation of the stresses in the half-space. These will be severest when the tractions take their maximum values and hence we will also consider the case for maximum coefficient of friction $\mu=1$, supposing that $q(y)=\mu p(y)$. Equations (2.6-8) were integrated numerically using the rigid-punch distribution (Equation (2.15)). The integration was performed after the normalisation of the integration interval, so that the total pad foot length extends from -1 to 1, instead from -L to L. The integrand has singularities at the end-points -1 and 1, but commercially available routines, such as these belonging to the NAG library, can easily cope with this kind of problems. For this purpose, the NAG library subroutines (NAG Code D01AJF)

were used and the program results were validated by comparing the results for uniform distribution with known solutions in closed form (Timoshenko and Goodier (1970)). The agreement was excellent up to the fourth decimal digit.

The corresponding stresses σ_{yy}, σ_{xx}, τ_{yx}, as well as the Von Mises stresses found under the punch are shown in Figures 2.9(a-b) for μ=0.0 and μ=1.0 and load P=1MPa. It can be seen from the figures that high stress concentrations occur just under each corner of the pressing punch. This is due to the singularity which exists at this point and it was the reason why the integration did not proceed beyond a depth of equal to (normalised) L/2. For shallower depths, not only the computing time increases disproportionally, but also the application of the small-strain elastic theory is in practice questionable.

In order to demonstrate the possible points of failure, the Von Mises and Tresca criteria of failure are next considered. The Von Mises criterion requires the shear strain energy per unit volume to reach a critical value and when expressed in terms of principal stresses σ_i, i=1,2,3, uniaxial yield stress σ_{ys} and yield stress in simple shear τ_y, it predicts failure when:

$$\frac{1}{6}\left[(\sigma_1-\sigma_2)^2+(\sigma_2-\sigma_3)^2+(\sigma_3-\sigma_1)^2\right] = \frac{\sigma_{ys}^2}{3} = \tau_y^2 \qquad (2.16)$$

(The stresses σ_i, i=1,2,3 can be determined by the standard transformations of the Mohr's circle (Timoshenko and Goodier (1970)). The yield of ductile materials may also be taken to be governed by Tresca's maximum shear stress criterion:

$$\max\left[\,|\sigma_1-\sigma_2|\,,\,|\sigma_2-\sigma_3|\,,\,|\sigma_3-\sigma_1|\,\right] = 2\tau_y=\sigma_{ys} \qquad (2.17)$$

In general, the difference in the predictions of the two criteria is not significant when the anisotropy of most materials is taken into account (Peterson (1974)). Both yield criteria are physically acceptable, but the Von Mises criterion usually produces better agreement with experimental results, whilst the Tresca's one is often easier to use in practice.

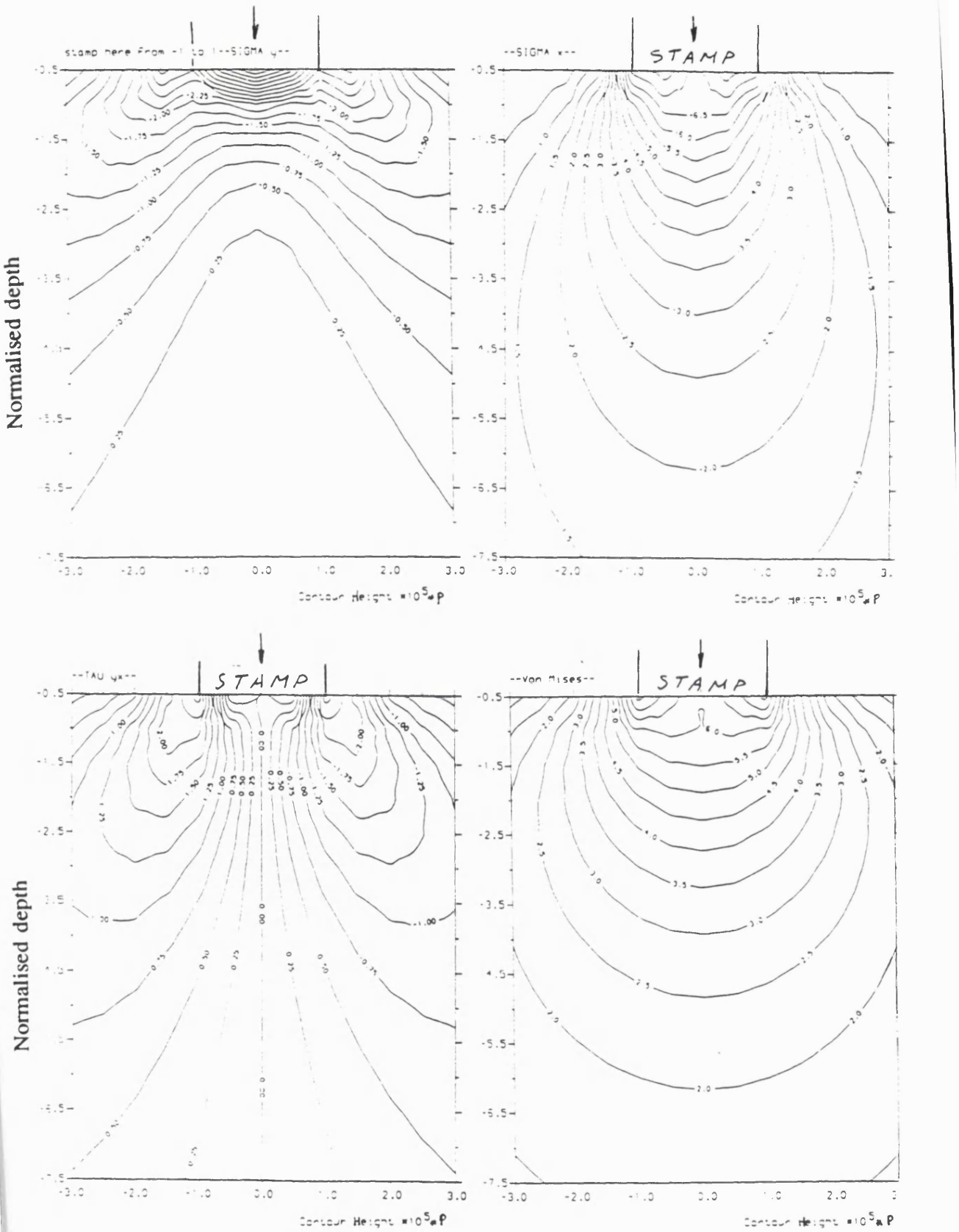

Figure 2.9a *"Rigid punch" configuration of Figure 2.8. Coefficient of friction μ=0. The figures correspond to the stresses given by Equations (2.6-8) and the Von-Mises Equation.*

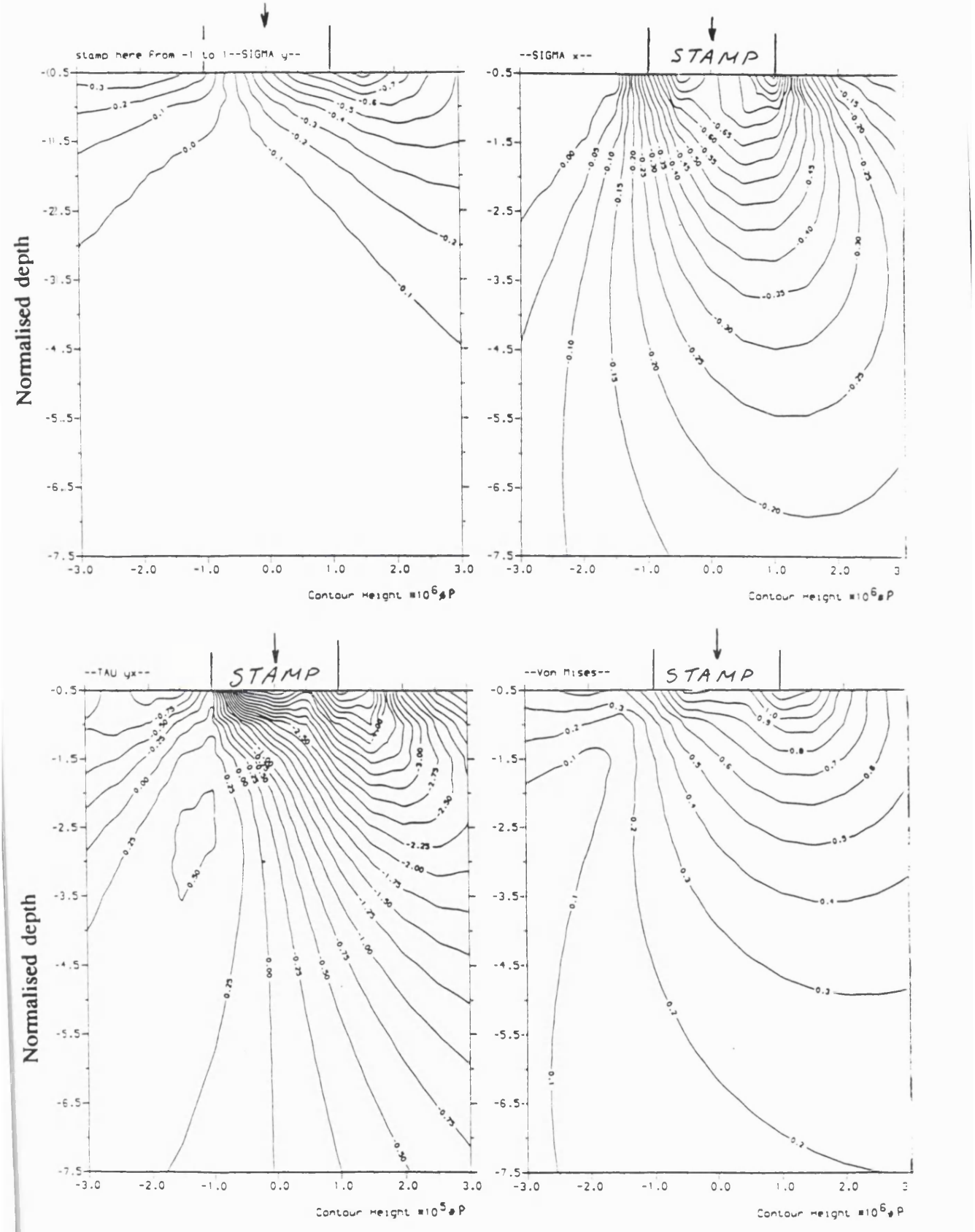

Figure 2.9b *"Rigid punch" configuration of Figure 2.8. Coefficient of friction μ=1.0. The figures correspond to the stresses given by Equations (2.6-8) and the Von-Mises Equation.*

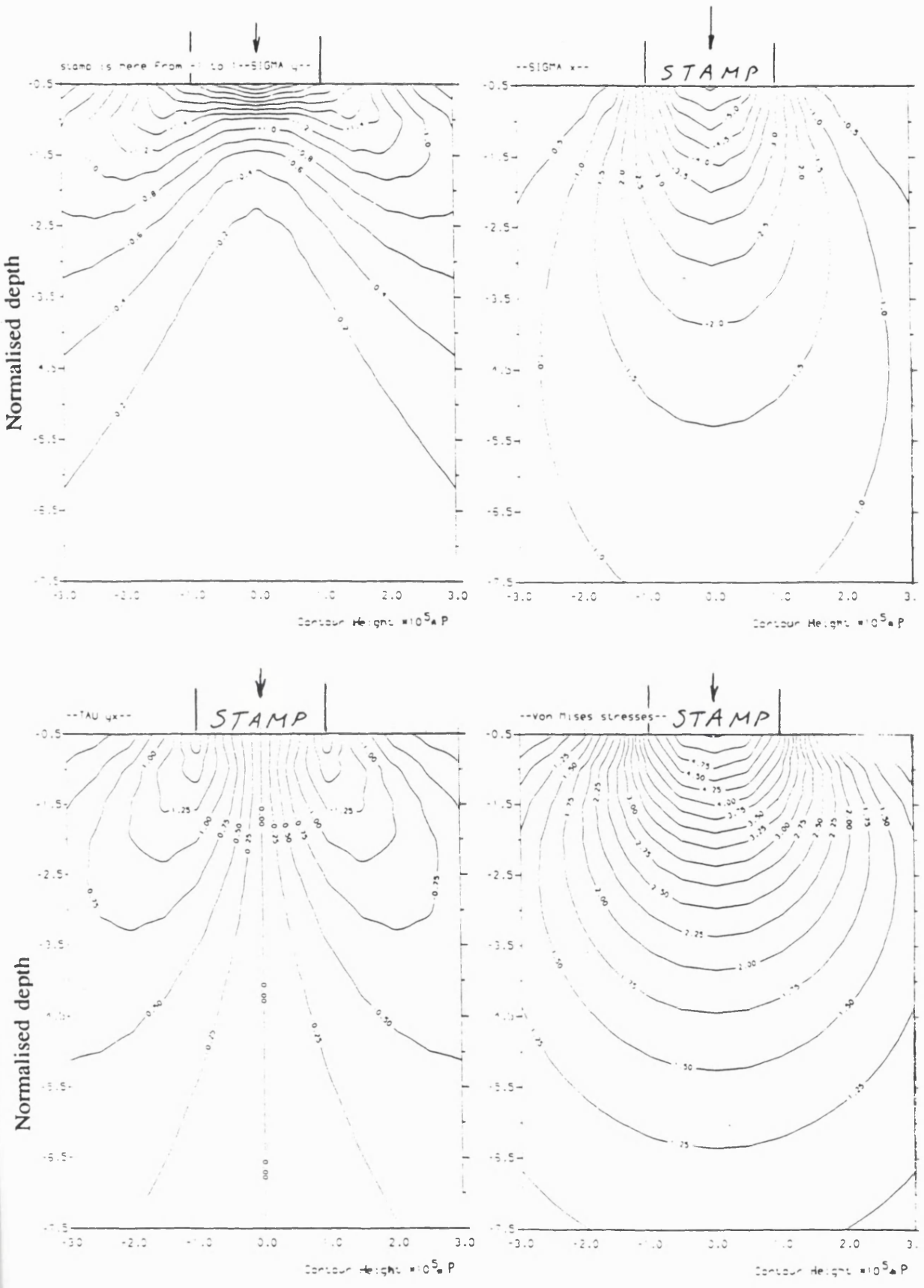

Figure 2.9c "Uniform" configuration of Figure 2.8. Coefficient of friction μ=0.0. The figures correspond to the stresses given by Equations (2.6-8) and the Von-Mises Equation.

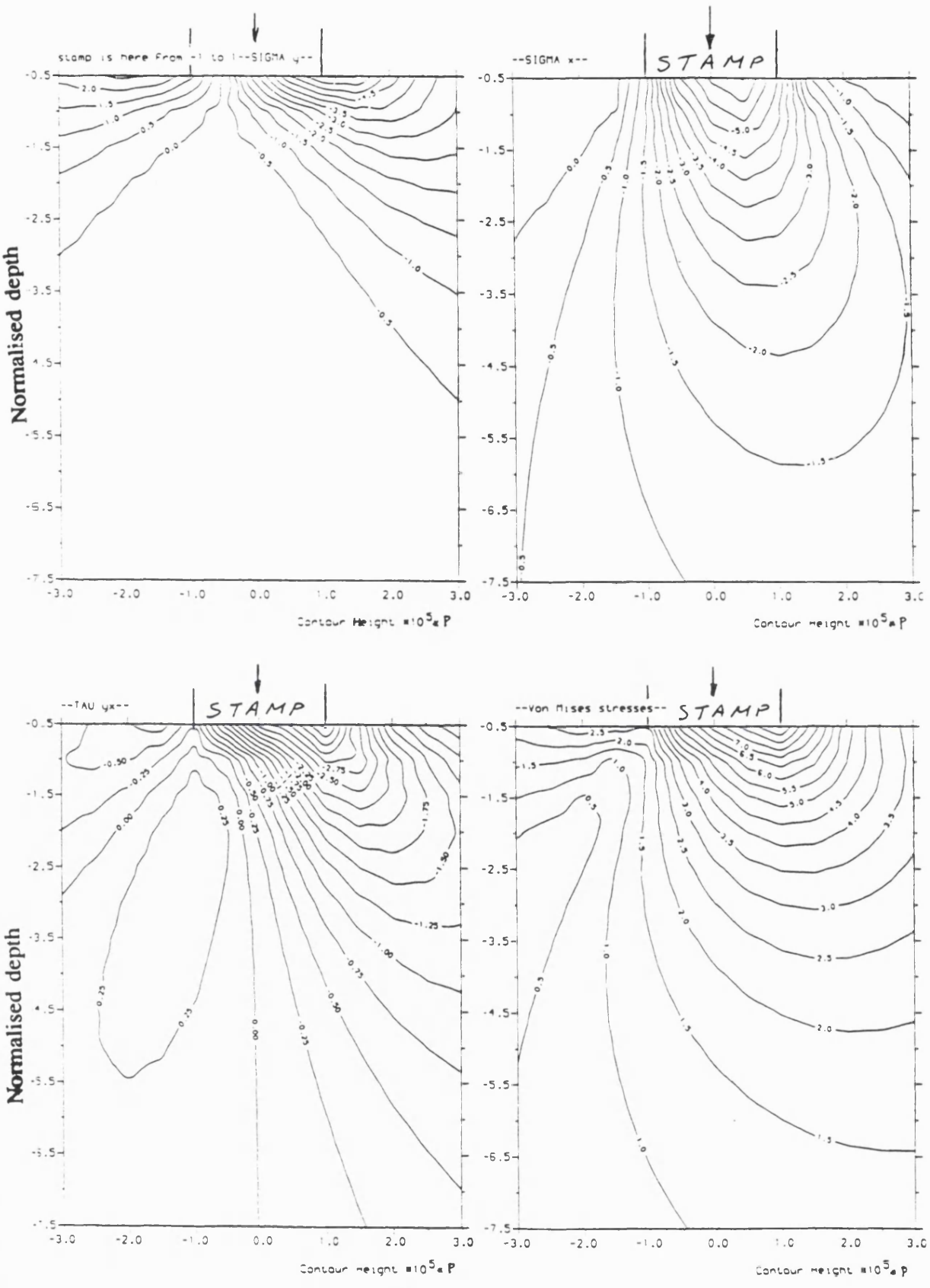

Figure 2.9d *"Uniform" configuration of Figure 2.8. Coefficient of friction μ=1.0 The figures correspond to the stresses given by Equations (2.6-8) and the Von-Mises Equation.*

According to what was mentioned in the last subsection, the infinite elastic pressure at the corners will give rise to theoretically infinite stresses and hence infinite differences in principal stresses, which will cause plastic flow. Although the contours of Figure 2.9 indicate high stress concentrations, especially under the pad corners, the stresses have already become finite at a depth 0.5L from the surface onwards. Whether the material will yield or not depends on the criteria above. For the Von-Mises criterion, the contours of Figures 2.9 in conjunction with Equation (2.16) can be used to ascertain whether the plastic zone has penetrated beyond the depth of 0.5L. The results can be used for the fracture mechanics model, but for smaller depths in a presence of a crack, an assessment based on LEFM may be proved dubious, due to the additional complexity of the small overall lengths of the cracks involved.

It is also interesting to compare the contours of Figures 2.9 (a-b), which refer to the rigid punch configuration, with those under a pad foot where uniform distribution $p_0=P/\pi$ has been assumed (Figures 2.9(c-d)). The two cases are not directly comparable, since they do not fulfil the same boundary conditions. The rigid punch case imposes the condition that the normal displacement under the punch be uniform and constant, or equivalently, that the punch be stiff enough so as not to tilt. On the other hand, in the uniform distribution case, it is the stresses that are specified and the displacements are then produced by the solution of Equations (2.12-13). Even though the difference between the corresponding contours should narrow distant from the contact, as it is expected from St. Venant's principle, the resulting stresses are invariably lower in the case of the uniform distribution. It is clear, therefore, that assuming a simpler uniform distribution only results in an approximation for the stresses in the half-space. Nevertheless, this assumption facilitates a solution based on the uncoupling of the crack and contact problems and offers rapid solutions for the SIFs (Rooke and Jones (1977)). How severe the influence of different distributions is, in conjunction with the limits of application of the LEFM, will be discussed in Chapter 4.

With regard now to the Tresca's criterion, in 2-D contact the condition of plane strain ($\gamma_{xz}=\gamma_{yz}=\varepsilon_z=0$ or $\tau_{xz}=\tau_{yz}=0$) generally ensures that the stress component σ_z is the intermediate principal stress (Johnson (1985)). Therefore, the Tresca's yield criterion is governed by the maximum shear stress or maximum principal stress difference $\tau_1= 0.5*(\sigma_1-\sigma_2)$ in the plane x-y of the cross-section. Contours of this principal stress difference or principal shear stresses, are presented in Figure 2.10 (taken from Johnson (1985)) in the form of photoelastic fringe patterns (Further

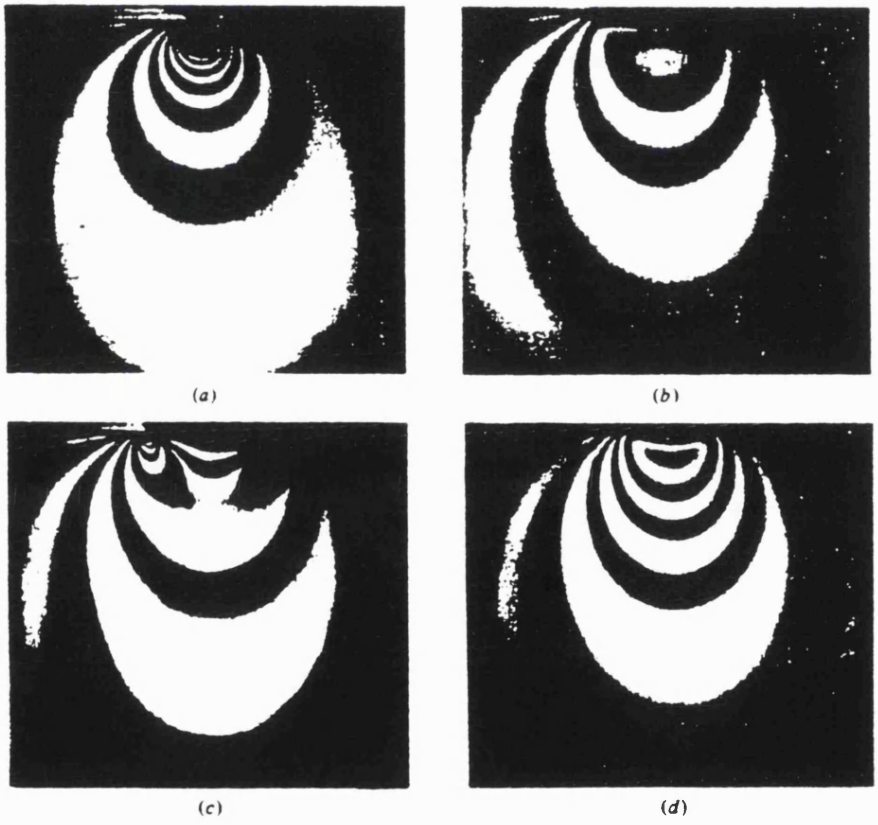

Figure 2.10 Two dimensional photo-elastic fringe patterns (contours of principal shear stress): (a) point load; (b) uniform pressure; (c) rigid flat punch; (d) contact of cylinders (from Johnson (1985))

photoelastic studies for various punch corner angles and friction coefficients can be found in Comninou(1976)). It seems from both Figures (2.9) and (2.10c) (which of course are not directly related, since they illustrate different stresses), that in the case of a rigid punch there are strong stress concentrations exactly under the pad edges, where the material might reach its yield point and possible crack nucleation can start. The result is useful for the non-destructive inspection of the fretting specimen, as it justifies the assumption that the crack is approximately located under the pad corner. Note also that the stresses are more evenly distributed for uniform distribution of pressure, as it should be expected. Figure 2.10d refers to a model of two cylinders pressed together (Equation 2.14), like that used by Nowell and Hills (1987b) in their different experimental test rig. Apparently, this model produces quite different stress distribution from that of the rigid-punch model and the results are not directly comparable.

Returning to Figures 2.9, it is obvious that the stresses increase under the leading edge of the punch as the friction coefficient increases. At the same time, the area just under the trailing edge is subjected to lower stress. The observed stress concentration in front of the pad foot due to the elevation of the frictional force is a common assumption in many fretting fatigue analyses. For this reason, some investigators (Tanaka *et al* (1985)) did not use the standard uniform, triangular or parabolical distribution of tractions of other authors (for example Edwards *et al* (1977 etc)), but they "weighted" them in a way that the leading edge conveys more traction. The numerical visualisations of Figures 2.9 seem to justify their choice, but it is usually difficult to beforehand predict what fraction of the frictional force is concentrated on the front of the fretting pad.

Another observation is that the stresses under the pads are negative (compressive). When the SIFs are calculated in the following Chapter 3, they will be negative due to these stresses, which press their faces together. It is known that a crack can normally grow only when it is subjected to a tension force in mode-I

(namely normally to its faces). The compressive environment of fretting fatigue would not favour the growth of cracks, at least according to the standard fracture mechanics, so long as there is no additional tensile bulk (axial) fatigue loading (σ in Figure 2.5) and crack arrest would eventually occur (Sato *et al* (1986)). However, the stresses induced by the tangential loading due to the fretting reduce very quickly with depth, depicting the local nature of the phenomenon.

A last comment is that the preceding 2-D analysis was based on the assumption that the frictional and tangential forces, irrespective of their shape, were distributed over the entire foot area. Close examination of the photographs of the surface morphology of the experimental specimens (for example in Lindley and Nix (1985), Tanaka *et al* (1985), Sato (1988)), as well as engineering intuition, lead to the conclusion that this is not the case, except for testing close to the fatigue limit. The fretting damage is usually confined to patches, indicating that contact occurs only partially (Nix and Lindley (1985)), as a result of the undulations present in the as-machined specimen surface. As the materials grind over each other on the fractured surface, features called "tongues" and "chips" (after Waterhouse (1981)) are formed which impair full contact and certainly contribute to the production of debris and the consequent progress of fretting wear. Although this phenomenon, which is a subject of a tribology assessment, plays an important role in the wear formation, it cannot easily be used for the fretting fatigue characterisation. In a series of experiments by Nix and Lindley (1985) the partial contact exerted little effect on the fretting fatigue findings, as no two specimens showed exactly similar wear scars. Hence, a fretting fatigue analysis based on the evaluation of surface damage is indeed difficult in practice. The general conclusion is that, although a 2-D analysis of fretting fatigue based on fracture mechanics ignores some factors, mainly the wear of the mating surfaces, it can still fully rationalise the relationships between important parameters that influence the material strength.

3. THE FRETTING FATIGUE MODEL: FORMULATION AND SOLUTION

3.1 Introduction

The knowledge of the stress field allows the prediction of the probable site of crack initiation. This was done in the previous Chapter. However, as yet there is no means of the predicting the number of cycles to initiate a crack and therefore a finite crack can only be analyzed by determining the crack tip SIF. When this is known, a fatigue threshold analysis or integration of the Paris fatigue law enables a critical crack length or a life curve to be predicted.

For this reason, a modelling technique is implemented in the following for the easy determination of opening mode (Mode-I) and sliding mode (Mode-II) Stress Intensity Factors for open edge cracks in a normally and tangentially loaded half-space. The technique makes use of distributed edge dislocations for any type of loading and the crack can be inclined at any angle to the surface. It will be shown that good precision can be achieved with less computing time than other numerical methods, such as the Finite Element Method.

After an introduction to the concept of dislocations, the numerical problem of a half-space with an edge crack in plane strain is formulated and solved. A popular approach to the problem is its formulation as a set of integral equations which satisfy the boundary conditions. These conditions can be obtained by using various methods (e.g. the Fourier transform of displacements, or by introducing a

distribution of dislocations etc). Most of these methods yield to a system of Cauchy-type singular integral equations, which can then be solved numerically.

An analysis based on the continuous dislocations distribution is quite straightforward and the steps followed in such an approach are outlined in this Section. New SIF results will be produced by applying the numerical procedure in the case of a normally and tangentially loaded half-space with an edge crack.

3.2 The dislocations method for finding the SIF

3.2.1. The concept of dislocations

Dislocations were initially used in fracture mechanics analyses to model the plastic deformation which usually occurs as slip between the blocks of crystals of the material (For bibliography on dislocations, the reader may see fracture mechanics

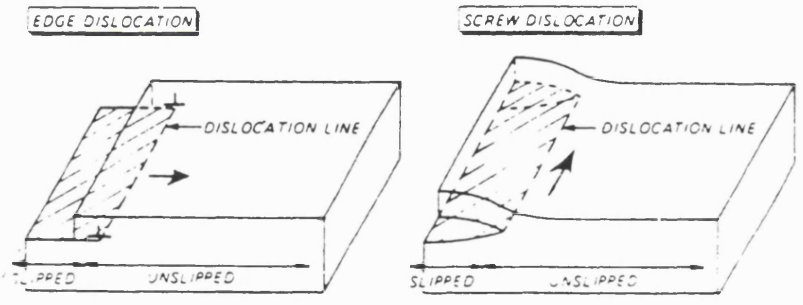

Slip owing to movement of pure edge and pure screw dislocations.

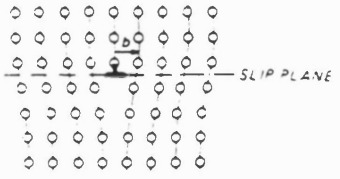

Figure 3.1 Slip due to the movement of dislocations and idealized representation of a dislocation (from Ewalds and Wanhill (1984))

texts, as e.g. Ewalds and Wanhill (1984)). A dislocation is basically the boundary that separates the slip and non-slip areas. The two main types of dislocations are depicted in Figure 3.1. When the displacement is normal to the dislocation line, it is called an edge dislocation, and when the displacement is parallel to the dislocation line, it is a screw dislocation.

The symbol $\perp$ is used for an edge dislocation and it depicts the dislocation as an extra half-plane of atoms, which lies above ($\perp$) or below ($\top$) the slip plane. The displacement (b) in Figure 3.1 is called the Burgers vector and it is constant along the dislocation line and perpendicular to an edge dislocation line.

3.2.2 Dislocation Models and cracks

One of the integral transform methods used for solving the elastic problem of finding the SIF, is the "dislocation method". In this case the dislocations are considered as a quite fictitious mathematical tool enabling us to model the crack. Nowell and Hills (1987) say that this operation resembles the process of inserting "darts" in dress making. The same authors point out that the method was originated in the USA with a team of researchers in Ann Arbor, Michigan, which included J. Dundurs, T. Mura, D. Smueser, M. Comninou, D.A.Hills and others.

The dislocations method for SIF evaluation is virtually a mixed boundary value problem, solved using standard transform techniques. It belongs to a category of methods where the problem can be reduced to a solution of the integral equation which takes the form:

$$L(x) = \int_0^a K(c,x)\phi(c)dc \qquad (3.1)$$

where "a" is the crack length, L(x) is the known stress along the crack in the

uncracked specimen, K(c,x) is a known kernel and $\phi(c)$ is an unknown function, related to the stress field induced by the dislocation in the cracked body. Once $\phi(x)$ is known, standard interpolation methods can be employed to find the SIF (Gupta and Erdogan (1973)), namely:

$$K_I = \lim_{x \to a} \sqrt{\pi(a-x)}\, \phi(x) \tag{3.2}$$

It is assumed that the crack has been modelled as a continuous distribution of displacement discontinuities, or dislocations. Of course, as it has already been mentioned, these are not real dislocations (i.e. lattice flaws), but one can imagine that this entirely mathematical concept arises by making a slit in the body, inserting or removing material, so that residual stresses exist.

Consider a half-space containing a (fictitious) dislocation at (c,0) in the inclined coordinate system $\hat{x}$-$\hat{y}$ (Figure 3.2) whose Burger's vector has components (b_x, b_y), after being resolved in x and y directions. The stress field induced by the presence of this edge dislocation, in the x-y coordinate system, is given by Hills and Nowell (1989) as:

$$\bar{\sigma}_{xx}(x,y) = \lambda[b_x(c)G_{xxx}(x,y,c)+b_y(c)G_{yxx}(x,y,c)] \tag{3.3}$$

$$\bar{\sigma}_{yy}(x,y) = \lambda[b_x(c)G_{xyy}(x,y,c)+b_y(c)G_{yyy}(x,y,c)] \tag{3.4}$$

$$\bar{\sigma}_{xy}(x,y) = \lambda[b_x(c)G_{xxy}(x,y,c)+b_y(c)G_{yxy}(x,y,c)] \tag{3.5}$$

where $\lambda=G/(\pi(\kappa+1))$, with G the shear modulus, $\kappa=3-4\nu$ in plane strain and $\kappa=(3-\nu)/(1+\nu)$ in plane stress. The full form of functions G_{ijk} and their derivation can be found in the Appendix.

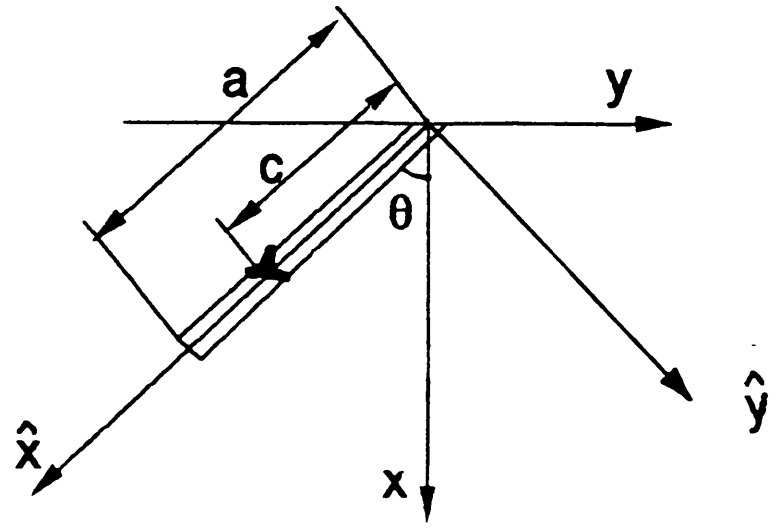

Figure 3.2 Crack geometry and coordinates system

In the rotated coordinate system $\hat{x}$-$\hat{y}$ the induced stresses given in terms of b_x and b_y are:

$$\bar{\sigma}_{\hat{y}\hat{y}} = \lambda\ (b_y K_y^N + b_x K_x^N) \tag{3.6}$$

$$\bar{\sigma}_{\hat{x}\hat{y}} = \lambda\ (b_y K_y^S + b_x K_x^S) \tag{3.7}$$

where K_i^N and K_i^S (i=x,y) are kernels dependent on the angle θ and the coordinates of the crack, derived from the functions G_{ijk} after using the Mohr's circle and the relationships given as Equations (3.3-5) to find the stresses in the rotated system $\hat{x}$-$\hat{y}$ (Timoshenko and Goodier (1970)):

$$K_i^N = \frac{G_{ixx}+G_{iyy}}{2} + \frac{G_{ixx}-G_{iyy}}{2}cos2\theta + G_{ixy}sin2\theta \tag{3.8}$$

$$K_i^S = \frac{G_{ixx}-G_{iyy}}{2}sin2\theta + G_{ixy}cos2\theta \tag{3.9}$$

with i=$\hat{x}$ or $\hat{y}$

In an elastic continuum a Burger's vector of $B_i(s)ds$ is used to model the

infinitesimal dislocation of density $B_i(s)$ at location s. Then the Burger's vector of a continuous array of dislocations is given by:

$$b_i = \int_S B_i(s)d(s) \tag{3.10}$$

where S is a path along the dislocation distribution. The Burger's vectors in our case, can be written:

$$b_x = \int_0^a B_x dc \tag{3.11}$$

$$b_y = \int_0^a B_y dc \tag{3.12}$$

If the shear and normal components of the stresses in an uncracked body due to external loading are $\sigma_S(\hat{x})$ and $\sigma_N(\hat{x})$, (resolved parallel to $\hat{x}$-$\hat{y}$ axes, after making use of the Mohr's circle to transform them into $\hat{x}$-$\hat{y}$ coordinates), the requirement that the net normal $N(\hat{x})$ and shear $S(\hat{x})$ tractions at the crack be zero, is:

$$S(\hat{x}) = \sigma_S(\hat{x}) + \bar{\sigma}_{\hat{x}\hat{y}} = 0 \tag{3.13}$$

$$N(\hat{x}) = \sigma_N(\hat{x}) + \bar{\sigma}_{\hat{y}\hat{y}} = 0 \tag{3.14}$$

and the integral equations expressing this equilibrium are obtained from Equations (3.6-7) and (3.13-14) to give:

$$S(\hat{x}) = \sigma_S(\hat{x}) + \lambda\left[\int_0^a B_x(c)K_x^S(\hat{x},c)dc + \int_0^a B_y(c)K_y^S(\hat{x},c)dc\right] = 0 \tag{3.15}$$

$$N(\hat{x}) = \sigma_N(\hat{x}) + \lambda\left[\int_0^a B_x(c)K_x^N(\hat{x},c)dc + \int_0^a B_y(c)K_y^N(\hat{x},c)dc\right] = 0 \tag{3.16}$$

The original problem has thus been reduced to one of finding the stresses that

the external field induces along the crack. The integrals, representing the stresses that the crack introduces in the half-space, have kernels with known values. What is additionally needed, is the stress analysis of the uncracked space and this can in most cases be easily carried out, as in the last Chapter. The solution follows by using superposition techniques. However, the method is in the following section further extended by considering the complete coupled crack-contact problem.

3.3 Extension of the method to the case of two elastic bodies

In the formulation of the problem which was considered in the previous section, it was assumed that no coupling occurs between the crack and the contact problems. This allowed the application of the superposition technique to Equations (3.13) and (3.14), where the stresses due to external forces (the contact problem), and the stresses due to the crack presence equal each other. The effects of the elastic nature of the solids were considered without taking into account the influence of the crack.

Nevertheless, the present problem is a coupled crack-contact problem in which the distribution of the transverse loads is not known. An analysis must be performed to compare the simplified models, which were considered previously which the problem of two elastic bodies in contact, in the presence of a crack in one of them. The present problem is different from the standard cracked strip problems, which were addressed by Erdogan and his co-workers (Erdogan *et al* (1973), Nied and Erdogan (1979)). The authors obtained the Green's function for the strip case, but they did not investigate angled cracks or the present configuration of rectangular blocks. It will be shown that by employing the mathematical model of dislocations a quicker solution can be achieved and new results for the fretting fatigue problem can be obtained.

In order to simplify the configuration studied it will be again assumed that the coefficient of friction μ is constant across the contact area and therefore $q(s)=\mu \cdot p(s)$ between $-L \le s \le L$. Equations (2.12) and (2.13) give the displacements at the surface of the half-space. It will be assumed that analogous relations give the normal surface displacements U_p for the punch, which will be considered as a half-space at least for smooth contact. These assumptions give:

$$\frac{\partial}{\partial y} U_p(y,0^-) = -\frac{2(1-\nu_p^2)}{\pi E_p} \int_{-L}^{L} \frac{p(s)}{y-s} + \frac{(1-2\nu_p)(1+\nu_p)}{E} \mu\, p(y) \qquad (3.17)$$

0^- and 0^+ are the positions just above and just under the line x=0, respectively.

The continuity of displacements in the contact line between the specimen and the pad can be expressed as follows:

$$\frac{\partial}{\partial y} [u(y,0^+) - U_p(y,0^-)] = \frac{d}{dy} U_0(y) \qquad |y| \le L \qquad (3.18)$$

where $U_0(y)$ describes the profile of the pad ($U_0(y)=0$ for a flat pad).

The quantity describing the normal displacement of the specimen $\partial u_x(y)/\partial y$ has been calculated in the Appendix, according to the dislocation theory (Equation A.14) for x=0, namely on the surface. Its value can be substituted in Equation (3.18). After some manipulation, the Equations (3.17-18) yield:

$$A\, p(y) + B \int_{-L}^{L} \frac{p(s)}{s-y} ds + \int_0^a B_x(c) K_x^{surf}(\hat{x},c) dc + \int_0^a B_y(c) K_y^{surf}(\hat{x},c) dc = 0 \qquad (3.19)$$

where the kernels K_i^{surf}, i=x,y on the surface are given by Equation A.14 and

$$A = \frac{1}{4} \left(\frac{\kappa-1}{G} - \frac{\kappa_p-1}{G_p}\right)\mu , \qquad B = \frac{1}{4} \left(\frac{\kappa+1}{G} - \frac{\kappa_p+1}{G_p}\right) \qquad (3.20)$$

G refers to the modulus of rigidity of the half-space and G_p to that of the punch, and $\kappa=3-4\nu$ for plane strain.

Equation (3.19) can be added to the system of Equations (3.15) and (3.16) providing another set of unknowns (the stresses p(y)), on the understanding that these resulting stresses need to be calculated using the restrictions which apply to the problem.

3.4 Formulation of the numerical model

3.4.1 Normalisation of the integration interval

The kernels K_i^N and K_i^S, i=$\hat{x}$ or $\hat{y}$, defined in Equations (3.8-9), are, of the Cauchy type, namely: $K \to \infty$ as $\hat{x} \to c$. The first step for the numerical solution of the system of Equations 3.15-16 is the normalisation of the interval of integration which is achieved by setting:

$$\begin{aligned} \frac{\hat{x}}{L} &= \frac{a}{2L}(1+v) \qquad 0 \le \hat{x}, c \le a \\ \frac{c}{L} &= \frac{a}{2L}(u+1) \qquad -1 \le u, v \le 1 \end{aligned} \tag{3.21}$$

so that the Equations 3.15-16 are now functions of u and v instead of $\hat{x}$ and c. The u and v will provide the integration and collocation points for the numerical solution.

Equations (3.15-16) refer to the stresses in the local coordinate system $\hat{x}$-$\hat{y}$ (Figure 3.2). The value of $\hat{x}$ from Equation (3.21) is used to find the stresses in the (normalised) half-plane along the crack. The stresses which are due to the external loading can be determined in the local $\hat{x}$-$\hat{y}$ system by the application of the Mohr circle. This procedure leads to the determination of the stress field at the collocation points along the crack.

3.4.2 Discretization of the integration interval

Following the procedure given in the classical work of Muskhelishvily (1954), we write the solution for $B_{x,y}(u)$ in Equations (3.11-12) as a product of a bounded function $\phi(u)$ and a fundamental function:

$$B_i(u) = \phi_i(u)\ (1+u)^{1/2}\ (1-u)^{-1/2} \qquad i=x,y \qquad (3.22)$$

The choice of this fundamental function depends on the shape of the crack and the expected positions of singularities. In our case we expect a singularity in the crack induced stress $\sigma_{\hat{y}\hat{y}}$ near the crack tip (u=1) and a finite value at the crack mouth at $\hat{x}\rightarrow 0$ (u=-1). For the case of a buried normal crack, the fundamental function of the second part of Equation (3.22) would be $(1-u^2)^{-1/4}$, due to the expected singularities at both ends of the crack (u=±1). The reader is referred to the mathematical analyses by Erdogan and Gupta (1972) and Krenk (1975), who investigated all the possible forms of the function $(1+u)^a(1-u)^b$ with a,b=±1/2.

We now consider the Gauss-Jacobi integration formula, which is a particular case of the more general Gauss-Chebychev quadrature: (Abramowitz (1965))

$$\int_{-1}^{1} B(u)K(v,u)du = \int_{-1}^{1} \phi(u)\frac{1+u}{(1-u^2)^{1/2}}K(v,u)du \qquad (3.23)$$

$$= \sum_{i=1}^{n} \frac{2\pi(1+u)}{2n+1}\phi(u)K(v,u)$$

By employing Equation (3.23), we can obtain the discretized numerical form of the integral equation system of Equations (3.15-16)

$$-\sigma_s(v_k) = \lambda \sum_{i=1}^{n} \frac{2\pi(1+u)}{2n+1} [K_x^S(v_k,u_i)\phi_x(u_i)+K_y^S(v_k,u_i)\phi_y(u_i)] \quad (3.24)$$

$$-\sigma_N(v_k) = \lambda \sum_{i=1}^{n} \frac{2\pi(1+u)}{2n+1} [K_x^N(v_k,u_i)\phi_x(u_i)+K_y^N(v_k,u_i)\phi_y(u_i)] \quad (3.25)$$

where the integration and collocation points for a surface crack are given by the following relations:

$$u_i = \cos\left(\frac{2i-1}{2n+1}\pi\right); \quad i=1,...,n$$
$$v_k = \cos\left(\frac{2k}{2n+1}\pi\right); \quad k=1,...,n \quad (3.26)$$

Note that these points depend on the fundamental function of Equation (3.22) and are different for other crack configurations. (Krenk (1975a,b))

In the system of Equation (3.24) and (3.25), we have 2n simultaneous equations in the 2n unknowns $\phi_x(u_i)$, $\phi_y(u_i)$, which are the bounded functions representing B_x, B_y. The first part of each of these Equations represents the stresses which are induced by the external loading. The system of equations can easily be solved, using one of the standard library subroutines, such as in the NAG library (NAG Code F04ATF for the solution of a linear system). The solutions for $\phi_x(u_i)$, $\phi_y(u_i)$ in the case when the crack is inclined to the surface are coupled.

3.4.3 Determination of the SIFs

By solving the 2nx2n system of Equations (3.24-25) we can obtain the n values of the function ϕ_y and the n values of the function ϕ_x at certain points u_i (Equation 3.26) between -1 and 1. Interpolation is next required to find $\phi(1)$ for each set of the $\phi_j(u_i)$, j=x,y. From Krenk (1975) we take:

$$\phi_j(1) = \frac{2}{(2n+1)} \sum_{i=1}^{n} \cot\left[\frac{2i-1}{2n+1}\frac{\pi}{2}\right] \sin\left[\frac{n}{2n+1}(2i-1)\pi\right] \phi_j(u_i) \tag{3.27}$$

where j=x or y.

Since these values of ϕ have been found by interpolation, we can transform them into the local coordinates set, as they behave like vectors (Li Yinghzi and Hills (1990)). This can be accomplished by employing the orthogonal transformation formulas for rotation of axes through an angle θ:

$$\begin{aligned} \phi_{\hat{x}}(1) &= \phi_x(1)\cos\theta - \phi_y(1)\sin\theta \\ \phi_{\hat{y}}(1) &= \phi_x(1)\sin\theta + \phi_y(1)\cos\theta \end{aligned} \tag{3.28}$$

We can now proceed to the SIF determination. From the definition of dislocation densities and the nature of the stress field at the crack tip, we have the following equation in local coordinates: (Li Yingzhi and Hills (1990))

$$B_{\hat{y}} = \frac{1+\kappa}{2G}\sigma_{\hat{y}\hat{y}}(\hat{y}=0) \tag{3.29}$$

$$B_{\hat{x}} = \frac{1+\kappa}{2G}\sigma_{\hat{x}\hat{y}}(\hat{y}=0) \tag{3.30}$$

The SIFs are then given by the relations:

$$K_I = \lim_{\hat{x}\to a} \sqrt{\pi(a-\hat{x})}\ \sigma_{\hat{y}\hat{y}}(\hat{y}=0) \tag{3.31}$$

$$K_{II} = \lim_{\hat{x}\to a} \sqrt{\pi(a-\hat{x})}\ \sigma_{\hat{x}\hat{y}}(\hat{y}=0) \tag{3.32}$$

By using Equations (3.22), and (3.29-32) and noting that at the crack tip when $\hat{x} \rightarrow a$ then $u \rightarrow 1$, we have:

$$K_I = \lim_{u \rightarrow 1} \sqrt{\pi a(1-u)} \; \frac{2G}{1+\kappa} B_{\hat{y}}(u)$$

$$= \lim_{u \rightarrow 1} \sqrt{\pi a(1-u)} \; \frac{2G}{1+\kappa} \phi_{\hat{y}}(1) \; \frac{(1+u)^{1/2}}{(1-u)^{1/2}} \qquad (3.33)$$

$$= \sqrt{2} \; \sqrt{\pi a} \; \frac{2G}{1+\kappa} \phi_{\hat{y}}(1)$$

and in an analogous manner:

$$K_{II} = \sqrt{2} \; \sqrt{\pi a} \; \frac{2G}{1+\kappa} \phi_{\hat{x}}(1) \qquad (3.34)$$

Thus, it has been shown that the mode I and II SIFs are proportional to $\phi_{\hat{y}}(1)$ $\phi_{\hat{x}}^{(1)}$ respectively, namely, at the values of ϕ at the crack tip with coordinates u=1. This is in agreement with the analysis by Gupta and Erdogan (1973). The values of $\phi_{\hat{j}}(1)$, $\hat{j}=\hat{x},\hat{y}$ from Equation (3.28) can be substituted into Equations (3.33) and (3.34) to yield the SIFs. Solving in this way, i.e. working mainly in a global coordinate set x-y and then employing Equation (3.28) for the rotation of axes, shows a considerable saving in computation.

3.5 The general case of a cracked half-space pressed by a stamp

3.5.1 Formulation

The analysis has so far treated the crack and contact problems separately by superimposing their contributions to the stress field. It was mentioned in Section 3.3 that the influence of the tractions and of the different materials of the two bodies in contact can be investigated by considering the coupled crack-contact problem. If we

assume that the distribution of tractions is unknown, and in order to formulate the numerical model, we should again suppose that the normal traction p(s) is a product of a bounded function m(s) and a fundamental function: (in an analogous manner as in Equation (3.22)).

$$p(s) = m(s)\ (1+s)^a\ (1-s)^b \tag{3.35}$$

This value of p(s) can be substituted in the Equations (2.6-8), which give the stresses in the half-space: σ_y, σ_x and τ_{yx} are now functions of p(s) and of the coefficient of friction μ (when $q(s)=\mu\ p(s)$. The kernels of the stresses σ^S and σ^N, along and across the crack, can be found by the application of the Mohr's circle to transform Equations (2.6-8) into the $\hat{x}$-$\hat{y}$ coordinate system. The procedure followed for the implementation of this approach is similar to that which has been expounded earlier. The only difference is that there is the additional unknown p(s) and the system is now described by three Equations (3.15), (3.16) and (3.19), instead of only the two Equations (3.15) and (3.16) of the uncoupled case.

3.5.2 Numerical treatment

Equation (3.19) needs a special manipulation in order to be numerically solved. It is of the general form: (Erdogan (1978):

$$A\phi(x) + \frac{B}{\pi}\int_{-1}^{1}\phi(t)\frac{dt}{t-x} = g(x) \tag{3.36}$$

where

$$\phi(x) = f(x)(1-x)^a(1+x)^b, \qquad -1\le x\le 1 \tag{3.37}$$

In Equation (3.36) the A and B are real constants which represent the

influence of the material, taken from Equation (3.20)) and the exponents α and b of Equation (3.37) are given in terms of A and B as:

$$\cot\pi b = \frac{A}{B}, \qquad \cot\pi a = -\frac{A}{B} \tag{3.38}$$

The index of the singular integral equation (SIE) is defined as: $k=-(\alpha+b)$. For similar materials $\alpha,b=\pm 1/2$, but not for this case where the materials are dissimilar. In order to get integrable singularities, k must be restricted to -1,0,1. The k=1 case represents the present model, that is the indentation of the strip by a sharp-edged stamp (Yahsi and Demir (1990)). The reader is referred to Krenk (1975a,b), who studied the cases k=-1 and k=0, which of course represent different configurations. We can proceed now to the solution of the system of the integral equations in the case when k=1 ($\alpha<0$, $b<0$) by making use of the standard Gauss-Jacobi integration formula. The numerical form of Equation (3.36) consists of the following system of n Equations (Abramowitz and Stegun (1965)):

$$\left\| \begin{array}{l} \sum_{i=1}^{n} W_i^n m(t_i)\left[\frac{B}{t_i - x_k}\right] = g(x_k), \qquad k=1...n-1 \\ \\ \sum_{i=1}^{n} W_i^n m(t_i) = \frac{1}{\pi} \end{array} \right. \tag{3.39}$$

where t_i and x_k are the zeroes and W_i^n the weights of the Jacobi polynomials, which provide the two additional sets of integration and collocation points. Once $m(t_k)$ are found, numerical interpolation is required to find their values at the points ± 1, namely just under the edges of the pads.

3.5.3 The numerical system

In this case, we have the following system of 3n equations in 3n unknowns:

$$\sum_{i=1}^{n}[(\lambda\frac{2\pi(1+u)}{2n+1}\ (K_x^{N}(v_k,u_i)\phi_x(u_i)+K_y^{N}(v_k,u_i)\phi_y(u_i)))+(W_i\ S^{N}(v_k,t_i)m(t_i))]=0$$

$$\sum_{i=1}^{n}[(\lambda\frac{2\pi(1+u)}{2n+1}\ (K_x^{S}(v_k,u_i)\phi_x(u_i)+K_y^{S}(v_k,u_i)\phi_y(u_i)))+(W_i\ S^{S}(v_k,t_i)m(t_i))]=0$$

$$\sum_{i=1}^{n}[(\lambda\frac{2\pi(1+u)}{2n+1}(K_x^{surf}\ (x_k,u_i)\phi_x(u_i)+K_y^{surf}\ (x_k,u_i)\phi_y(u_i)))+(W_i[\frac{\beta}{t_i-x_k}]m(t_i))]=0$$

$$\sum_{i=1}^{n}W_i\ m(t_i)=\frac{1}{\pi} \qquad (3.40\text{-}43)$$

where u_i, v_i , i=1...n are the integration and collocation points along the crack (Equation 3.21), and t_i, (i=1...n) and x_k, k=1...n-1 are the Jacobi zeroes (integration and collocation points) referring to the part of the surface pressed by the pad. The kernels S^S, S^N correspond to the kernels of the stress field Equations (2.6-8), after their transformation into the $\hat{x}$-$\hat{y}$ coordinates system and their normalisation. The first two sets of the above Equations (2n equations with 3n unknowns each) correspond to the system of Equations (3.24-25) with the additional unknowns $m(t_i)$, due to the unknown pressure distribution. The remaining two sets of the above Equations (3.42-43) (n-1 and 1 in number respectively, with 3n unknowns each), correspond to Equation (3.19) which effectively acts to introduce the influence of the different materials into the system.

Although the above analysis looks rather cumbersome, the numerical solution can be easily carried out. After the formulation of the problem, there is no need for the calculation of the zeroes and weights of the Jacobi polynomials, since there are powerful formulas which can be found in many special books on quadratic integration (for example Stroud and Secrest (1967)). All the zeroes and weights of the Jacobi polynomials were calculated by a handy program taken from the above mentioned book. The only inputs to the program were the constants A and B which describe the influence of the material and the coefficient of friction according to Equation (3.38). For the present program it was supposed that the specimen material was aluminium alloy and the pad was of steel with Poisson's ratio 0.33 and 0.25 respectively.

3.6 Check of convergency and accuracy

3.6.1 Comparison with known data

a) Edge crack in axially loaded half-plane

The method used was initially validated against known results obtained from the literature, using various numbers of iterations (n) for the numerical solution of the system of Equations (3.24-25). The well known results for an edge crack in a stressed half space were first calculated. For $\theta=0°$ (normal crack) the percentage discrepancy from the generally accepted value of $K_I/(\sigma\sqrt{\pi a})=1.1215$ (Nowell and Hills (1987)) in terms of n, is shown in Table 3.1 (σ is the tensile stress)

Iterations number n	% error
5	2.12
10	0.32
20	0.09
30	0.05
40	0.03

Table 3.1 Numerical percentage error for normal crack ($\theta=0°$)

For angles $\theta\geq 0°$ (Figure 3.2), convergence occurred with n set to 30. The normalised SIFs are presented in Figure 3.3. The results are also compared with those published by Murakami (1985) for two values of numbers of iterations n (10 and 30) and the resulting errors are shown in Table 3.2

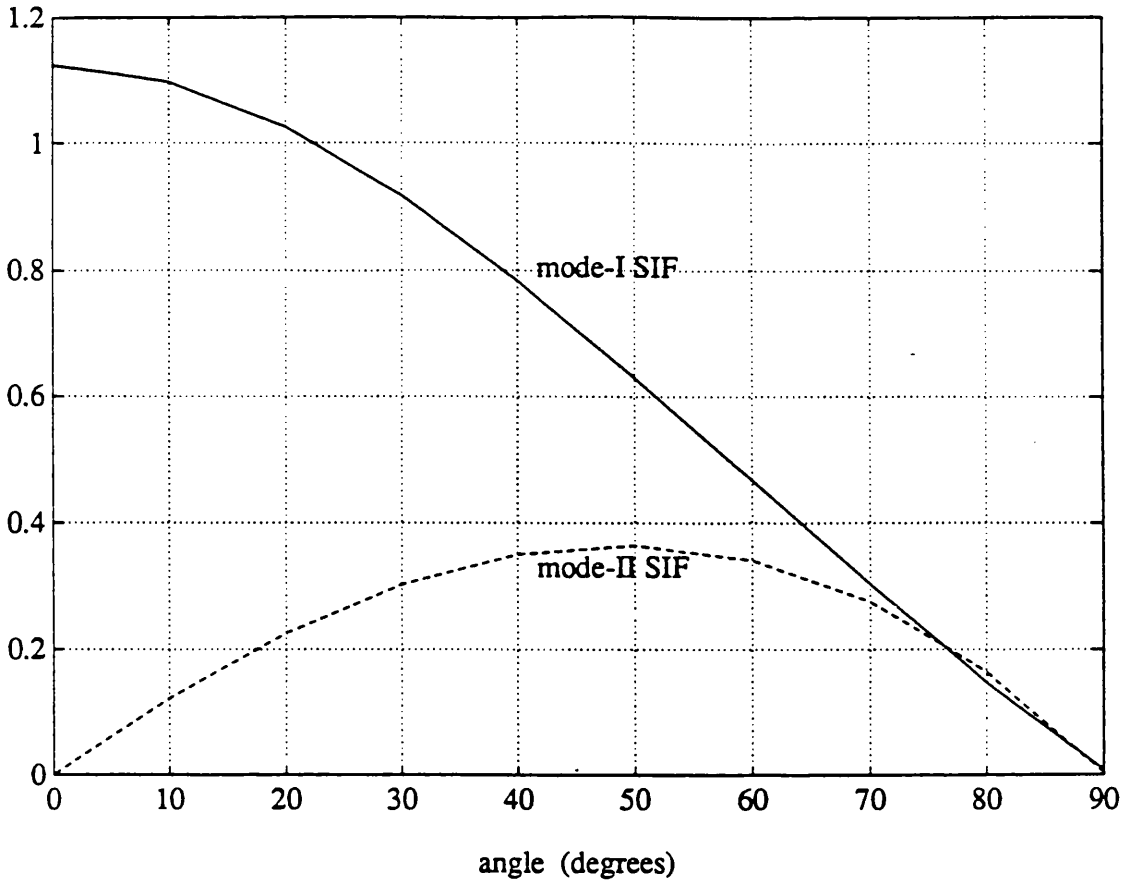

Figure 3.3 Normalised ($K/(\sigma(\pi a)^{1/2})$) SIFs for an angled crack.

From the data shown in Table 3.2, it seems that there is a fluctuating discrepancy in the values in the case of inclined cracks. This is due to the selection of the fundamental function (3.22). This function exhibits eigenvalue singularities of order -1/2 at the crack tip and +1/2 at the crack mouth, respectively. However this may not be exactly the case at the mouth and the stress singularities in there depend on the angle of the corner. Williams (1952) suggests that the analysis for the free-free case (Figure 3.4) be applied to determine the stress variations at the base of V-shaped notches, according to the angle of the vertex.

θ	Y_I	Y_{II}	% difference in Y_I for n=10	% difference in Y_{II} for n=10	% difference in Y_I for n=30	% difference in Y_{II} for n=30
0°	1.1215	0.0	-0.32	0.0	-0.05	0.0
10°	1.0978	0.1186	-0.35	-0.19	-0.06	-0.06
20°	1.0286	0.2243	-0.43	-0.18	-0.07	-0.04
30°	0.9201	0.3058	-1.00	-0.23	-0.14	+0.09
40°	0.7818	0.3543	+0.82	-0.70	+0.07	-0.04
50°	0.6251	0.3648	+0.10	+0.41	+0.11	-0.03
60°	0.4630	0.3360	+4.10	-0.40	+2.40	-0.29
70°	0.3050	0.2710	+1.11	-3.00	-0.08	+0.03

Table 3.2 **Normalised SIFs $Y_i=K_i/(\sigma\sqrt{\pi a})$ i=I,II from Murakami (1985) and comparison of their values with the corresponding values found by the numerical method employed in this work for various numbers of iterations n.**

From the Figure 3.4 we can deduce that the order of the stress eigenvalue at the crack mouth is not actually +1/2 for normal cracks (α=90° in this figure) and this also applies for other vertex angles. When the exponents of Equation (3.22) are not of order ±1/2, then the determination of the roots of the Jacobi polynomials is required, as was shown in Section 3.5.

We decided to proceed with a fundamental function given by Equation (3.22),

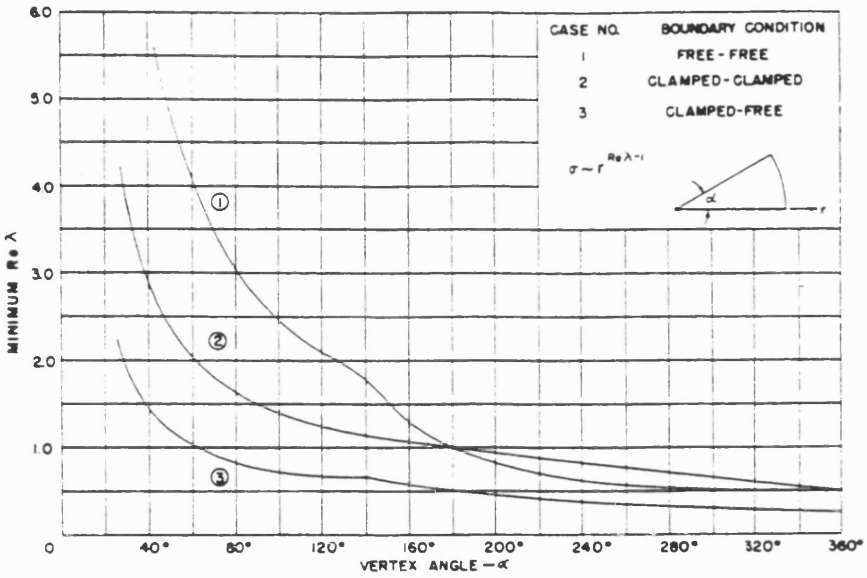

VARIATION OF MINIMUM REAL PART OF EIGEN VALUE WITH VERTEX ANGLE

Figure 3.4 Stress eigenvalues resulting from various boundary conditions (from Williams (1952))

because what we really wanted was a fast and versatile method for determining SIFs and the accuracy was excellent for normal cracks and good for most angled cracks. The main advantage of this method was the handling of any desired loading by simply providing the appropriate discretized system of integral equations (3.24) and (3.25) with a new set of left hand sides, namely new values for the stresses σ_i, i=S,N due to the external loading.

b) Edge crack in a normally and tangentially loaded half-plane

The method was then employed to give data for comparisons with the results calculated by the formulae given by Rooke and Jones (1979), who assumed uniform distribution of tractions. Because their results refer to point load, these were integrated for a distributed uniform load that presses onto the surface of a specimen identical

to that of Figure 2.7 for a pressure of 31MPa. The load is distributed over the entire contact area which is divided into a number of individual elements (n) each of width T/n, where T is the total pad width 2L (Figure 2.8). The SIFs due to each individual force K_{tn} and K_{nn} are summed to yield a total SIF due to frictional (tangential) forces (K_t) and normal pressure (K_n):

$$K_t = \sum_{n}^{1} K_{tn}(y) \tag{3.44}$$

$$K_n = \sum_{n}^{1} K_{nn}(y) \tag{3.45}$$

The integration was performed with 60 integration points, implementing a computer library routine (NAG D01AJF). The adopted number of integration points is adequate, provided the crack depth is not less than the individual element width (=T/n). The results are compared with those derived by the continuous dislocation method for crack depths 0.2-1mm and they are shown in Figures 3.5. The number of iterations for the continuous dislocations method was set to n=20, and the error should be less than 0.1% (Table 3.1).

For the determination of the SIFs, which were due only to the normal traction a value of coefficient of friction μ=0 was used. Again there was very good agreement between the results obtained by these two methods (about 1%), and the convergence became better with increasing crack length. As this was a comparison between two entirely different approaches, it further increased our confidence that the analysis was correct.

It was decided to use n=30 in all calculations reported throughout the rest of this work. Some results, especially for large angles (θ=50°) would have been more accurate had we used n>30, but as good convergence occurred with fewer iterations, it was felt that the method would lose its simplicity and consequent advantages over other much more time-consuming methods (e.g. the Finite Element Method).

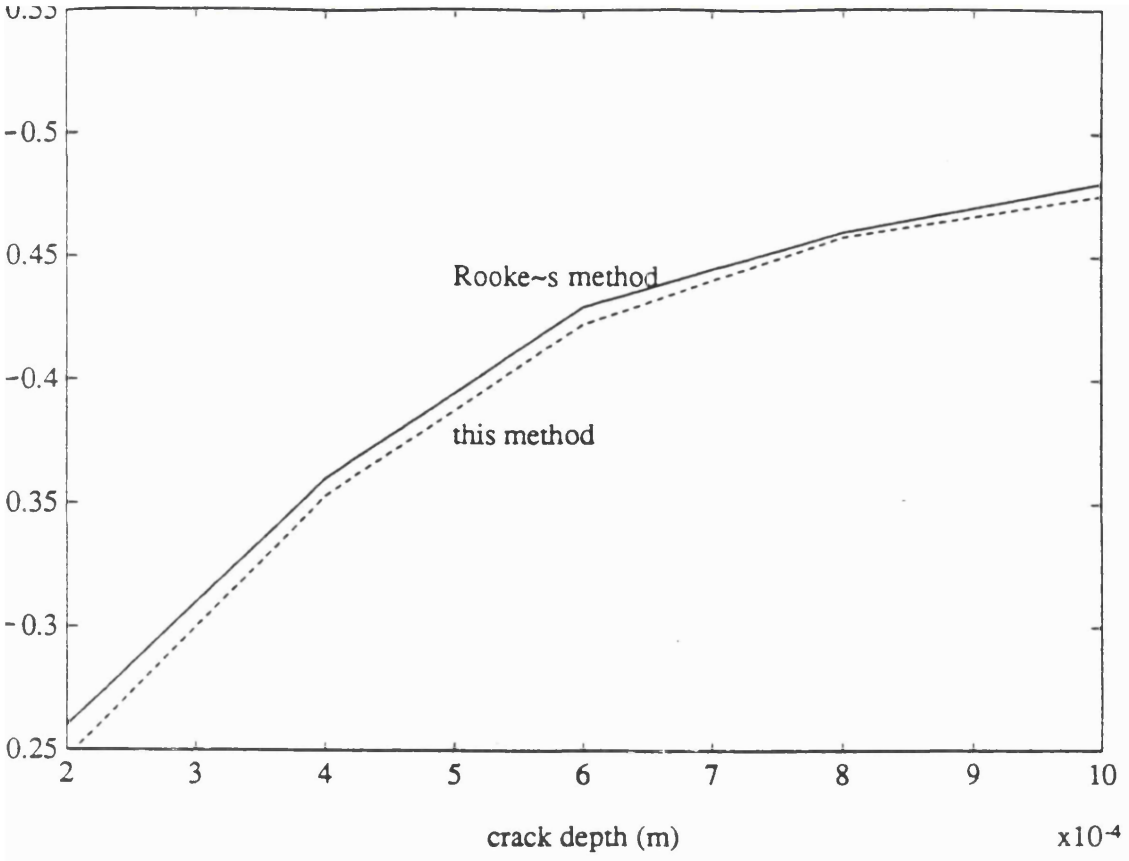

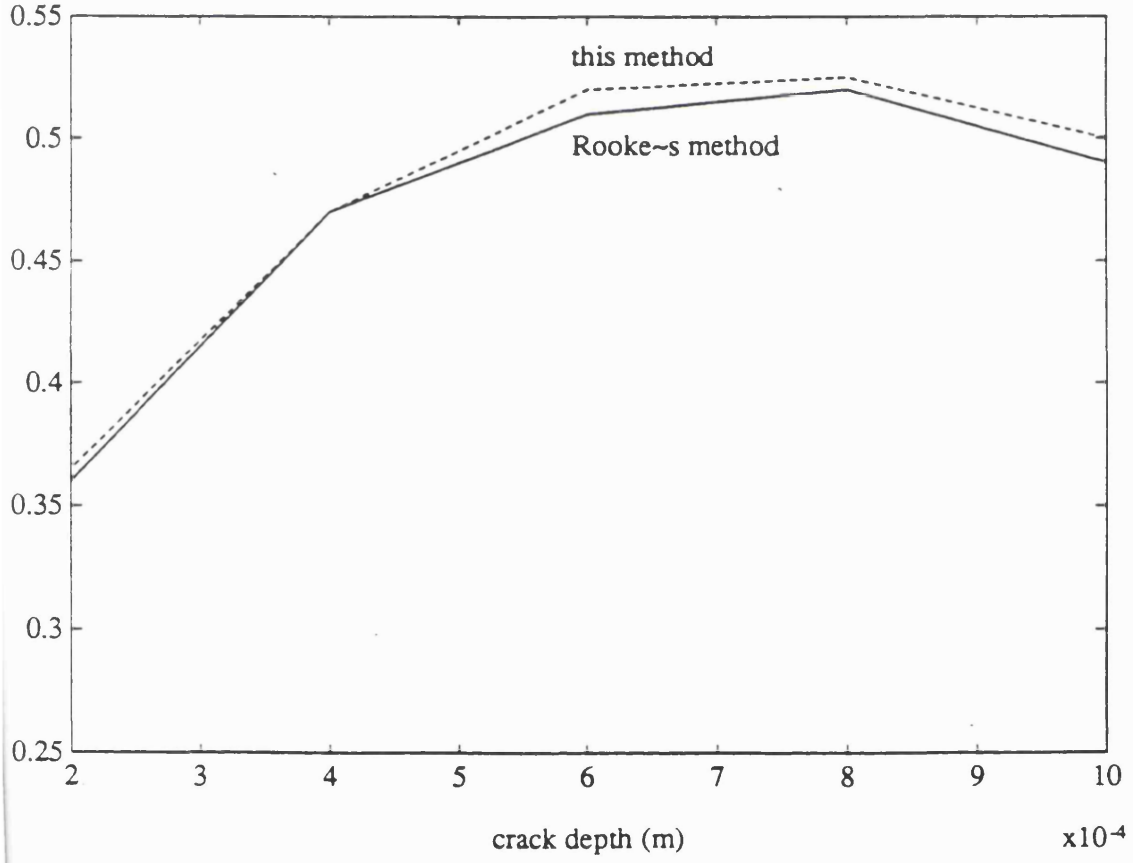

Figure 3.5 Agreement between the method by Rooke and Jones (1977,1979) and the method employed in this work. The SIFs refer to the dimensions of the specimen of Figure 2.7 for a normal pressure of 31MPa.

For the model results to be valid, the faces of the crack should always be open and not pressed together, so that they don't suffer Coulomb friction. The case of partially closed cracks has been studied by Hills and Nowell (1989) and Hills and Comninou (1985), but it is outside the scope of this work. Of course, the check on the validity of the LEFM and on the plane strain conditions of the problem must be always taken into regard (Section 2.5-6).

3.6.2 Suitability of the method

The continuous dislocation method employed in this work has been well established in the literature the recent years and it features some advantages over the Finite Element Method (FEM), when it is used for the determination of the SIFs. One can consider the continuous dislocation method as a special case of the BIM (Boundary Integral Method), where the base function used in the BIM has been substituted by the displacement function of Equation (3.1). The most obvious of the advantages over the FEM are:

1. There is no need for the time consuming meshing of the model. This is especially beneficial in the case when various angles of crack propagation are to be examined. Some researchers used finite element analysis for the stress study of specimens in contact, but they did not introduce a crack into their mesh (Hattori *et al* (1988). Their models would need re-meshing for the examination of different angles and lengths and this demands additional laborious operations. As the FEM mesh must be dense enough for stress analysis, the introduction of a crack for every angle considered, would make the numerical effort prohibiting.

2. The resulting matrices are small and we could use even a personal computer for the numerical calculation. The analysis is rapid and convergence is easily obtained in most cases. The SIFs are easily extracted and the whole procedure is

straightforward. Indeed, for n integration points along the crack, the size of the matrix to be inverted was:

Single crack normal to the surface:	n x n
Angled crack (superposition method):	2n x 2n
Angled crack (coupled problem by considering the influence of the material	3n x 3n

3. The quadrature used is easy to adapt for the $1/\sqrt{r}$ discontinuity, which occurs at the crack tip and so the method is particularly suited for cracks where, unlike the FEM, there is no need for any special crack tip elements.

Of course there are some cases where the method used in this study cannot be applied satisfactorily. One special shortcoming of the method was in the "forcing" of the singularity at the crack mouth to be of order +1/2 (Equation (3.22)) and of B_y to be there not only bounded but also zero. The dislocation density corresponds to dw/dx, where w is the separation of the faces, and therefore forcing $B_y \rightarrow 0$ means that the crack faces remain parallel at the crack mouth, which in reality cannot hold true.

Nevertheless, the results obtained for SIFs are quite satisfactory as they refer to the crack tip (where the order singularity was correctly assumed) away from the crack mouth. Indeed Dewyenne *et al* (1992) showed that the variation of $B_y(x)$ with x from its actual value is significant only in the last 10% of the crack length close to the mouth. Moreover, according to the Table 3.2 the method gives correct results with less than 1% inaccuracy for most angles even with small values of n. However, in terms of the calculation of the crack opening displacement on the surface the use of a modified scheme is recommended *(ibid)*.

It must be also stated that there are some drawbacks to the Gauss-Chebychef method, which is expressed by the Equation (3.23) with collocation and integration

points taken from Equation (3.26), especially in more complicated cases due to the fact that the roots cannot be calculated at the limits ±1, and interpolation is thus needed. One alternative would be the Lobatto-Chebychef method (Theocaris and Ioakimidis (1977)), which gives directly the values $\phi(\pm 1)$ without recoursing to interpolation procedures, or other recurrence formulae (Tsamasfyros and Theocaris (1982)). However, the use of the Gauss-Chebychef integration formula was preferred in this study because it is the one most commonly used for straight cracks. As long as the coefficients α and b of Equation (3.22) are ±1/2, it does give excellent accuracy.

4. RESULTS AND DISCUSSION ON THE FRETTING FATIGUE MODEL

4.1 SIFs for fretting fatigue cracks

4.1.1 SIFs for straight cracks normal to the surface

The main independent variables of the problem are the crack length/pad length ratio a/L, the friction coefficient between the pad and the specimen surface μ and the inclination of the crack θ (Figure 3.2). All the results reported here were derived for ratios $a/L \geq 0.5$, so that the calculations start some distance away from the surface. The numerical method tends to be ineffective closer to the surface, since the number of summations n increases significantly, and, moreover, the application of an elastic stress analysis in this area is uncertain, due to possible yielding of the material. The "short" crack effects (Section 2.6), which are due either to the small physical length of the crack in small scale systems or to high stresses under the pad edges (which imply that the plastic zone penetrates some considerable distance into the bulk of the body), can render the whole phenomenon so complicated in the vicinity of the surface, that the validity of a more detailed LEFM analysis is questionable. When the results obtained are to be interpreted for actual cracks, the length L should be taken as the half-pad foot length, because the integration was carried out between -L and L (or from -1 to 1 in the normalised region). The values of the normalised SIFs in all the following figures should be multiplied by $(\pi a)^{1/2}p$ to yield their actual numerical values. (where p is the normal pressure). The frictional pressure is implied to be: $q=\mu p$ and in the following figures the symbol 'cf' stands for the coefficient of friction μ.

The specimen SIFs for pad pressure of uniform and "rigid punch" distribution and for various friction coefficients, were calculated and are shown in Figure 3.1. Data calculated by taking into account the different elastic properties of the specimen and pad materials are also considered (aluminium alloy and steel; Section 3.5). This elastic model involves more computational effort, but is closer to reality, as it has been already mentioned in Section 3.5. There seems to be a small difference among the corresponding values of the mode-I SIFs due to these three stress distributions, especially close to the surface. This difference tends to become zero at a depth less than the pad foot length.

The main conclusion which can be drawn from the comparison of the three sets of data, is that the simpler uniform distribution can adequately describe the phenomenon at some distance away from the surface. The common assumption in almost all fretting fatigue analyses of the literature of uncoupling the contact and crack problems and superposing their solutions is therefore quite justifiable. Although, the uniform stress model is the most conservative of all in terms of mode-I SIFs, normally no safety problems should be introduced by its application. However, when the specimen dimensions are generally bigger and consequently the crack lengths involved are longer, the difference between the SIFs derived from the real elastic model and the simplified models near to the surface might be of greater importance. Of course, the checks concerning the plastic yield of the material should be again carried out.

From the data depicting the mode-II SIFs, it can be inferred that the difference between the simpler models ("uniform" and "rigid punch") and the real case elastic model (Steel-aluminium alloy) for mode-II SIFs is more profound than in the mode-I case. It seems that the influence of the shear stresses is more significant for the elastic model. The mode-II SIFs are invariably smaller for the elastic steel-aluminium alloy model, namely when the punch is considered somewhat elastic with a specific Poisson's ratio and not absolutely rigid. This implies lower

shear deformation of the body, as it should have been expected for a less stiff pressing pad. Therefore, at least for the early stages, when a possible mode-II extension may be important, the "simpler" models are conservative. Nevertheless, the use of this conclusion for LEFM calculations is again rather qualitative, as there is no satisfactory model for the early crack nucleation stages which connects the growth with SIFs.

The rapid approach to zero of the mode-I SIFs verifies the local nature of the fretting influence. The mode-II SIFs are less influenced by the crack length in terms of their tending to zero with increasing length, especially for higher friction coefficients. This phenomenon is not surprising, if one considers Figures 2.9, which depict the stress distribution in the bulk of the specimen. The contact problem does not favour the crack opening mode to the same extent as it does for the sliding mode, since the stresses perpendicular to the crack faces (σ_y) are considerably lower than those along the crack (σ_x). Moreover, the former diminish with depth faster than the latter, even though the presence of a frictional force parallel to the surface increases both stresses. Therefore, in the absence of friction the contact loading forces the crack faces to slide on each other (hence the high mode-II SIF values) and suppresses their tearing apart, yielding negative mode-I SIF values. Only when a force normal to the crack faces in the form of the frictional force is present, the mode-I SIF starts to increase with increasing friction and eventually becomes positive. Finally, by collective reference to both Figures 4.1, it can be shown that although the increase in friction elevates the SIFs, its influence is local and decreases after some distance from the surface (at about 2 times the pad width).

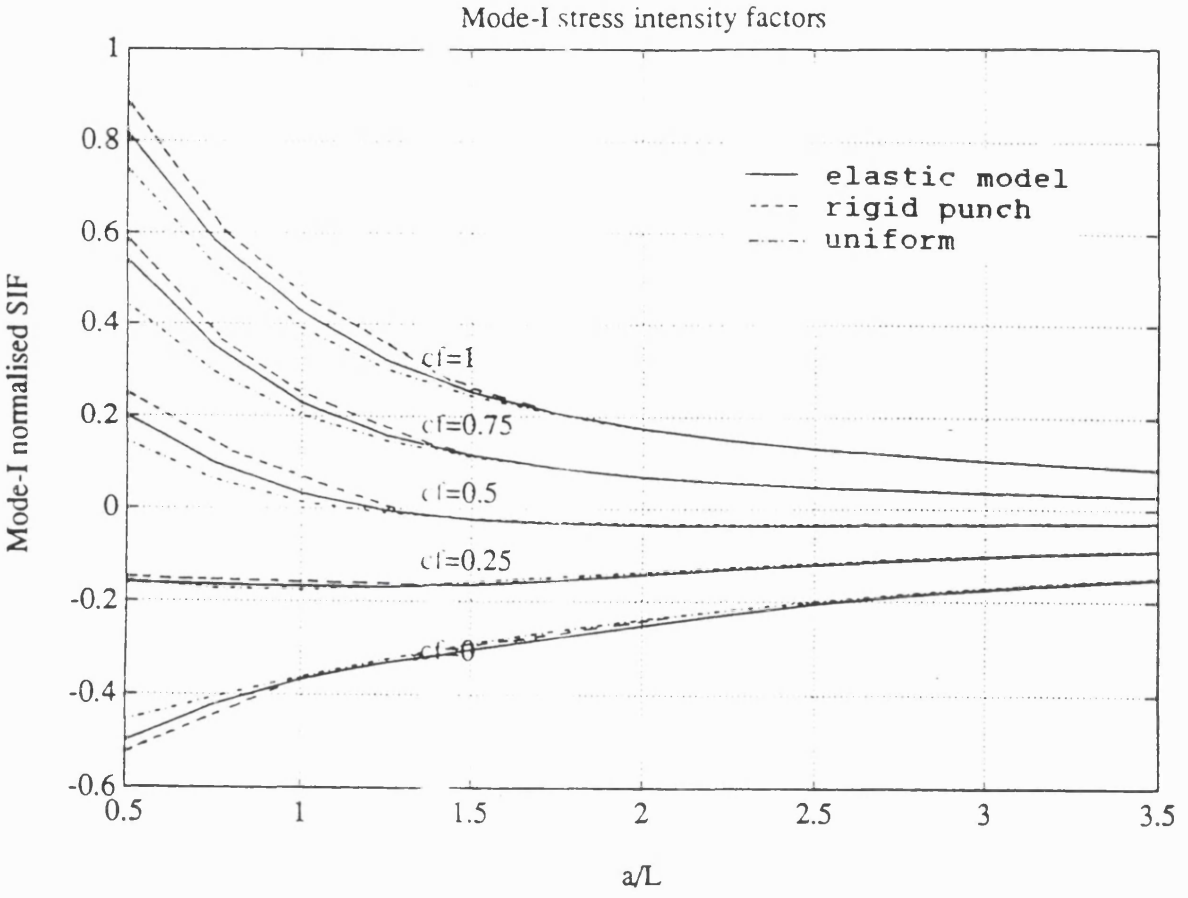

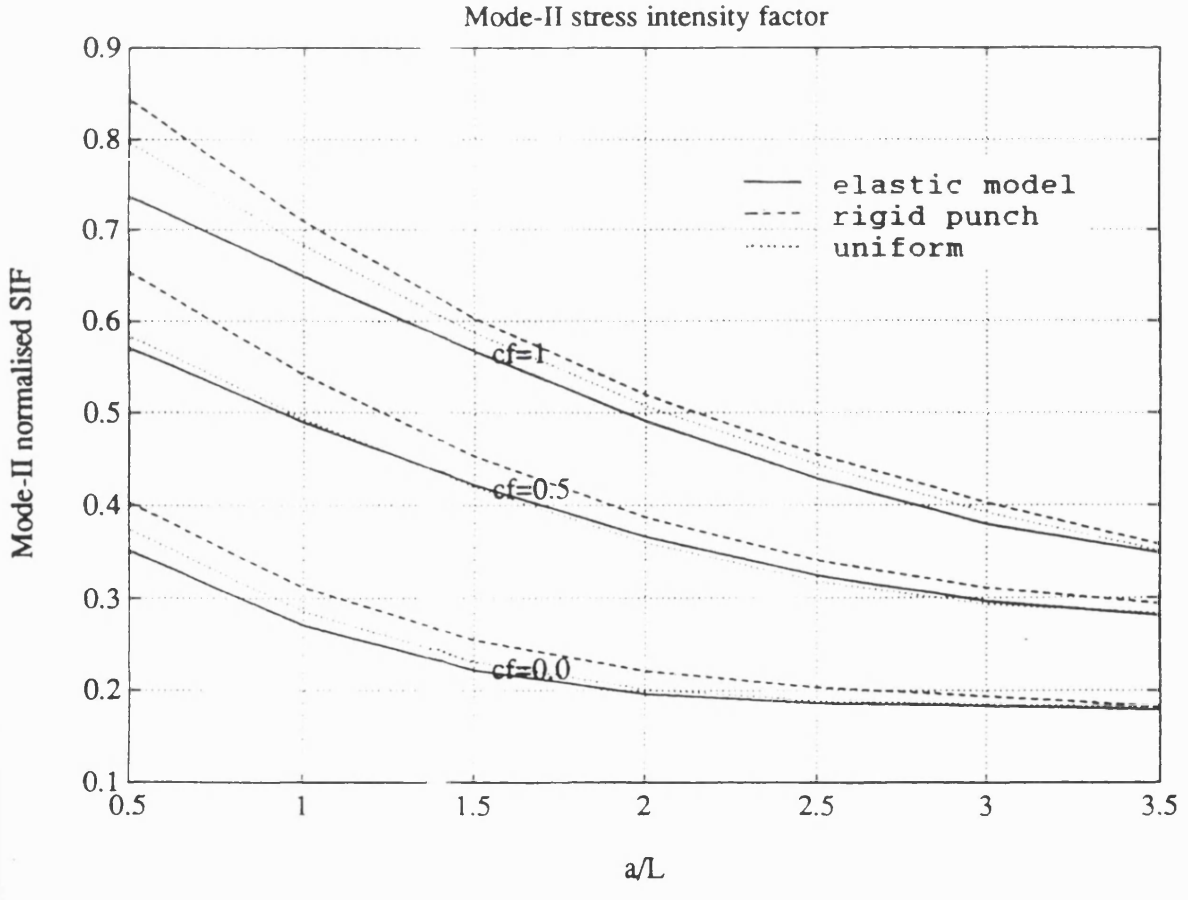

Figure 4.1: Normalised ($K/(p(\pi a)^{1/2})$) SIFs for various pressure distributions in terms of length and coefficient of friction. Normal crack L:pad foot half-length p: normal pressure

4.4.2 SIFs for angled cracks

The dependence of the SIFs on the angle of the crack and the a/L ratio has been calculated and some results are shown in the following Figures 4.2-14. To our knowledge, there are no published results for angled fretting fatigue cracks for the case of sharp ended pads (Figure 2.5). The new results presented here can be useful for the analysis of the general case of fretting fatigue, provided that there is no severe influence of the short crack effects.

Following the conclusions of the previous subsection, the uniform stress distribution was used for the study of the angled cracks. A solution based on the uniform distribution saves computational time and simplifies the formulation of the problem. It was also shown that this solution is scientifically correct for cracks longer than half the pad width, when the difference with the elastic model tends to become zero. It is repeated that, for shallower depths, the cracks may be too small for a successful application of the LEFM theory, depending of course on the scale of the problem. A summary of the cases which were considered is presented in Table 4.1 and the figures are arranged as follows:

Figures 4.2-4.12: SIFs when there is simultaneous action of both tangential and normal forces. The plots refer to various combinations of depths, angles, and coefficients of friction 'cf'.

Figures 4.13 and 4.14: SIFs due to the separate action of either normal or tangential load in terms of the crack angle and the depth. There are useful for fatigue calculations, when one needs to know the separate influence of the normal or the tangential load, so that their action can be superposed.

Although cracks generally grow in mode-I, it cannot be excluded that they will not grow in mode-II under the pads in their very early stages (Section 2.1.2).

However, as the cracks grow and enter the Stage-II of Forsyth's notation (Figure 2.4), a progressive transition to mode-I should take place. The mode-I SIFs are negative under the pads, especially for high angles under the pads, indicating that the cracks suffer crack closure and eventually the influence of mode-I will prevail and crack arrest will happen. Of course, if the simultaneous presence of the bulk tensile stress can sustain on its own the continuous propagation of the crack, the crack will continue to grow as a plain fatigue crack, not being affected any more by any fretting influence. These negative mode-I SIFs can be considered as "relieving" factors for the influence of the bulk fatigue stress, which provides the positive SIFs to force the crack open. The crack closure phenomena in fretting fatigue were also discussed in the experimental studies by Sato *et al* (1986). The authors postulate that one of the main factors for growth retardation in fretting fatigue is this closure due to the oblique cracks, and the theoretical findings of this study seem to justify their hypothesis.

The figures 4.8-12 show an increase in the negative mode-I SIFs with increasing angle, denoting a severer crack closure for a crack situated under the pads. However, for angles close to the normal direction (0°), the mode-I SIFs can become positive, provided that the friction force is high enough, so that it can pull the crack open. In general, higher coefficients of friction elevate the mode-I SIFs. This influence of friction and angle is not so dramatic for mode-II SIFs.

The main conclusion from the above discussion is that cracks at angled orientations will soon enter a zone of tip closure, where further growth is unlikely. The cracks will self-arrest, unless a bulk tensile stress (σ in Figure 2.5) provides the positive SIFs which are necessary for further propagation. Of course, in this case their trajectory changes to become normal to the tensile stress. The crack shape then becomes kinked and the crack continues to propagate perpendicularly to the principal tensile stress, implying that the influence of the fretting loading has almost disappeared. The kinked cracks are discussed in the next Section.

Figure number	Coeff. of friction cf	Angle of the crack
4.2	0.0 (0.3) 0.9	0°
4.3	0.0 (0.3) 0.9	10°
4.4	0.0 (0.3) 0.9	20°
4.5	0.0 (0.3) 0.9	30°
4.6	0.0 (0.3) 0.9	40°
4.7	0.0 (0.3) 0.9	50°
4.8	0.00	0° (15°) 45°
4.9	0.25	0° (15°) 45°
4.10	0.50	0° (15°) 45°
4.11	0.75	0° (15°) 45°
4.12	1.00	0° (15°) 45°
4.13	Normal load only	0° (10°) 50°
4.14	Tangential load only	0° (10°) 50°

Table 4.1 Data used for the calculation of the normalised SIFs in Figures 4.2-4.14. The symbols 'A (B) C' imply: 'From A to C, step B'. The angle of the crack is denoted as θ in Figure 3.2.

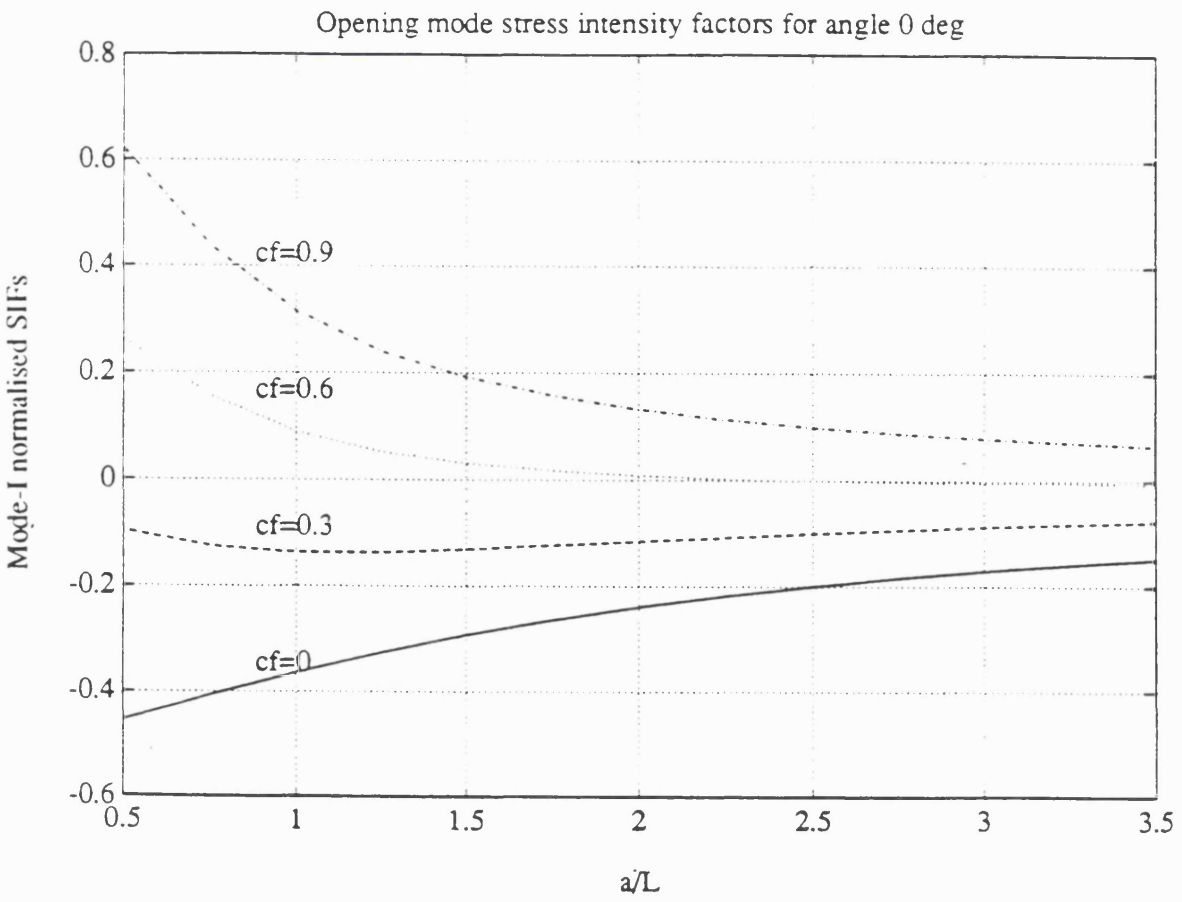

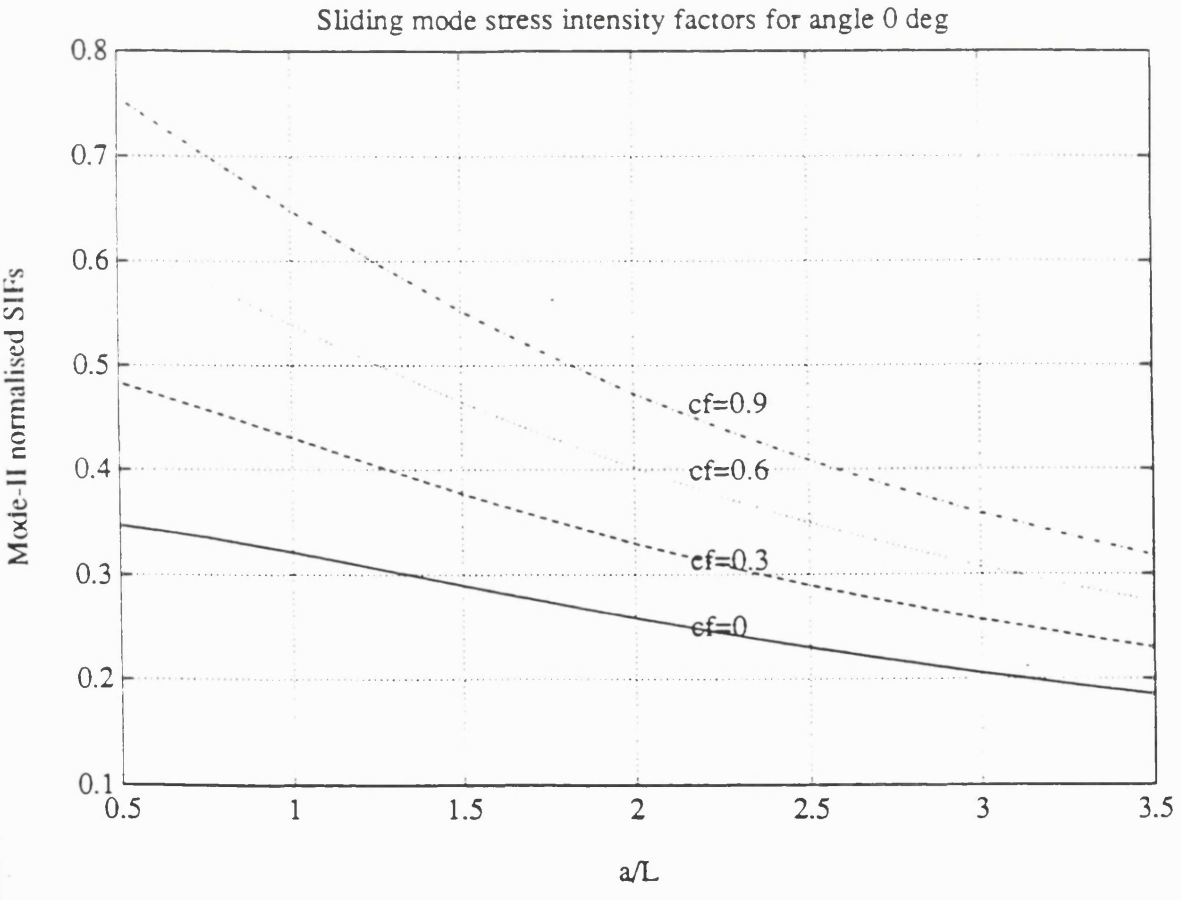

Figure 4.2 Normalised ($K/(p(\pi a)^{1/2})$) SIFs in terms of length and coefficient of friction. Angle=0°. L: pad foot half-length. p: normal pressure

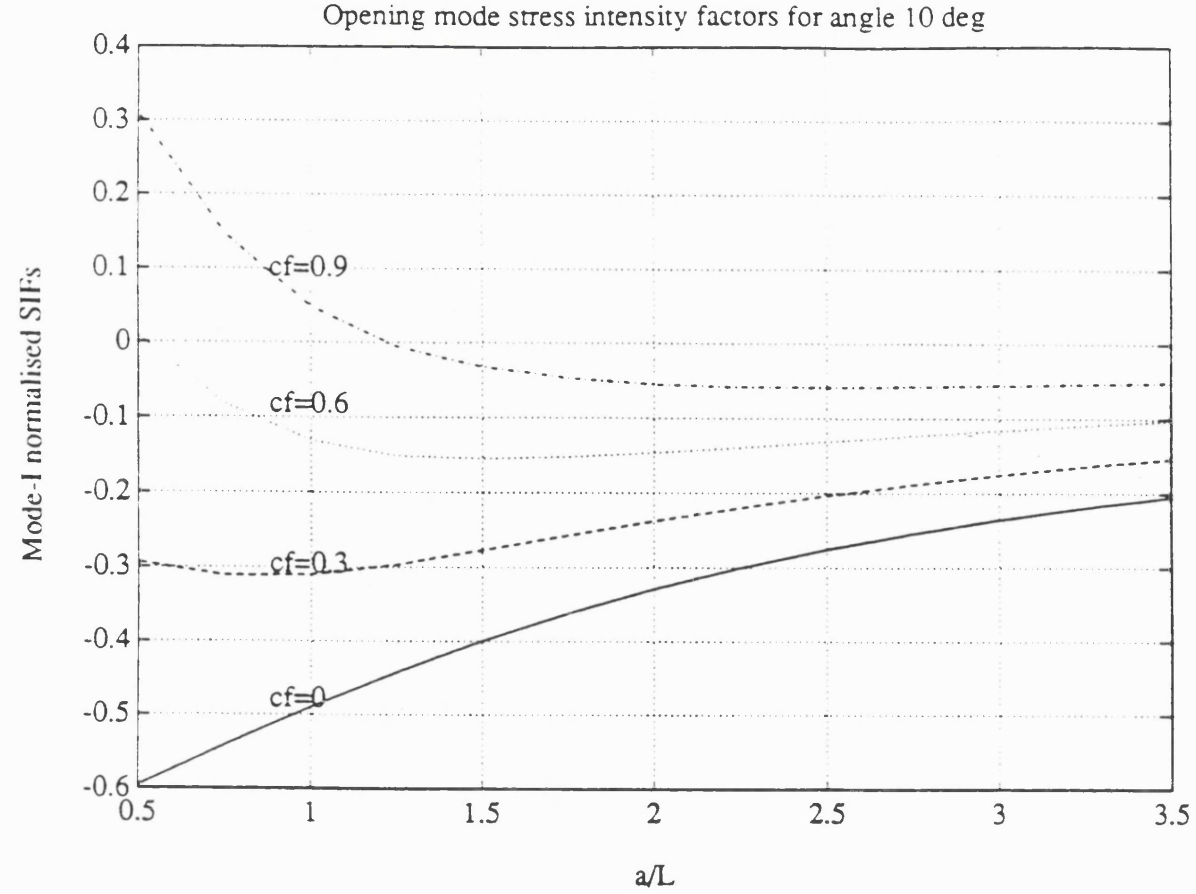

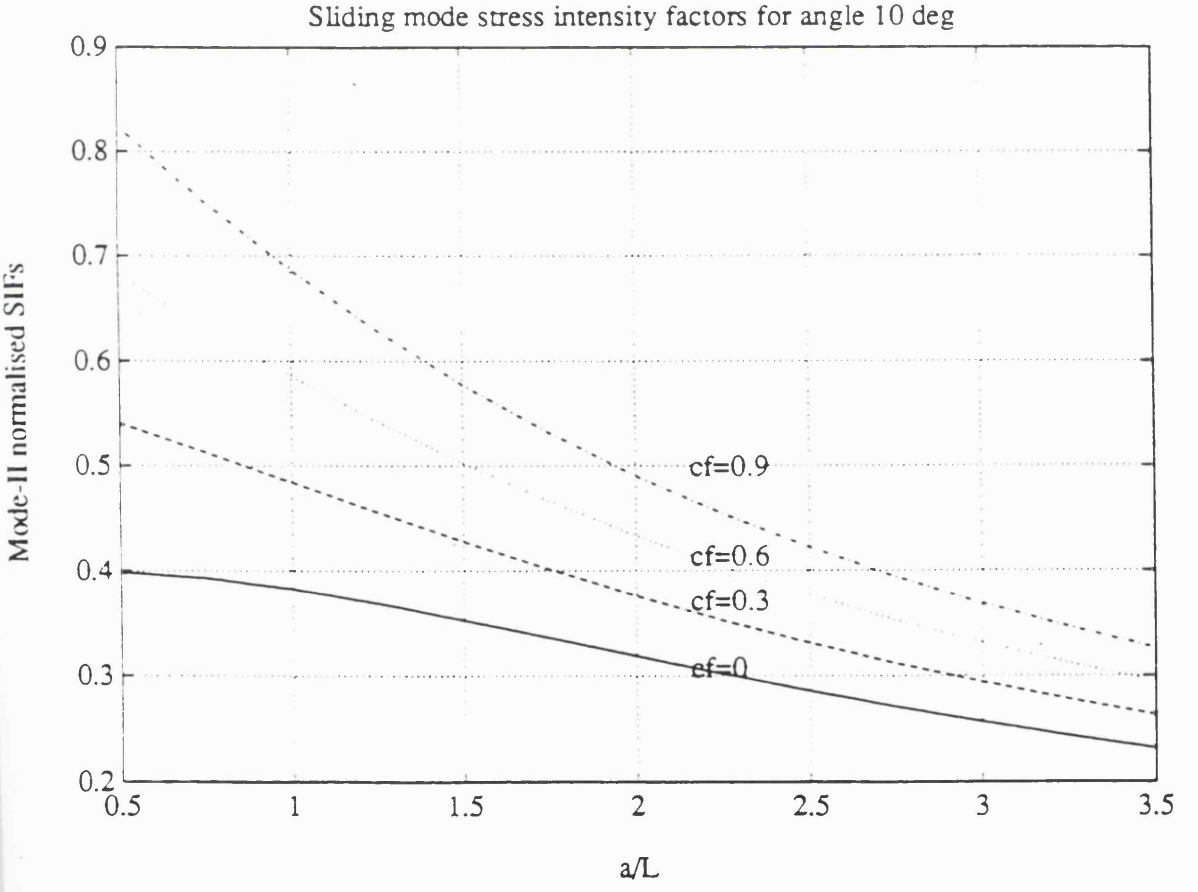

Figure 4.3 Normalised ($K/(p(\pi a)^{1/2})$) SIFs in terms of length and coefficient of friction. Angle=10°. L is the pad foot half-length. p is the normal pressure

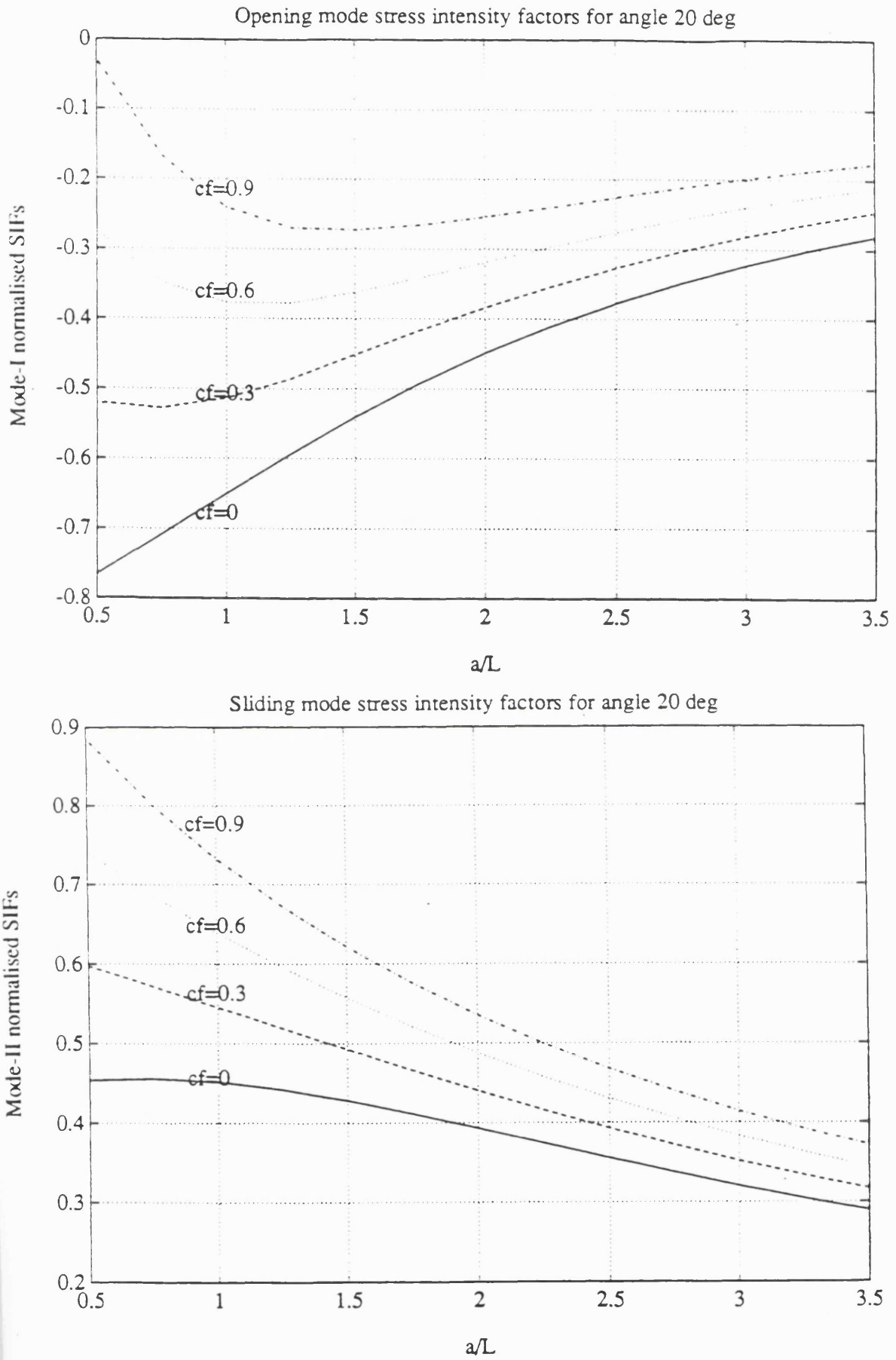

Figure 4.4 Normalised ($K/(p(\pi a)^{1/2})$) SIFs in terms of length and coefficient of friction. Angle=20°. L is the pad foot half-length. p is the normal pressure

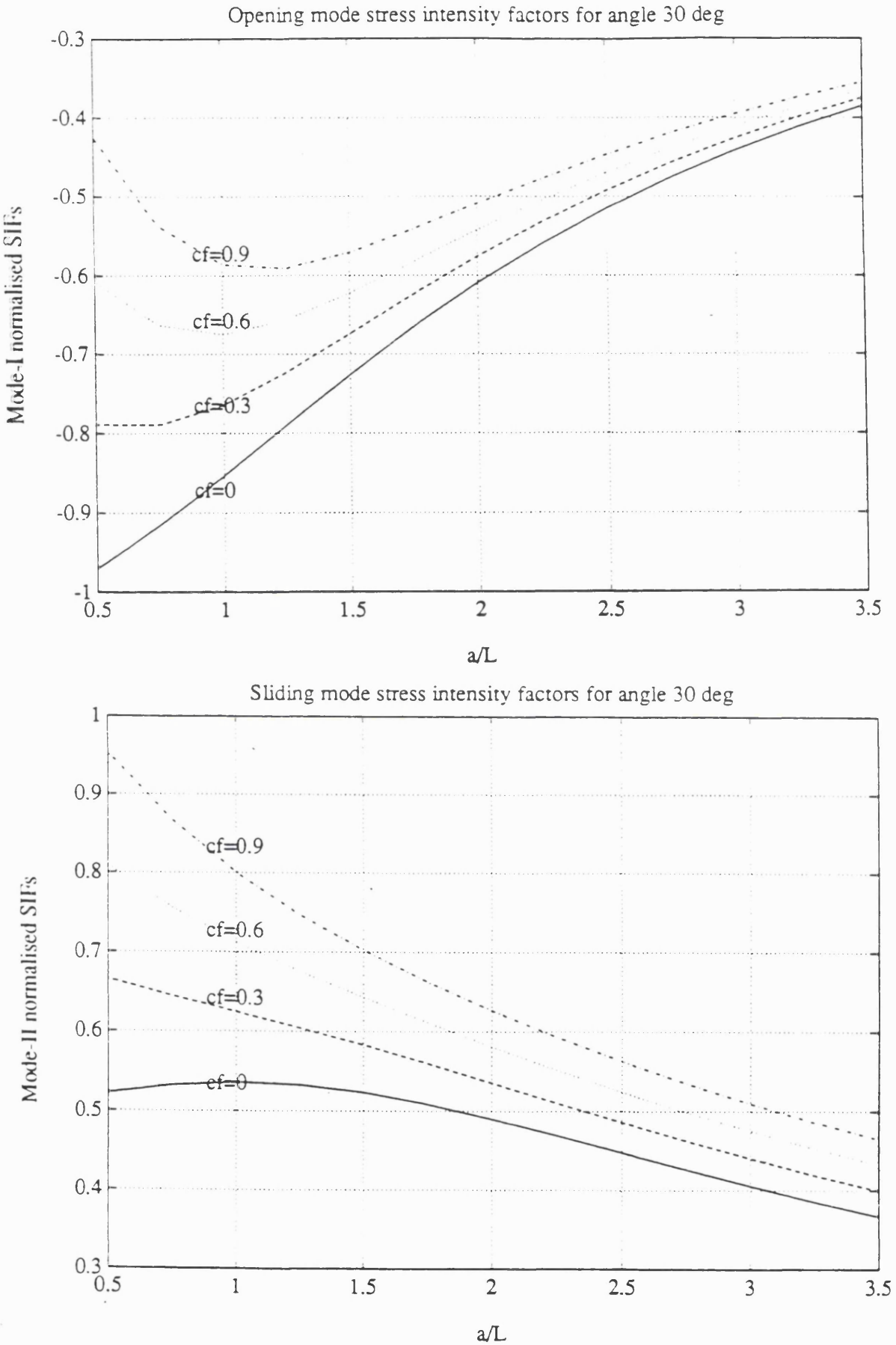

Figure 4.5 Normalised ($K/(p(\pi a)^{1/2})$) SIFs in terms of length and coefficient of friction. Angle=30°. L is the pad foot half-length. p is the normal pressure

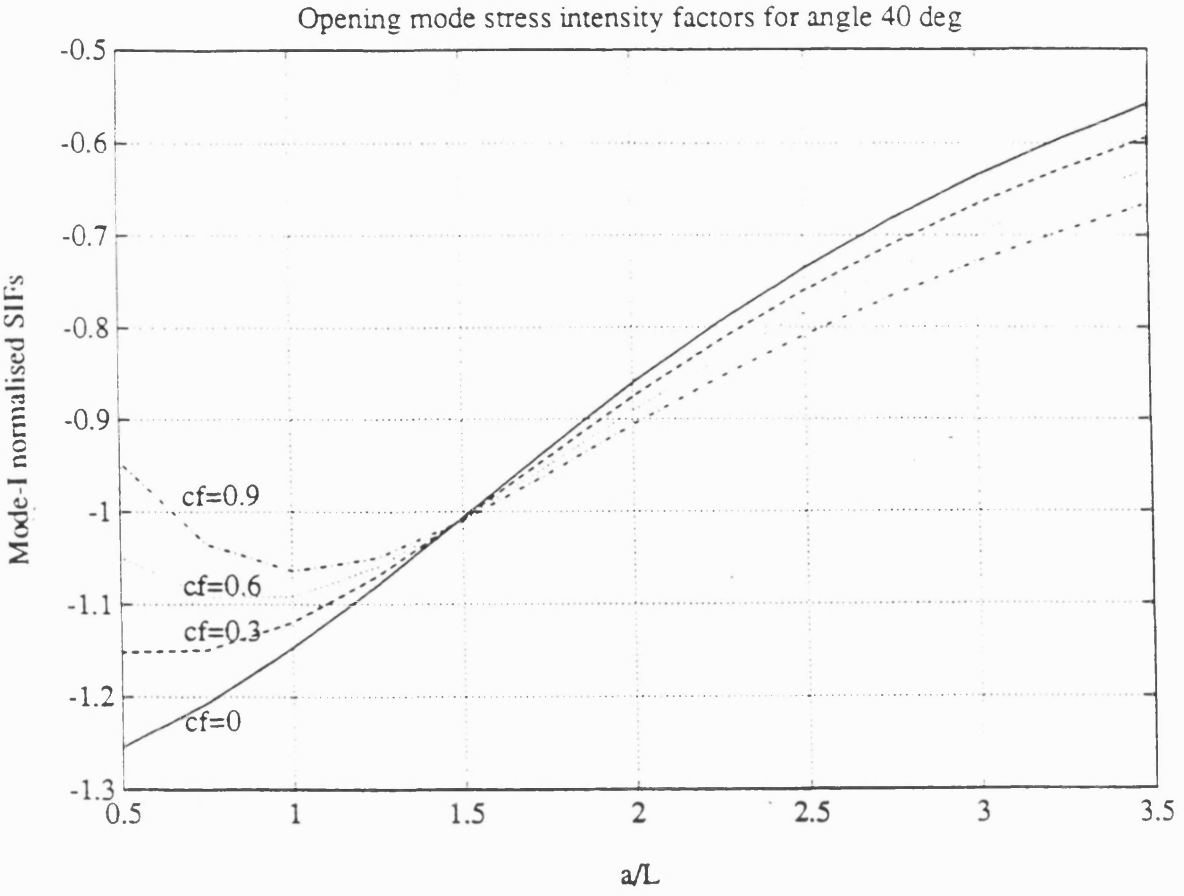

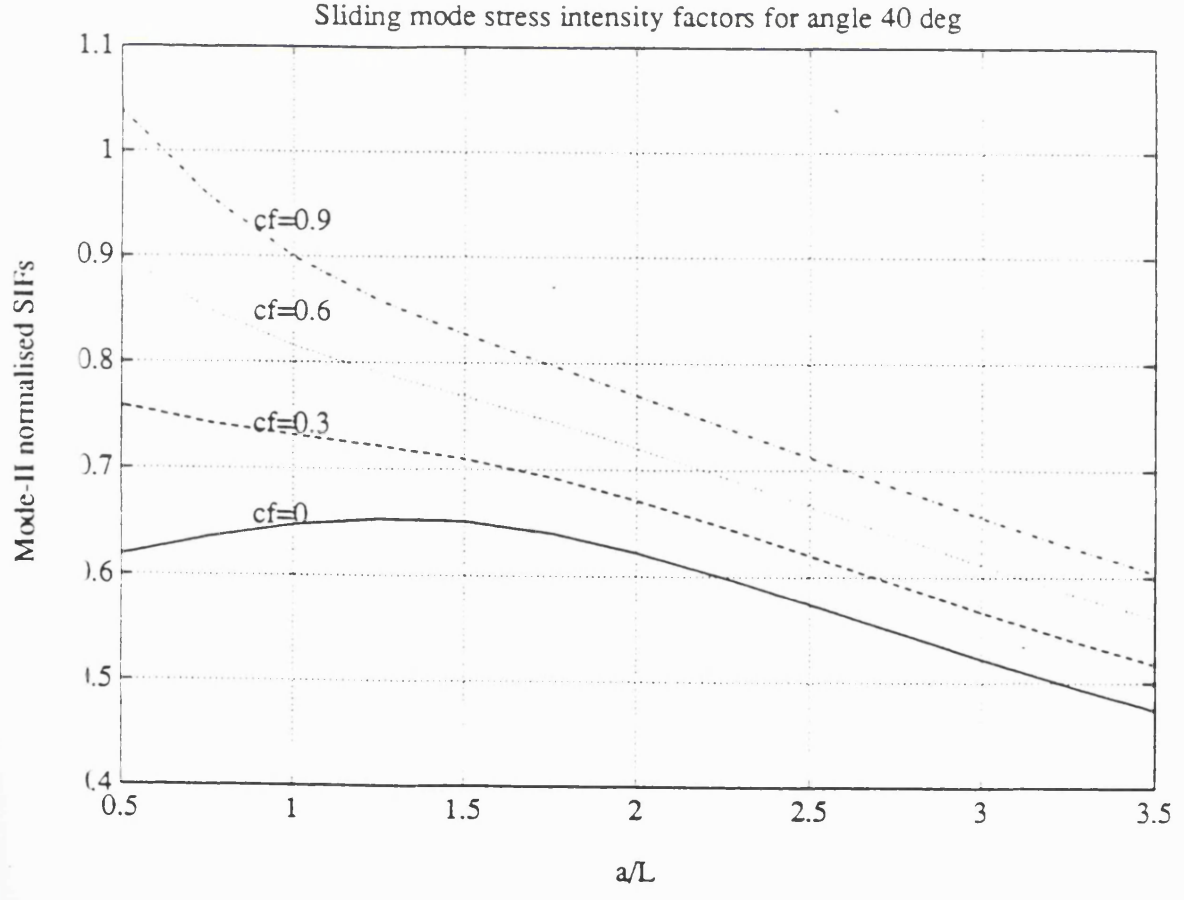

Figure 4.6 Normalised ($K/(p(\pi a)^{1/2})$) SIFs in terms of length and coefficient of friction. Angle=40°. L is the pad foot half-length. p is the normal pressure

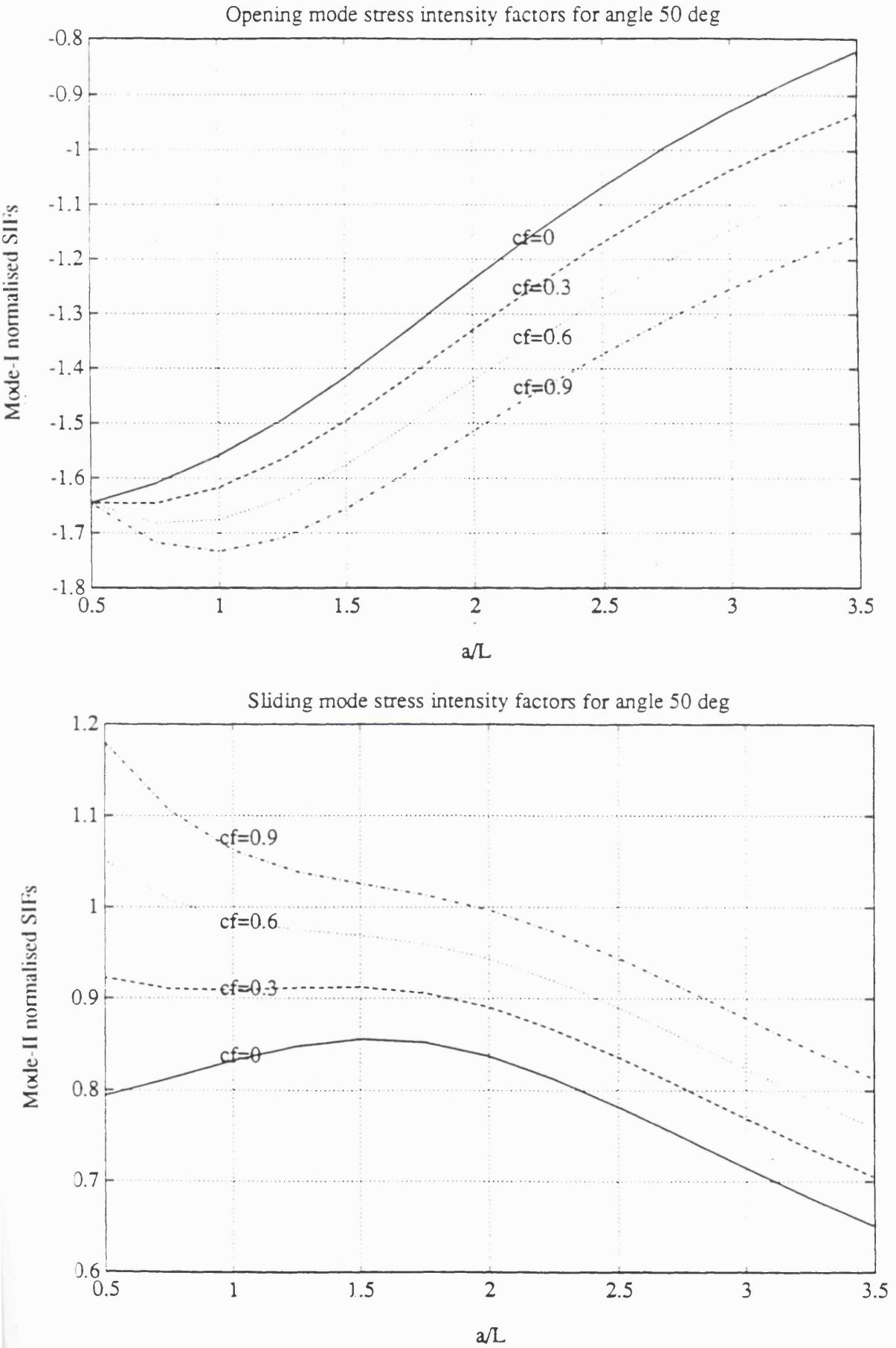

Figure 4.7 Normalised ($K/(p(\pi a)^{1/2})$) SIFs in terms of length and coefficient of friction. Angle=50°. L is the pad foot half-length. p is the normal pressure

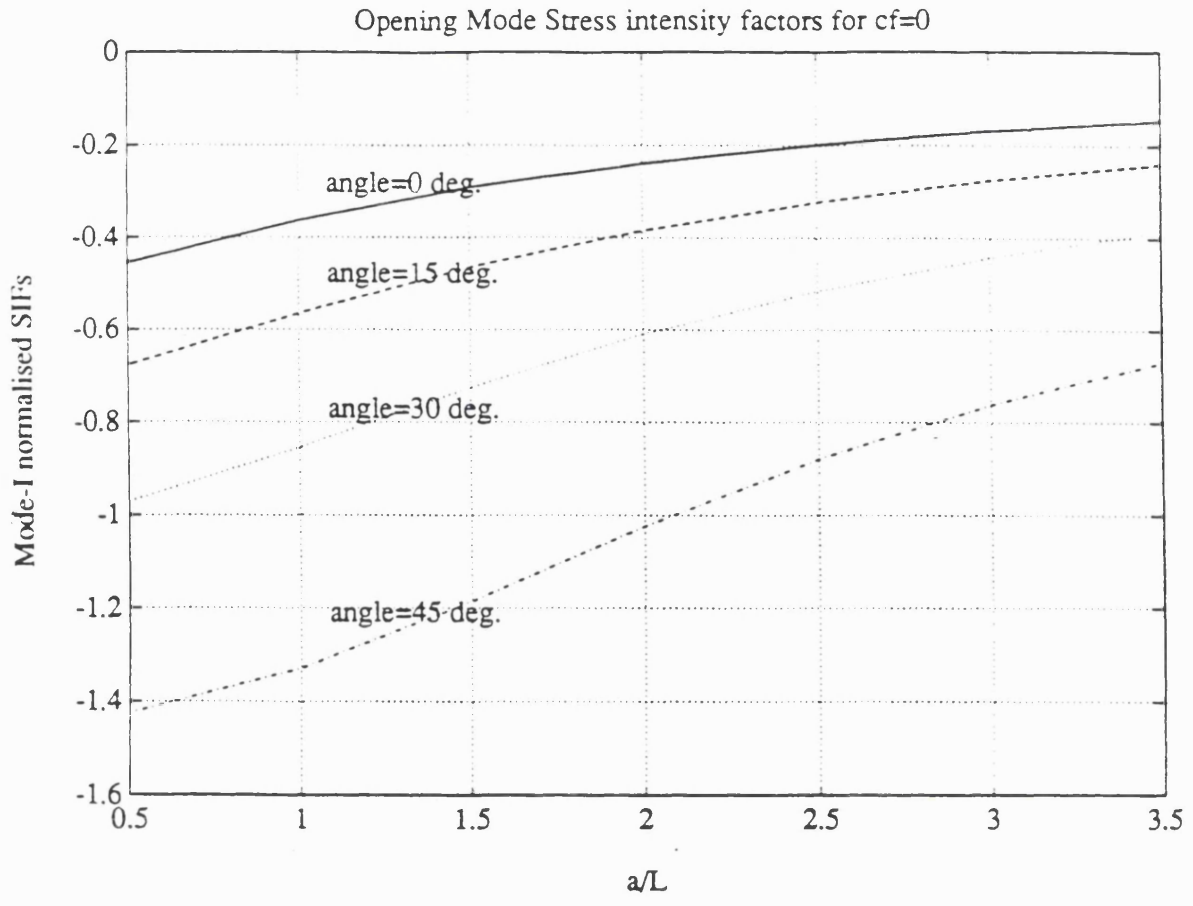

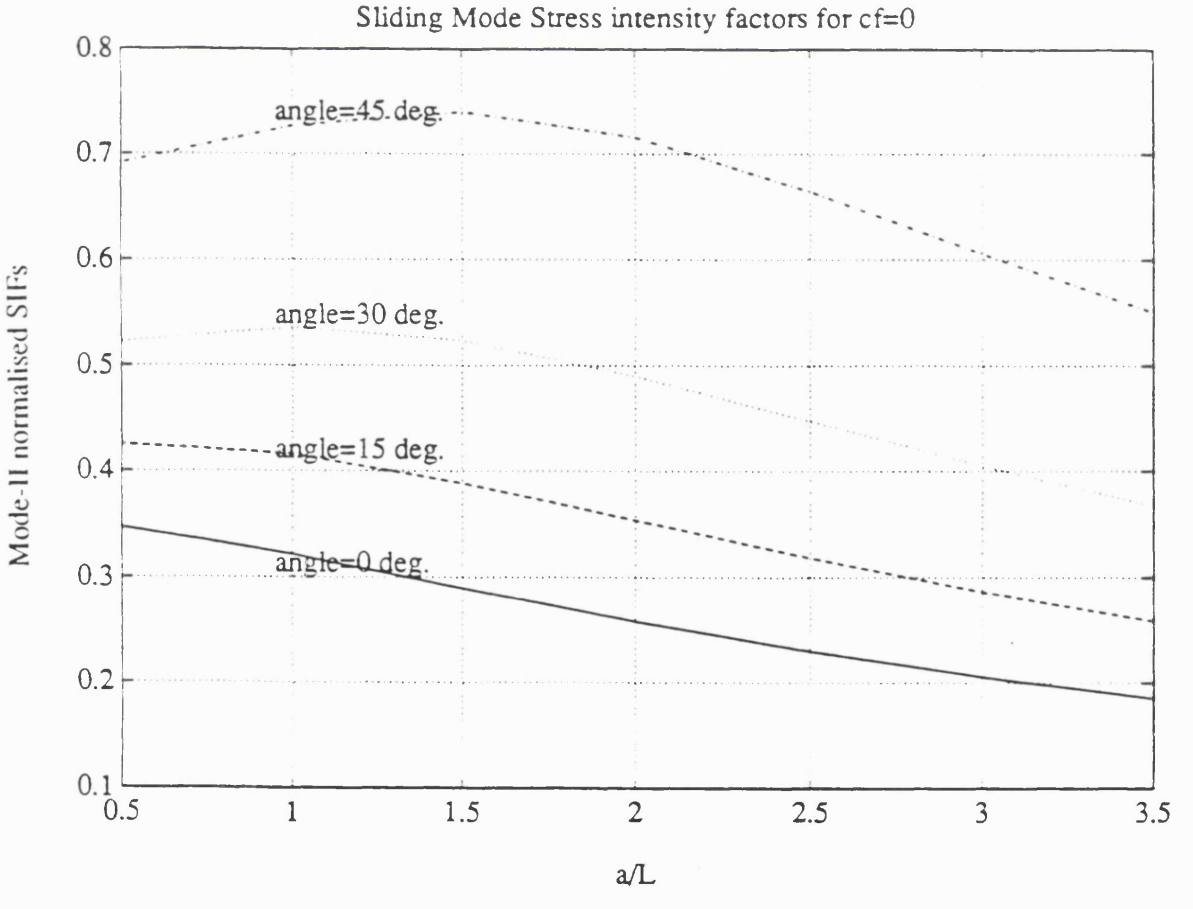

Figure 4.8 Normalised ($K/(p(\pi a)^{1/2})$) SIFs in terms of angle and length. Coefficient of friction cf=0. L is the pad foot half-length. p is the normal pressure

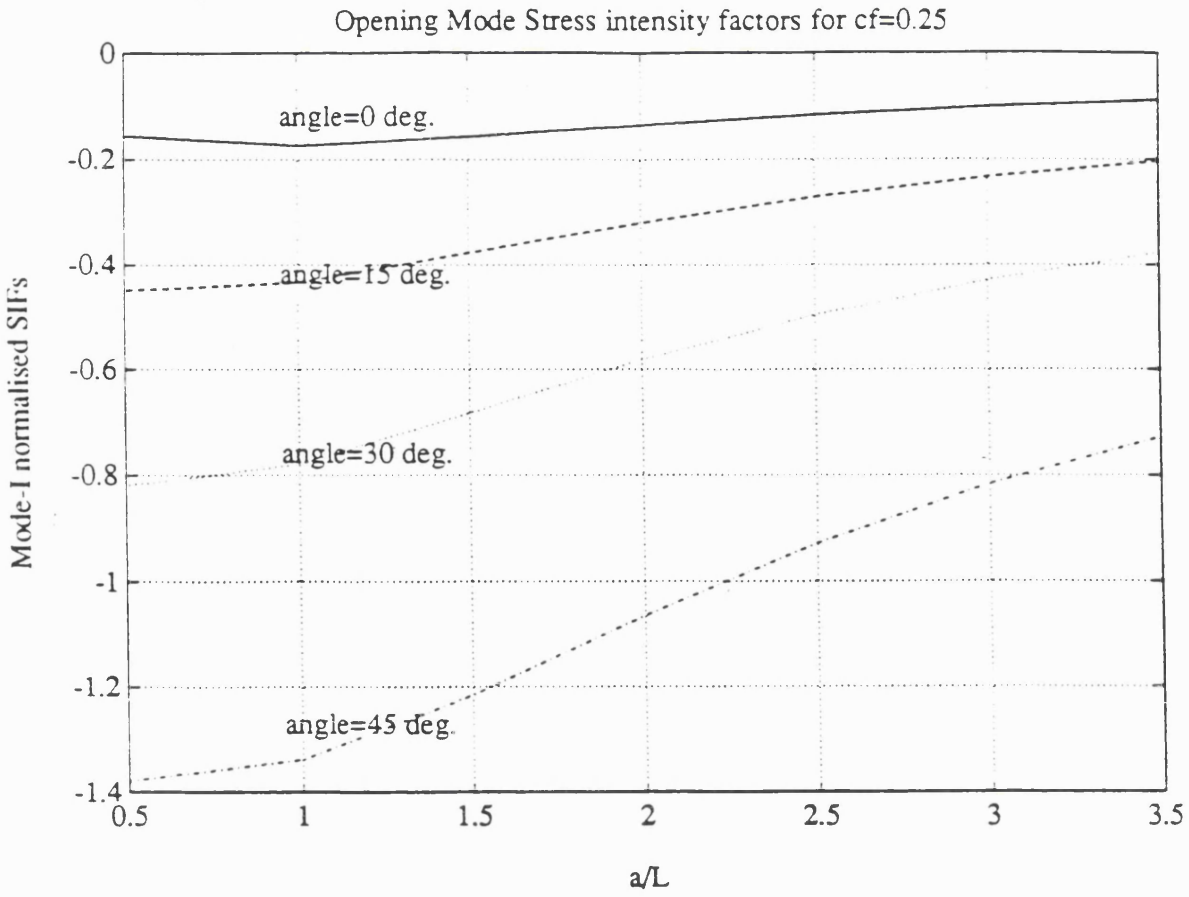

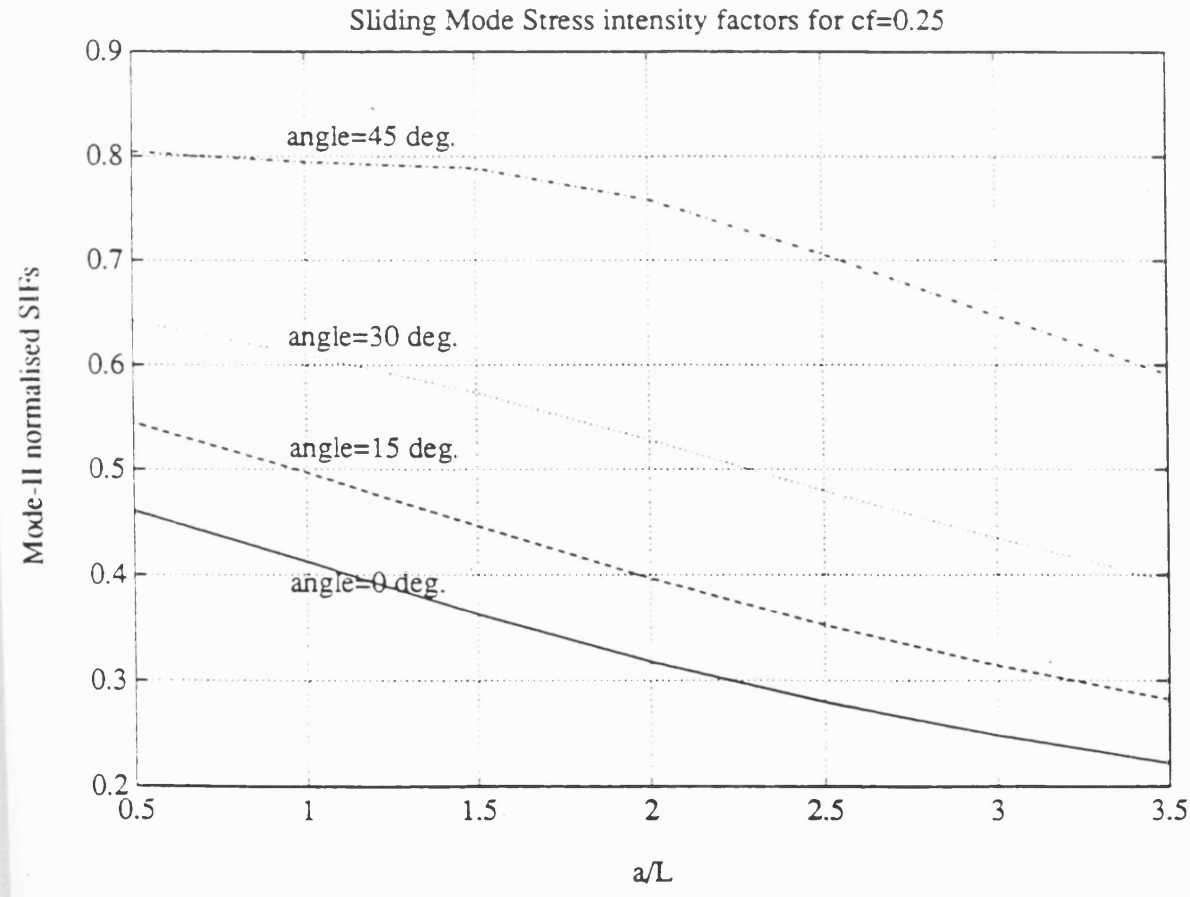

Figure 4.9 Normalised ($K/(p(\pi a)^{1/2})$) SIFs in terms of angle and length. Coefficient of friction cf=0.25. L is the pad foot half-length. p is the normal pressure

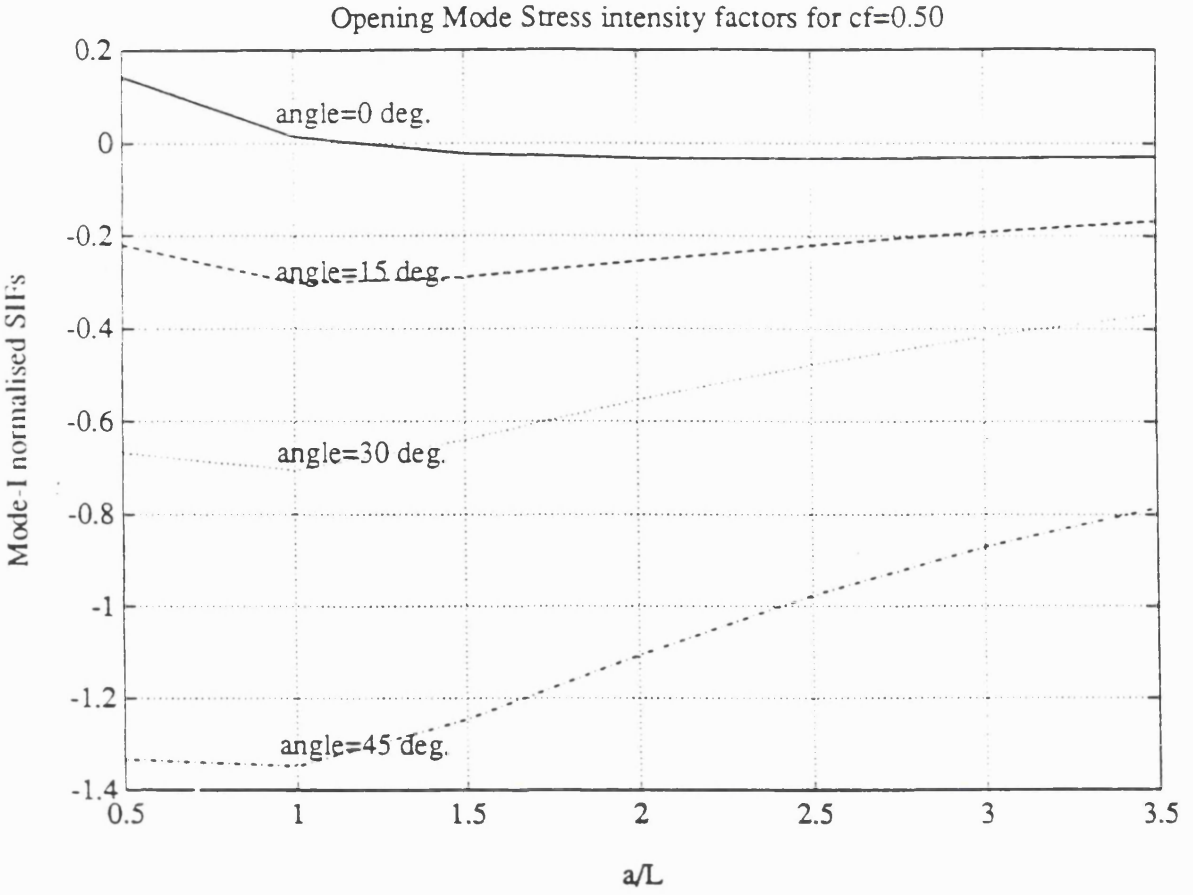

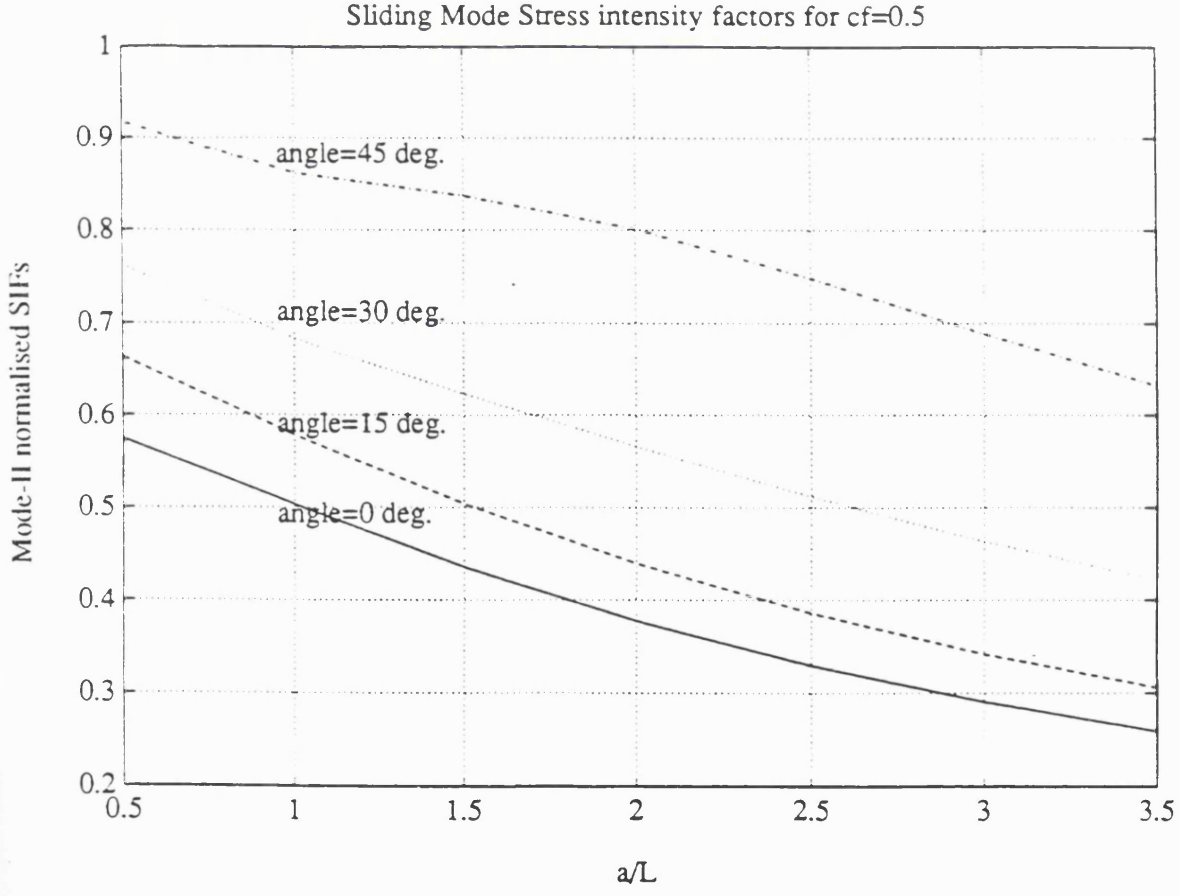

Figure 4.10 Normalised ($K/(p(\pi a)^{1/2})$) SIFs in terms of angle and length. Coefficient of friction cf=0.50. L is the pad foot half-length. p is the normal pressure

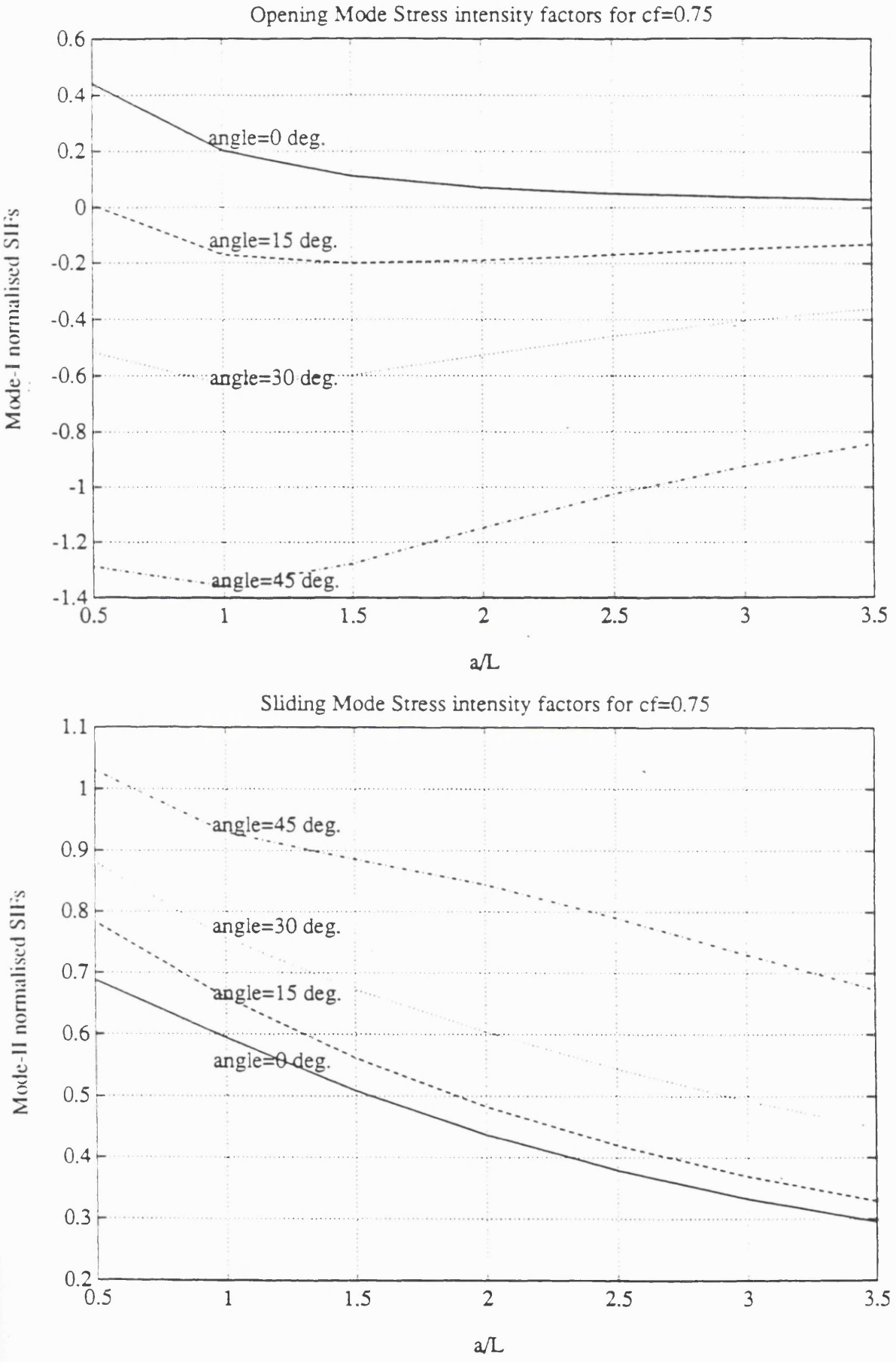

Figure 4.11 Normalised ($K/(p(\pi a)^{1/2})$) SIFs in terms of angle and length. Coefficient of friction cf=0.75. L is the pad foot half-length. p is the normal pressure

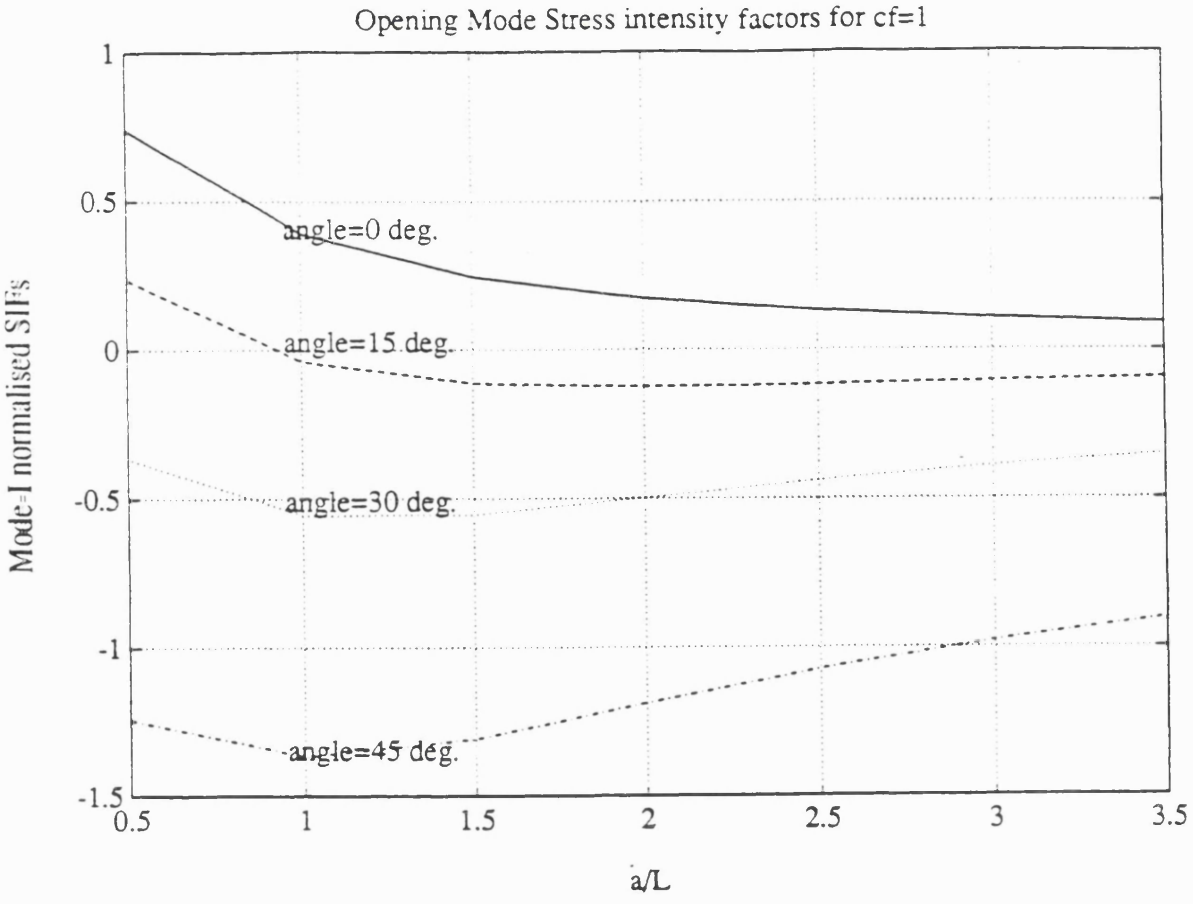

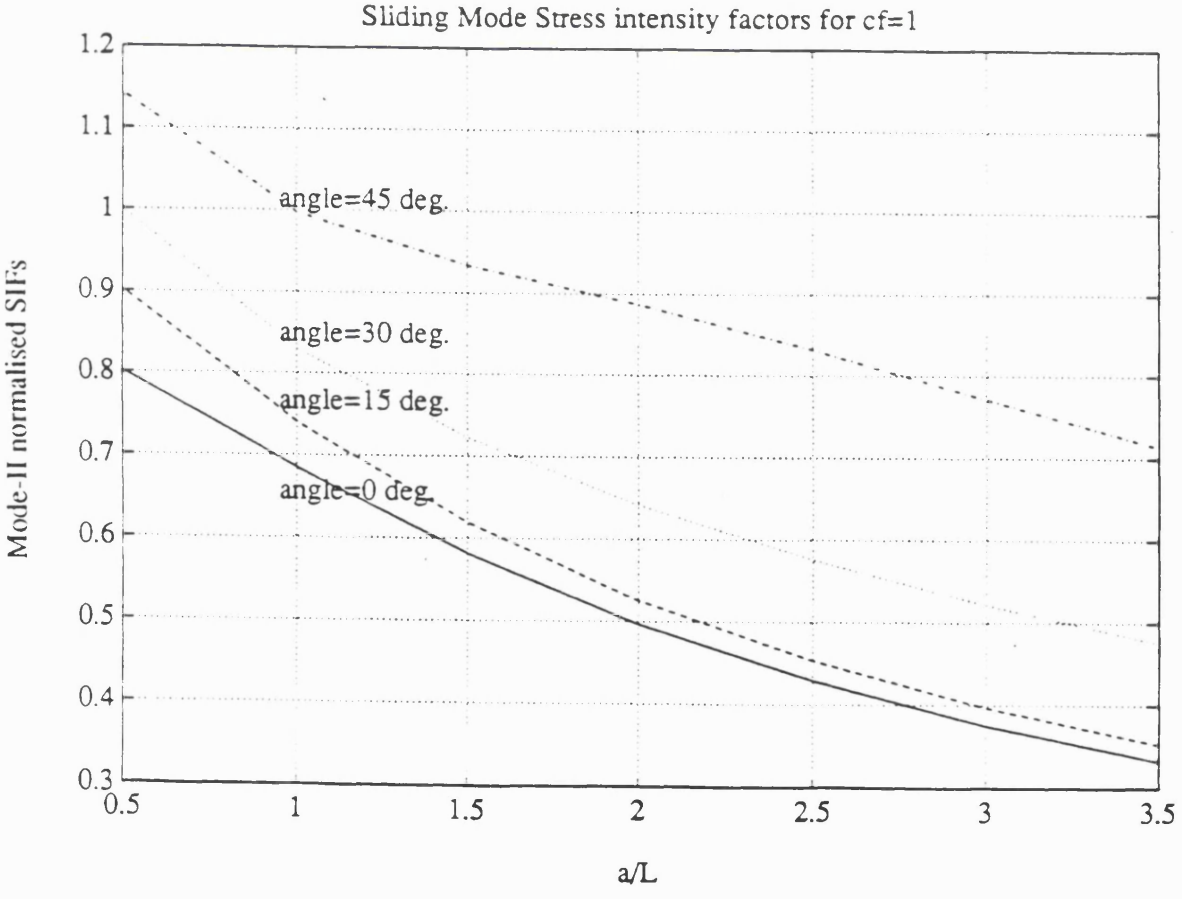

Figure 4.12 Normalised ($K/(p(\pi a)^{1/2})$) SIFs in terms of angle and length. Coefficient of friction cf=1.0. L is the pad foot half-length. p is the normal pressure

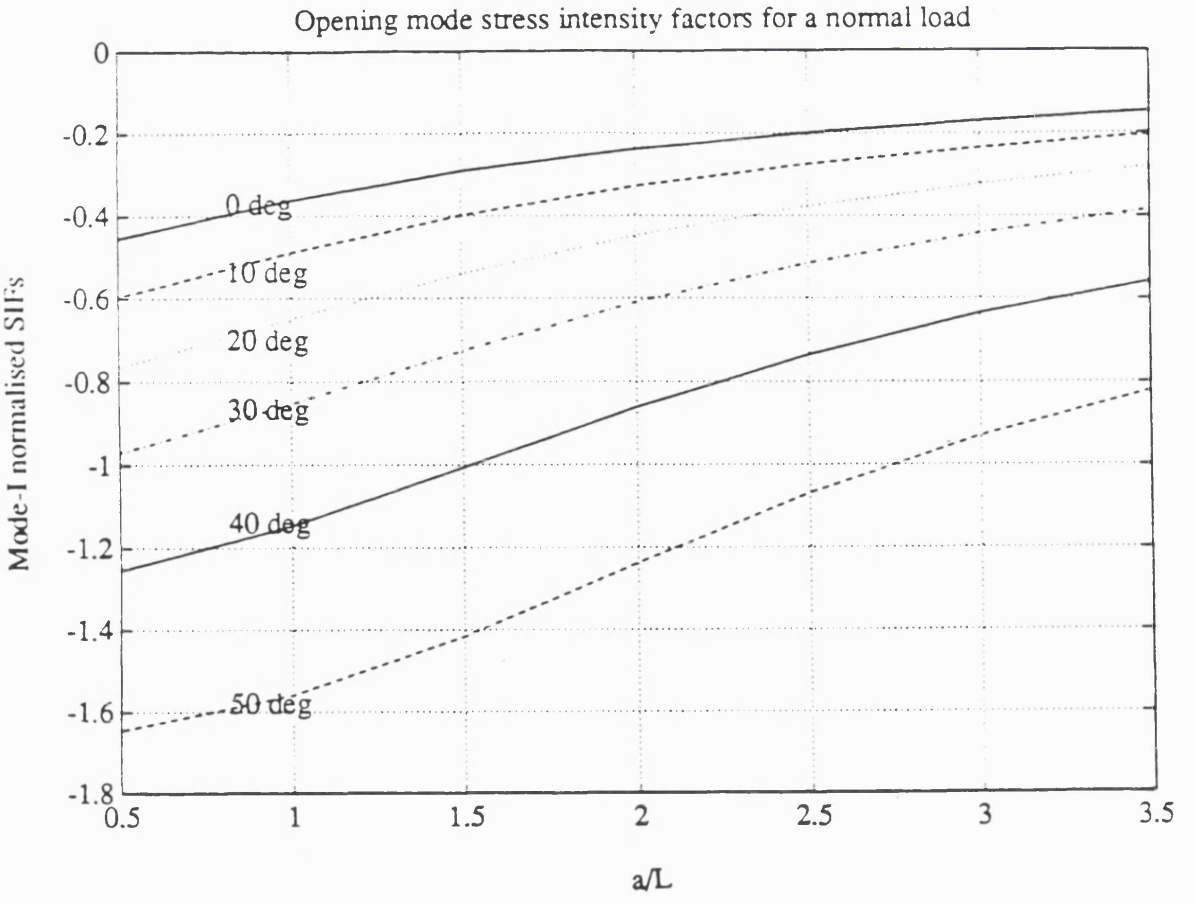

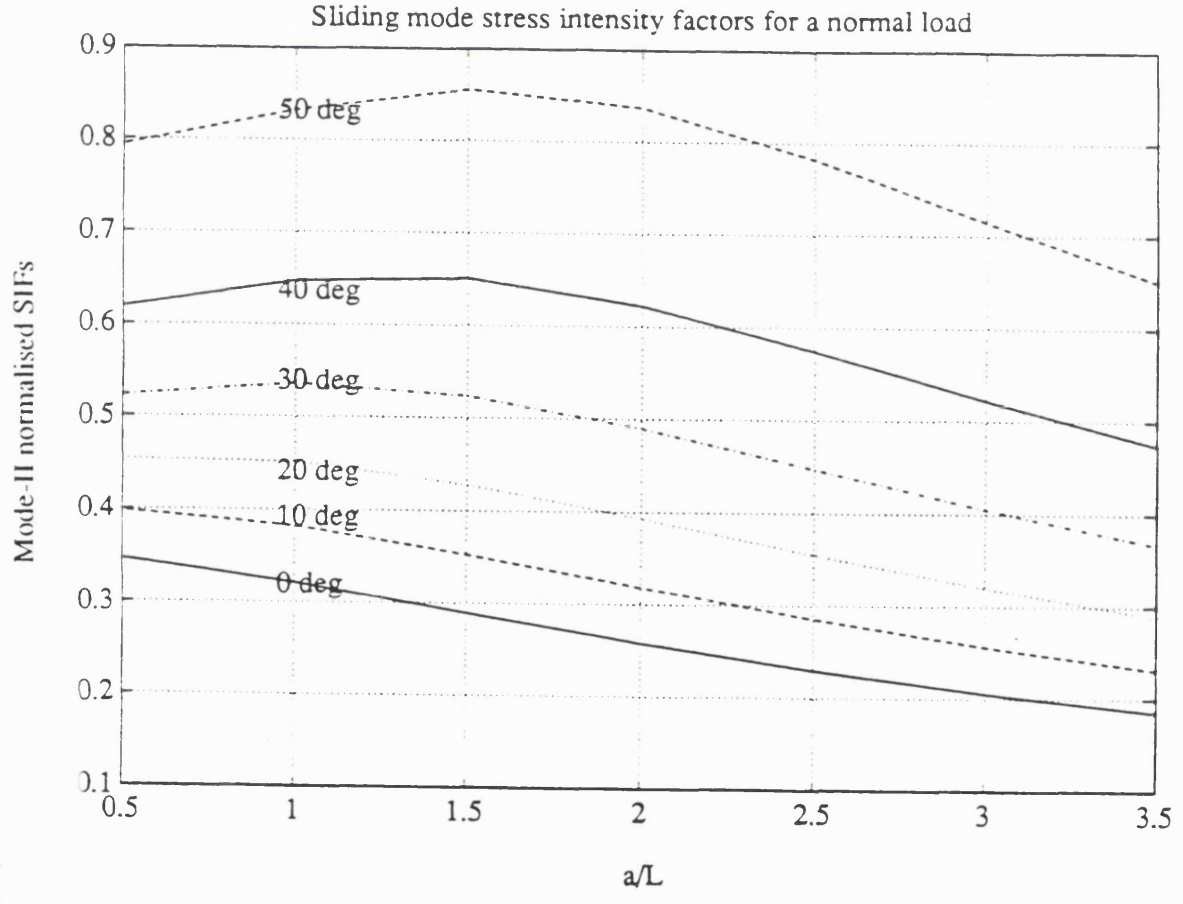

Figure 4.13 Normalised ($K/(p(\pi a)^{1/2})$) SIFs in terms of angle and length. Normal load only. L is the pad foot half-length. p is the normal pressure

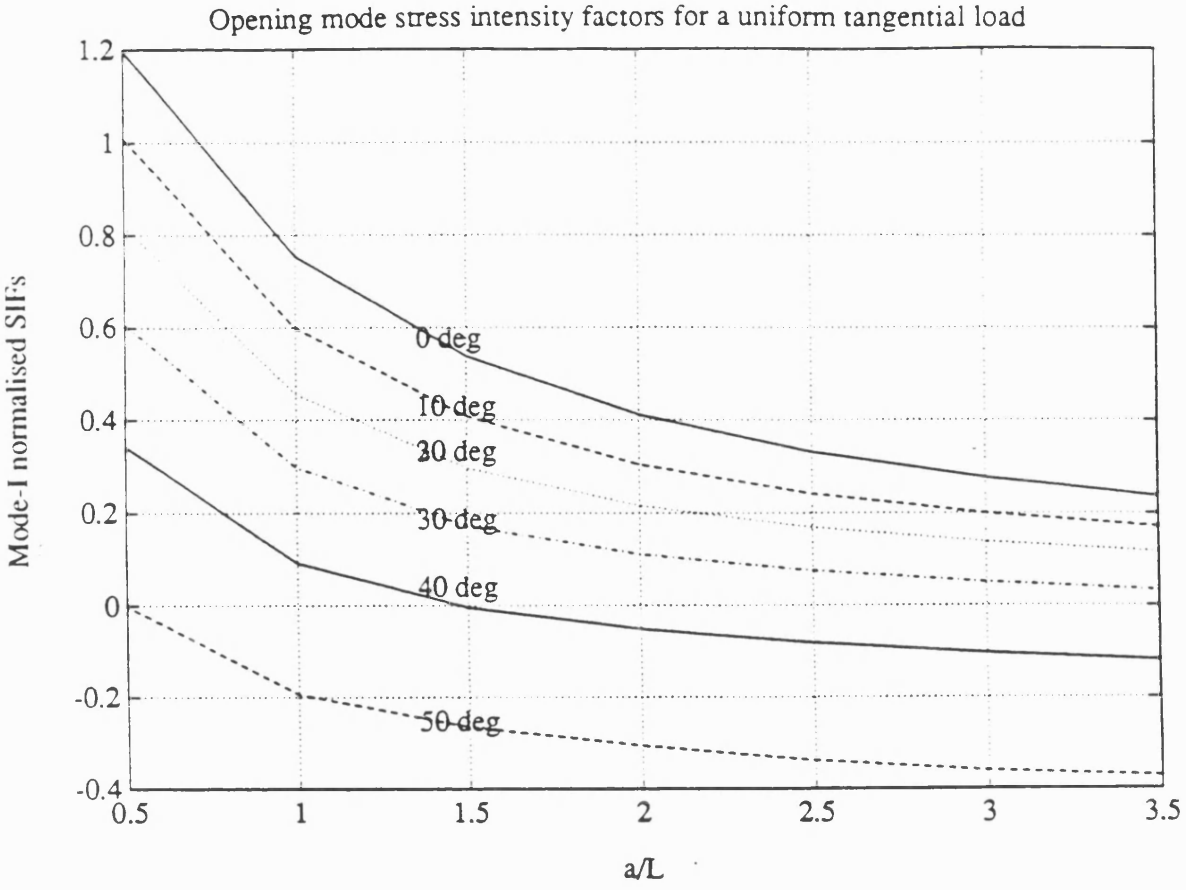

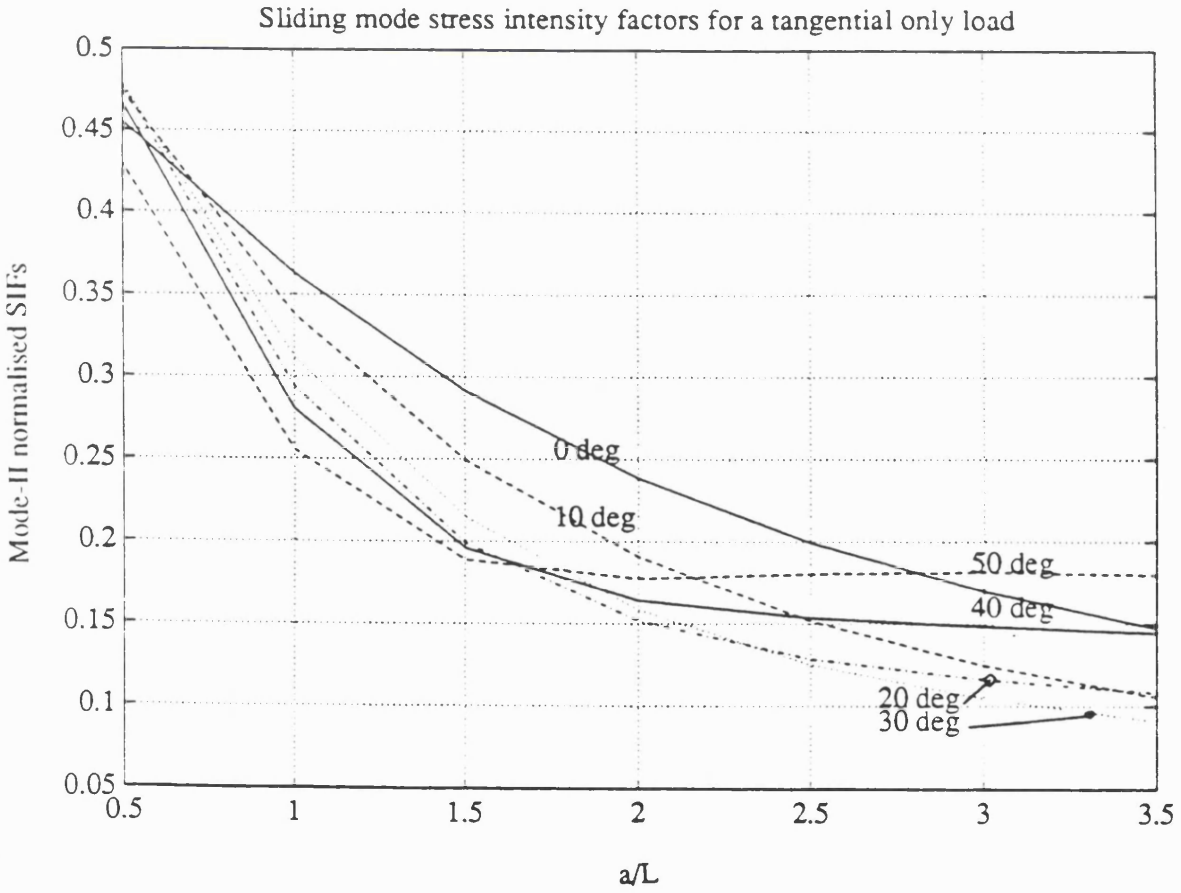

Figure 4.14 Normalised ($K/(p(\pi a)^{1/2})$) SIFs in terms of angle and length. Tangential load only. L is the pad foot half-length. p is the normal pressure

4.2 Kinked crack effects

Detailed determination of the crack growth trajectory is not possible with the present state-of-the-art calculations based on fracture mechanics, because of the lack of satisfactory criteria for the formation and initial propagation of very small cracks. It is to be noted that the microstructure of the material plays an important role in dictating the direction of the crack growth. It can be assumed, however, that the fretting fatigue cracks are initiated under maximum repeated shearing stress which is the combination of tangential stress and repeated stress. The influence of maximum shear stress seems to be more significant than the maximum normal stress in the early growth stages where the yielding phenomena are intense (Ewalds and Wanhill (1984), Miller (1989)). However, the propagating depth of these Stage-I shear type cracks (Figure 2.4) is small and the crack eventually grows perpendicular to the direction of the repeated principal tensile stress which includes the tangential stress of fretting. This is the area where the cracks are oblique to the surface, and the tangential stress exists together with the repeated stress σ. When the crack becomes longer, its propagation direction is normal to the principal stress of the repeated stress (the direction of the axis of the specimen (Figure 2.4)), since the effect of the tangential stress on the contact surface becomes small. This analysis is in agreement with the experimental findings of Endo and Goto (1976).

For the present fretting fatigue model there is obviously combined loading in both mode-I and mode-II. However, the applicability of the mixed mode criteria for crack growth (like these according to the maximum stress theory (Erdogan and Sih (1963) or energy density (Gdoutos (1984)), is questionable especially for small cracks in their initial growth stages. If the angled crack is long enough not to be considered a small crack and provided the plane strain conditions are satisfied, one could apply the maximum stress theory for crack propagation, which is usually more reliable. It is equivalent to calculating approximate stress intensity factors for a small branch at a tip of a crack in terms of the main crack stress intensity factors and

predicts the direction of the instantaneous angle of crack propagation θ, which satisfies the Equation:

$$\Delta K_I \sin\theta + \Delta K_{II} \sin\theta \, (3\cos\theta - 1) = 0 \qquad (4.1)$$

Unfortunately, this approximate model depends on the arbitrary choice of the depth at which the SIFs are calculated as well as on the crack growth segments Δa_1, Δa_2 etc (Sih and Barthelemy (1980), Williams (1984)). The crack closure effects and the effects of the contacting asperities on the effective SIF ranges should also be taken into account (Abdel Mageed and Pandey (1990)). Furthermore, the crack may not follow a regular pattern and its trajectory might change progressively until it adopts a path normal to the surface. This arc shaped crack might be the subject of a further study (Xiaping Lu and Comninou (1989)), but this is out of the scope of this study, which deals with model kinked cracks. Even if we assume an initial angle for the initiation (say 45° for stage-I cracks), and apply one of the crack growth criteria, once the existed crack has adopted an unknown non-normal to the surface pattern, the expressions for K_I and K_{II} are altered and cannot be easily determined.

As regards the kinked crack effects, the K_I for an edge crack that starts obliquely to the surface and eventually grows normally to it, is almost identical to that of a normal crack (Murakami (1985)), provided that a "projected" length is used for its calculation. This length corresponds to the projection of the angled part d_1 onto the perpendicular crack direction plus the normal part d_2, namely it is $d_1\cos\theta+d_2$. Indeed, Li Yingzhi and Hills (1990) calculated the SIFs for a kinked crack subjected to a tensile stress field σ. They found that for a crack which starts at 45° to the surface, develops to a length d_1 and then it turns perpendicularly to the surface and grows to length d_2, the relation given below predicts accurately the SIFs for a kinked crack in the range: $0.01 \leq d_2/d_1 \leq 10$:

$$\frac{K_I}{\sigma\sqrt{\pi d_1}} = 1.1215 \sqrt{\cos\theta_1 + (\frac{d_2}{d_1})} \qquad (4.2)$$

When the slant length becomes smaller than 1/4 of the normal part, as the crack grows away from the surface, the K_I is identical to the corresponding SIF of the normal crack up to the second decimal digit (Figure 4.15). For this reason if there is no considerable angled crack growth for the scale of the model, or the employed NDE method is not very effective for the small size of the angled part involved, the angled and kinked part effects are not taken into account for design purposes, once the crack is long enough to be studied by LEFM calculations.

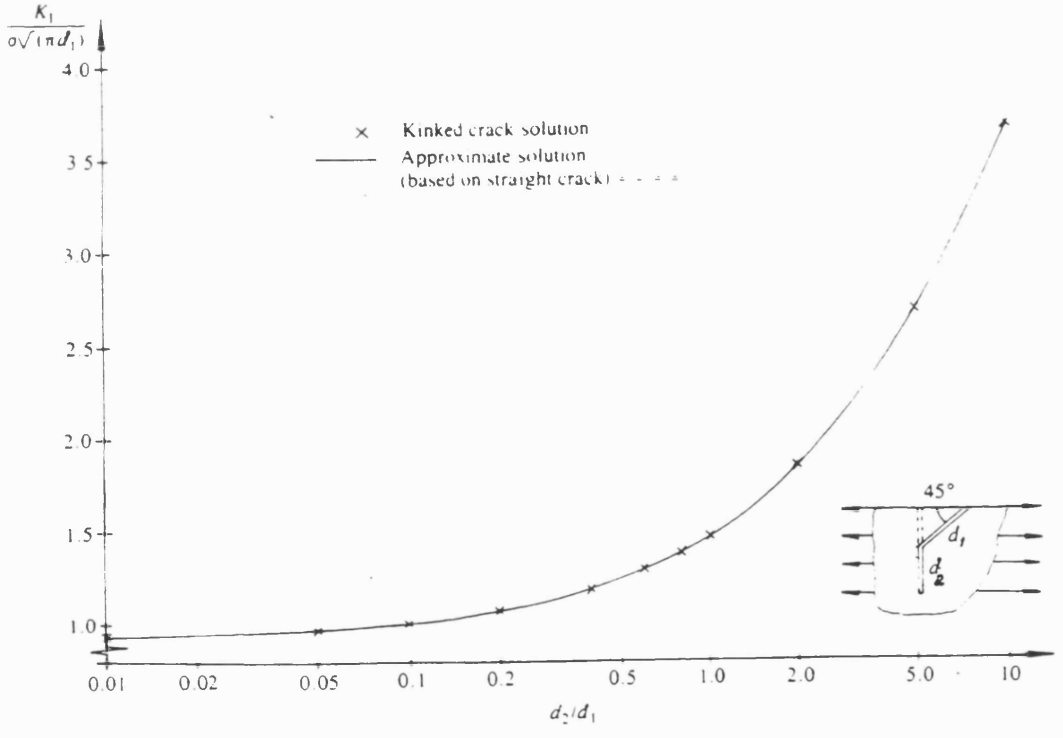

Figure 4.15 Relationship between the SIF for a kinked crack of initial angle 45° and length d_1+d_2 and the SIF for the corresponding normal crack of length $d_1\cos\theta+d_2$

4.3 Fretting fatigue threshold analysis

4.3.1 Mean and alternating SIFs under fretting conditions

In the following, the results of the present study will be employed for the analytical study of the experimental model of Figure 2.7. The specimen material is aluminium alloy 2014A and the fretting pads are made of 3.5NiCrMoV steel. The new results allow a refinement of the existing analyses which are mainly based on data derived for normal cracks. Fretting fatigue limits are estimated by comparing the SIF ranges with the threshold SIF of the material. These calculated results are then compared with experimental results of fretting fatigue tests. Provided LEFM is applicable, the calculated critical crack size for crack growth at the fatigue limit should correspond to the maximum observed defect size.

The discussion on the SIF results revealed that the influence of the different materials of the fretted components on the fatigue strength is small. For this reason the uniform loading model is used in the following analysis, as its main properties are the simplicity and the rapid solutions it provides. Another finding, which is justified by the analytical study of the preceding Chapter, is the uncoupling of the contact and crack models and the superposition of the solution of the independent contact and crack problems. For this purpose, the SIF data of Figures 4.13-14, which refer to the separate action of the tangential and normal loadings, can be used. Under these conditions, the SIF at the crack tip is considered to be the combination of three individual contributions:

a. that due to the body stresses, which is caused by the applied fatigue stress.

b. that due to the frictional forces through the fretting pads

c. that due to normal pad loads.

The first two contributions are alternating and hence damaging, while the third one is static, compressive and tends to be beneficial, as it will become evident.

The total mode I SIF range ΔK_a, which corresponds to tensile stress range $\Delta\sigma$, is the sum of the components due to the externally applied stresses (ΔK_{ax}) and to fluctuating frictional force (ΔK_{fr}) (Nix and Lindley (1985)):

$$\Delta K_a = \Delta K_{ax} + \Delta K_{fr} - \Delta K_r \tag{4.3}$$

where ΔK_r accounts for the fact that the specimen alternating body stress is lower under the pads, because some load is diverted through the pads. The individual terms of Equation (4.3) can be expanded as follows:

$$\Delta K_{ax} = \frac{M}{C} \Delta\sigma \sqrt{\pi a} \tag{4.4}$$

$$\Delta K_r = \frac{M}{C} \frac{\Delta F_t}{A} \sqrt{\pi a} \tag{4.5}$$

$$\Delta K_{fr} = K_t \frac{\Delta q_t}{C} \sqrt{\pi a} \tag{4.6}$$

where A is the cross sectional area of the specimen, Δq_t is the distributed tangential (frictional) pressure, K_t is the tensile mode SIF given by Figure 4.1 and M and C are front surface and crack shape correction factors respectively. For the deepest point of the crack, the equations for M and C are: (Scott and Thorpe (1981)):

$$C = [1+1.47(a/c)^{1.64}]^{0.5} \tag{4.7}$$

$$M = 1.13-0.07(a/c)^{0.5} \tag{4.8}$$

where a/c is the aspect ratio (depth over semi-surface length) of the crack. From fretting fatigue tests in a similar configuration like that of Figure 2.7, it has been found that the cracks are highly extended across the specimen surface along the z axis and consequently a/c$\rightarrow$0 and M$\approx$1.12 (*cf* Figure 3.1) and C=1 (Nix and Lindley (1985,1988)). Hence, these values of M and C do not produce very conservative

results for fracture mechanics calculations.

The total mean mode I SIF is the sum of the contributions of the externally applied stresses (K_{me}) and of these due to the normal contact pressure (K_{mc}), or, when expressed by expanding the individual terms:

$$K_{mean} = K_{me} + K_{mc}$$
$$= 1.12\sigma_m \sqrt{\pi a} + K_n p_n \sqrt{\pi a} \qquad (4.9)$$

where σ_m is the applied mean stress and p_n is the applied normal pressure. The term K_n is in fact always negative *(cf* Figure 4.14).

Pook (1976) suggested that there is a short crack length effect, which has to be included in the K_{mean} calculation. The threshold for short crack propagation is smaller than that for longer cracks or, in other words, short cracks may propagate faster than longer ones. This might be due to the fact that the plastic zone at the tip of the crack is more effective for short cracks, so that the crack does not close until it is well into compression. No length correction term was incorporated into the SIF calculations, since very little is still known about short crack propagation and there is lack of a general analytical model. However, Edwards *et al* (1977) have given some empirical results for short crack corrections in fretting fatigue calculations.

The input parameters in the above mentioned Equations (4.3) and (4.9) are the applied stresses (stress amplitude range $\Delta\sigma$, applied mean stress σ_m and normal pressure p_n) as well as the specimen dimensions. However, the frictional force range ΔF_t and the coefficient of friction μ should be determined experimentally.

Numerous techniques have been developed for the measurement of friction. For the test rig configuration considered in this work, the measurement technique is based on the attachment of strain gauges on the lower part of the pads and taking

into account both their bending and uniaxial extension (There are various experimental publications in RAE Technical Reports, see e.g. Edwards and Cook (1978b) and also Endo *et al* (1974)). A common property of the fretting fatigue tests of the literature is that the frictional force achieves a limiting value equal to the contact force, namely the maximum coefficient of friction μ under alternating stresses greater than a critical value, becomes approximately equal to unity after some time (Nix and Lindley (1985)). If an analytical study is to be undertaken, it is suggested that a mean coefficient of friction of 0.7-1 be used, on the basis of observed results of contact surface damage in the fretting tests of the literature (see and Chapter 2.8.2c).

In order to study the failure mechanisms for mode-I fatigue crack growth, the mode-I fatigue threshold range ΔK_0 must be known. It can be derived from the data in Figure 4.16 that for aluminium alloy 2014A the mode-I threshold range in terms of the stress ratio R is given by the relation (Nix and Lindley (1985)):

$$\Delta K_0 = 2.67 - 1.87\ R \tag{4.10}$$

for the least square best fit to the data and:

$$\Delta K_0 = 2.1 - 1.42\ R \tag{4.11}$$

for the lower bound to the data. The ratio of minimum to maximum SIF for mean stress σ_m and stress range $\Delta\sigma$ is given by the equation:

$$R = \frac{\sigma_m - \Delta\sigma/2}{\sigma_m + \Delta\sigma/2} \tag{4.12}$$

for no fretting and

$$R = \frac{K_{mean} - \Delta K_d/2}{K_{mean} + \Delta K_d/2} \tag{4.13}$$

for fretting. Note that in the absence of fretting the above ratio is constant as it depends only on external testing parameters. For fretting conditions the ratio

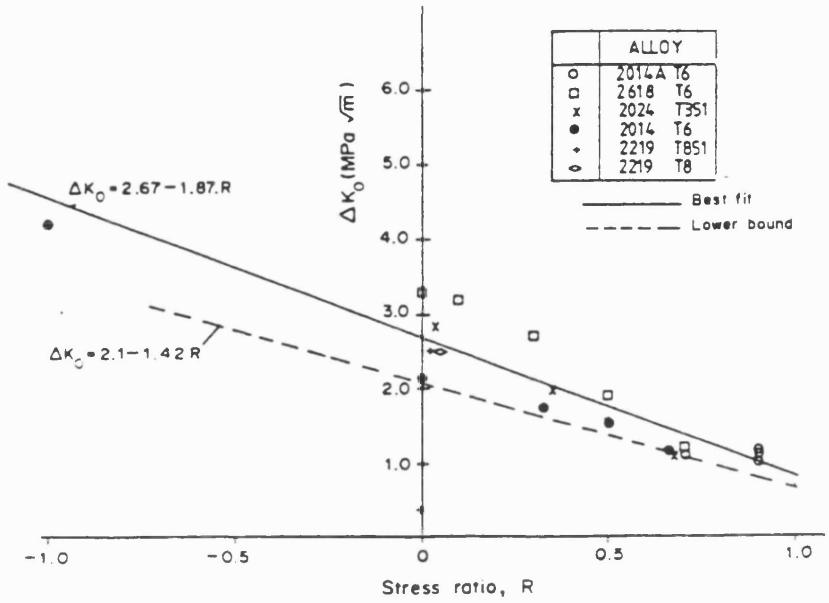

Figure 4.16 Fatigue thresholds for Al-Cu alloys (from Nix and Lindley (1985))

(Equation 4.13) depends on the SIF (ranges) which change with crack length as the influence of the pressing and tangential loading diminishes.

4.3.2 Influence of the mode-II loading

For edge cracks perpendicular to the surface a constant K_{II} occurs, that causes relative sliding of the crack faces. Additionally for angled cracks, there is a fluctuating ΔK_{II} component. The growth direction under mixed-mode loading is still perpendicular to the normal stress in the crack tip field. However, the incorporation of the influence of the mode-II loading on the crack growth indicates that fatigue crack growth can start at $\Delta K_I < \Delta K_0$, where ΔK_0 is the SIF threshold range in mode-I. The mode-II component in the near threshold fatigue crack growth increases the size of the crack tip reversed plastic zone, facilitating the growth, but at the same time,

increases the contact and rubbing of the surfaces, leading to crack arrest and delay of failure. (Gao Hua *et al* (1982)). This influence must be very intense at the early stages of fretting fatigue (Stage II in Figure 2.4; see and Tanaka *et al* (1985)).

The problem one encounters here is the choice of a suitable mixed mode fracture criterion. There is a selection of criteria in the literature, most of which seem to compare a function of the range of SIFs $\Delta K_v(KI,K_{II})$ with the threshold for mode-I ΔK_0:

$$\Delta K_v \left(K_I , K_{II} \right) = \Delta K_0 \qquad (4.14)$$

enabling failure envelopes to be obtained. The most commonly used of them are:

1. criterion of maximum tangential stress (Erdogan and Sih (1963))
2. various criteria of the energy density. For example see the just mentioned and Gdoutos (1984) for the strain energy criterion proposed by Sih.
3. J-integral criterion (Yu (1982))
4. Energy release rate criteria (Broek (1974)).

Additionally, there are numerous empirical criteria, for example Tanaka (1974). These criteria were developed for a specific application and their adaptation to other testing conditions may be difficult without the knowledge of all the conditions involved. The failure envelopes constructed by the various criteria may refer to different thresholds and crack growth stages and the reader is referred to Pook (1985, 1989) for a discussion about their inconsistencies and the construction of failure mechanism maps. Especially for the fretting fatigue case, the study of the mixed mode crack growth is compounded by the small physical length of the cracks and the compression stress field induced by the pad (Otsuka (1991)). Furthermore, the loads may be applied out of phase and be dependent on the history of traction distribution (Hills and Comninou (1985)).

Despite the fact that little is still known about the behaviour of small cracks

in fretting fatigue, an attempt can be made to evaluate the influence of the mode-II loading. For this purpose, the criterion set out by Di Leonardo (1979) was chosen, mainly because the input data for the materials of our configuration were given in the same paper. This is virtually a combination of the conventional fracture toughness characterization and the Griffith instability criterion, given by a combination of ΔK_I, ΔK_{II} and ΔK_0 of the type:

$$[\frac{\Delta K_I+m}{\alpha}]^2 + [\frac{\Delta K_{II}}{\beta}]^2 = 1 \qquad (4.15)$$

For aluminium alloy 2014: ν=0.33 and:

$$\alpha = \Delta K_0 + m = \Delta K_0 (1+M)$$

$$\beta = \alpha [\frac{3(1-2\nu)\Delta K_0}{(2-2\nu-\nu^2)(\Delta K_0+2m)}]^{1/2} \qquad (4.16)$$

where $m=M\,\Delta K_0$ with M=0.5 for ν=0.33, so that Equation (4.15) becomes:

$$[\frac{\Delta K_I/\Delta K_0+0.5}{1.5}]^2 + [\frac{\Delta K_{II}}{0.9625\Delta K_0}]^2 = 1 \qquad (4.17)$$

with $\Delta K_I=\Delta K_a$ from Equation (4.3) and ΔK_0 from Equation (4.11) so that it depends on the stress ratio R. The value of ΔK_{II} is due to the mode-II contributions of the frictional forces. It can be calculated from the numerical system developed in the last Chapter, with input parameters the contact pressure and the coefficient of friction.

4.3.3 Results

In order to investigate the influence of the various testing parameters, the critical crack length was found for the specimen shown in Figure 2.7 for normal pressure of 31MPa and 139MPa. Experimental data, derived by Nix and Lindley (1985,1988), were available for the same model. The numerical values for the stress ranges involved were: mean fatigue stress σ_m=125 MPa, stress amplitude range

$\Delta\sigma$=15 MPa and contact pressure 31 MPa and 139 MPa. The authors found an upper bound defect depth of about 0.25mm by breaking open the fretting fatigue cracks in their experiments, under the same numerical parameters of this study.

Uniform traction distribution was chosen for both the normal and the tangential loading and the general error of the calculations by the continuous dislocation method, is within the bounds which have been mentioned in Section 3.6. In plain fatigue, that is in the absence of the fretting pads, the critical defect size is given by the respective point of intersection of the curves which express the Equations (4.3) and (4.15):

$$\Delta K_{ax} = \Delta K_0 \tag{4.18}$$

where the ratio R refers to no-fretting conditions. In this case ΔK_{ax} gives the SIF range for fatigue due only to main tensile stress and ΔK_0 is constant throughout the examined area, as it is not dependent on the crack length. In this case the critical crack depth was a_c=400 μm (Figure 4.17).

Next, two sets of numerical results were examined corresponding to two values of contact pressure. The value of the stress ratio R is given by Equation (4.13). The critical crack length can be found as the point of intersection for the curves giving ΔK_0 and ΔK_a.

With fretting present the critical crack depth was drastically reduced to a_{c1}^1=195 μm, when the total contact pressure was 31MPa and to a_{c2}^1=260 μm for contact pressure 139 MPa. Some interesting conclusions drawn from these values will be discussed in the following section.

When the influence of mode-II effects are incorporated by using Equation (4.15), the critical depth is the intersection point of the above equation with unity. The results are a_{c1}^2=180 μm and a_{c2}^2=230 μm for contact pressure 31 MPa and 139

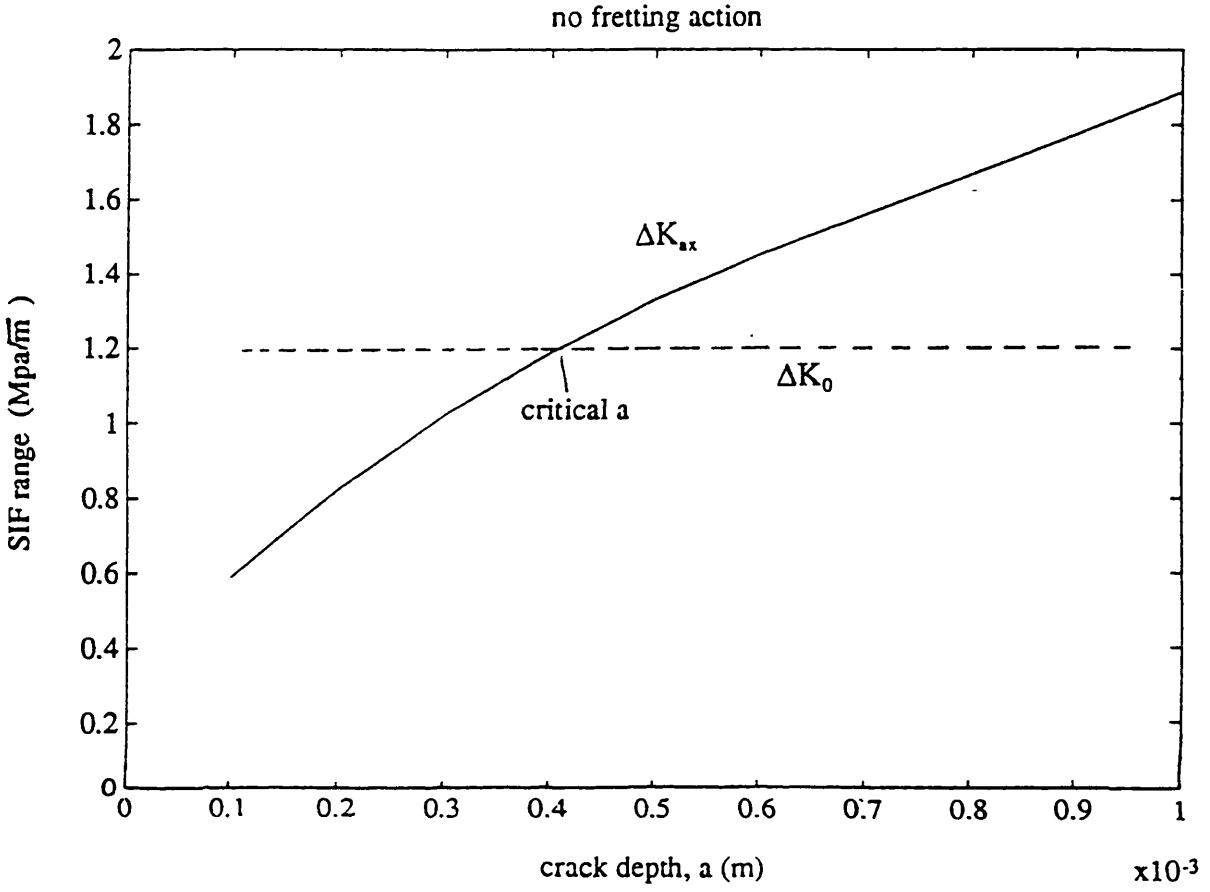

Figure 4.17 Critical defect size when there is no fretting action

MPa respectively.

All the above results refer to normal cracks. Two further sets of data were derived for cracks inclined at 20° and 45° under the pads. For a normal pressure of 31MPa, the corresponding critical crack lengths were found 260μm and 410μm for the two angles. For the higher pressure the lengths were 310μm and 470μm, respectively (Figure 4.19).

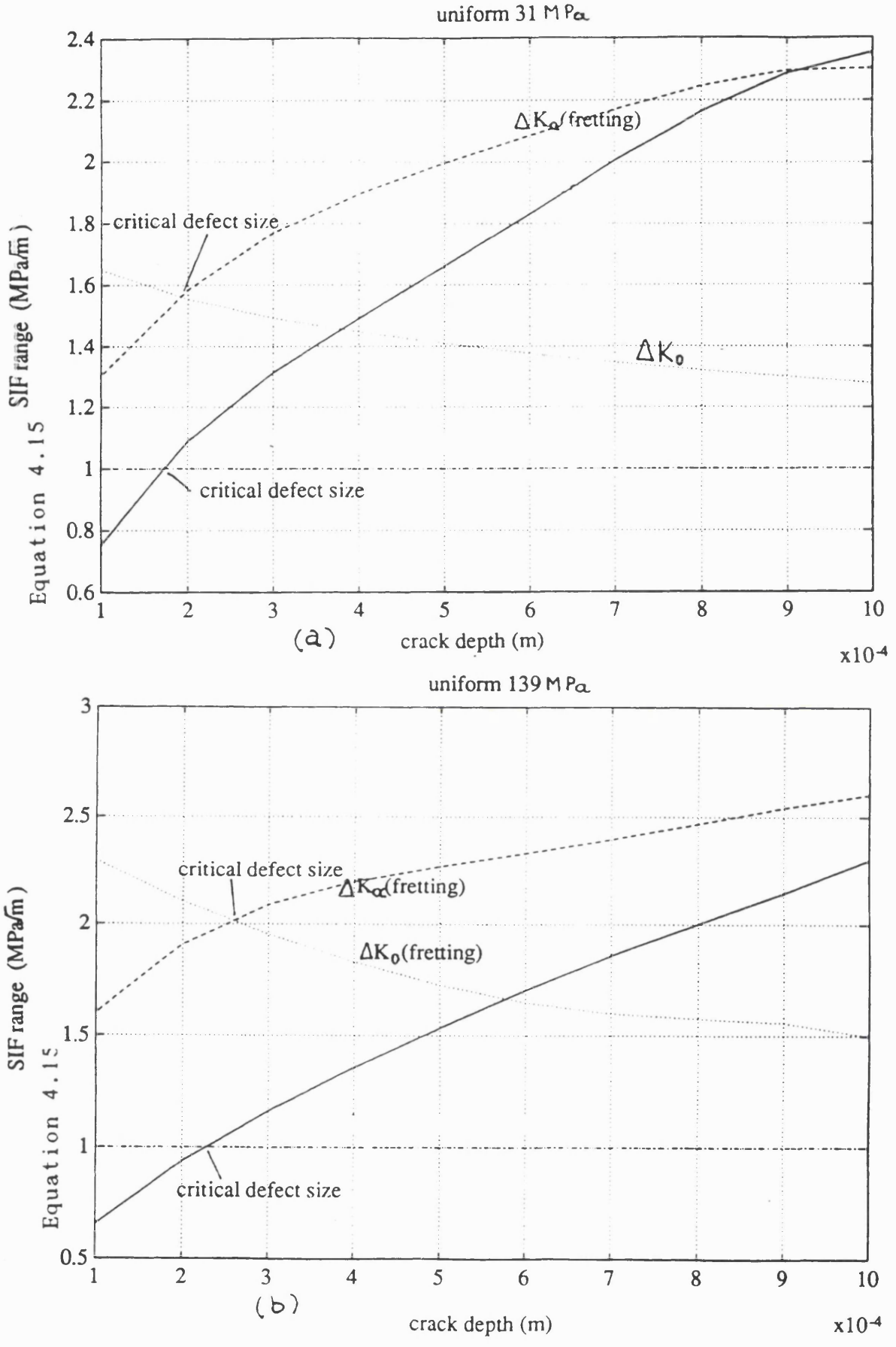

Figure 4.18 Contact pressures: (a) 31MPa (b) 139MPa. Upper curves: Total applied (ΔK_a) and threshold (ΔK_0) SIF ranges in fretting. Lower curves: Equation (4.15)

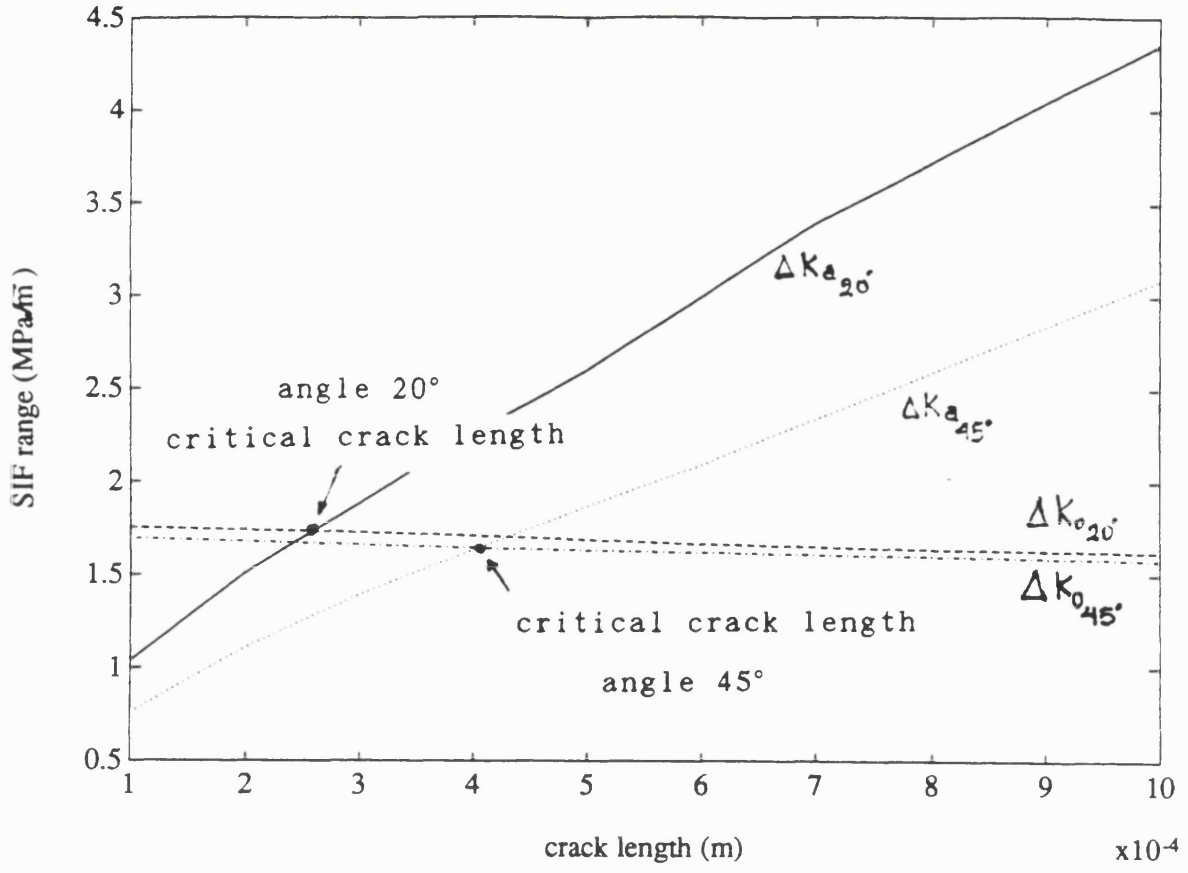

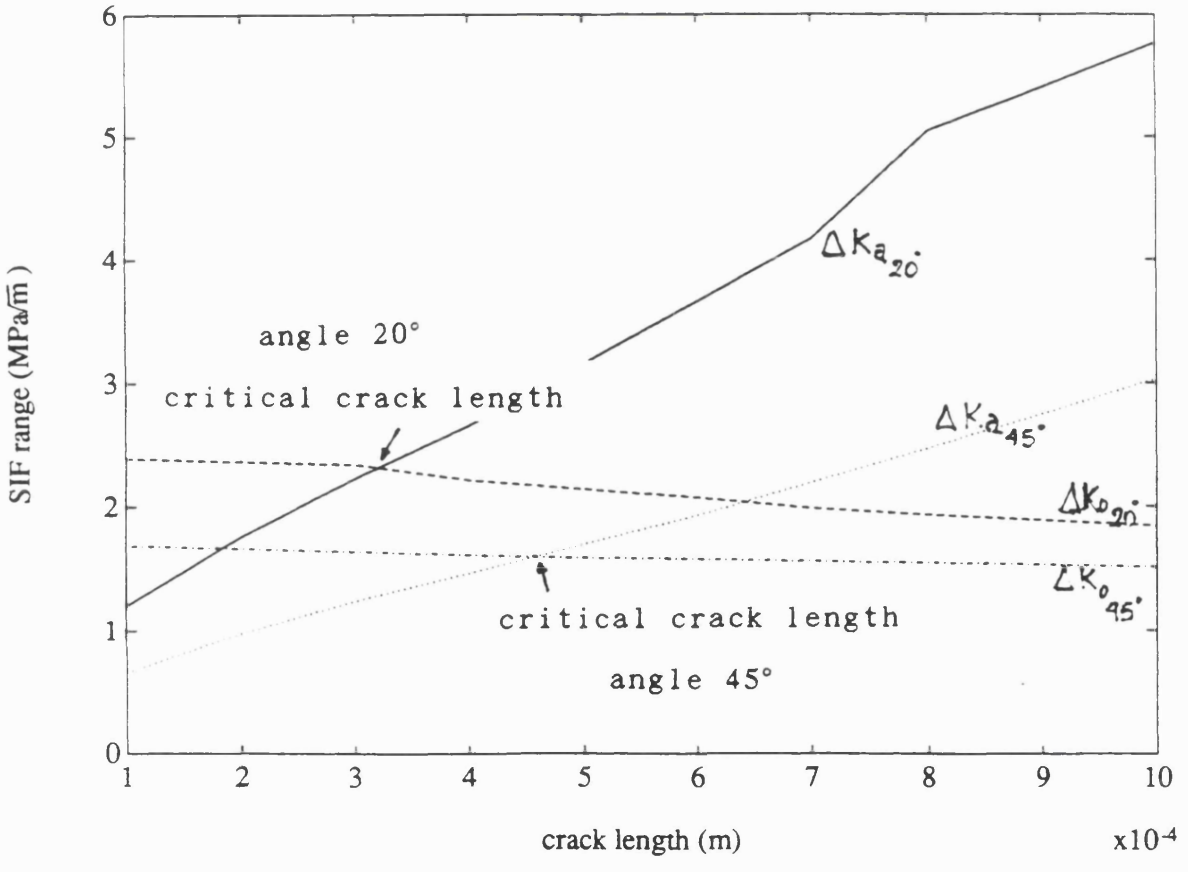

Figure 4.19 Critical defects sizes for contact pressures (a) 31MPa and (b) 139Mpa. The cracks are inclined at 20° and 45° under the fretting pads

4.4 Discussion

The main conclusions that can be drawn from the data given in Figures 4.17-19 are: First, the fretting reduces significantly the critical defect size, and second, contact pressure has little effect on the critical size; in fact a considerably higher contact pressure produces slightly longer critical crack lengths. Under fretting conditions, the curves show that both ΔK_a and ΔK_0 are modified and the critical crack length a_c can be reduced by a factor of two to three, compared to that shown in Figure 4.17. This is due to the depression of the ratio R, which tends to increase the active threshold SIF range ΔK_0 above its corresponding non-fretting value (Equation 4.11). Although one would thus expect a further increase in the critical crack length, the rise in the total range ΔK_a, due to the additional influence of the frictional force component ΔK_{fr} (Equation 4.3), brings about the demotion of the point of intersection of ΔK_0 and ΔK_a. The influence of the stress field induced by the pressing pad becomes thus obvious: it acts to increase the negative component K_n which depresses the total mean SIF (Equation 4.9) and consequently reduces the ratio R. It simultaneously increases the tangential (frictional) component ΔK_{fr}, which is dependent on the coefficient of friction, and hence the total mode-I SIF.

The relatively higher values of R for shorter cracks imply that short cracks should propagate faster than longer ones, since they effectively grow under higher positive stress ratios. This is reasonable, because it was found that the SIFs in fretting fatigue depend on the crack length and reduce with the diminishing influence of the fretting pad. So, the ratio R tends to decrease with increasing crack length under fretting conditions, whilst it is not dependent on the crack length for non-fretting conditions.

Higher pressing forces do not produce a proportionate increase in the critical crack lengths, since in the second case (139 vs. 31MPa) the critical crack length increased only marginally. Although the crack faces are forced to a crack closure

state, the effective range ΔK_a (which depends on the frictional force) still manages to force the crack open and reduce the critical crack length, hence the detrimental effect of fretting fatigue. The normal pressure, on the other hand, contributes mainly to a shear mode of crack extension, which is only significant for Stage-I cracks and it does not favour the tensile extension mode. The obvious engineering implications of this are well known, e.g. a "tighter" connection is preferable in pin-lug combinations or in "shrunk-on" components. In these cases the benevolent effect of tighter connections includes the reduction of the interface movement which can initiate fretting fatigue cracks, even though this influence cannot be quantified (Section 2.2).

If the angled effects are taken into account (Figures 4.19), the resulting critical crack lengths are invariably higher than those corresponding to normal cracks and increase with increasing crack angle under the pads. A crack growing at an angle is increasingly subjected to the compression stress field which is induced by the pressing pad, as implied from Figures 4.8-12 and the negative SIFs of Figures 2.9, and this of course does not favour its growth. Recalling that the experimentally found critical lengths were about 250μm, it seems that best agreement with the experimental data occurs when the model assumes normal cracks. A more plausible scenario, substantiated by the fractographic observations of the literature, is that the crack grew initially obliquely to the surface, but the angled part is very small compared to the critical crack length. The SIF analysis above still holds, because the kinked and normal cracks are approximately characterised by the same SIFs, as long as the angled part is shorter than about 1/4 of the overall length (Section 4.2).

The close agreement with experimental results showed that LEFM did not break down for the higher contact pressure, which apart from its influence to the crack tip condition, it could have introduced near-surface plasticity. It has been already mentioned (Section 2.6) that no absolute values for the "short" crack effects can be given, as these are dependent on the conditions of the particular experiment.

However for a qualitative estimation, according to Taylor's (1986) criterion, the crack length should be longer than 10 times the plastic zone in fatigue, expressed by Equation 2.5. For the problem at hand, the fatigue limit $\sigma_{y,c}$=135MPa (Lindley and Nix (1985)) and for $\Delta K \approx 2\text{-}3 MPa\sqrt{m}$ (the higher values of ΔK_a from Figure 4.18), the criterion dictates that the corresponding crack length for the LEFM to be valid be at least 80μm. This roughly coincides with the additional requirement that the crack be longer than 10*(grain size≈10μm)=100μm. However, the LEFM hypothesis should always be confirmed by careful experimental validation, as the underlying plastic zone mechanism is very complicated. The high stresses under the pads may lead to yielding of the material undermining the LEFM calculations, if the crack has not grown sufficiently into the bulk of the body, so that its overall length is much longer than the yielding zone size. Some reports in the literature claim that fracture mechanics studies produced good predictions even for cracks shorter than 0.1 mm (Section 2.4). For example, Tanaka *et al* (1986) found that they can make predictions for cracks as short as 12 μm by using Elasto-Plastic FM (EPFM) (J integral). Even though the EPFM principles can be applied for shorter cracks than the LEFM ones, the above crack depths are excessively short. Great care is therefore needed when the results from a particular materials development programme are used for design purposes and the particular conditions of the experiments must always be taken into regard.

It also transpires that the mode-II contribution is not as important in the stage where the crack has already grown away from the surface. This can be deduced from the second set of curves in Figures 4.18, from where we can see that the data derived by taking into account the mode-II effects do not differ from the others. In the initial stage, where the mode-II effects may be more important causing intense sliding of the crack faces, the crack is usually very small and the LEFM analysis fails. As mentioned, the application of a mixed mode criterion of propagation is extremely difficult for a fretting fatigue model. However, the procedure followed can be useful

when the dimensions of the specimen are much larger than a few millimetres. Again the reader is referred to the stress analysis Figures 2.9 and the SIF curves (Figures 4.1-14) where it is shown that the influence of fretting fatigue does not persist to large depths.

The discussion so far showed that an analysis based on fracture mechanics can adequately describe the problem of fretting fatigue. Fundamental to this analysis is the characterisation of the crack size. If a certain NDE method is to be implemented for this purpose, it should be able to answer whether the crack is length is less than its critical value, when the design philosophy requires "infinite life" of the component (the "energy industry" approach; Section 2.1.2). If crack propagation is of interest, the NDE method should provide the crack length data, so that a Paris type law can be applied for life predictions (the "airframe structures" approach) The development of an ultrasonics NDE method is the subject of the subsequent chapters of this thesis.

literature. It treats both forward and inverse problems in ultrasonics and particularly those using Rayleigh waves. Due to the complexity of the problem, the crack will be simplified as follows: Initial angle 45°, angled length d_1 and normal length d_2 (Figure 5.1). Note that in the subsequent analysis the slot angle is implied relatively to the surface of the specimen. The angled length can seriously change the scattering signature, because most of the energy of the incident Rayleigh waves is contained near the surface. This depends on the relation between wavelength and length of the angled part and will be a subject of investigation in this work. The specimen is considered to be a half-space, long in the z-direction (normal to the plane of the half-space), so that the present study is a two dimensional analysis of the problem. Additionally, it has been assumed that the transducer can only be placed on one side of the crack, as the other side is occupied by the fretting pads, under which the crack grows (Figure 2.5). The initial angle was chosen on the grounds of many observations of fretting fatigue cracks, as it was explained in the Introduction, but the basic arguments of the model can be extended to any angle. The crack faces are assumed to be open for the following analysis and any implications due to the crack closure will be discussed.

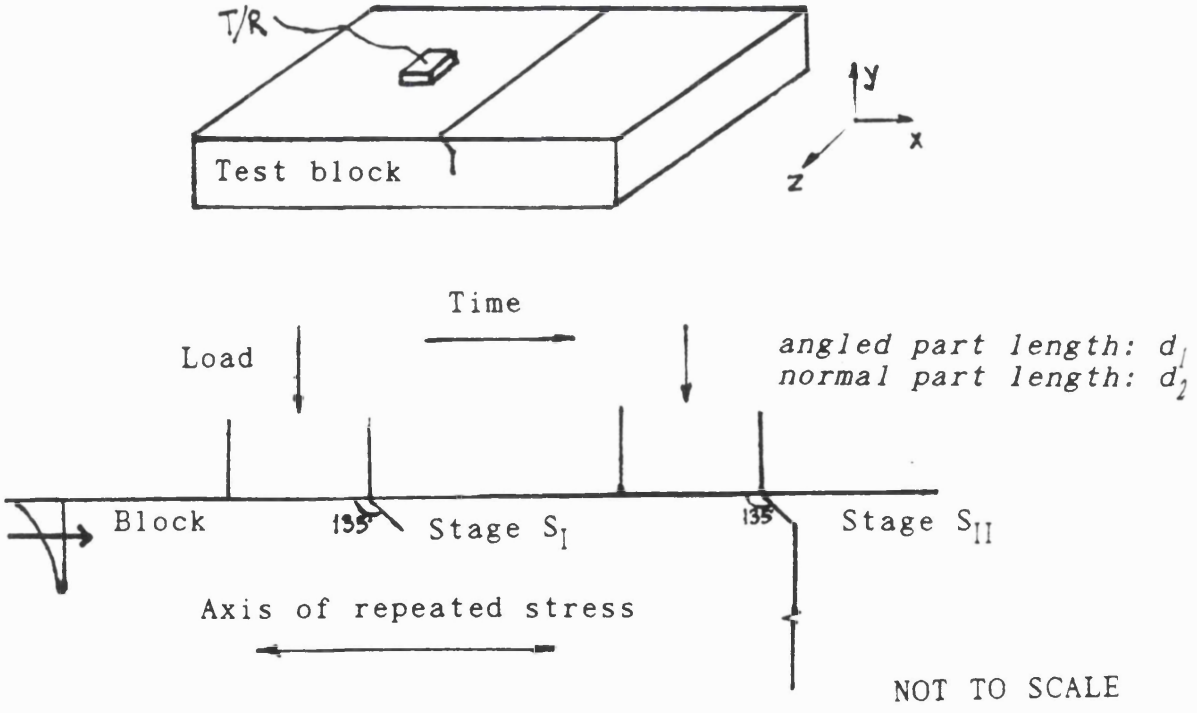

Figure 5.1 Modelling of fretting fatigue cracks

5. THEORETICAL AND EXPERIMENTAL BACKGROUND FOR THE RAYLEIGH WAVES SCATTERING

5.1 Introduction

Following the analysis of fretting fatigue cracks in the previous chapters, an ultrasonics testing method will now be examined with a view to determining the shape and the size of a kinked crack. For this reason, the response of a kinked crack will be compared with that of an angled and of a normal crack. The method of testing will make use of ultrasonic Rayleigh waves and the purpose of the analysis is to choose a suitable range of wavelengths, so that the initial crack growth stages can be monitored.

Rayleigh waves are attractive for investigating surface and near surface defects (Vu and Kinra (1981)). Their amplitude decays exponentially with the normal distance from the surface, retaining about 4% of its value at a depth equal to two wavelengths (Graff (1975)). Besides, they are non-dispersive in an isotropic homogeneous half-space and will travel for long distances without significant attenuation. Their amplitude decays with distance as $(k_R R)^{-1/2}$ (k: wavenumber, R distance from the emission source), while the analogous decay law for the body waves is $(k_{L,T} R)^{-1}$ (Viktorov (1967)). It is this property of the Rayleigh waves which makes them very useful in the area of non-destructive testing and evaluation and flaw detection in particular. (see Pao (1983) for a review of the elastic waves generally and Thomson (1983) for examples of Rayleigh waves applications).

This chapter deals with the background material against which this work was performed and discusses some methods of solution which are available in the

5.2 Equations of Motion for an Elastic Solid

Lord Rayleigh (1885) was the first to derive the equations describing the propagation of Rayleigh waves by solving the bulk wave equations subject to the boundary conditions imposed by the surface. Some properties of the Rayleigh wave propagation are given next. A more rigorous analysis can be found in Pao and Mow (1973) and Harker (1988).

Consider a particle in an elastic solid, whose position can be determined by the cartesian coordinates (x,y). We have assumed that there is no particle motion in a direction normal to the plane of the half-space and the free surface is characterised by y=0 (this coordinate system was chosen, because it is almost invariably used in the literature for surface waves propagation). In the absence of body forces, the displacement equation of motion for a linear elastic isotropic and homogeneous medium is: (Pao and Mow (1973)

$$\rho \ddot{u} = \mu \nabla^2 u + (\lambda + \mu) \nabla \nabla u \tag{5.1}$$

where ρ is the density and λ and μ are the Lamé parameters.

A non-trivial solution to the above equation is found by obtaining the so-called "Rayleigh Equation" *(ibid)*:

$$\eta^6 - 8\,\eta^4 + c_R^2 \left(\frac{24}{c_T^2} - \frac{16}{c_L^2}\right) - 16\left(1 - \left(\frac{c_T^2}{c_L^2}\right)\right) = 0 \tag{5.2}$$

where $\eta = c_R/c_T$ and c_R, c_L, c_T are the velocities of Rayleigh, longitudinal and shear waves, respectively. There is only one real root η_R of this equation that satisfies the decaying amplitude conditions and is usually approximated by the value: (Graff(1975))

$$\eta_R = c_R/c_T = (0.87+1.12\nu)/(1+\nu) \qquad (5.3)$$

For ν=0 to 0.5, the ratio c_R/c_T varies from 0.874 to 0.955. Especially for steel (ν=0.25-0.28) and aluminium (ν=0.33-0.34), the ratio c_R/c_T takes the values 0.92 and 0.93 respectively. Obviously the Rayleigh wave velocity depends only on the body waves velocities and consequently on the elastic constants of the material, while it is not a function of the frequency, rendering the wave non-dispersive. The particle motion consists of sine and cosine waves at right angles and has an elliptical path. Both components decay exponentially with depth and the rate of fall-off is greater for higher frequencies. The whole of the energy of the wave is contained in a layer closely to the surface of thickness only one to two wavelengths, making the Rayleigh waves ideal for the detection of surface and near-surface defects.

Another characteristic of the Rayleigh wave is that it is a combination of longitudinal and shear waves, balanced at the surface to satisfy the necessary boundary conditions. If a Rayleigh wave impinges on a defect, it will have to satisfy a new set of boundary conditions. This separates its constituent longitudinal and shear waves, which are then scattered separately. Thus, in addition to the directly scattered Rayleigh waves, a quantity of body waves will also be generated, which may recombine later to give another portion of the scattered Rayleigh wavefield. The phenomenon is termed mode-conversion (Bond and Saffari (1984b)).

It transpires that the Rayleigh waves velocity is very close to that of the shear waves, sometimes rendering the unique identification of Rayleigh waves in the time domain difficult (Table 5.1). For this reason in the case of NDE measurements, the transducer can be coupled at different distances from the target and displacement histories recorded. The various wave traces can be identified according to their relative arrival time and attenuation, as the body waves attenuate faster than the Rayleigh waves (Harker (1988)).

ν	c_T/c_L	c_R/c_T
0.00	0.707	0.862
0.25	0.577	0.919
0.33	0.500	0.932
0.40	0.408	0.941
0.50	0.000	0.955

Table 5.1 Elastic wave speed relations in terms of the Poisson's ratio ν (Harker (1988))

5.3 Rayleigh waves in NDE

5.3.1 Rayleigh waves scattering

Workers in the NDE area are interested in the interaction of Rayleigh waves with numerous geometries and, although there are no closed-form analytical solutions, a vast relevant literature is available (Doyle and Scala (1978), Bond *et al* (1984a), Bond and Saffari (1984b)). The Rayleigh waves which are employed for conventional contact testing of crack-like defects usually have wavelengths comparable to the anticipated defect size, namely of the order of a few millimetres, or frequencies of testing in the region from 0.2 kHz to 10 MHz. Frequencies up to 100 MHz are increasingly being used for commercial applications, such as acoustic microscopy (Som (1991)).

When a surface wave interacts with an irregularity, be it corner or crack, part

of its energy is reflected in the form of a surface wave, part is transmitted past the feature, also as a surface wave, and the remainder is propagated into the interior in the form of various bulk waves. The analytical treatment of this problem is very difficult. Further complications of geometric and algebraic nature are introduced when the medium under consideration contains other boundaries, as is invariably the case in "real-life" applications. In these cases, additional mode-conversion occurs rendering the situation extremely complicated. In general three scattering situations can be distinguished, depending on the relative size of the wavelength and the surface feature.

i) When the wavelength 'λ' is very much smaller than the main dimension of the surface feature 'd', namely $d/\lambda >> 1$, the Rayleigh wave can be viewed as following the smooth contours of the defect and being scattered only at sharp corners. Here, it is assumed that the wave interacts with each corner separately and achieves its asymptotic form in between these scattering events (Achenbach *et al* (1980)).

ii) When the wavelength is much larger than the inhomogeneity ($d/\lambda << 1$) much of the incident energy diffracts around the object and the pulse does not deviate much from its original path. Some perturbation and quasistatic approximation theories have been proposed in order to describe aspects of this problem (Glass *et al* (1981), Kino (1987)).

iii) When the wavelength is of the same order of size as the inhomogeneity ($d/\lambda \approx 1$), the scattered wave pattern is often complicated and very dependent on the characteristics of the defect, such as shape, position, orientation, size, material properties and surface state. Such a complex and sensitive inter-dependence on the defect features gives ultrasonic scattering in this region great potential for defect characterisation and this is thus the regime of most interest in ultrasonic NDE.

In practice, one has also to consider the factors which reduce the energy in an ultrasonic beam (Auld (1973), Kino (1987), Bray and Stanley (1989)). Attenuation

of ultrasonic beams may be due to transmission loses, interference effects and beam spreading. There are also losses due to generation of unwanted modes as well as coupling losses which greatly influence system response. One has also to consider the unwanted scattering which occurs because the material is not truly homogeneous, as there are grain discontinuities, inclusions etc. In general this effect is highly dependent on the relationship between (grain size)^3 and wavelength (Bond (1978)). When the grain size is less than 0.01 wavelengths, this unwanted scattering does not influence much the Rayleigh waves propagation. On the other hand, scattering is intense and non-destructive inspection may become impossible for grain sizes greater than 0.1 wavelengths. A similar adverse influence is due to the surface roughness which results in diffraction and noise signals. Unfortunately, apart from some trivial cases (Section 7.8.2) only qualitative guidelines can be provided for this case.

The basic difficulty for an exact solution of the problem of the Rayleigh waves scattering is introduced by the complexity of the geometry and the ensuing phenomena. Theoretically, the elastodynamic scattering problems belong to the general category of mixed initial boundary value problems. The stress free boundary conditions, which involve derivatives of the displacement field, are of the generalised Neuman type and the continuum equations are of hyperbolic form (Pao and Mow (1973). However, some analytical solutions for general simple elastodynamic problems can be found in standard texts (Eringen (1974) or Auld (1973)). The 2-D features which have attracted most attention are, in ascending complexity, the wedges, steps and troughs (slots and cracks). A brief description of the main features of interest in the field of ultrasonics testing will be presented in the following sections, along with the main methods for studying such scattering problems.

5.3.2 Scattering from wedges

The interaction of Rayleigh waves with a corner or infinite wedge constitutes the first major increase in complexity of the scattering geometry above that of a half-space. The problem is of interest of its own right, but also provides insight into the scattering mechanism of more complicated geometries, such as downsteps and slots. One of the earliest investigations of this problem was conducted by Knopoff and his co-workers (Hudson and Knopoff (1964)). They used a combination of Green's functions to describe the displacement field. Many other researchers (Bond (1978)) tried similar methods leading to integral transforms. Unfortunately the agreement between analytical theory and experimental results is generally poor, since it is very difficult to solve the resulting set of integral equations and the coupling of the wavetypes along the surface prevents the use of straightforward methods for the treatment of these equations.

Victorov (1967), in his classical text, presents various experimental results for the wedge problem. The general conclusion is that the Rayleigh wave interaction with the corner gives rise to reflected and transmitted Rayleigh waves and produces additional bulk waves which represent losses from the energy of the Rayleigh waves in the system.

Since there is no characteristic dimension in the problem of Rayleigh waves scattering at a corner, the reflection and transmission coefficients are independent of the wavelength and therefore of frequency. The coefficient values vary with the wedge angle θ (Section 7.8.2). As θ approaches 180°, the reflection coefficient approaches zero and the transmission coefficient approaches the unity, as it is expected.

Numerous investigators have utilised numerical techniques to compute the reflection and transmission coefficients and phase changes upon transmission and

reflection at the corner in a quarter space and due to a step change in elevation. These methods have provided invaluable data for the study of the interaction of a wave with a feature, no less because they allow a real time visualization of the incurring phenomena. Pure finite difference schemes with pulsed Rayleigh wave initial conditions have been developed by Munasinghe (1973) and Bond (1978, 1979), while a hybrid finite element/finite difference scheme has been used by Blake (1988) and Blake and Bond (1990a-b, 1992). Among recent efforts for developing a numerical method for the solution of the integral equations arising from the application of Fourier transform techniques are those of Momoi (1985) for a 270° degree wedge. Also, Gautesen (1987) has found very useful results for various wedges and values of Poisson's ratio. He used a Green function to generate a boundary integral formulation and solved the problem of obtuse wedges by employing a numerical method similar to that presented in the first part of this thesis (Erdogan *et al* (1973)). His results, given in graphical form can be used when a single coefficient of transmission or reflection is needed in a ray theory analysis.

The most studied of wedges is the 90° corner. It can be used as reference for experimental studies, due to its frequency-independence. A selection of the transmission and reflection coefficients for a 90° corner as a quarter-space, and for different materials is given in Table 5.2. The value for the reflection coefficient cited by Victorov seems rather high, and has since been found by most researchers to be about 0.40.

Attention is also drawn to the normalized scattering cross section of a crack $\gamma_N=1-R^2-T^2$, where R and T are the transmission and reflection coefficients, respectively (Kinra and Vu (1985-1986)). With the values of R and T from the Table 5.2, γ_N is about 0.43-0.50. This suggests that when a Rayleigh wave interacts with a quarter-space, approximately half of the energy is radiated in the form of mode-converted body waves; the remainder is transmitted and reflected in the form of Rayleigh waves. This observation may be useful in the field applications of NDE

for the calibration of the required power of the related instruments.

Author	Poisson's ratio ν	Reflection coefficient	Transmission coefficient
Victorov (1967) experimental	0.34	0.60	0.70
Bond (1979) Numerical	0.34	0.47±0.05	0.59±0.05
Bond (1979) Experimental	0.34	0.36±0.02	0.60±0.01
Achenbach *et al* (1980) Ray theory	0.33	0.40	0.60
Kinra and Vu (1985) Experimental	0.34	0.43±0.02	0.59±0.03
Gautesen (1987) Analytical	0.33	0.40	0.60
Gautesen (1987) Analytical	0.25	0.35	0.68
Blake (1988) Numerical	0.25	0.35±0.05	0.68±0.05

Table 5.2 Reflection and Transmission Coefficients for a quarter space

5.3.3 Scattering from Steps

The next level of complexity in the scattering geometry is that of a step and this introduces spatial dimensions in the form of step height. Here, unlike the wedge geometry, the spectral scattering coefficients are strongly dependent on the Rayleigh wavelength and step height 'd' (Munasinghe and Farnel (1973)). The step length to wavelength ratio d/λ is important in determining the precise form of the scattered wavefield.

If d/λ is small, the problem can be solved by perturbation techniques, since the feature can be considered as a minor deviation from the half-space geometry. For large d/λ ratios (usually larger than 2), multiple scattering techniques can be employed to calculate a good approximation to the overall scattered wavefield. The incident Rayleigh wave interacts first with the top corner, travels down the step and subsequently interacts with the bottom corner (Achenbach *et al* (1980)).

An analysis of the scattering in the mid-frequency regime (d/λ in the range from 0.2 to 2) can only be attempted with numerical methods. The partial differential equations are discretised and then integrated along parallel lines in the time direction (Munasinghe and Farnell (1973)). These discretisation methods (finite element/difference) are very useful as they help explain phenomena which occur in the interaction of Rayleigh waves with cracks of similar dimensions (Blake and Bond (1990a,b)).

5.3.4 Scattering from slot-like defects

Cracks are usually modelled either as slots or as troughs, where there is the additional parameter of the width 'w' of the feature. When this width 'w' tends to become zero at the bottom of the slot, then the configuration approaches that of the

crack tip. Due to the complexity of the problem, most authors have removed the angle and curvature variables from the crack problems.

Visscher (1986) applied a boundary integral method which gives better results for the low frequency regime, as did Zhang and Achenbach (1988) for an inclined surface-breaking crack. Kino (1978) and Auld (1979) adapted the reciprocity relations and the scattering matrix formalism of the electromagnetic theory to obtain formulas for scattering of elastic waves from flaws. However, their results are only valid for the long wavelength regime.

Various numerical studies have been also performed (Bond (1979), Georgiou and Bond (1987) and Blake and Bond (1990 a,b-1992)). These make use of the finite difference and/or element method, with considerable success, as it will become evident in the analysis of the experimental data of this work. Also, Datta and Shah (1987) used a hybrid technique combining a representation of the scattered field in the half-space with the finite element method. This allows them to deal successfully with complicated geometries (non-planar and branched cracks).

Another approach to the same problem is a spectral technique based on the elastodynamic ray theory, which was developed mainly by Achenbach, Gautesen, Mendelsohn and co-workers after 1978 (Achenbach *et al* (1982)). The Achenbach group investigated the scattered field generated by either body or Rayleigh waves incident from a point at infinity upon a normal crack. Also, Doyle (1986) and Doyle and Scala (1987,1990) have employed a similar method to tackle various crack geometries in corners. They examined the Rayleigh waves interaction with a crack of an arbitrary angle at a corner and presented reflection and transmission coefficients for these geometries. In the spectral technique, the total field in the cracked half-space is considered as the superposition of the incident field in the uncracked half-space and the scattered field in the cracked half-space generated by the surface tractions on the crack faces. These tractions are equal and opposite to

the tractions which are due to the incident field in the unscattered half-space. The total field is written as $u^t=u^i+u^s$, where the superscripts denote the total, incident and scattered field, respectively. Due to the substantial computational effort required to obtain the exact solution of the resulting equations, the authors have resorted to the ray theory to solve the scattering problem (Achenbach *et al* (1982)).

Strictly, the ray theory can only be applied to problems in which the crack length is much longer than the wavelength, hence it is valid for $d/\lambda>>1$. Under this condition, the reflection and transmission coefficients exhibit an oscillation with 'kd', where 'k' is the wavenumber. In terms of the inverse NDE problem, this finding is very important, since it allows the characterisation of the crack length by simply measuring the spacings between the successive peaks or valleys in the spectrum. The spacing ΔK (or Δf, in terms of frequency), is connected with the crack length 'd' by the simple relation:

$$\Delta(kd) = \pi \quad or \quad d = \frac{C_R}{2\Delta f} \qquad (5.4)$$

As the modulations are of periodicity such that a half wavelength corresponds to the crack length, they can be attributed to the destructive and constructive interference phenomena, due to the Rayleigh waves reflected from the top and bottom of the slot (Achenbach *et al* (1980), Saffari and Bond (1987b)). The signal is maximum at slot lengths equal to odd numbers of half wavelengths and minimum at even numbers. The spectral technique will be employed in the next Chapters for evaluating the crack length in idealised fretting fatigue cracks and the implications of a NDE method based on Rayleigh waves will be discussed.

The review so far referred to modelled 2-D features. The analysis of 3-D cracks is more complicated, but numerous efforts have been made for their characterisation, especially by using the quasistatic approximation and Born inversion (Kino (1987). For the interaction of surface waves with "real" fatigue

cracks the reader is referred to the works by Weston-Bartholomew (1981a,b) for the prediction of fatigue failure, and Hirano *et al* (1987) and Buck *et al* (1990) for the monitoring of crack tip closure behaviour. Some recent Russian work on this subject is reported in Damaskin *et al* (1991).

5.4 Experimental procedures for contact measurements

5.4.1 Contact techniques

The development of quantitative experimental methods for non-destructive evaluation has been hampered by the lack of adequate explanations of the phenomena which take place during the Rayleigh wave/defect interaction. Nevertheless, from the insights gained from the theoretical and numerical models, many of the proposed defect characterisation techniques can be better evaluated. On the other hand, ultrasonic measurements can provide valuable data for the validation of the various theoretical explanations of the complex scattering phenomena.

In ultrasonic NDE, all the contact measurement techniques involve transmitting an ultrasonic stress wave in the medium under test (Coffey (1980)). In this way, any defect in the medium can be detected by measuring the portion of stress wave scattered by the defect. The simplest way is by comparing the amplitude of the scattered wavefield with those from reference features (Doyle and Scala (1978)).

Contact measurements are liable to errors and in most cases the technique requires a high degree of patience and care to make the results reproducible. Conventional ultrasonics testing, in contrast to the laser ultrasonics, requires coupling between the specimen and the probe. The acoustic coupling is normally

accomplished in any of the following three ways:

1. By placing a thin ($\approx\lambda/100$) film of liquid couplant (e.g. oil or grease) over the surface of the part to be tested. The piezoelectric probe is then pressed onto the part. The technique is simple, but it needs careful calibration to give lowest attenuation and reproducible signals. The thickness and viscosity of the film cannot usually be uniform and therefore the coupling sensitivity varies. Besides, the pulses incident on the thin film are multiply reflected at the two interfaces bounding the film. This extends the incident pulse length and changes its amplitude, due to interference amongst the multiply reflected components (Coffey (1980)).

2. By immersing the part in a liquid medium. In this case, the piezoelectric transducer radiates acoustic energy through the medium and into the part. The method needs precise separation of transducer and specimen, so that multiple reflections from the specimen surface do not interfere with any signal of interest (Coffey (1980), Bond and Saffari (1984)).

3. By placing a piezoelectric transducer inside a nozzle which directs liquid couplant onto the surface of the tested part; acoustic energy radiated from the transducer is waveguided along the liquid stream onto the surface of the part. See also texts like Krautkrämer and Krautkrämer (1983) and Harker (1988) for special transducer arrangements for railways, gas pipes etc.

A relatively new technique, that provides at least a partial solution to the couplant problems, is the generation of ultrasound by laser (Scruby *et al* (1982)). This is a noncontacting method, that can be used remotely in hostile environments and on awkward-shaped specimens and also provides reproducible waveforms and amplitudes. However, it is at present more expensive and less portable than the conventional methods. Moreover, the generation of large signal amplitudes might cause surface damage and, most important of all, the method is hazardous to health and needs special laser safety precautions.

In the following a brief description of the main techniques for sizing surface

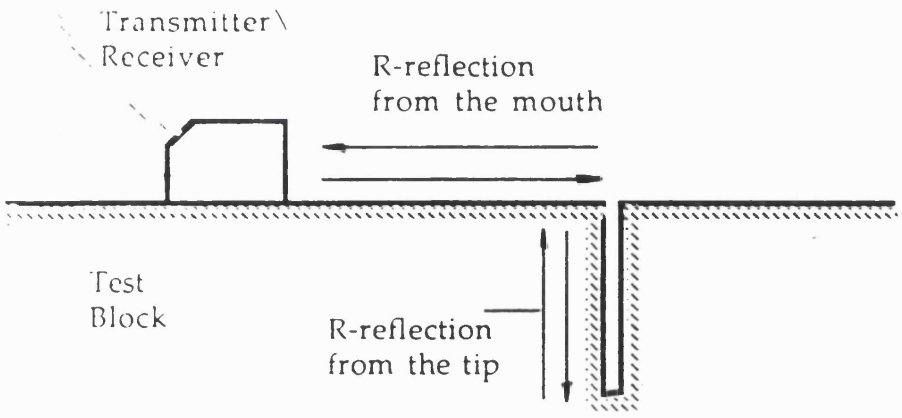

R=Rayleigh pulse

Figure 5.2 The pulse-echo approach to sizing surface defects

defects is given. In the pulse-echo method (Figure 5.2), one transducer is used for both transmitting ultrasonic pulses and receiving the returning echoes. The essence of the pulse-echo method is that it is possible to separate the Rayleigh wave pulses reflected from each feature of the defect and thus calculate their relative distances according to the arrival time of the corresponding Rayleigh pulse.

If there is access to both sides of a known crack, two transducers can be placed, one on each side of the defect (Figure 5.3). When a single Rayleigh pulse from the first probe interacts with the crack, the second transducer first receives the faster body waves scattered from the crack tip and later a second pulse due to the Rayleigh waves along the free surface. This pitch-catch type of measurement allows the crack length to be determined from the difference in time between the arrival of the Rayleigh waves in an uncracked surface and a cracked surface. The method is also efficient for spectral measurements, because, the modulation in the spectra are often more evident in the transmitted pulse than in the reflected one (see discussion in Section 6.2.3). The main drawback with the method is the identification of the

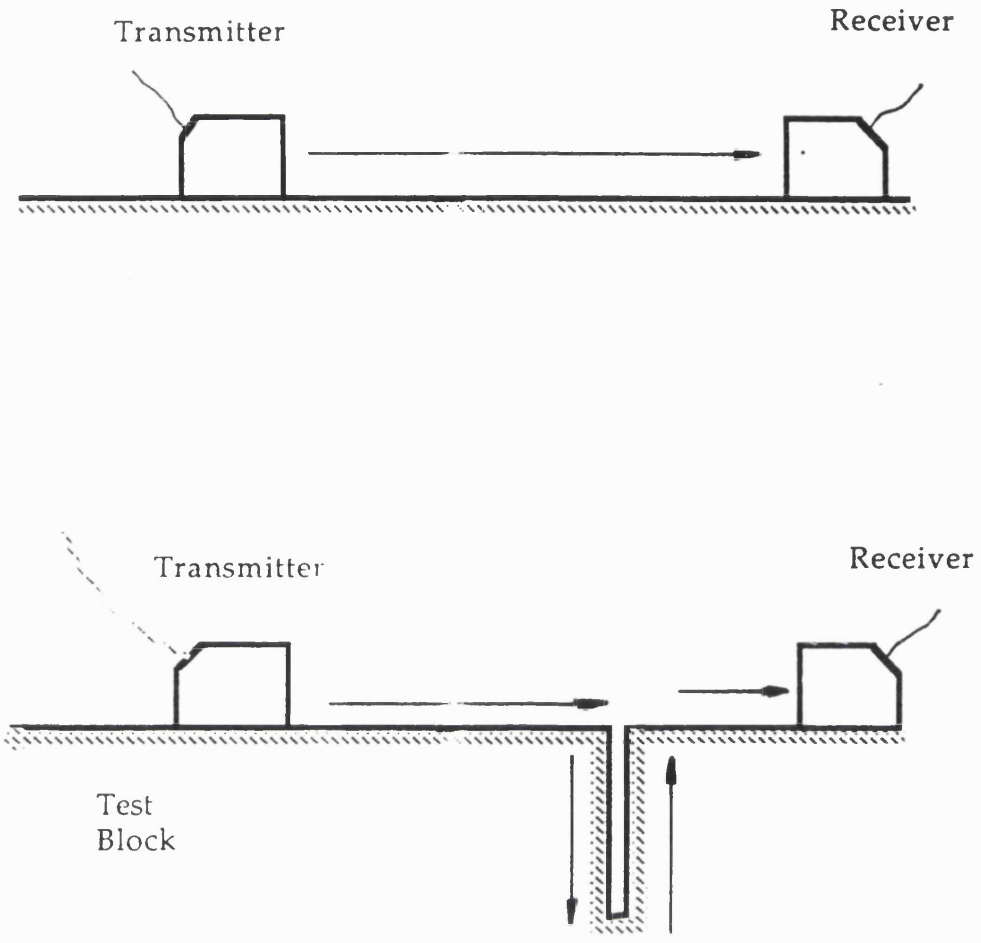

Figure 5.3 The Rayleigh waves transmission approach to sizing surface defects

Rayleigh wave which has been transmitted along all the surfaces of the crack, because additional types of wanoves are generated at the crack tip and edges due to mode-conversion. Also, the energy reaching the receiving transducer is usually very low due to the multiple scattering events that the Rayleigh waves undergo while transmitting past the crack. Besides, the problems associated with the experimental variables, such as coupling and transfer characteristics of the transducers and surface condition, can be more intense in this type of testing. An advantage of the method is that can be used to measure the depth instead of the length of the crack and consequently its inclination to the surface. This approach has been proposed by Silk (1977) and makes use of the arrival time of the shear wave originating at the tip and

reaching the receiving probe through the bulk of the body. However this technique has only been used for conveniently deep (22-30mm) cracks.

One of the problems in all contact measurements is to identify the Rayleigh wave and choose the right window for gating. If other type of waves arrive within the gate, they will modulate the Rayleigh waves amplitude from the features of the crack and perhaps obscure some of them. For this reason, a careful investigation into the nature of all the echoes appearing in the time domain traces is important. Indeed, numerical visualisations (Blake (1988)) showed that the body waves generated at features of the crack tend to interfere with the transmitted Rayleigh pulse. Similarly, Yew *et al* (1984) and Saffari *et al* (1987b) recorded shear waves generated at the crack tip, which eventually immerse at the surface as Rayleigh waves, after being mode-converted there. A discussion on these phenomena is given in Section 7.7.3.

If the measurements are conducted in a plate rather than in half-space, there is a back wall reflection and a variant of the previous time-of-flight methods has been proposed by Hudgell *et al* (1974) and verified by Silk (1977) and Tittmann and Buck (1980) (Figure 5.4). The Rayleigh wave travelling down the first face of the crack, mode-converts into a shear wave at the tip, travels through the bulk of the body, reflects back at the back-wall and eventually converts again to Rayleigh wave at the crack tip. The transit time between the echo at A and the echo from the back wall is:

$$\Delta T = \frac{2d}{c_R} + \frac{2(t-d)}{c_T} \qquad (5.5)$$

The crack depth can be determined by precision measurement of ΔT and plate thickness t. However, this model is valid when $d/\lambda > 1$, a condition not readily accessible in most practical applications. The major difficulties are due to very small difference between shear and Rayleigh wave velocities (Table 5.1), which make the unequivocal interpretation of the signals difficult in some cases.

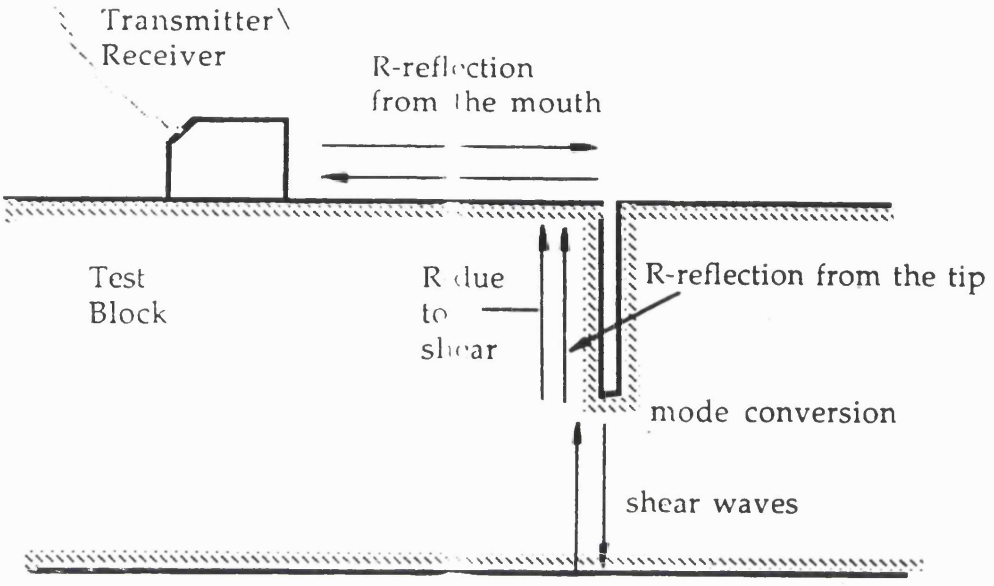

Figure 5.4 The Rayleigh waves interaction with a surface crack in a plate (after Hudgell et al (1974))

Recently, Saka *et al* (1989) employed shear waves to study partially closed fatigue cracks. The first and second back wall echoes were used instead of the weak crack-tip echo for the measurement of the time-of-flight. They found that the time-of-flight changes proportionally to the ratio of the crack depth to the specimen width. The method proved successful for tightly closed fatigue cracks in austenitic stainless steel.

It must also be added, that there are numerous examples in the literature, where the practical implications of the Rayleigh wave scattering demand that more than one techniques be employed and complement each other to give adequate explanation. For example, Saffari *et al* (1987b) combined the finite difference method with experimental results from laser generated Rayleigh waves, trying to interpret the various forms of the waves scattered at a slot. Also, Bond and Taylor

(1991) combined three techniques in their effort to analyze the interaction of Rayleigh waves with a rib on a plate: finite differences numerical simulation, an energy partition model and wave arrival time measurements.

5.4.2 Ultrasonics spectral techniques

There has also been a significant development in the spectroscopic defect sizing methods. When the ratio $d/\lambda \approx 1$, the various scattered signals which are captured by the receiver, overlap or interfere with each other, being so closely mixed that they cannot be considered as due to separate scattering events. In these cases, the spectroscopic analysis technique can be applied as a useful method of defect characterisation (Fitting and Adler (1981)). By employing digital spectral analysis, the time signal can be decomposed into its frequency components using a computer or a special-purpose hardware. The basic assumption behind spectroscopy is that a frequency-domain description is likely to reveal important information which is not apparent in the time-domain signal.

These techniques are based on the observation that when a pulse which is emitted from a broadband transducer hits a defect, then each of the frequency components it contains interacts independently with the defect. In addition, echoes from different scattering centres in a small defect, which overlap in the time signals, produce a periodic modulated structure in the frequency domain, which can be of interest for the defect characterisation. In practical measurements, a Fast Fourier Transform (FFT) is applied to the time domain signal of the gated scattered waves and the transducer response deconvolved from it. The comparison of the pulse spectra before and after interaction, yields information about the defect size and orientation. This information is contained in both the phase and the amplitude spectrum of the pulse.

The advantage of the spectroscopic technique is that the locations of the maxima and minima of the amplitude spectrum are determined expediently and with a high degree of accuracy. However, the general amplitude errors in the spectroscopic measurements are significantly larger than those of other methods, like the tone-burst method (Vu and Kinra (1981)), which can be more accurate in determining the magnitude of the amplitude spectrum. An extensive study of the overall spectral response of a two-dimensional pulse-echo system can be found Stepanishen (1981), who established a transfer-function model by combining the transducer and the acoustic media response.

Furthermore, Singh and Singh (1981) used the photoelasticity method (analogous to that used by Zachary *et al* (1979)) in conjunction with standard FFT techniques to obtain frequency spectrum data from the diffracted Rayleigh waves at an edge crack. They reached the useful conclusion that Rayleigh waves of wavelength equal to the penetration depth (≈1.5 wavelength) and less are substantially reflected by the leading face of the crack. Besides, a portion of the low frequencies in the broadband pulse, which have wavelengths significantly longer than the crack depth, will cut under the crack and continue across the surface with little interaction. The crack can thus be considered as a low pass filter with cut-off close to the frequency that corresponds to the penetration depth. However, it is extremely difficult to isolate a selected portion of the Rayleigh wave which contains the desired information.

Another spectral technique, called the cepstral method, has been used by Morgan (1974). His object was to determine the shape of defects with complicated contours. The important property of this technique is the second transform of the spectrum of the reflected signal back into the time domain, after taking out the system response. The information about the defect contour could be obtained from the resulting signal in the time-domain, the so-called "cepstrum". In it the peaks due to the reflection at different points on the defect contour are supposed to be

separated, as the signal can now loosely be considered as a "cleaned up" equivalent of the original signal. Unfortunately, the limited frequency bandwidth of the Rayleigh wave transducers do not easily provide sufficiently short pulses to separate the expected echoes from small slots (Cooper *et al* (1986)) and the method has not gained wide acceptance in terms of NDE applications. It is however used in other fields, for example in Geology (Fitting and Adler (1981)).

6. THEORETICAL AND EXPERIMENTAL MODEL OF THE RAYLEIGH WAVES CHARACTERISATION METHOD

6.1 Introduction

In this chapter a theoretical analysis is first presented based on the interaction of time harmonic elastic waves with an edge crack. The problem at high frequencies ($d_1/\lambda>1$) can be decomposed into a number of canonical problems whose solutions are available in the literature. The resulting solutions are valid at a frequency range which includes some cases of practical importance, at least for some 'longer' fretting fatigue cracks, which can be examined at sufficiently high testing frequencies, without considerable complications due to surface roughness and materials grain size. In any case, the findings from the high frequency study help significantly the interpretation of the whole scattering problem.

Next, a experimental spectral ultrasonic technique is utilised to complement the time-domain considerations. The basic assumption underlying spectral analysis is that a frequency-domain analysis is likely to reveal important information which is not directly apparent in the time-domain signal. In Section 6.3, a description of the experimental configuration is given. The specimen, transducer and data-capture apparatus are described and then the method which was employed for the experimental study of the scattering by kinked cracks is presented. The aim is to explain the reasons for the choice of the particular testing parameters and to highlight some problems which were encountered in the process. The interdependence between some parameters will also become obvious. The results of the measurements and the discussion on them are reported in the following Chapter 7.

6.2 Spectral techniques for depth measurements

6.2.1 Normal and angled cracks

It was mentioned in Section 5.3.4 that Achenbach *et al* (1980) proposed a simple spectral technique for crack length measurement, based on the elastodynamic ray theory, which holds true for $d/\lambda>1$. For this range of frequencies, a solution for the Equation (5.1) for waves travelling in the x-direction, giving the Rayleigh wave displacement at the point $x\vec{i}+y\vec{j}$ can be expressed as:

$$u_i = A\, e^{ikx}\, (\vec{i}+\tau\vec{j}) \tag{6.1}$$

In Equation 6.1, $\tau=\cot 2\theta^T$ and wavenumber $k=2\pi f/c_R$. The Rayleigh wave is composed of longitudinal and shear components, each incident at purely imaginary angles θ^L and θ^T respectively. These are related to the longitudinal and transverse wave speeds by:

$$\frac{\cos\theta_L}{c_L} = \frac{\cos\theta_T}{c_T} = \frac{1}{c_R} \tag{6.2}$$

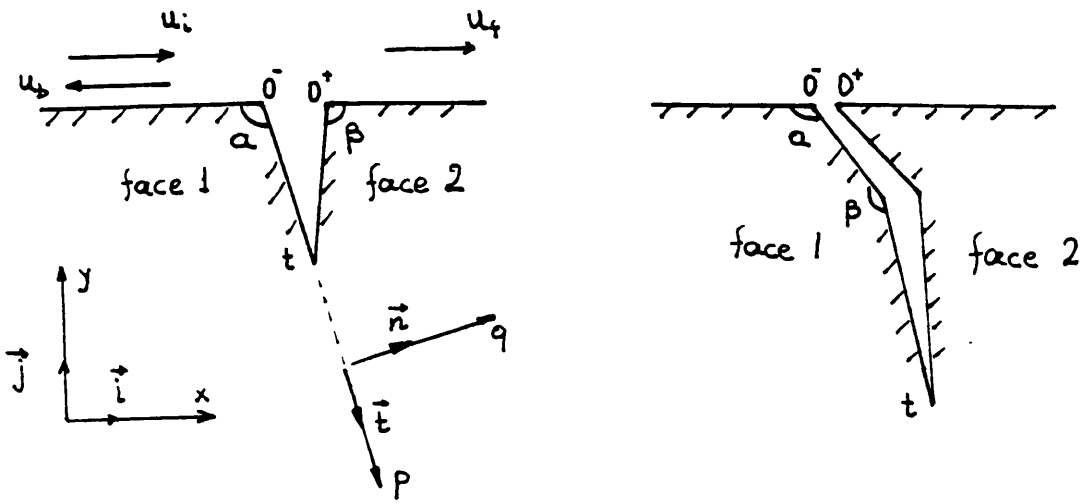

Figure 6.1 Coordinates system for the ray theory analysis

Consider now a Rayleigh wave with surface displacement u_α impinging on an angled crack. Let R_α and T_α be the reflection and transmission coefficients respectively for the crack edge corner α at O^-, which is the first feature of the crack that scatters the incident Rayleigh wave. The crack tip is characterised by the corresponding coefficients R_t and T_t and the other crack edge corner at 0^+ by R_β and T_β. The back-scattered wave u^b is the sum of the wave u^r_o, which is reflected by the edge corner at O^-, plus those waves which are subsequently reflected back to the surface by the features of the crack and include a contribution from the crack tip. Consequently, the backscattered wave is given by:

$$u^b = u^r_o + \sum_{n=0}^{\infty} u^r_n \tag{6.3}$$

Strictly speaking, we should have added a term u_{diff} at the end of Equation 6.3 which is due to the diffraction of Rayleigh waves. The wavefront of the incident wave, exponentially damped for $y<0$, impinges on the crack tip and mouth, producing directly diffracted bulk and surface waves. These additional surface waves can be found by treating the incident Rayleigh wave as a sum of longitudinal and shear waves and then using results available for the canonical problem of the bulk waves diffraction by a straight edge (Achenbach *et al* (1980, 1982). The resulting diffraction corrections u_{diff} involve damping factors, which decay exponentially. This damping results in no significant influence by the diffraction corrections for crack lengths such that $d/\lambda>1$ (Doyle (1986)). Therefore, the influence of the edge diffraction can be ignored for the present high frequency approximation, whereas for low frequencies the whole reasoning of the geometrical approximation for crack measurements breaks down *(ibid).*

By moving the origin of the coordinates to the crack mouth, we have from Equation (6.3).

$$u^r_o = AR_\alpha H(-x) U^r_o \tag{6.4}$$

with

$$u^b = A[R_\alpha + T_\alpha^2 R_t e^{2ikd} + T_\alpha^2 [R_\alpha R_t^2 + R_\beta T_t^2] e^{4ikd}] H(-x) U^r{}_O \tag{6.8}$$

where the terms pertaining to the second wave arrivals from the crack tip have been multiplied by T_α to transmit back to the surface.

In a similar way, the transmitted wave is given by:

$$u^f = A T_\alpha \, T_t \, T_\beta e^{2ikd} * [1 + R_t \, (R_\alpha + R_\beta) \, e^{2ikd}] H(g) W^r{}_O \tag{6.9}$$

where the last two factors refer to the transmitted wave at a distance g from O^+. The second order contributions are due to waves whose route was back to 0^- and crack tip respectively, after their reflection at 0^+ .

It is interesting to notice that u^f does not alter by the interchange of α and β, that is the Rayleigh wave transmission is indifferent to which crack side faces along its path, whereas u^b does depend on the first angle choice (Kinra and Vu (1986), Doyle and Scala (1990)). The simple spectral technique which was expressed by Equation 5.4 and relates crack depth to the spacing of the interference fringes in the frequency spectrum can now be inferred by examining Equations 6.8-9. The frequency enters in them only through factors e^{2imkd} for an integer m. Therefore, the spacing Δk of periodicity in spectra is governed by crack depth via $2\Delta kd = 2\pi$ (Equation 5.4) or in terms of frequency f: $\Delta f = c_R/2d$. Note that in Equations 6.8-9 the omitted higher order terms will also involve 'd' only via integral powers of e^{2imkd}.

Doyle and Scala (1990) in their analysis of angled cracks in corners extended the normal crack model of Achenbach *et al* (1980). Instead of considering a coefficient R_t at the crack tip, they assumed the existence of symmetric and antisymmetric waves generated at the crack tip. Their configuration leads to some lengthy calculations for the determination of the scattering parameters at the crack

tip, according to an asymptotic model developed in the original paper by Achenbach *et al* (1980). However, the model can equally well be described in the way just reported, by using at the crack tip the reflection coefficient given by Freund (1976): R_t=0.085. In any case, the usefulness of this method for crack length measurements is not dependent on the knowledge of the absolute values of the reflection coefficients of each corner (tip, mouth) of the crack, but on frequency considerations. As crack length may be determined by simply measuring the spacing between successive fringes in the frequency spectrum according to Equation 5.4 the exact knowledge of the values of the reflection coefficients plays no significant role.

6.2.2 Kinked cracks

In this case additional scattering occurs at the knee of the crack. The back reflected wavefield can be expressed by a relation similar to Equation 6.8, where the reflection and transmission coefficients with subscript β now refer to those of the knee corner and the crack length corresponds to the angled part length d_1. There is also an additional term due to the reflection from the crack tip (distance travelled: $2d_1+2d_2$)) and the whole equation is now given by:

$$u^b = A[R_\alpha + T_\alpha^2 R_\beta e^{2ikd_1} + [T_\alpha^2 R_\alpha R_\beta^2 e^{4ikd_1} + T_\alpha^2 T_\beta^2 R_t e^{2ikd_1+2ikd_2}]\ H(-x)U^r{}_o \qquad (6.10)$$

Clearly, the frequency in the exponents of 'e' is no more entered exclusively through factors which are multiplied by d_1, like the factors e^{2imkd} of the previous case. The last term, being a function of d_2, should further modify the spectrum modulations due to d_1. It must hold $d_1/\lambda>1$, so that the regular interference fringes referring to the angled length d_1 become evident. Additionally, the wavelength λ should be less than d_2 for the modulations due to the crack tip reflections to be superposed on the fringes which characterise the angled part reflection coefficient. Further discussion is reported in Section 7.7.1

6.2.3. Discussion

Before the experimental investigation, the implications of some of the findings of the above analysis will be discussed. It is repeated that the whole analysis holds for high frequencies, so that the reflection coefficient between the scattering events attains its frequency-independent value for the corresponding corner (Section 7.7.1). The reflection and transmission coefficients for infinite wedges or corners of angle α and β can be taken from Gautessen (1987), although they are not always in exact agreement with the experimental results of Viktorov (1967). For a specific corner angle, both coefficients depend only on the Poisson's ratio ν of the particular material (see discussion in Section 7.8.3 and Figure 7.21).

It was earlier mentioned that reflections beyond the second order ones are minute. This can be obtained for a normal crack ($\alpha=\beta=90°$) as follows: the incident pulse first interacts with the leading edge of the crack, which it "views" as a 90° corner ($R_{90}=0.4$, $T_{90}=0.6$, Table 5.2). The pulse is subsequently transmitted past the apex of the corner and is reflected from the crack tip with a reflection coefficient of $R_t=0.085$, from a sharp 360° crack tip (Freund (1976)), or $R_t=0.10$ from the first 270° corner at the rectangular "tip" of a slot simulating a crack (Bond (1978)). The second reflected pulse must thus consist of multiple scattering contributions to the reflected wavefield and its amplitude is estimated as: $(T_{90})(R_t)(T_{90})=(0.60)(0.10)(0.60)\approx 0.036$, namely about 10 times smaller than the amplitude of the first reflected signal $R_{90}=0.40$. The corresponding amplitudes of the pulse from the second order reflections are $(T_{90})^2(R_{90})(R_t)^2=(0.60)^2(0.40)(0.10)^2=0.001$ and $(T_{90})^2(R_{90})(T_t)^2=(0.60)^2(0.40)(0.18)^2=0.005$ (value of $T_t=0.18$ from Freund (1971)), which are much smaller than the reflection coefficient of the leading angle. Referring to Equation 6.8, it becomes clear that there is no need for the introduction of higher order terms, as the contribution from returning waves which are subjected to more scattering events, is indeed tiny.

For angled cracks, if α=135°, then R≈0.12, T≈0.60 (Kinra and Vu (1986), Gautessen (1987)). The first arrival of the waves reflected by the crack tip has amplitude $T^2R_t=(0.60)^2(0.10)=0.036$, which is now a fairly big value relatively to the first reflection R=0.12 (about 1/3 of it).

For kinked cracks with $\alpha=\beta$=135°, the amplitude terms in Equation 6.10 become approximately:

0.120 for the first reflection from 0

0.043 for the reflection from the knee point

0.013 for the reflection from the crack tip

0.0006 for the reflection from the waves travelling up and down the length d_1. The reflection from the knee point should yield some visible ripples on the main reflection coefficient 0.120, having amplitude equal to about 1/3 of it. The case is analogous to that of the last paragraph, if one considers for a moment that the role of the angled slot is taken up by the angled part of the kinked slot. As already mentioned, the returning echo from the crack tip introduces another periodicity in the scattering. While the spacing of the interference fringes pertaining to the knee point is $\Delta f_1=c_R/2d_1$, the fringes due to the crack tip are superposed on the former with regular spacing $\Delta f_2=c_R/(2d_1+2d_2)$. In practice, very careful measurements should be taken, because the amplitude of the returning echo from the crack tip is almost ten times smaller than the first return from the crack mouth (0.013 vs 0.120) and possibly comparable with the measurement noise.

A useful quality of the back reflected signal is revealed by close examination of the leading terms of Equations 6.8 and 6.10 on one hand, and 6.9 on the other: the pulse-echo method is more suitable for this type of ultrasonic inspection than the 'pitch-catch' method of Figure 5.3, where access to both sides of the crack was necessary. Indeed, the back reflected signal is always greater than the forward transmitted, which is subjected to more scattering events. This is rather reassuring for fretting fatigue measurements, where the disassembly of the two fretted bodies

is thus avoided, of course so long as there is no normal pressure and the crack faces remain open.

6.3 The ultrasonic spectroscopy system

The ultrasonic spectroscopy system is shown schematically in Figure 6.2. It is centred around a Gould Biomation digital oscilloscope, which performs the data acquisition with a sampling rate of 100 MHz at 8 bit resolution. The pulser-receiver is a Panametrics 5052 PR, which excites the transducer with a sharp voltage spike. The digital oscilloscope samples and digitises the pulse-echo time domain signal from the pulser/receiver and transfers it to an IBM PC, via an IEEE 488 data bus. There is a serial link between the PC and the University of London mainframe computer, which allows the transfer of data files between the two machines, making easy the access of the extensive computing facilities of the University.

Once the digitised signal is stored in the PC memory, a commercially available program (MATLAB) can be used for gating and signal processing. A routine can select any portion of the time domain signal and perform operations such as Fast Fourier Transform (FFT), deconvolution and plotting.

6.4 Selection of the specimen and slots dimensions

a) Rayleigh waves velocity

The specimen dimensions were chosen to match the range of frequencies used in this work. The "dog-bone" specimen (Figure 2.6) was modelled by a plate of aluminium alloy Al 2014. This aircraft material was easy to machine and its

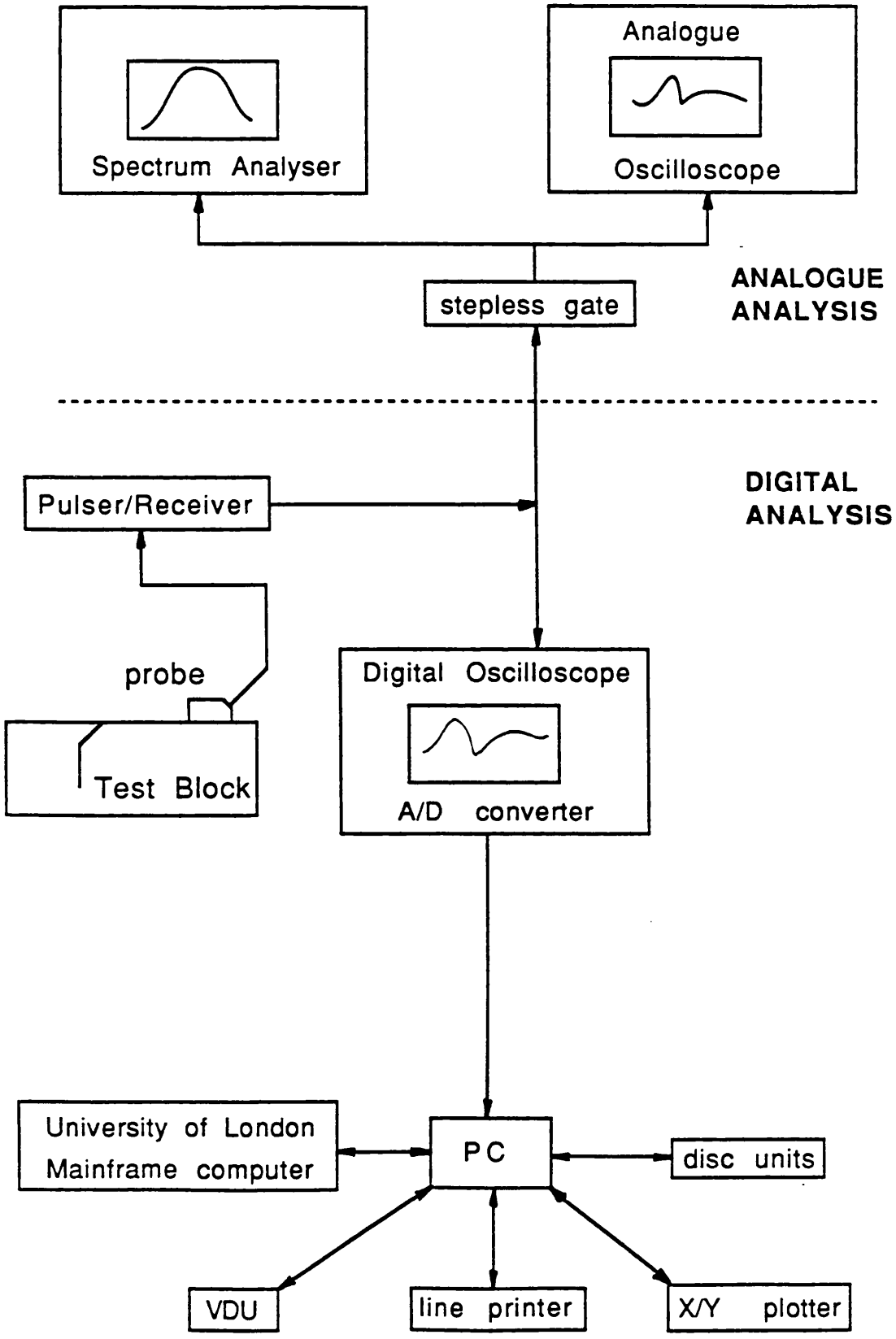

Figure 6.2 Block diagram of the spectroscopy system

material attenuation is negligibly small in the desired frequency range of 1 to 5 MHz. The plate was assumed to be elastic, homogeneous and isotropic.

The Rayleigh waves velocity c_R should be known as accurately as possible if time-of-flight measurements are to be undertaken, bearing in mind its proximity to the shear waves velocity. Handbook values for Rayleigh wave velocities are not sufficiently accurate, as they usually refer generally to "aluminium". For example, Krautkrämer and Krautkrämer (1983) give the shear wave velocity c_T and suggest that c_R/c_T =0.93. The value of the Rayleigh wave velocity was determined using the arrangement shown in Figure 6.3, to be 2930±20 m/s. The waves were allowed to reflect from the top A and bottom B corners of the specimen (thickness 'h'=23.5mm) and measuring the time difference ΔT between the signals from A and B:

$$c_R = \frac{2h}{\Delta T} \qquad (6.11)$$

The digital oscilloscope offers excellent accuracy in terms of time domain measurements (about 0.5% discrepancy between different measurements). The values for the acoustic wave velocities in aluminium are given in Table 6.1.

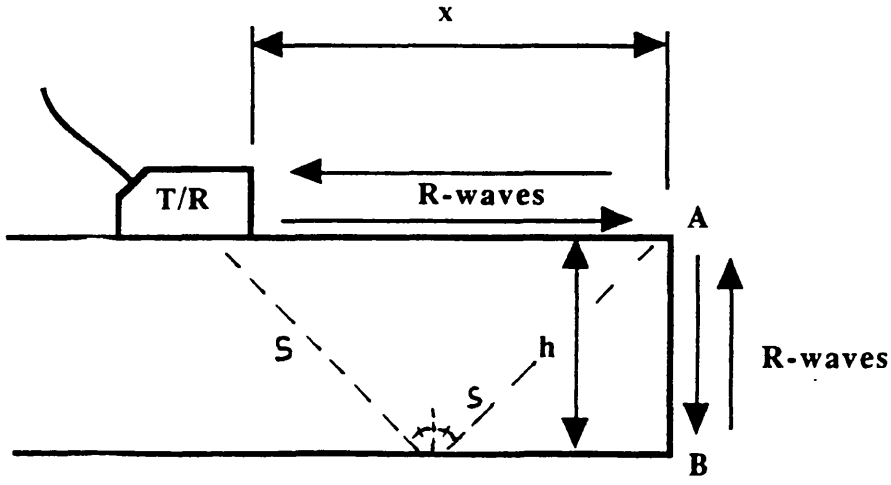

Figure 6.3 Contact testing configuration. A and B depict the Rayleigh waves path for reflection from corners A and B respectively

Some interesting problems associated with the velocity are mentioned at this point. The measured Rayleigh wave velocity on a stress-free surface is not necessarily the actual velocity of the waves travelling along the faces of the crack, due to the presence of a residual stress in the vicinity of the crack tip. However, Tittman and Buck (1980) suggest that the Rayleigh wave velocity on a stress-free surface can be the same as that for the waves along the crack faces, on condition that the specimen plate is homogeneous and the roughness of the crack faces is negligible (roughness affects the Rayleigh waves attenuation, too, perhaps to a greater degree (Section 7.8.2)). Besides, they argue that the residual stress in the vicinity of the crack tip, is more likely to influence the shear waves velocity u_T than the Rayleigh waves velocity u_R. Therefore, the measured Rayleigh wave velocity can be used for time-of-flight calculations in the experimental model (as in Hudgell *et al* (1974)).

One testing parameter, which is often overlooked, is the choice of the suitable transducer according to the material. Krautkrämer (1983) quotes that if the material has a transverse velocity which differs more than approximately 5% from that for which the transducer has been designed, either no Rayleigh waves at all or oblique transverse waves are produced in the specimen. Since many of the commercially available transducers are specially produced for measurements in steel, there must always be a calculation to see whether they are suitable for a given material. The transducers used in the following experiments were specially manufactured for testing in aluminium alloys. However, the transducers for steel should also be acceptable for most aluminium measurements, as the shear wave velocity of steel (3.23 km/s) is very close to that of the aluminium alloy (3.13 km/s from Table 6.1).

Specimen	Spec. Gravity 10^3 kg/m^3	c_L m/s	c_T m/s	c_R m/s
Al 6061-T6 Kinra-Vu 1986	2.7	6400	3130	2926 ±20
"Aluminium" Krautkrämer 1983	2.7	6320	3130	2910
"Aluminium" Cooper *et al 1986*	-	-	-	2900
Al 2014-T3 This work	-	-	-	2930 ±20

Table 6.1 Acoustical properties of aluminium alloys and comparison of values obtained in this study with other available in the literature.

b) Dimensions of the specimens

The wavelength $\lambda_R=c_R/f$ in aluminium, for the previously mentioned velocity and for transducers with nominal frequencies from 1 MHz to 5 MHz varied from 3mm to 0.6mm, approximately. In all the measurements, it was desirable to obtain plane strain conditions, so that the results are comparable with those from the literature (e.g. Achenbach *et al* (1980), Kundu and Mal (1981), Kinra and Vu (1986), Gautessen (1987)). The significance of plane strain follows from the usual equations describing the Rayleigh waves propagation on the surface. Without loss of generality, the Rayleigh wavefield in an elastically isotropic medium is completely described by

two spatial dimensions (x-y) and time. The z component of displacement and all derivatives of the displacement field with respect to z are assumed to be zero. The solution of the equations describing the wavefield in the plane strain state results in the Rayleigh Equation 5.2 (Pao and Mow (1973)), whose solutions yield reasonable accurate values for the Rayleigh waves velocity. For these plane strain conditions to be valid, the width of the specimen along the z axis should be adequately large, but and as there is no known analytical treatment of this extremely complicated problem, the following procedure was followed to justify the choice of the specimen thickness.

Two specimens of the same material (aluminium) were machined, each containing a slot. If 'h' is the specimen width and 'd' the slot depth, then the dimensions in millimetres for the two specimens were $(h,d)_1=(12.7,3.6)$ and $(h,d)_2=(12.7,6)$ respectively. The first specimen was to be examined with a incident Rayleigh wave frequency of 1.6 MHz, corresponding to a wavelength of $\lambda_R=1.8$ mm, and the second one with a frequency of 1 MHz, corresponding to $\lambda_R=3$ mm. In this way the dimensionless quantities d/λ_R were the same for both specimens (3.6/1.8 for the first and 6/3 for the second), while the h/λ_R ratios were 7.05 and 4.23, respectively. The spectral responses of both situations were obtained and their amplitudes in the neighbourhood of $d/\lambda_R=2$ were found to agree within 5-10% (<0.8 dB), which is a reasonable error for spectroscopic methods (Kinra and Vu (1985)). Therefore the possible errors produced by the deviation from the plane strain conditions are very small to be recorded.

Even though smaller specimen were thus shown to be acceptable, their overall dimensions were chosen considerably larger for experimental convenience: 300x150x23.5mm and 300x150x47mm. The second specimen was used for examination with the longer wavelength of 4mm (for 0.7 MHz frequency).

c) Shape and dimensions of the slots

As a first approach to the problem the cracks were considered to be always open, with smooth crack faces which were not filled with dirt or any other kind of fluid or solid impurities. The specimen surface was very smoothly machined in order to reduce the attenuation of the travelling Rayleigh waves.

The available broadband Rayleigh wave transducers had nominal peak frequencies in the range from 1-6 MHz. Generally, there is no easy way of artificially creating model slots as small as those encountered in the first part of this work (some hundreds of microns or smaller in length). Fortunately, the situation can be studied with the help of a scale model where the d/λ ratio remains the same with the corresponding ratios as for the real cracks. Under these conditions, the results from the scale model can be applied to the real crack. Some extra care is still needed on the application of the scale model results to very small cracks, where the use of very high frequencies is necessary, because in this case the wavelength becomes comparable to the surface asperities. This condition can cause testing problems due to the increased dispersion and attenuation of the Rayleigh waves.

The slots were cut in a wire-cut spark erosion machine. The width of a slot cannot be near zero, due to the limitations of the machining process. The ideal condition would be if the slot was of virtually zero width, like a line crack. As a reasonable compromise, it was decided to maintain a slot length over width ratio of 10 at all times, that is for a slot depth of 2 mm, the corresponding width ought to be about 0.2 mm. For this reason, the thinnest possible wire was used for cutting them. The cutting wire was 0.15 mm in diameter and the slot width was found to be less than 0.2 mm, by checking with an optical microscope. Although the exact shape of the slot "tip" cannot accurately be determined, care was taken by the contractor so that it was machined to be adequately sharp so as to provide a scattering source.

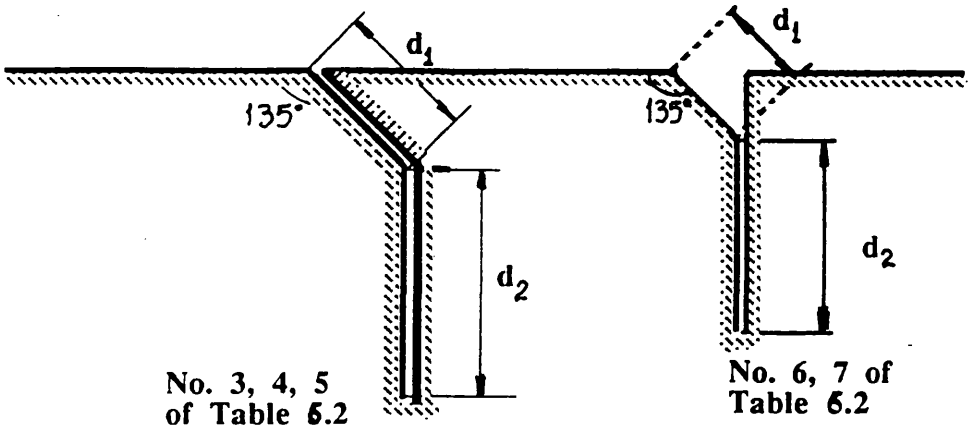

Figure 6.4 Shape and dimensions of the kinked cracks

Slot No	Type	Angled part d_1 (mm)	Normal part d_2 (mm)	Total length (mm)	Max d_1/λ	Min d_1/λ
1	normal	-	2	2	4.0	0.6
2	angled	1.6	-	1.6	3.2	0.5
3	kinked	2	2	4	4.0	0.6
4	kinked	2	4	6	4.0	0.6
5	kinked	2	11	13	4.0	0.6
6	'kinked'	0.5	5	5.5	0.25	0.12
7	'kinked'	0.5	8	8.5	0.25	0.12

Table 6.2 Slot dimensions and slot length over wavelength ratios for the available transducers. The d_1/λ values for kinked slots 3,4, and 5 refer to the transducer of Figure 7.3. The d_1/λ values for "kinked" slots 6 and 7 refer to the transducer of Figure 7.4

The kinked slots started with a part of 2 mm length which was inclined at 45° to the surface. After that oblique length, the slot turned perpendicular to the surface, so as to resemble a kinked crack. Three kinked slots were machined (Nos. 3, 4 and 5 in Table 6.2); the ratios of their normal part over their inclined part were: 2:1, 3:1 and 5.5:1 (Figure 6.4), namely their total length 'a' was 2+2mm, 2+4mm and 2+11mm respectively. Two additional slots were cut and examined with a transducer of lower nominal frequency in order to study the interaction of longer wavelengths with the angled part. These slots (Nos 6 and 7 in Table 6.2) were not exactly kinked, because it was difficult to machine an angled part as small as 0.5mm; they were shaped as in Figure 6.4. No comparison problems associated with their different shape should normally arise and this was confirmed in the experiments.

d) Position of the transducers

In fretting fatigue situations one does not have the additional difficulty of locating the crack. Its position is approximately known, usually within or at the edge of the fretting zone under the outer corner of the pad (Section 2.9). If for some reason (discontinuities in the material, abnormal wear of the fretting specimen, corrosion etc) the crack has initiated and grown at some other point in the vicinity of the area which is pressed by the pads, its detection should not normally pose any considerable difficulties and only details of the following discussion are affected.

One of the problems which was encountered early in the experimental procedure was the selection of the position of the transducers relative to the defect. As already mentioned, much of the Rayleigh wave energy incident on the crack is converted to body waves. After the scattering, both body waves and Rayleigh waves are present near the imperfection; sufficiently far from it, however, the body waves attenuate as a consequence of either cylindrical expansion or mode-conversion to Rayleigh waves. The fraction of body waves directed towards the receiving transducer as a longitudinal wave is resolved in time from the scattered Rayleigh

wave, although the shear wave at the receiver may not have enough time to separate from the Rayleigh wave. Indeed, a change of just few tenths of a millimetre in the transducer position can significantly alter the overall pulse shape. The spectroscopic measurements should thus be confined to the scattering far-field in order to be meaningful, where Rayleigh waves reflection is the predominant mode and clearly separated from the primary bulk waves reflections, especially from these due to the shear waves. Experience showed that a distance from the scatterer of 5-10 times the wavelength was sufficient to guarantee far-field conditions. A series of measurements at various distances from the target were taken and that contributed to the identification of the different waves in the returning signal, because the relative arrival time between the directly reflected Rayleigh waves from the same scattering features remains constant.

The pulse-echo Rayleigh wave measurements were conducted in three positions: at distances of 20, 30, 40 mm from each feature. These were considered to be suitable choices, since the longest wavelength in the incident spectrum (Figure 7.4), corresponding to less than 1 MHz, was about 3.5 mm and the distance was at least 6 times longer than that. The spectra of the signals corresponding to different distances (20, 30 and 40 mm) for the various defects were found to be almost identical (their discrepancies were smaller than the experimental errors), indicating that far-field conditions had been achieved.

6.5 Signal Processing

a) Spectrum analysis

The output signal contains information not only about the flaw, but also the combined characteristics for each system component involved. A standard deconvolution procedure was used to eliminate the experimental responses which are

due to the system and not related to the flaw itself. The procedure which was followed for the signal processing and the determination of the transducer frequency response is outlined in the following.

Suppose that a measured flaw signal can be modelled in the time domain as the convolution of the measurement system impulse response function $v_2(t)$ with the flaw's impulse response function r(t), plus noise n(t). The incident field, namely the field generated by the transducer is still not known. The model can be described as: (Fitting and Adler (1981),Neal *et al* (1992))

$$v_1(t) = v_2(t) * r(t) + n(t) \tag{6.12}$$

and it can be stated in the frequency domain, after the application of complex FFT on all the signals, as:

$$V_1(f) = V_2(f) * R(f) + n(f) \tag{6.13}$$

Here $v_1(t)$ is a blurred and noise-corrupted estimate of the flaw's true signature r(t), as $V_1(f)$ is a band-limited, distorted and noise-corrupted estimate of the flaw's true frequency domain signature R(f). A common approach to the problem of defining R(f), the flaw's far-field scattering amplitude, is via the application of a filter of the Wiener type 'W' in the frequency domain:

$$R(f) = \frac{V_1(f)\ V_2^*(f)}{|V_2(f)|^2 + W^2} \tag{6.14}$$

where * denotes the complex conjugate. $v_2(t)$ usually represents the signal from a reference feature, where the coefficients of transmission and reflection are known.

The use of a Wiener filter, which desensitizes the deconvolution to division by near-zero values in $|V_2(f)|^2$ is suggested by some authors (Murakami *et al* (1978)). The filter is usually set at around 10% of the maximum of the reference magnitude frequency spectrum $V_2(t)$: $W=0.1 \cdot \max(V_2(f))$ (Chaloner and Bond

(1977), Neal *et al* (1992)). However the application of a filter in this work did not improve the spectrum, because of the fact that 25% of the peak response was chosen as the cut-off point (-12dB) and at this rather high point the influence of the filter was measured to be negligible (see and Murakami *et al* (1978)).

b) Determination of the incident field

The incident and the reflected wave from an infinite wedge are connected through a constant relation, as they are not dependent on the frequency (Section 5.3.2). If a 90° wedge has been taken as the reference feature, then the spectrum of the reflected pulse from it, is proportional to the spectrum I(f) of the incident pulse, according to the relation:

$$V_2(f) = 0.4 \times I(f) \tag{6.15}$$

(the value of the reflection coefficient for aluminium was taken 0.40, although it varies from 0.37 to 0.43 in the literature (Table 5.2)). Equation 6.15 implies that we have to divide the amplitude of every single frequency in the reference spectrum by the "scale factor" 0.4 in order to obtain the incident pulse. Obviously, the transfer function of the reflection coefficient R(f) which corresponds to the defect, without taking into regard the filter influence of Equation 6.14 is now given by:

$$R(f) = \frac{V_1(f)}{I(f)} = \frac{V_1(f)}{V_2(f)} \times 0.4 \tag{6.16}$$

c) Implementation of the spectral technique

The steps taken to implement this procedure were:

i) The ultrasonic backscattered spectrum of the feature to be measured was

obtained, which is convolved with that of the interrogating system. The return amplitude is very sensitive to the orientation of the transducer relatively of the slot; the error in phase was estimated at ±0.4 radians for 1 to 5 MHz and it requires a degree of skill and patience to optimize the signal.

ii) The transducer transfer function was obtained from the backscattered echo of a reference scatterer. The reference spectrum was taken from a sharp 90° edge, where the reflection coefficient is frequency independent.

iii) The scattering signal of the flaw was deconvolved from the reference signal. This was carried out in the frequency domain. The absolute value of the reflection coefficient for a feature can be found by simply multiplying its value for each frequency component by the reflection coefficient for a 90° corner (≈0.4; Equation 6.15)

d) Gating and windowing

The sampling rate should be high enough, so that no distortion phenomena in the frequency domain (termed 'aliasing' (Fitting and Adler (1981)) occur. It is generally suggested that the sampling rate be at least $2f_c$ (the so-called Nyquist rate), where f_c is the maximum expected frequency in the signal *(ibid)*. In the present case, the sampling rate of the oscilloscope (100 MHz) was well above the highest frequency component in the signal (about 6 MHz).

In order to increase the resolution in the frequency domain, many commercially available subroutines allow the selection of the number of points in the FFT operations. This is performed by allowing the truncated portion of the time-domain signal to occupy part of the array to be Fourier transformed and padding the remainder with zeroes. In the experimental process 2048 points were used for the FFT of the signals. This number gave both good resolution and moderate computing time.

It became necessary to isolate a portion of the time-domain signal in order to apply the FFT to transform it into the frequency domain. This gating operation is equivalent to truncating a signal and it thus introduces a discontinuity at its ends, leading to spectral spreading or leakage in the frequency domain (Papoulis (1977), Brook and Wynne (1988)). It is therefore common practice to multiply the original signal, before transformation, with a suitable window function. By choosing an appropriate window, we can arrange that the undesirable effects of spectral leakage are damped out. A good FFT window has a narrow main spectral lobe and low sidelobe levels to reduce 'distant' spectral leakage.

The FFT operation just described implies that the time-domain signal had been multiplied by a rectangular, or 'do-nothing', window function. Applying a rectangular window produces the best main lobe in the spectrum *(ibid)*, in exactly the area where most of the energy of the transducer is contained, namely at frequencies both below and above the central frequency. The rectangular window, however, causes spectral leaking at the spectrum edges and thus large side lobes, leading in difficulties of interpretation there. For this reason a high cut-off level was chosen, so that only the frequencies of the main lobe were used in the subsequent FFT processing. Of course, setting at a lower cut-off level would widen the effective bandwidth of the transducer, meaning that the transducer would excite and respond to a wider range of frequencies. From the experimental point of view, however, the choice of the exploitable bandwidth is not of vital importance. If testing at a wider range of frequencies, that is at frequencies below the cut-off level, is needed, it is suggested that another transducer of appropriate nominal frequency be used. In this way, it is always guaranteed that the resulting spectra do not misrepresent the fundamental frequency contents of the pulse, which are roughly concentrated around its central portion. The use of other window functions (for example Hanning, Hamming, Bartlett and others contained in the MATLAB library) reduces

the
substantially distant spectral leakage, but as they constitute a different compromise, they distort the central portion of the spectrum, which is more of interest.

6.6 Errors of measurements

As the general scattering problem even for the simple case of the reflection from a corner still defies an exact analytical solution, there are no universally accepted values for the reflection coefficients (*cf* Table 5.2). For this reason, it may be more appropriate to speak in terms of the underlying "uncertainty" of the experimental procedure, rather than of the absolute "error" (Holman (1978)). However, in the following the term "error" will be used, as in most experimental publications, implying the deviation of each measurement from the mean value for the same set of measurements.

The spectral response of an imperfection was deduced from the FFT of two signals (Equation 6.16), so that it is invariably deconvolved from the system's response. Consequently the sources which make up the total error are the differences, and not the absolute values, in the following features of the two signal acquisitions:

1. Pressure on the transducer as well as thickness, density, temperature and other non-controllable properties of the couplant. The main difficulty in the contact measurements is caused by the sensitivity of the signal to the thickness and uniformity of the couplant. Even small variations in the couplant thickness can produce considerable distortions to the measurements.
2. Surface finish, slot impurities and wear due to multiple measurements at the same positions.
3. Orientation of the wedges relative to the slots, affecting both the phase and amplitude, and distance of the transducer from the target. A micrometer was used to control these parameters.

All those errors are random in nature and contribute to the general random error of the experiments, because it is impossible to break the composite error into its constituents. As their main influence is on the repeatability of the experimental results, an attempt to circumvent it was made by increasing the number of measurements; 4 of them were taken for each individual case.

Although the absolute values of the above errors is immaterial in ultrasonic spectroscopy, the evaluation of modelling errors is important. These are errors produced by the deviation of a laboratory specimen from the idealised conditions that it is supposed to represent. One source of these errors is the presence of some plane stress conditions, which cannot be always eliminated. Another error could be introduced by surface roughness. Although most of the theoretical analyses in the literature treat the scattering problems as having perfectly smooth surfaces, in the present case the machined faces of the slots could not be polished nor could their surface roughness measured. The roughness of the upper free surface of the specimens was measured to be in the range $0.25 \leq e \leq 0.40 \mu m$, as communicated by the contractor who machined the specimens. The range of the Rayleigh wavelengths used was $0.5 \leq \lambda \leq 3.5$mm (Section 7.2). Therefore, the range of $\varepsilon = e/\lambda$ was $7 \times 10^{-5} \leq \varepsilon \leq 8 \times 10^{-3}$, which, for the most part, is quite small (Kinra and Vu (1985)).

A third modelling error is due to the geometry of the machined specimens. As mentioned already, a 90° corner was taken as the reference scatterer. The condition that its reflection coefficient is frequency independent requires that the corner be sharp, but in the course of machining a certain amount of roundness can be inserted. Especially the slot tip should necessarily be sharp enough for a scattering event to take place there. The reflection from the tip is the most important parameter, since it will be used to characterise the slot length. Unfortunately, exact measurement of the roundness at the slot tip is not possible, and, additionally, this can change across the width of the specimen. Care was taken by the contractor to machine the slot tip as sharp as possible, and its shape can be considered as resembling either a

crack tip or a rectangular bottom of a trough. In either case, the reflection coefficients do not differ much (Section 6.2.3), provided of course that a sufficient degree of sharpness does exist. Victorov (1967) states that for radius 'r' of the sharp corner such that $r/\lambda<0.05$ the effect of the roundness of the corner is small. The 90° corner which was taken as reference was adequately sharp (r=30 μm, due to the precision cutting machine): for the maximum frequency used (5 MHz), the ratio $r/\lambda_{min}\approx0.05$. Note that both this error and the errors due to the surface conditions and roughness are frequency-dependent and increase at higher testing frequency. Especially in the case of the wavelength becoming comparable to the asperities or to the large grain of the material, intense scattering takes place and the whole ultrasonics test breaks down due to the high attenuation.

Regarding now the apparatus, it can be stated that as noise and jitter in the electronics of the experimental system have probably a zero mean value, Fitting and Adler (1981) suggest signal averaging to improve signal to noise (S/N) ratio. The improvement in this ratio for M averages is $M^{1/2}$. The process of averaging 64 times the signal for every measurement was repeated 4 times and an average value was taken. The signal without any excitation (namely the "electronic" noise) was checked after averaging, and the noise was then measured to be negligible.

Taking all the above into regard, the repeatability of the measurements was found to be good and the discrepancies between the different measurements did not amount to more than ±1dB (<12%) of the measured quantity, which was the amplitude of the reflected signal in each measurement. The phase error was less than 0.2 radians at 5MHz. This seems to be in agreement with the error calibration by Kinra and Vu (1985-1986), who state that the experimental errors in ultrasonic spectroscopy are generally in the area of 10-15% (0.8-1.2 dB). Note that they did not use signal averaging in their experiments, which further reduces the errors due to the electronics of the apparatus (Fitting and Adler (1981)). When the whole procedure was repeated for 10 instead of 4 times for a corner measurement, the same sort of

random variations was observed. This suggests that the uncertainty associated with the inherent variability remains unchanged with additional sets of data, as it should have been expected (Holman (1978)), although the repeated measurements improve the experimental confidence through the rejection of the odd inexplicable data. A general remark on the whole experimental spectroscopy is that the spacings between the extrema along the frequency axis are determined with a higher degree of accuracy than the absolute values of the spectrum amplitudes. If a more accurate determination of the amplitude is necessary, one has to resort to other methods, like the tone burst method (Kinra and Vu (1986)), which are rather more complicated for field applications.

As regards the time-of-flight measurements, their repeatability was excellent: the digital facility of the oscilloscope produces time delay measurements with a repeatability of 100ns for the scale of 20μs, which corresponds to the 100MHz sampling rate. In this kind of measurements, the error is usually tiny: in a series of measurements like these of Figure 6.3, the distance between the first and second complex of echoes, which corresponds to '2h' (Equation 6.11) was found to be virtually the same. The two main contributors to the amplitude errors, namely the pressure on the transducer and the thickness of the couplant, do not influence much the time-of-flight measurements.

7. THE ULTRASONIC SPECTROSCOPY SYSTEM: RESULTS AND DISCUSSION

7.1 Introduction

As a check of validity and in order to identify the echoes which appear in the scattering events, the system described in the last Chapter is initially used for the study of the reflection of Rayleigh waves from a quarter-space, a normal slot and a 135° angled slot. In these studies, the reflections from the specimen boundaries are also investigated and consequently the model is treated as a plate rather than as a half-space. Not all the returning signals can easily be accounted for, since the generation of some may be attributed to the 3-D scattering in the plate and possibly to phenomena associated with the finite width of the plate and transducer. Predicting the time domain shape of the composite pulse at the receiver is not a trivial problem due to the complex relationship between rays arriving from different points of the boundary. In an attempt to study the nature of the most prominent of the secondary reflections, the transducer-target distance was set at 20, 30 and 40 mm, and plots of series of traces versus the distance were recorded and reported in the following.

7.2 Reflection from a quarter-space

The quarter-space was emulated by a sharp right angled corner in a plate, so that the reflections resulting from scattering at the corners and boundaries of the plate can be studied. The thickness of the plate was many wavelengths long, so that

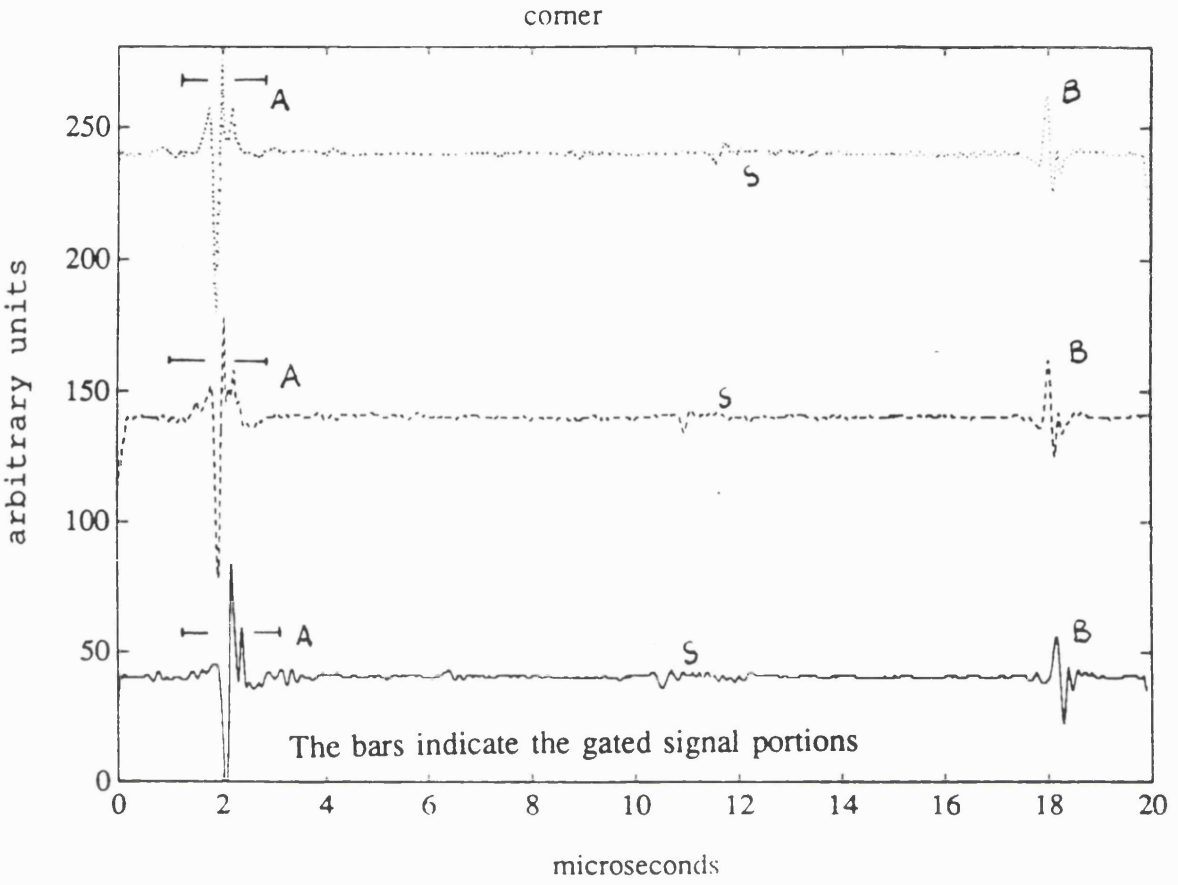

Figure 7.1 Time domain traces for a quarter-space. The transducer-target distance is 40 mm for (____), 30 mm for (- - -) and 20 mm for (...)

the reflection from the right angled corner resembles that from an infinite corner. The following analysis was carried out with a broadband transducer of nominal resonant frequency of 3 MHz in order to determine the frequency response of the system. The results given in Figure 7.1 correspond to time-domain measurements at distances 20, 30 and 40 mm respectively from the sharp 90° corner and the following echoes can be identified:

1. the reflected Rayleigh pulse from the apex of the 90° angle A of Figure 6.3, which are denoted by 'A'.

2. the reflected Rayleigh waves from the lower 90° corner B of Figure 6.3 which are denoted by 'B'.

3. some reflected waves, the most evident of them are shown as a series of

disturbances (S). The relative distance of these waves (S) from the waves denoted by 'A' and 'B' changes as the transducer approaches the corner, and therefore they are not directly reflected Rayleigh waves. A closer inspection (the "wet finger" test) suggested that these waves should not be mode-converted Rayleigh waves generated at the first corner, namely they are not due to the body waves generated at the first corner A and eventually reflected from the back wall surface. They should thus be due to scattering from the lower corner B. An investigation into their nature is carried out in Section 7.7.3.

The pulse denoted as 'B' is due to the Rayleigh wave which is transmitted past the first right angle and eventually reflected back from the bottom corner of the aluminium block. The transit time ΔT between the echoes from the two vertical corners remains constant in all three measurements (16 μs), since it corresponds to the time taken by the Rayleigh waves to travel down and up the vertical face of the specimen of Figure 6.3.

Next, and in order to carry out the frequency-domain analysis, the time-domain data from corner 'A' were gated and the DC component removed (Figure 7.2 for the signal corresponding to a transducer-target distance of 30 mm). Subsequently, the FFT was applied to the resulting signal and in this way the Fourier amplitude spectrum of the reflected pulse was obtained. In Figure 7.3 the spectra corresponding to the three different distances transducer-target are presented. They are identical, within experimental error, suggesting that even for the smallest distance of 20μm the far-field conditions had been achieved (Section 6.4d). An analysis of wave arrival times suggested that the disturbances within the gate for the 40mm signal should be due to the longitudinal wave generated at the top corner A, reflected at the bottom surface of the plate and transmitted back to the transducer. Longitudinal waves energy is mainly contained in a cone inclined at 45° to the surface and geometry calculations indicate that the scenario above is the only possibility. In any case, the disturbances did not seem to influence much the FFT operation and the resulting

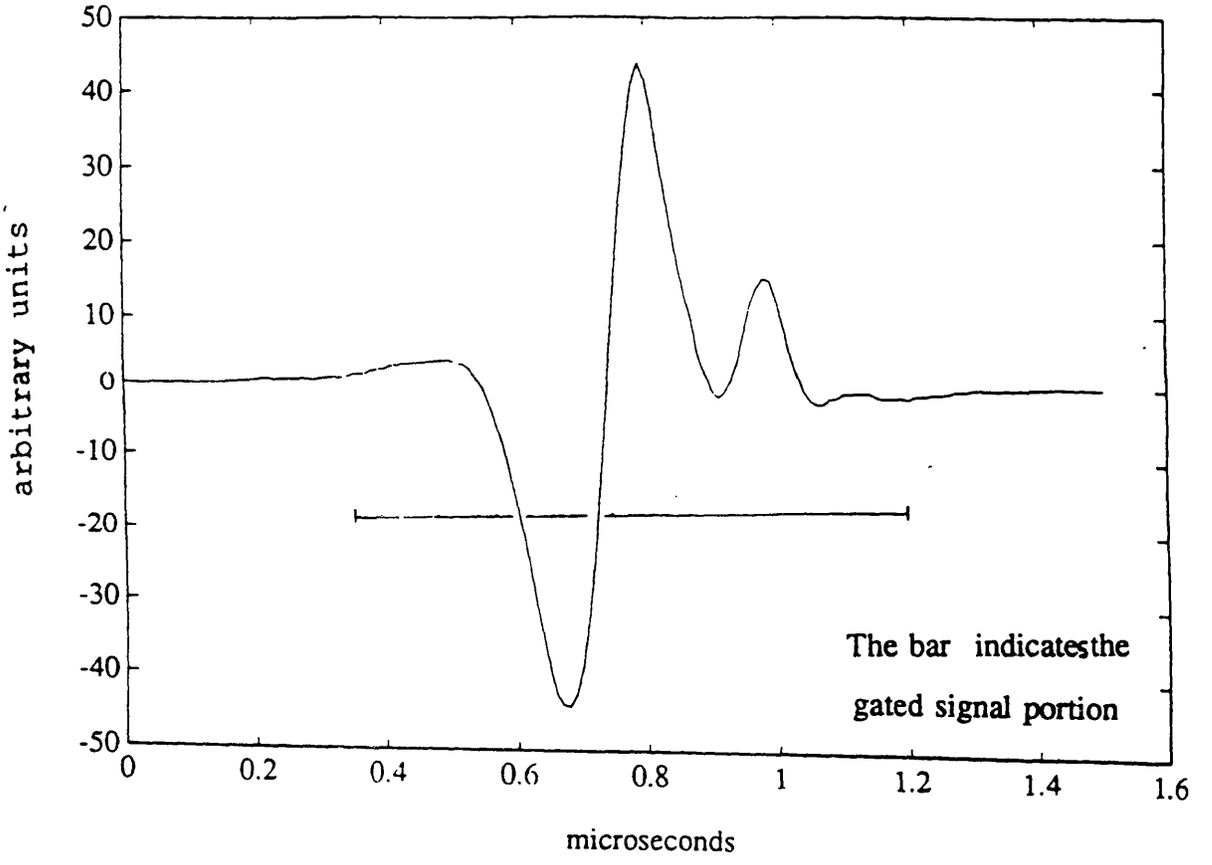

Figure 7.2 Time-domain backscattered signal from a 90° corner (distance transducer-corner 30 mm)

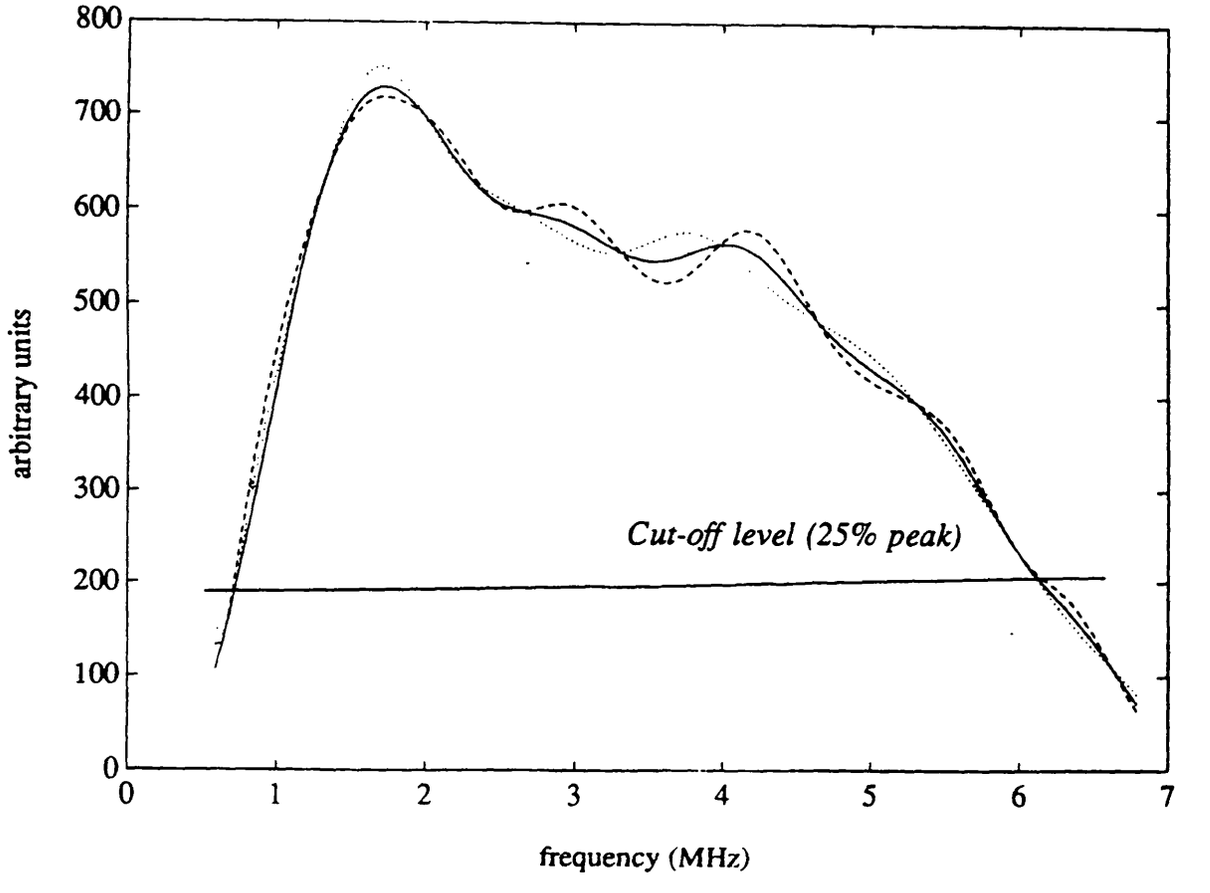

Figure 7.3 Magnitude frequency spectrum for a 90° corner.The transducer-target distance is 40 mm for (____), 30 mm for (- - -) and 20 mm for (...)

spectrum. The longitudinal waves attenuate fast as they travel through the bulk of the body and therefore the amplitude of the disturbances due to them is small compared to that of the main signal, as it can be seen from Figure 7.1.

The frequency spectrum shown in Figure 7.3 is connected with that of the incident pulse through Equation 6.15, namely every frequency component in it is about 0.4 times smaller than the corresponding frequency of the incident pulse. The intersection of the chosen cut-off level, which was set at about -12dB (25%) of the maximum of the reference magnitude spectrum, with the reference spectrum was used to estimate the available bandwidth. The spectrum of the incident pulse seems that it has a broad bandwidth of about 5 MHz ($0.8 \leq f \leq 6$ MHz) or available wavelengths λ in the range $0.5 \leq \lambda \leq 3.5$mm for Al 2014.

The sharp 90° corner was also examined by another transducer of nominal frequency 1 MHz, in exactly the same way and the spectrum of Figure 7.4 was obtained. If the cut-off level of -12 dB is applied on the maximum magnitude of Figure 7.4, it seems that the available bandwidth is from 0.7 to 1.4 MHz and the range of wavelengths from about 2 to 4mm. This narrow band transducer was employed for the examination of the sensitivity of the long wavelength interaction with very small cracks.

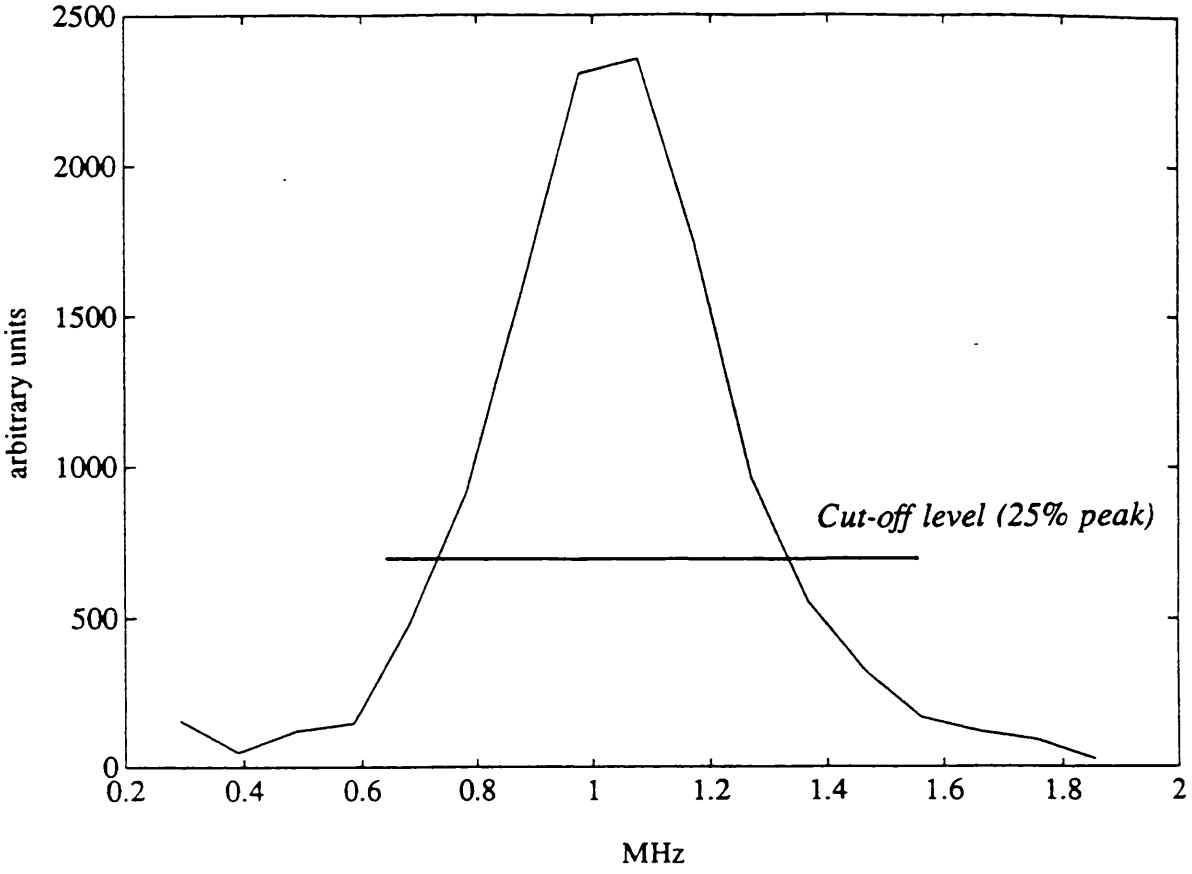

Figure 7.4 Magnitude frequency spectrum of a 90° corner examined with a transducer of 1MHz nominal frequency

7.3 Reflection from a normal slot

The time-domain traces from the three transducer-target positions (20, 30 and 40 mm respectively) and for a slot depth of 2 mm are shown in Figure 7.5. The first complex of echoes 'A' corresponds to the Rayleigh waves reflection from the slot and the second one 'B' to the reflection from the back wall, according to Figure 6.4. The spectral response of the transducer is given by Figure 7.3, as it was determined previously.

The time-domain signals were processed according to the standard method outlined in Section 6.5, where the reference signal from which they were

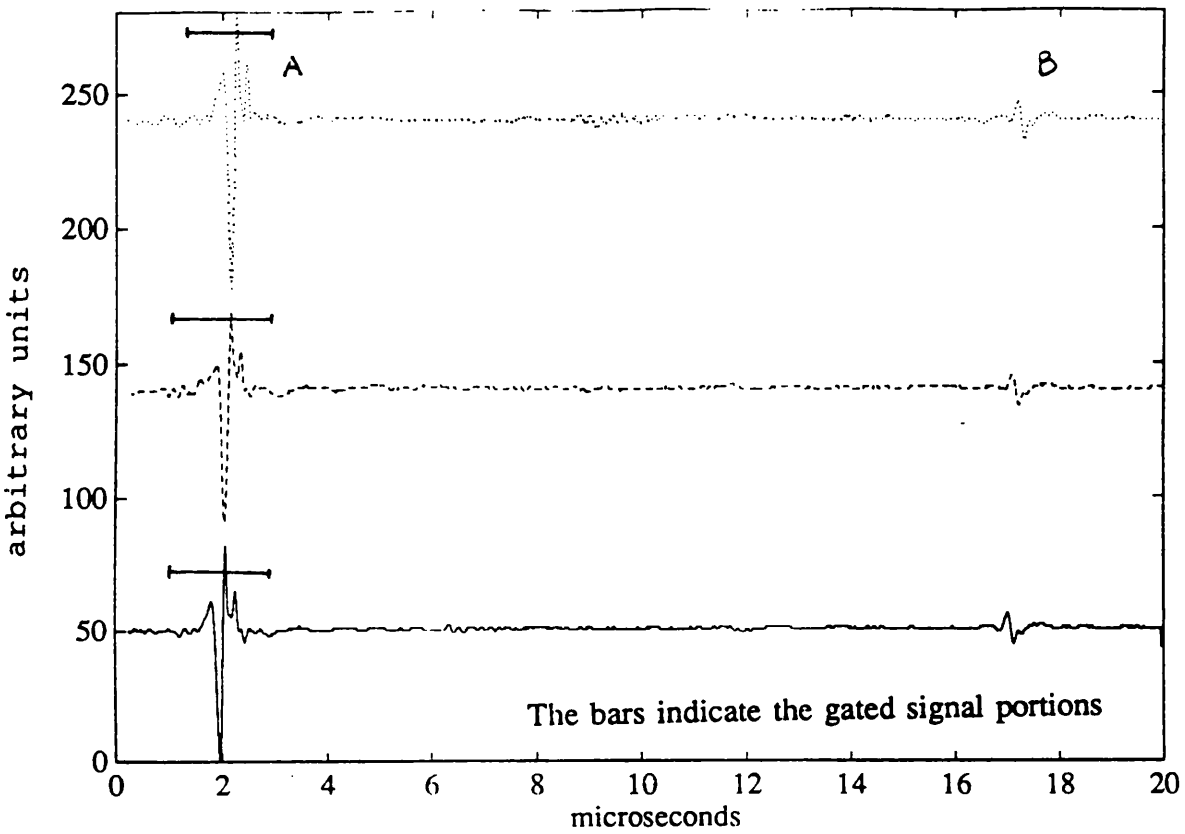

Figure 7.5 Time domain traces for a normal slot. The transducer-target distance is 40 mm for (____), 30 mm for (- - -) and 20 mm for (...)

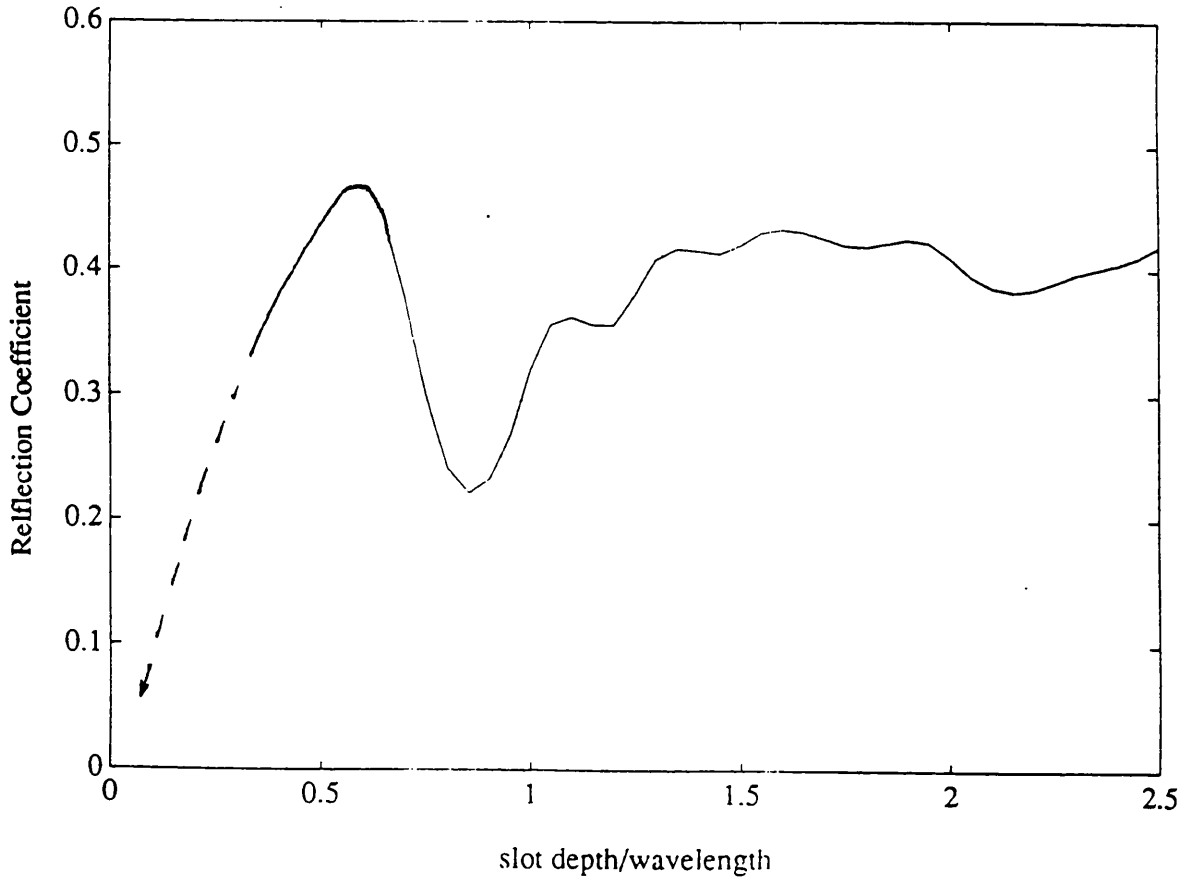

Figure 7.6 Reflection coefficient for a normal slot. Experimental results of this study.

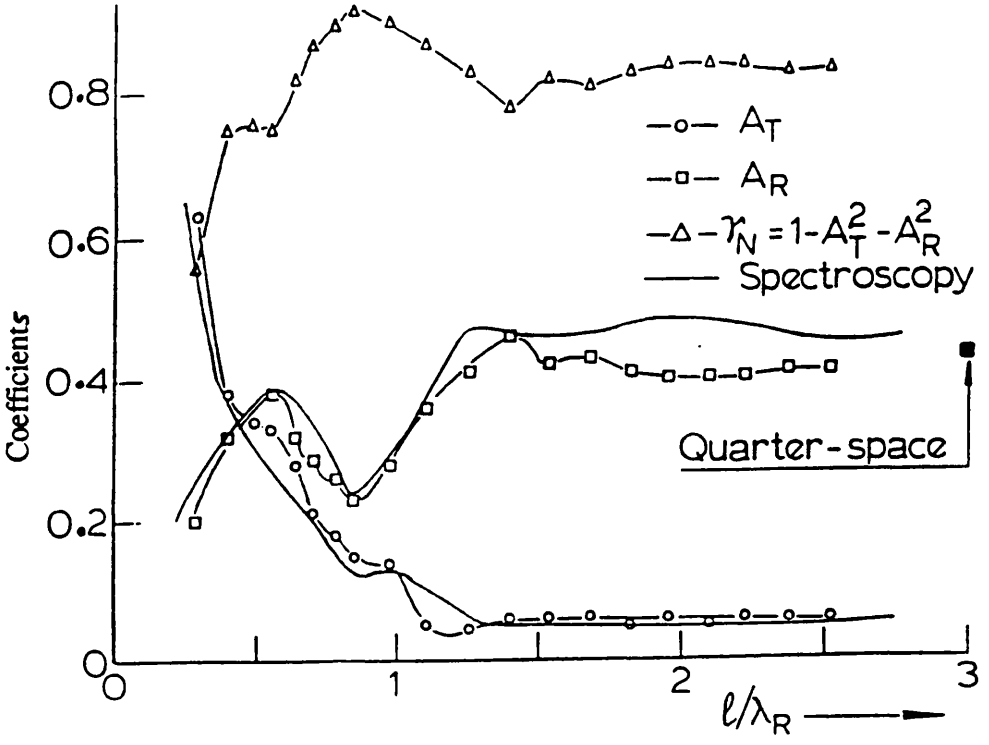

Figure 7.7 Reflection and transmission coefficients for a normal slot. Experimental results for Al 6061-T6 (Kinra and Vu (1986).

deconvolved is given by the transducer magnitude spectrum of Figure 7.3. The resulting spectral response curve for the slot in question is presented in Figure 7.6. It can be compared with Figure 7.7 where the experimental results of Kinra and Vu (1986) (material: Al 6061-T6) are shown.

From the plots shown in Figures 7.5 and 7.7 it can be seen that the reflection coefficient attains a maximum value at about $d_1/\lambda=0.5$. There is a minimum just before $d_1/\lambda=1$ and another peak at about $d_1/\lambda=1.5$. For higher values of d_1/λ, the reflection coefficient tends to reach its constant value of about 0.40, which is the reflection coefficient for the aluminium quarter-space (Table 5.2).

The reflection coefficient is therefore affected by the interference phenomena.

Indeed, the gated Rayleigh signal should contain two separate Rayleigh waves reflected from the top and the bottom of the crack. When the time separation of these signals is small compared to their pulse lengths, they overlap and appear as one long pulse, but the latter can still modulate the structure of the reflection from the top corner. However, the reflection from the crack tip is very weak, as its amplitude is theoretically only 1/10 of that of the first arrival from the crack mouth (Section 6.2.3)). Some regular spaced modulations would be expected to be visible in the reflection coefficient according to the spectral analysis of Section 6.2. In the region of validity of the ray theory (for $d/\lambda>>1$), the regular modulations should appear as distant ripples on the reflection coefficient ($\approx$0.40), but as their amplitude ($\approx$0.036, Section 6.2.3) is smaller than the measurement errors ($\approx$10% or $\pm$1 dB of the measured quantity, Section 6.6), they are usually barely discernible in the measurements of the practice.

The spectral analysis of Section 6.2 in conjunction with the experimental results revealed that when the wavelength becomes much smaller than the slot depth ($d/\lambda>2.5$-3), the reflection coefficient asymptotically approaches the frequency-independent value of the corresponding corner at the mouth. In this limiting case the returning tiny echo from the crack tip, arrives increasingly later than the reflection from the first corner, because it has to travel more wavelengths down and up the crack length. The length scale of the scattering geometry, namely the slot length, which introduces the modulations due to the scattering at the crack tip, tends to be lost, leaving only the first corner reflection almost unmodulated to characterise the reflection coefficient.

7.4 Reflection from a 135° angled slot

A 1.6mm long slot, angled at 135° to the surface, was ultrasonically tested by using a transducer with the spectral response of Figure 7.3. The time-domain signals are shown in Figure 7.8. They are more complex in appearance than those

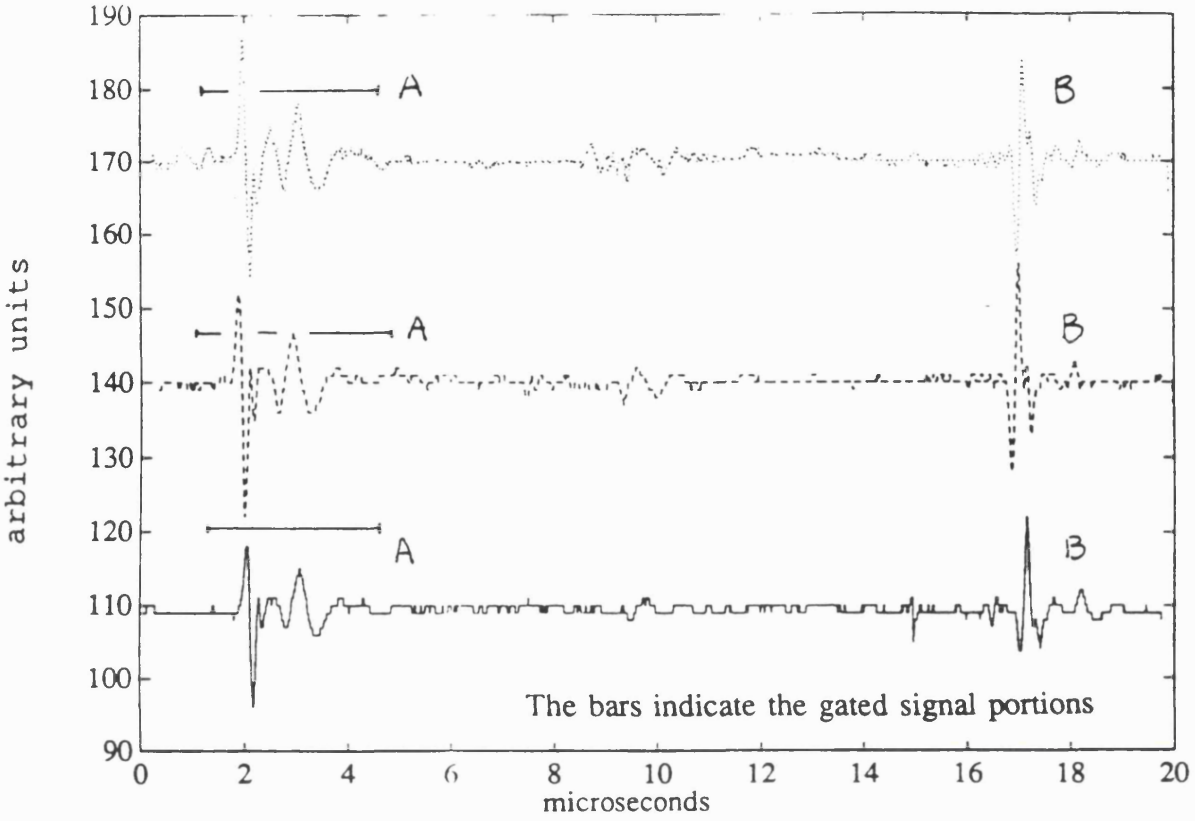

Figure 7.8 Time domain traces for a 135° angled slot. The transducer-target distance is 40 mm for (____), 30 mm for (- - -) and 20 mm for (...)

from the 90° corner and the normal slot. Notice that the distance between first and second complex of echoes (denoted as 'A' and 'B' in Figure 7.8 and corresponding to the slot and the back-wall echo) is again constant and that the signal is rather weak, due to a smaller reflection coefficient. Nevertheless, the crack tip arrival is more evident at 1.1μs for total path length 2*1.6 than the previous normal slot, since its relative amplitude is now 1/3 of the first pulse (Section 6.2.3).

The spectral response of the slot was obtained in the same way as for the normal slot and is shown in Figure 7.9. The corresponding plots which are available in the literature are presented in Figures 7.10 (for Al 6061, Poisson's ratio ν=0.34). The maximum value of the reflection coefficient is obtained for $d_1/\lambda \approx 0.5$. With

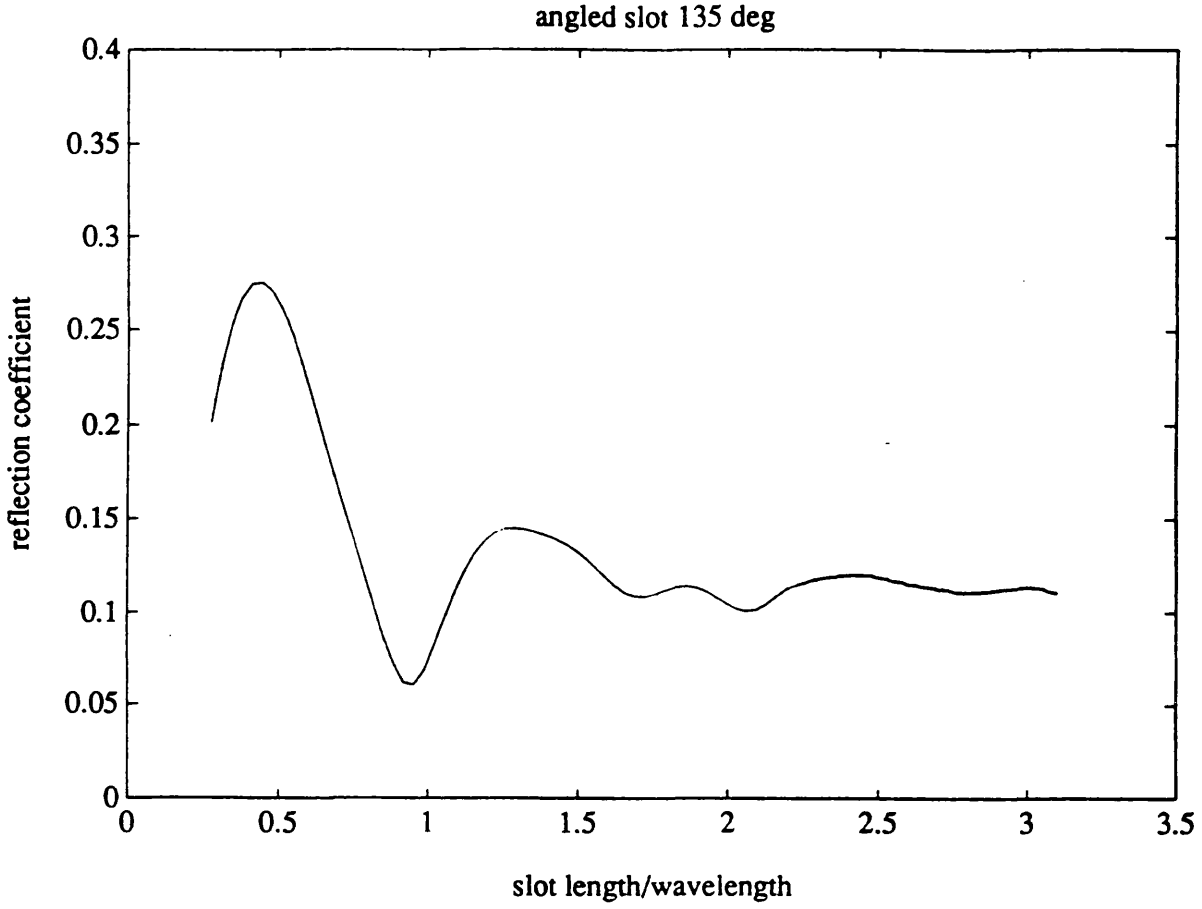

Figure 7.9 *Reflection coefficient for a 135° slot. Experimental results of this study*

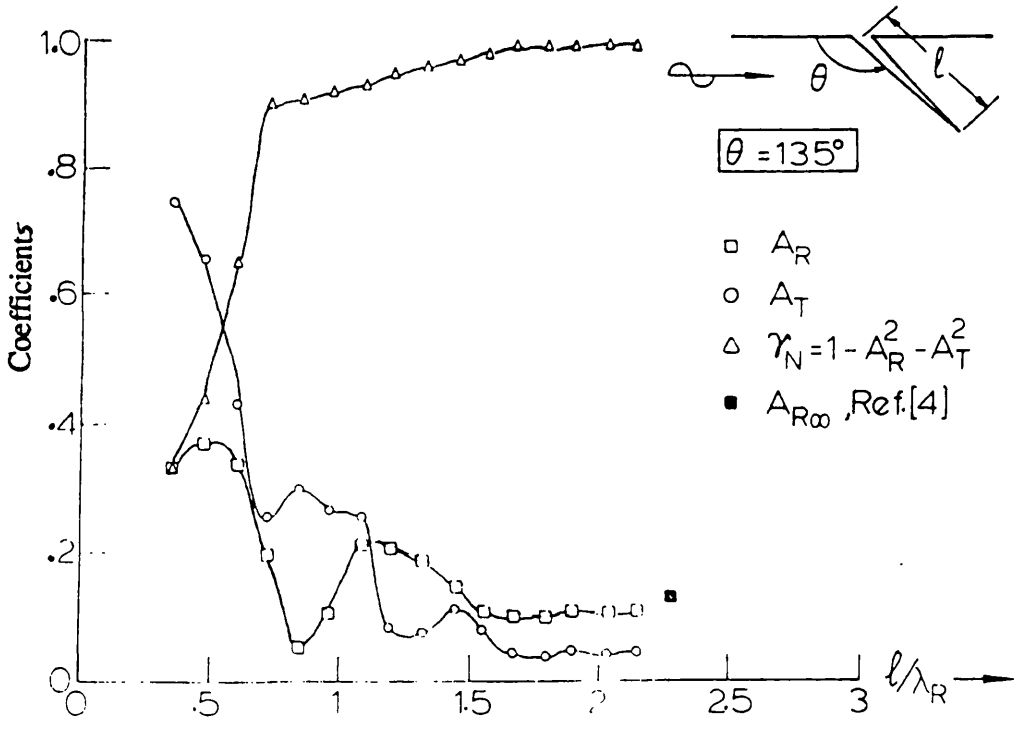

Figure 7.10 Reflection and transmission coefficient for a 135° slot. Experimental results for aluminium from Kinra and Vu (1986)

reference to both Figures 7.9 and 7.10 the next noticeable feature is a minimum just below $d_1/\lambda \approx 1$. The general reflection coefficient is indeed much weaker than that from a normal slot. It can also be inferred that the reflection coefficient has the tendency to attain a constant value between 0.12 and 0.14 in the short wavelength region. Taking into account the unavoidable error bounds of this study (±1 dB), then the agreement with the published results is good. The reflection coefficient for a 135° angled slot should approach 0.125 in the high frequency limit; the frequency-independent reflection coefficient for a 135° wedge, as it was explained in the last Section (Victorov (1967), Gautessen (1987)).

7.5 Reflection from kinked cracks

The time-domain signals from all three kinked cracks (Nos 3, 4, and 5 in Table 6.2) for the three different positions of the transducer (20, 30 and 50 mm) are presented in Figures 7.11-12. The slots were examined with testing frequencies contained in the broadband transducer which ranged from 1 to 6MHz (Figure 7.3). The ratio d_1/λ relatively to the common angled part of the slots d_1=2 mm ranged from 0.4 to 4, namely in the middle to high frequency regime. The normal parts of the kinked slots were 2, 4, 11 mm respectively. The overall length of the slots can therefore be some wavelengths longer than the longest wavelength (≈3mm for 1MHz frequency), but this does not mean that the present is a typical high frequency test. As most of the energy contained in the incident pulse is concentrated close to the surface, the angled part of the cracks plays an important role in the scattering mechanism, as it will become clear from the results and the discussion in Section 7.7.1.

Many of the signal characteristics can be easily accounted for. The first observation is that the first complex of echoes "A" is from the slot itself and the second one "B" is due to the back-wall echo. In the time space between them there are some reflections, which must be due to the presence of the plate boundaries.

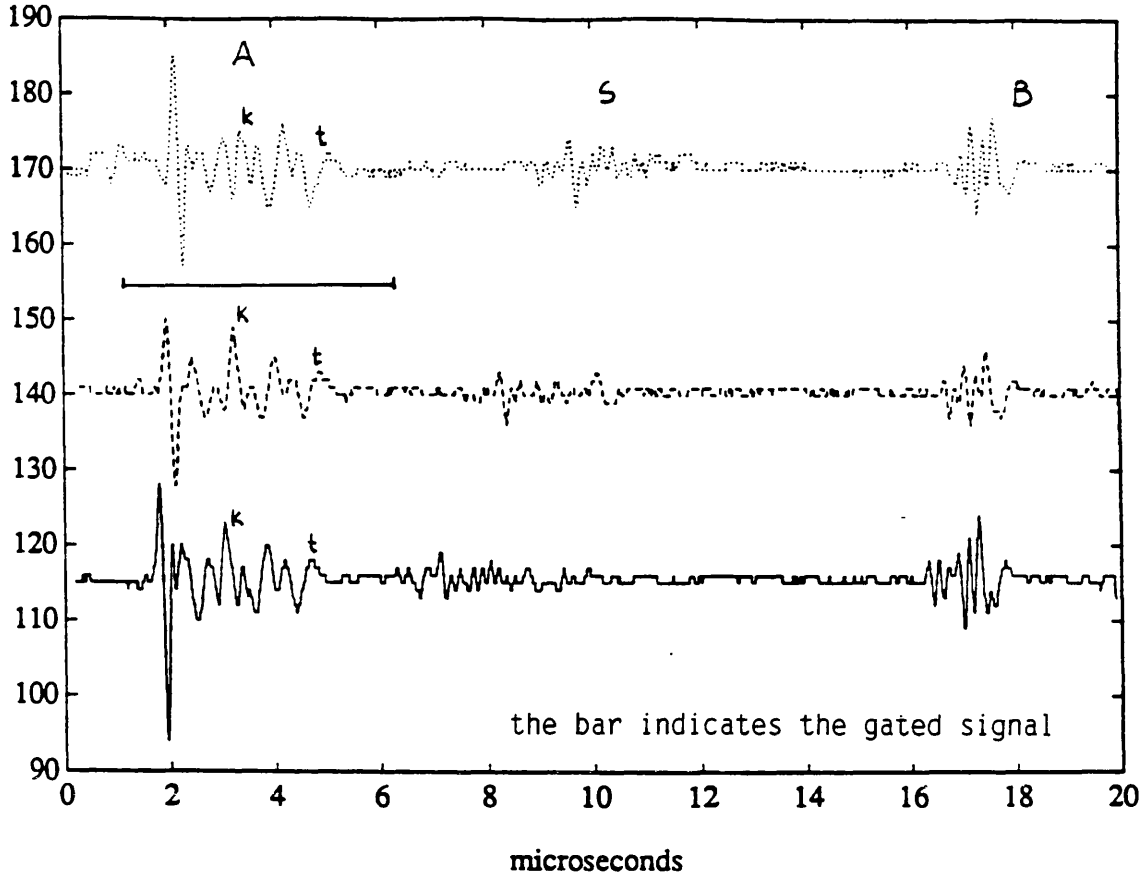

Figure 7.11a Time domain traces for a "short" kinked slot. Ratio of angled over normal part 1:1. The transducer-target distance is 40 mm for (___), 30 mm for (- -) and 20 mm for (...)

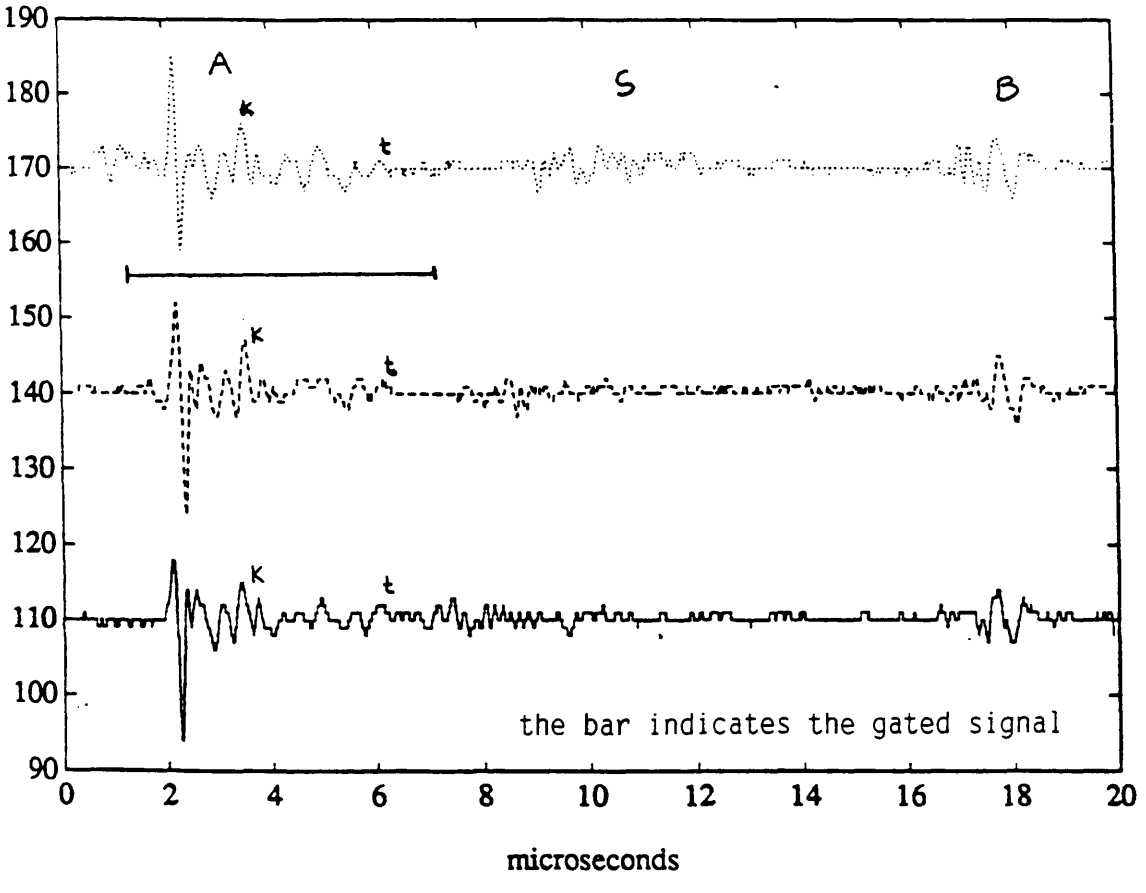

Figure 7.11b Time domain traces for a "medium" kinked slot. Ratio of angled over normal part 2:1. The transducer-target distance is 40 mm for (___), 30 mm for (- -) and 20 mm for (...)

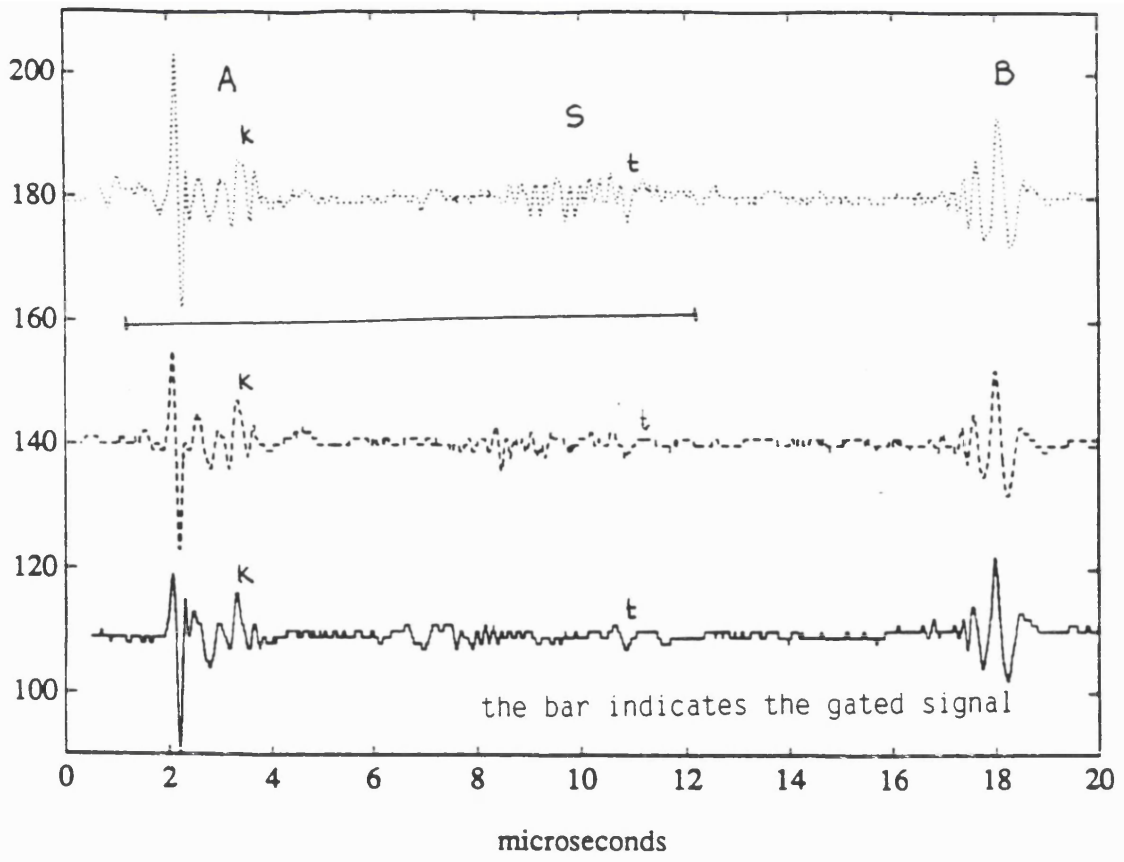

Figure 7.11c Time domain signals for a "long" kinked slot. Ratio of angled over normal part 5.5:1. The transducer-target distance is 40 mm for (___), 30 mm for (- - -) and 20 mm for (...)

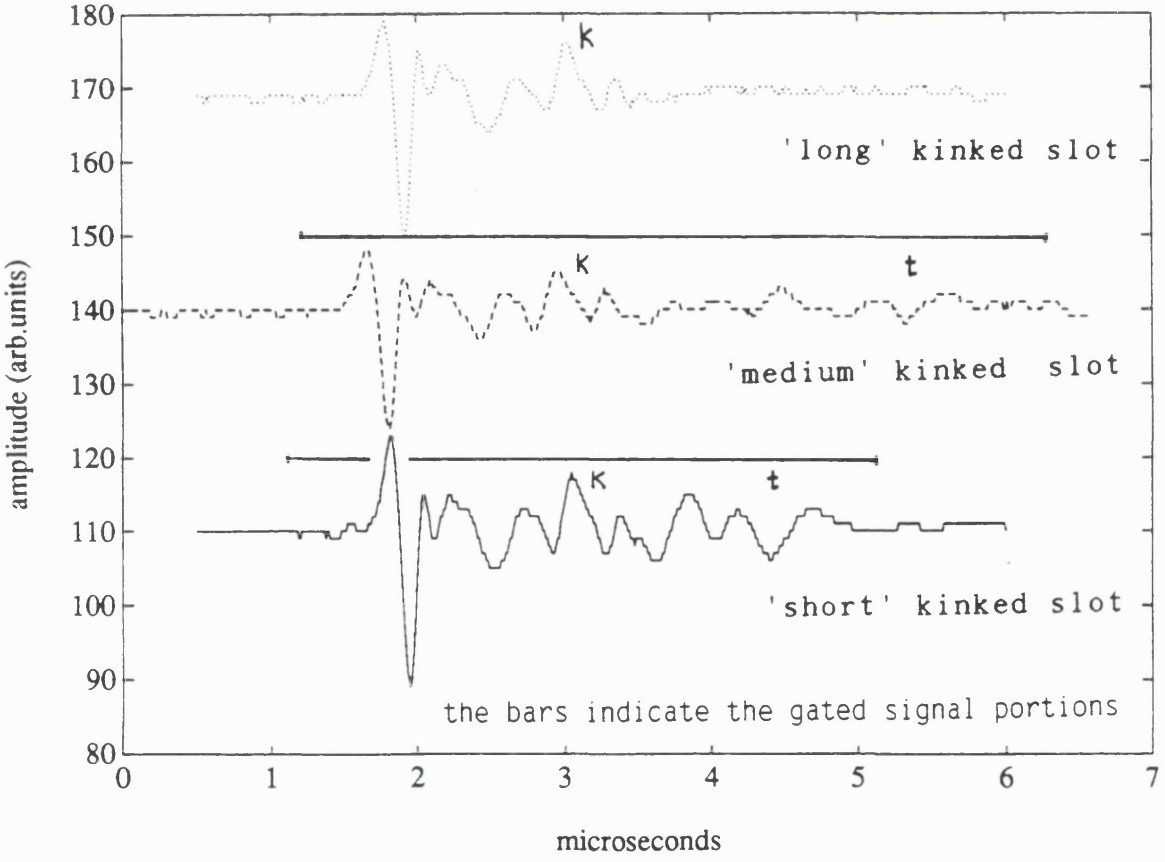

Figure 7.12 Time domain signals reflected from the angled part of the slots of Figure 7.11

These reflections might obscure some Rayleigh waves reflections from parts of the slot and therefore an investigation into their origin and nature is necessary, so that the transducer-target distance is properly chosen (Section 7.7.3).

One can discern the reflections from the knee point 'k' and the slot tip 't' in all three Figures 7.11 and 7.12. The 'second' high pulse 'k', which is constant for all three slots characterises this kind of scattering. It is also to be noted that the pulse 't' which is reflected at the slot tip has undergone a phase change compared to the reflections from the top corner and the knee 'k'. Several authors have calculated phase shifts (Achenbach *et al* (1980)), but none has interpreted them. Given the present level of understanding of surface waves scattering problems, this study will not concern itself with an analysis of the phase. Additionally, the amplitude of these reflections is higher than that predicted by the ray analysis of Section 6.2, implying a more complex operating scattering mechanism (see Section 7.7.1).

Slot (Table 6.2)	Length 'k' (mm)	error (%)	Length 't' (mm)	error (%)
No 3 (2+2mm)	1.85	7.5	3.85	3.75
No 4 (2+4mm)	1.88	6	5.45	9.1
No 5 (2+11mm)	1.87	6.5	12.95	0.4

Table 7.1 Experimental results from the time domain measurements of Figures 7.11-12. The slots nominal dimensions are given in Table 6.2. The length 'k' refers to the nominal angled part up to the knee. The length 't' refers to the nominal overall length up to the slot tip.

On the basis of the excellent accuracy of the time-of-flight measurements (Section 6.6), one can assume that the measured values of the slots lengths are closer to the reality than the nominal ones. The rather high discrepancy of the experimentally found values of slot lengths from their nominal values can be mostly attributed to the fact that, especially for the angled parts, the scattered wavefield travels on the leading face of the slot which should be slightly shorter than the 'centre line' of the slot that corresponds to the nominal machined length of 2mm. Impurities, surface roughness and residual stresses do affect the surface waves velocity (Section 6.4a) and therefore the experimentally found lengths, but to a negligible degree.

The spectral responses of the three kinked slots, in terms of the testing frequency, are presented in Figure 7.13. The scattering signals are deconvolved from the chosen reference signal of a sharp 90° corner (Figure 7.3), according to the procedure given in Section 6.5c. The study on the nature of the secondary reflections (Section 7.7.3) helped the isolation of a suitable portion of the signal for the FFT processing. For the "long" slot (No 5) the portion of the signal that is occupied by the secondary reflections is substituted by zeros. In reality, this portion that separates the reflected pulse complexes from the angled part ('A') and the slot tip ('t') is filled with the unavoidable electronic noise for the particular measurement. When instead of zeros, this portion was artificially padded with only the electronic noise and no secondary reflections, the resulting spectra remained almost the same.

A common characteristic in all three Figures 7.13 is the position of a minimum corresponding to a frequency of 2.6MHz or to $d_1\cos45°/\lambda = 1.2$ (in terms of the normal depth of the common angled part $d_1\cos45°$). As regards the absolute strength of the reflection coefficient, the three spectra do not exhibit considerable differences: they all tend to a value between 0.10-0.15 for high frequencies. This value corresponds to the reflection coefficient for a slot slanted at 135° to the surface. In order to verify the angled part influence, the relative spectra deconvolved

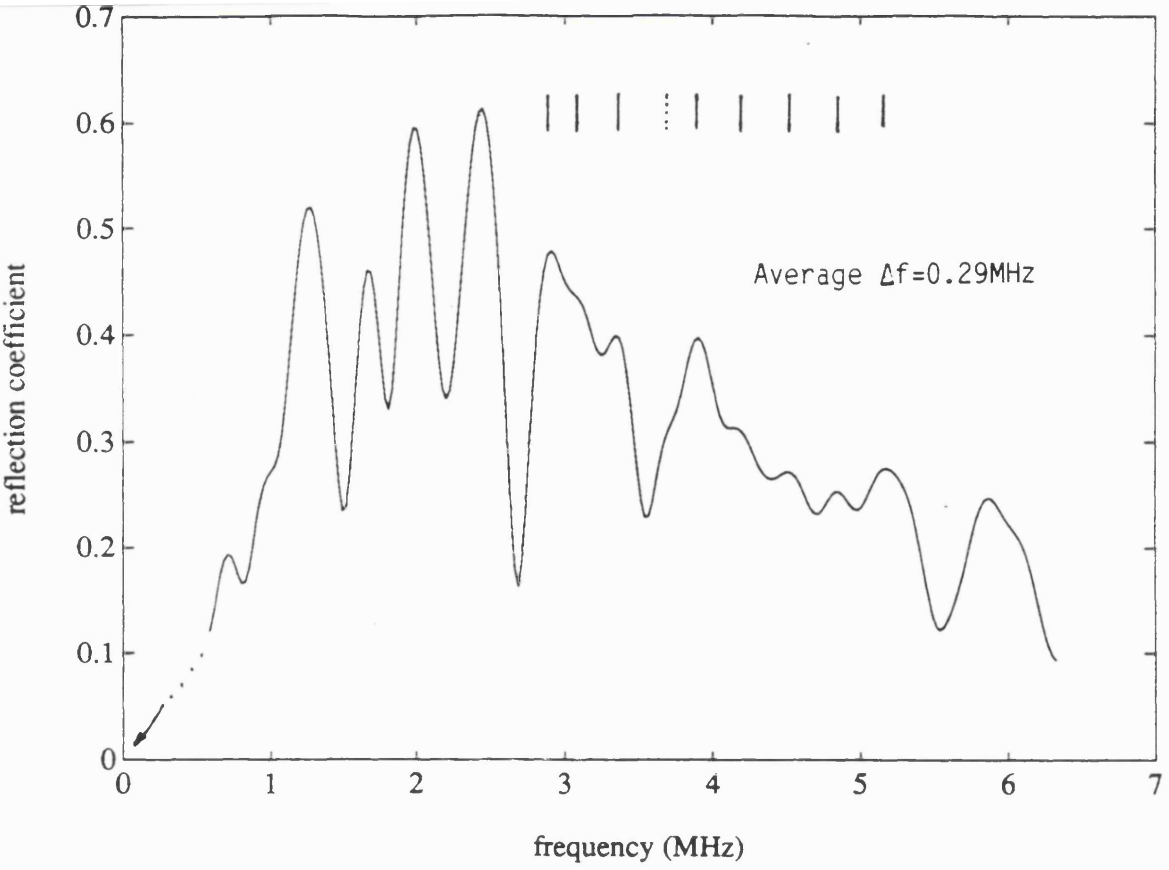

Figure 7.13a Reflection coefficient for a 135° angled kinked slot (No 3 of Table 5.2). Experimental results of this study.

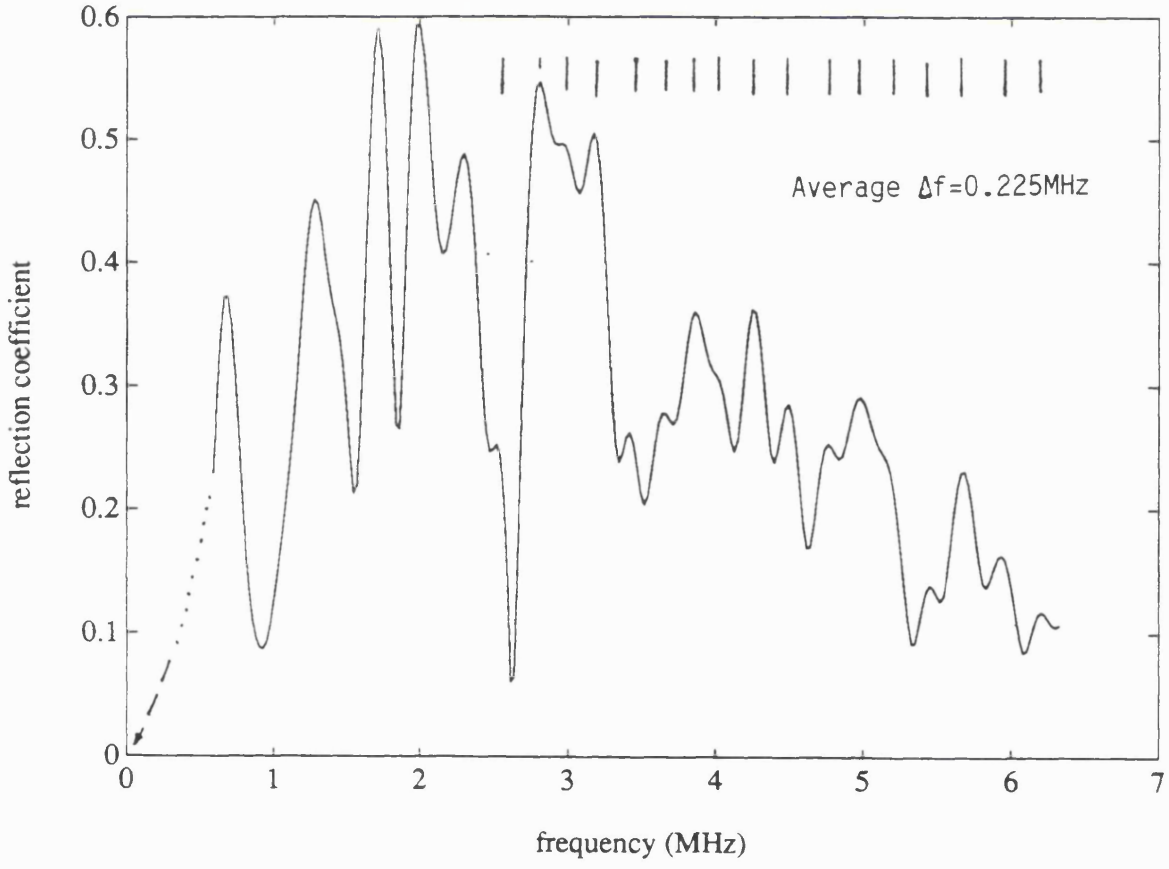

Figure 7.13b Reflection coefficient for 135° angled kinked slots (No 4 of Table 5.2). Experimental results of this study.

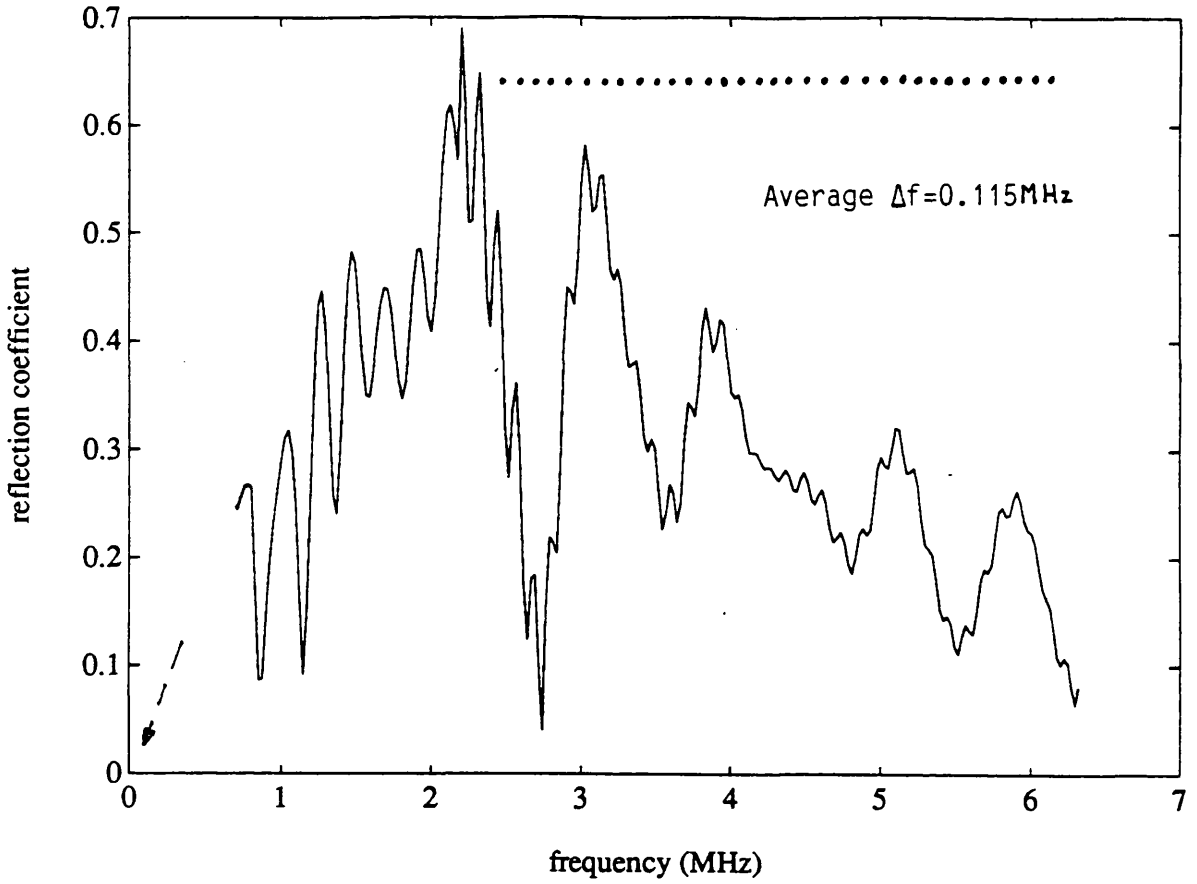

Figure 7.13c Reflection coefficient for a 135° angled kinked slot (No 5 of Table 5.2). Experimental results of this study

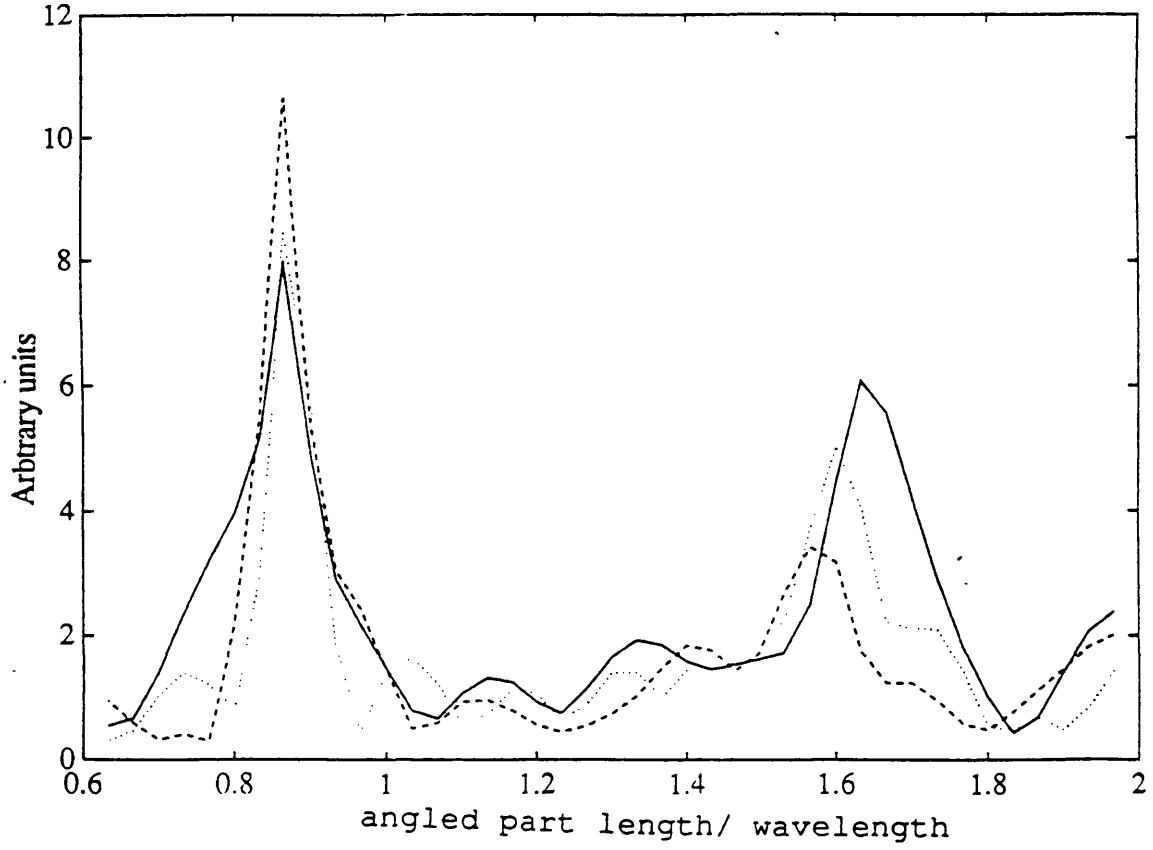

Figure 7.14 Spectral reflection responses for kinked cracks of Table 5.2 (No 3:(___), No 4: (- - -), No. 4:(...)) deconvolved from an angled corner of the same length

from a 135° corner of 2mm length were taken and are shown in Figure 7.14. A first conclusion, substantiated by this figure, is that the first inclined part dominates the scattering for this wavelengths regime, as it should have been expected, since most of the wavelength components of the incident pulse interact strongly with the angled part (Section 7.7.1).

Furthermore, two distinct regions are evident in each spectrum of Figures 7.13, which are approximately separated by the minimum at f=2.6MHz. It is remarkable that this frequency marks the approximate beginning of the validity of the spectral technique expressed by Equation (5.4), namely $d/\lambda>1$. For frequencies higher than 2.6MHz or $d_1\cos45°/\lambda>1.2$, regular spacings between the successive peaks and troughs of the spectra are visible. It is to be noted that these modulations are superposed on the modulations of the reflection coefficient of an angled slot. These modulations are a consequence of the destructive-constructive interference between the slot tip return and the returns from the angled part.

Measuring the average Δf between these successive peaks and troughs the total length of the slots, which corresponds to the travel path of the returning echo from the crack tip, can be found from the relation: $d=d_1+d_2=c_R/(2\Delta f)$ for $d_1/\lambda>1$ (Section 6.2.2)

short slot (No 3 of Table 6.2):	d=5mm,	app. error: +25%
medium slot (No 4 of Table 6.2):	d=6.43mm,	app. error: +7.2%
long slot (No 5 of Table 6.2):	d=12.69mm,	app. error: -2%

The error tends to reduce with increasing normal slot length. This is not unreasonable if one considers the relationship between the total slot length and the wavelength. Although the ratio d_1/λ that refers to the angled part is the same for all three slots, the case of the long slot is closer to a "real" high frequency testing. For this slot the wavefield reflected from the tip is clearly separated from the first complex of echoes, having to travel many wavelengths down the length of the

normal part. Conversely, it becomes increasingly inaccurate to apply the multiple scattering techniques of Section 6.2 for the measurement of shorter slots. Other types of waves may be generated which interfere with the Rayleigh waves and destroy the otherwise recognisable regular modulations (Section 7.7.1).

The slot tip echoes do also modulate the spectra for frequencies lower than those above, namely in the region $d_1/\lambda<1$. There is an indication of periodicity for these frequencies, which should be a consequence of the interference from the tip reflections, since the distance between the extremities (peaks or valleys) diminishes with increasing normal part length. However in this frequency regime the strong wavefields generated by the whole pulse interaction with the angled part undermine a regular periodicity in the spectra.

To examine experimentally the interaction of longer wavelengths with the angled part of a kinked crack, a further series of experiments were conducted. In these, a transducer with the frequency spectrum shown in Figure 7.4 was used ($0.7 \leq f \leq 1.4$ MHz). The two kinked slots interrogated were Nos 6 and 7 of Table 6.2 and the d_1/λ ratio was from 0.25 to 0.12. The resulting time traces and spectral responses in terms of the testing frequency are presented in Figure 7.15. Note that the ratios d_1/λ in terms of the angled part d_1 were the same for both slots, but their normal parts were different. For the slot No5: $1.25\leq(d_1+d_2)/\lambda\leq2$, whereas for the slot No6: $2\leq(d_1+d_2)/\lambda\leq4$ (approximatelly, in terms of the total slot length). The experiment was thus contacted in the high frequency regime in terms of the total length, but in the low frequency regime in terms of the angled part. The incident pulse which contains wavelengths considerably longer than the angled part, almost ignores the length d_1, seeing it as a minor perturbation in its path, and continues to interact eventually with the normal part d_2. The absolute value of the reflection coefficient for both cases is akin to that of a normal crack and considerably higher than that of an angled crack (*cf* Figure 7.13, where the testing wavelengths were shorter).

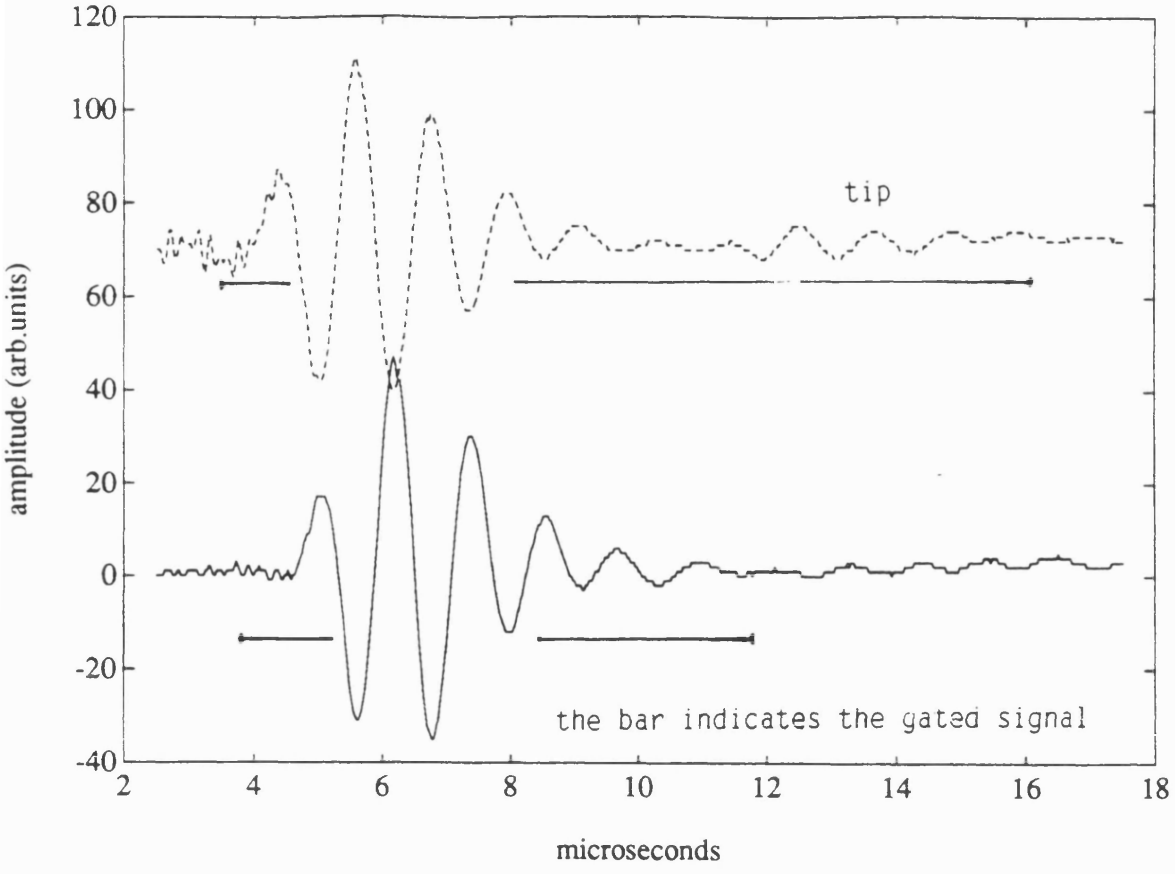

Figure 7.15 Time traces and reflection coefficients for 135° angled kinked slots (Nos 6 (top) and 7 (bottom) of Table 6.2)

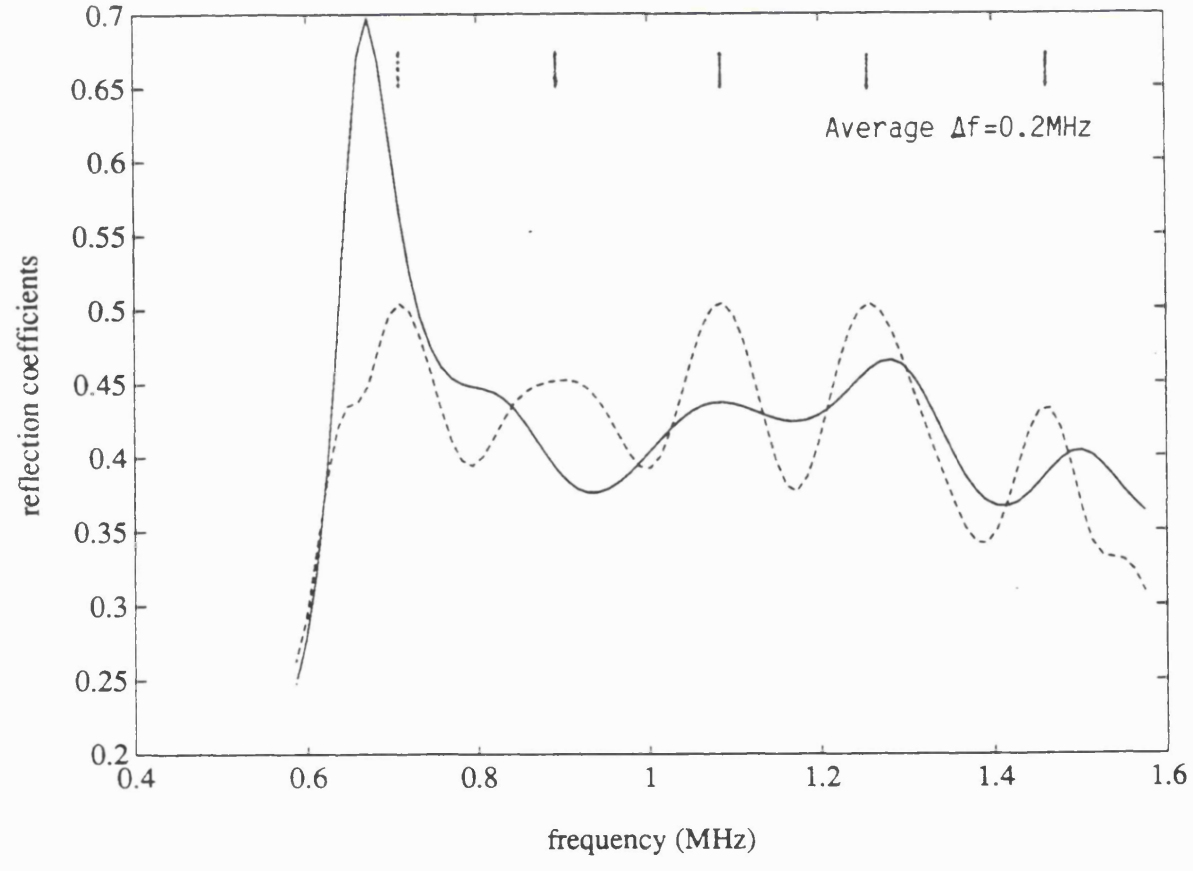

Figure 7.15b Spectral reflection responses from kinked slots of Table 6.2 (No5:(___), No 6 (_ _ _). Nominal testing frequency: 1MHz, distance from the slot: 40mm

In this high frequency regime in terms of the total length, both reflection coefficients tend to about 0.40, that is the frequency-independent value for a normal slot, modulated by the echoes from the tip. The spacing of the modulations is more regular for the longer slot No.6. Measuring the spacing (Δf=0.2MHz) between successive peaks in frequency domain, Equation (5.4) yields a total length of 7.25mm, which is in reasonable agreement with the nominal total length of less than 8.5mm (error less than 15%). For slot No.5 the modulations are not so visible, nor is the slot tip return in the time domain. The narrowband transducer has a broad spatial extent and the corresponding echoes overlap with those from the top corner.

7.6 Alternative inspection of the crack

For a fretting fatigue configuration, it is not always possible to interrogate the crack from the side normally occupied by the pressing stamp, if complete disassembly is undesirable. Nevertheless, it is possible to investigate how the signals change when the crack is examined from the other side of the crack, provided that the crack faces remain open. This examination was instigated by the observation that although the reflection coefficient oscillates with the wedge angle (Viktorov (1967) and Figure 7.21, Gautessen (1987)), it is sometimes stronger for acute than for obtuse angles. This property of the reflection coefficient would facilitate the NDE of angled cracks. For the present case the incident pulse would see an angled part inclined at the complementary angle of 45° to the surface, which is followed by the perpendicular part. Following the same experimental technique as for the previous cases, the reflection coefficient for a 45° inclined slot (Figure 7.16 for a 2mm long slot) was indeed found to be stronger than for its complementary angled slot.

The time traces that correspond to the examination of kinked cracks are presented in Figures 7.17. All the kinked crack signals resemble that from the

corresponding angled slot and the resulting spectra were found to be identical, within experimental error. Even the secondary reflections were almost the same in all the measurements, as were the corresponding spectra of all the time domain signal of Figure 7.17. The insensitivity of the scattering to the slot length is partly supported, if one reconsiders Equation 6.10, at least for the frequency range of its validity ($d_1/\lambda >> 1$). The high frequency asymptotic value of the reflection coefficient from the first 45° corner becomes now R_a=0.4 (Gautessen (1987)), instead of 0.125 for the 135° corner. Applying the multiple scattering theory of Section 6.2, the last term of Equation 6.10 which expresses the reflection from the crack tip is now $(T_{45})^2$ $(T_{225})^2$ $R_t=(0.60)^2$ $(0.60)^2$ (0.1)=0.012 (the transmission coefficient for the 225° angle at the knee was taken from Blake (1988) and for the 45° from Gautessen (1987) respectively). The first angle reflection is therefore about 30 times stronger than that

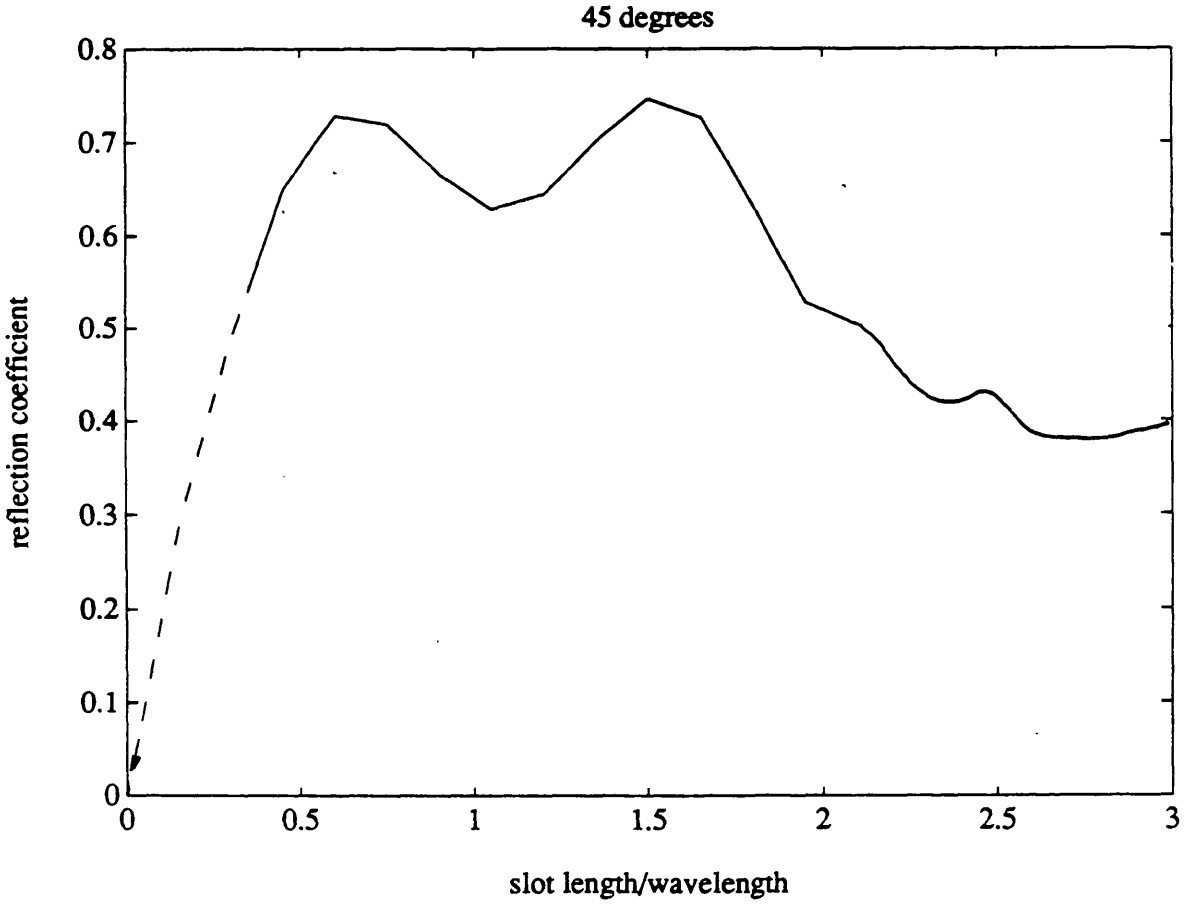

Figure 7.16 Reflection coefficient for a 45° slanted slot.

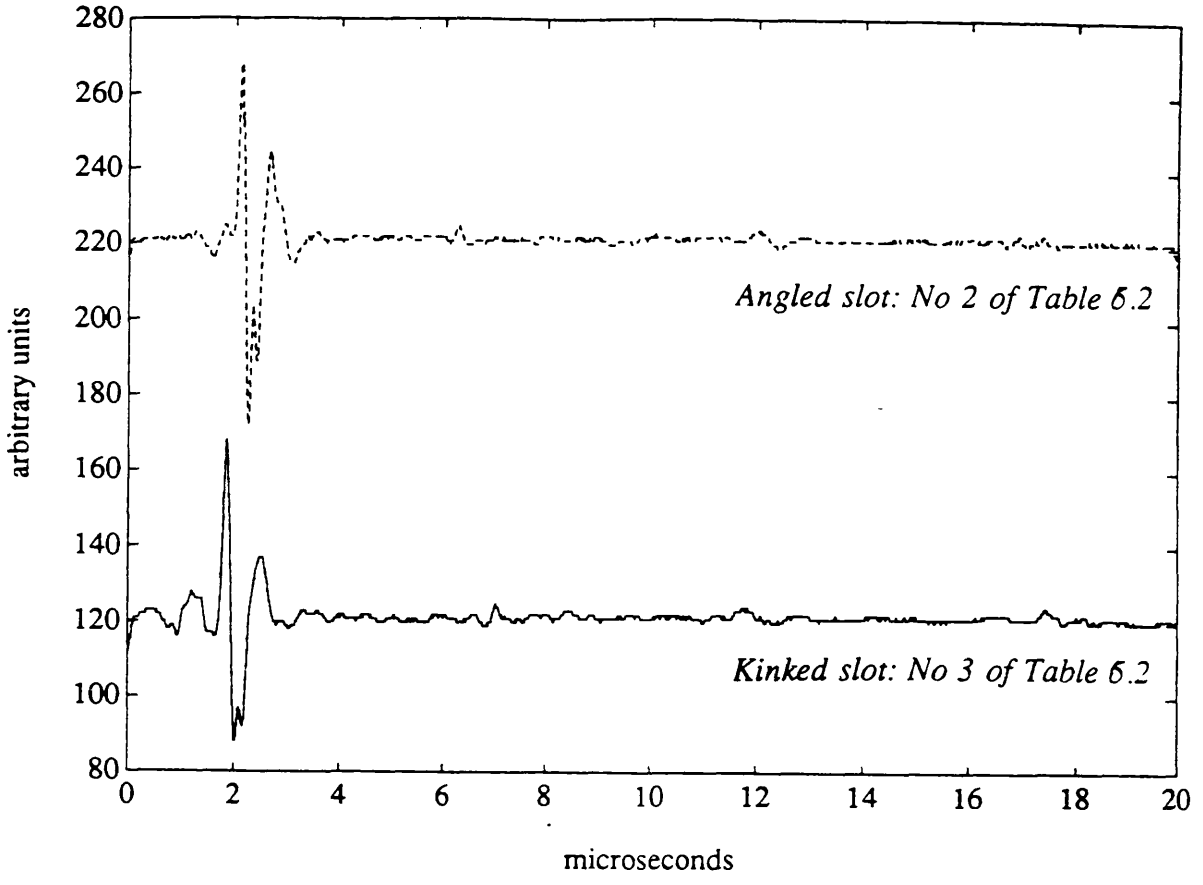

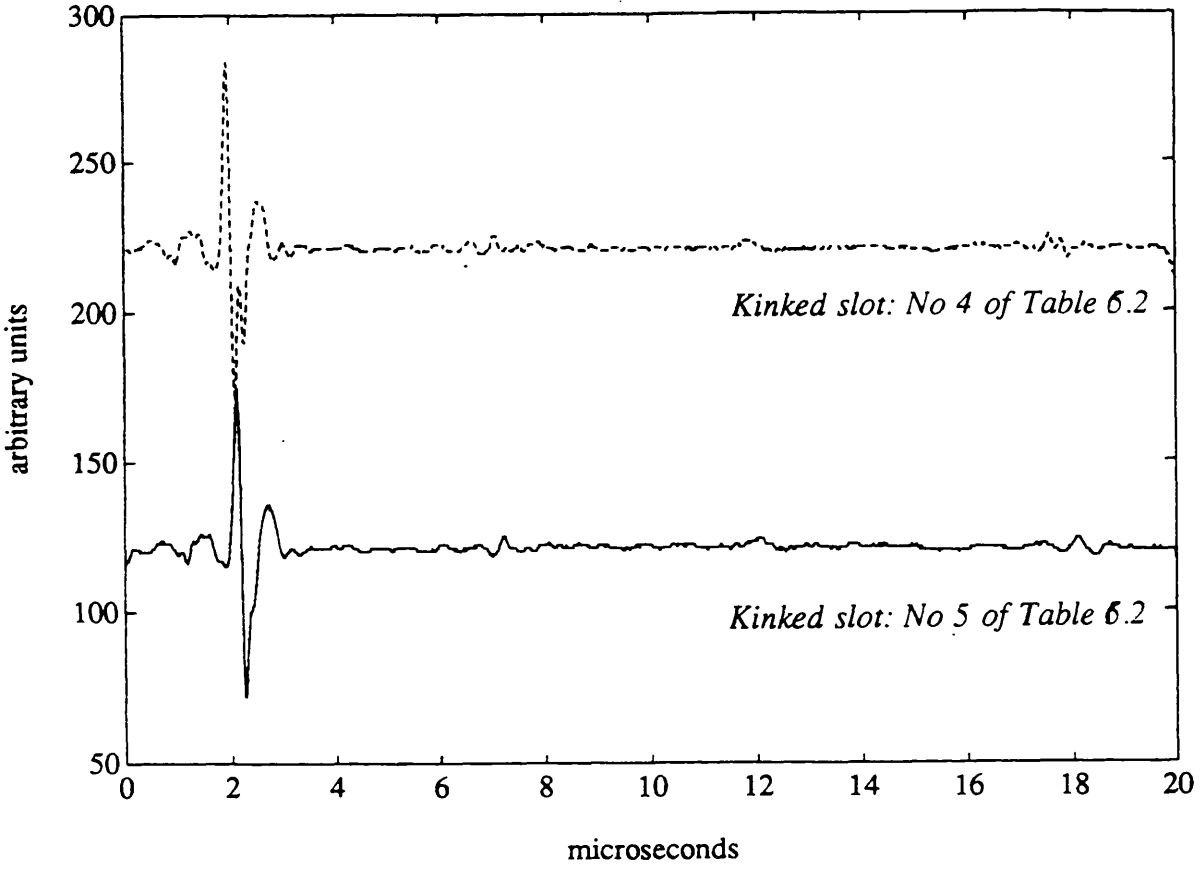

Figure 7.17 Time traces for various slots initially slanted at 45° to the surface. Transducer of Figure 7.3. Distance from the slot: 40mm

from the crack tip, implying that the echo from the tip is now too small. Of course, it should still be present in the time traces, but it cannot be easily disentangled from the measurement noise, nor is capable of modifying in a measurable way the first angle reflection in frequency-domain. The conclusion is that if time domain measurements are to be undertaken, the coupling of the transducer at the acute angle side of the crack is not as efficient as the coupling at the obtuse angle side. It is nevertheless remarkable that the reflection coefficient can efficiently be used to distinguish between an acute and an obtuse initial angle of a slot. Further discussion is presented in Section 7.8.3.

7.7 Discussion on the experimental results

7.7.1 The scattering mechanism

a) Interaction with corners and slots

An explanation of the various scattering phenomena is necessary in order to help clarify some of the scattering interactions which take place. Data given in a series of publications (Achenbach *et al* (1980), Achenbach *et al* (1982), Gautessen (1987), Blake and Bond (1990a,b)) may be used in order to investigate the scattering phenomenon and help its interpretation. Achenbach, Gautessen and their co-workers used mainly ray theory analysis, whereas Blake and Bond resorted to numerical formulations of the problem. In the latter studies, the incident pulse is simulated by a Ricker pulse sent towards surface features and the ensuing interactions were studied with the aid of numerical modelling (finite differences/finite elements). The so-called Ricker pulse has the advantage that it is representative of pulse shapes used in experimental surface waves NDE and is also suitable for the analytical formulation of the problem (Blake (1988)). The following discussion refers to the case where the angled part of a kinked slot is of the same order of size with the wavelengths

contained in the incident pulse ($0.5<d_1/\lambda<3$). This is mainly the regime of practical interest in conventional ultrasonic NDE with Rayleigh waves, when small physical crack lengths are involved. Testing with higher frequencies, i.e. shorter wavelengths, is usually difficult as a consequence of the limitations due to the surface roughness (Section 7.8.2).

Figure 7.18 presents numerical visualisations of the scattering of the incident pulse by a 90° corner, a 135° corner and a 135° down step. The reason for presenting the scattering mechanisms for corners and down steps is that their understanding provides a strong background for the study of the scattering from a kinked crack. As mentioned, the down step and slot geometries are virtually logical increases in complexity of the scattering geometry above that of the frequency-independent scattering from a single corner. The normal or sloping surfaces connecting the scattering centres in a down step or slot introduce a wavelength dependence into the problem and this manifests itself as resonances in the spectral scattering coefficients. It is a detailed interpretation of these resonances that is required for a Rayleigh waves based surface feature characterisation method.

After the interaction with a 90° corner, it is evident from Figure 7.18a that the incident pulse gives rise to pulses of reflected (Rr) and transmitted (Rt) Rayleigh waves, compression waves (C), shear waves (S) and von Schmidt head waves (vS). The shear-like head waves (vS) are generated because the surface grazing component of the compression wavefield cannot satisfy on its own the stress-free boundary conditions on the surface. Both the high and low frequencies contained in the incident pulse are reflected at the same time. The compression wave power is concentrated around a cone inclined at 45° to the surface, while the shear waves power is mainly contained in two lobes which are symmetric to either side of the wedge bisector (Portz *et al* (1980)).

When it comes to slots, there is an additional scattering source at the tip. Of

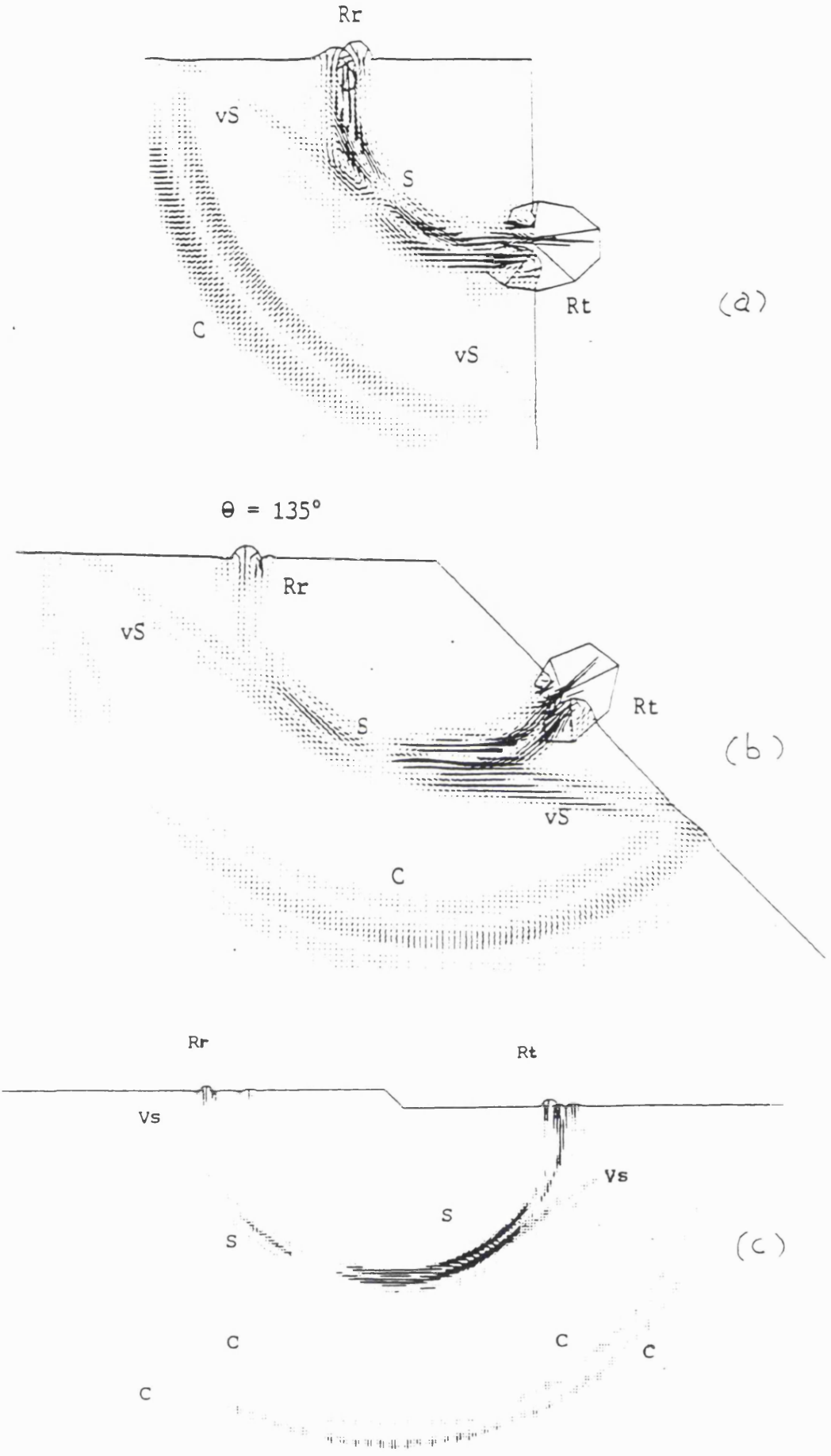

Figure 7.18 Numerical visualisation of Rayleigh waves scattering from a 90° corner (a), a 135° corner (b) and a 135° down step (c) (Blake and Bond (1990b))

course, some waves can be transmitted past the tip and scattered at the top corner of the trailing surface, but their contribution to the reflected wavefield is extremely weak (Section 6.2). A high frequency wavefield formed on the top corner of the leading surface propagates down the surface and interacts with the slot tip, producing a small reflected Rayleigh wavefield. This eventually propagates back up the leading slot surface and is transmitted onto the upper surface, contributing a small pulse to the reflected Rayleigh wavefield. Additionally, the middle and long wavefield components of the incident pulse create a Rayleigh wave pulse directly at the tip, provided that the Rayleigh pulse consists of such wavelengths that their penetration depth (1-1.5λ) is comparable to the slot depth. This wavefield is also transmitted back onto the upper surface (Munasinghe and Farnell (1973), Blake and Bond (1990a,b)). However, both these returns are hardly discernible in the time traces of normal cracks in Figure 7.5 due to their small amplitude when compared to the reflection from the crack top corner (Section 6.2).

As the angle of the top corner increases from 90° to 135°, the simultaneous interaction of the incident wave with the leading face of the crack is lost (Figure 7.18b). One could imagine its longer wavelength components impinging gradually on the sloping surface. Especially for 135° angled and kinked slots, the reflections from the tip and knee, respectively, are relatively stronger than the corresponding reflections of the normal slot when compared with the first corner reflection (Section 6.2.3). A "big" second pulse is evident in Figures 7.8 and 7.11-7.12, corresponding to the reflections from the tip 't' and the knee 'k', respectively. This pulse's amplitude is approximately equal to that predicted by the spectral technique of Section 6.2.3, namely 1/3-1/4 of that of the first reflection.

The irregular shape of the time traces, given in Figures 7.8 and 7.11-12, shows that there should be another strong source of Rayleigh waves, which interferes with the directly reflected pulse. By referring again to the numerical studies of Blake and Bond (1990b), the source of the extra mode-converted high frequency

wave is a surface grazing compression wave created at the first corner, which grazes down the first face of the crack and generates a reflected and transmitted Rayleigh pulse at the next scattering point (crack tip or knee point in kinked cracks). It should be remembered that for the same frequency, the compression wavelength is more than two times longer than the Rayleigh wavelength (see and Table 6.1 for the respective velocities). Hence the contributions due to the surface grazing compression wavefield may be significant and in fact they can be as large in amplitude as their accompanying Rayleigh wavefield for a 135° slot (*ibid*). Nevertheless, these contributions do not persist up to high frequencies: the surface grazing compression wave propagates as a part of a spherical wavefront which attenuates, due to cylindrical spreading, faster than the Rayleigh wavefield. Higher wavenumbers mean that the surface wavefront has to travel more wavelengths down the sloping surface and consequently is further reduced. After $d_1/\lambda \approx 2$, it should disappear and the reflection coefficients conform increasingly better to the predictions of the multiple scattering theory.

b) The resonances in the spectrum

The origin of the resonances in the scattered wavefield is more easily understood in the high frequency scattering regime. If the wavelength is small compared to the surface feature length, the Rayleigh wave attains its quiescent form rapidly after scattering from a corner. This is borne out by the curves expressing the reflection coefficients for the 90° and 135° slots (Figures 7.6 and 7.9) for high d/λ ratios. The reflection coefficients there tend asymptotically to their corresponding frequency-independent values for the corresponding corner. The scattering coefficients of the individual corners of a slot provide the basic ingredients for a multiple scattering approach to the problem, like that expressed by the analysis in Section 6.2. The wavefields, which are multiply scattered from top and bottom of the slots interfere in a constructive and destructive mode and this results in the periodic resonances in the spectral scattering coefficients (Section 5.4.2). .

As the ratio of d/λ decreases towards unity (the mid-frequency regime), there are still periodic resonances due to the wavefields generated at the scattering centres but their origins are more complicated. Here, the Rayleigh waves interacts with the whole of the sloping surface more or less instantaneously, depending of course on the angle of the sloping surface, as already explained. The wavefields scattered from the top corner do not reach their asymptotic forms before interacting with the next scattering source, and vice versa. The picture is further complicated by the fact that the surface grazing compression wavefield contributes another mode-converted Rayleigh pulse to the reflected wavefield. This pulse interferes with the returning pulse from the tip and further modifies the resonances, at least as long as the surface compression wave has enough amplitude ($d/\lambda<2$). As the wavelength increases still further, the surface feature geometry appears as a minor perturbation of the half-space geometry. The Rayleigh wave sweeps past the slot onto the other surface, creating a small scattered wavefield. In this long wavelength regime, the reflection coefficient increases more or less linearly with increasing frequency (Auld (1979)).

c) Kinked cracks

For kinked cracks, the analysis above would predict a mean amplitude given by the reflection coefficient of the angled part and modulated by the amplitude of the wavefield generated at the crack tip (pulse 't' in Figures 7.11-12). This modulation does provide a means for the inverse characterisation of the slots. It is reminded that most of the wavelength components of the incident pulse do not differ considerably from the angled part depth with which they interact. It is not therefore surprising that the spectra of the kinked slots are similar to that corresponding to the angled slot.

The regular modulations are clearly visible in the reflection coefficient of a long kinked crack (Figure 7.13c). As mentioned, this happens because the scattering

there refers to real high $(d_1+d_2)/\lambda$ ratios, allowing the wavefields to attain their asymptotic forms between the scattering events. The same applies, to a lesser degree, for the medium and short cracks. For the latter case, there is not enough time for the tip return to separate from the main event, that is the reflection from the whole angled part.

The tip pulse amplitude 't' is not that predicted by the analysis of Section 6.2, namely it is not about 1/10 of the amplitude of the top angle reflection, but significantly stronger. It is particularly reinforced for the shorter slot (Figure 7.12), being almost 1/4 of the amplitude of the first corner reflection and reduces with increasing normal parts. One can assume that a wavefield generated by the surface grazing compression wave is superposed on the wavefield created by the high frequency components at the crack tip. This leads to the amplification of the overall slot tip return. Because the compression wavefield is rapidly attenuated, the tip return is gradually reduced for cracks with longer normal parts, as the higher frequency wavefields are becoming the sole contributors to its formation.

For the particular experiments, the wavelength components of the incident pulse varied from 3.5mm (for 0.7MHz) to 0.5mm (for 6MHz). The normal depth of the angled part is approximately $2\cos45°=1.4$mm and for this reason the interaction of the incident pulse with the angled part mostly occurs in the middle frequency regime. Indeed, the tail of the incident pulse has enough structure for $\lambda=1.4$mm, so as to interact strongly with the knee point and create a wavefield there. This Rayleigh wavefield introduces an additional complexity to the scattering, as it propagates down the normal part and generates a wavefield at the tip. It seems that a second reason for the amplification of the amplitude of the pulse 't', apart from the influence of the surface grazing compression wave, is the overlapping of the wavefield generated in the way just described with the high frequency wavefield.

The amplitude of the modulations in the middle frequency regime, namely for

frequencies lower than those corresponding to the minimum of Figures 7.13 at f=2.6MHz, do not exhibit the same structure as the high frequency modulations. The longer wavelength components with are transmitted past the top corner have less time to reach their asymptotic forms, before being scattered by the knee. Also the reflected wavefield, which is due to the direct interaction of the tail of the incident pulse with the knee, is in the scattering near field of the top corner and this results in its amplification and enhances the modulations amplitude. However, an indication of length dependence can still be discerned in the middle frequency modulations, as their spacing tends to decrease with increasing normal slot lengths. This implies that whatever wavefields are instigated by the interaction of the middle and long wavelength components with the angled part, these are at the same time shorter than the overall slot length, especially for the longer slot. They can therefore travel down the longer normal part and effectively behave in way similar to that described for the shorter wavelengths. In this way, they produce the characteristic modulations. However, the spacing of these modulations cannot be quantified, because the presence of the surface grazing compression wavefield, which is strong for middle frequencies, interferes with them and alters their modulations periodicity.

The preceding discussion highlighted the fact that the angled part dominates the scattering, at least for the dimensions scale of the experiments. In terms of the general value of the reflection coefficient what really governs the scattering is the ratio of the wavelength over the angled part length and not the overall slot length. Nevertheless, a rather strong slot tip return is still discernible and can efficiently be used for crack measurements.

7.7.2 Time-of-flight considerations in a plate

Some methods of quantitative examination based on the back wall echoes will be considered in the light of insights gained from the experiments. The first topic is the possibility of applying the time-of-flight method, which is expressed by Equation 5.7. This equation, if solved for the depth d, yields for a normal crack:

$$d = \frac{c_R\ (\Delta T\ c_T - 2h)}{2(c_T - c_R)} \qquad (7.1)$$

where ΔT is the time difference between the first reflected pulse and the back-wall echo arrival time.

For the case of a 2 mm normal slot, the time difference is 15.1 μs in Figure 7.8. If c_T is taken as 3.13 km/s (Table 6.1), Equation 7.1 yields a crack depth of 2.1mm (error only 5 %). However, Equation 7.1 is very sensitive to the values of the velocities c_R and c_T, because its denominator is a difference of very similar quantities, the velocities c_R and c_T. The values of the velocities from the handbooks vary, as they depend on the particular experimental conditions (texture, stress field, residual stresses, temperature etc (Tittman and Buck (1980)). Because a change of 4% in c_T causes a 40% change in crack length, Equation 7.1 cannot in practice produce reliable results.

Nevertheless, this method of sizing is useful for qualitative estimation. It is based on Figures 5.4 and 7.19 where it has been assumed that the waves which travel from the crack tip to the back-wall and are reflected back are mode-converted shear waves (Section 5.4.2). Compare Figures 7.1 (90° corner) and 7.5 (normal slot) where the transit time ΔT refers to the same specimen thickness: there is an apparent decrease in the relative distance between the two echo complexes 'A' and 'B' in Figure 7.5 (ΔT=15.1 μs), due to the faster velocity of the shear waves between the crack tip and the back-wall, in contrast to the all-Rayleigh waves path of Figure 7.1

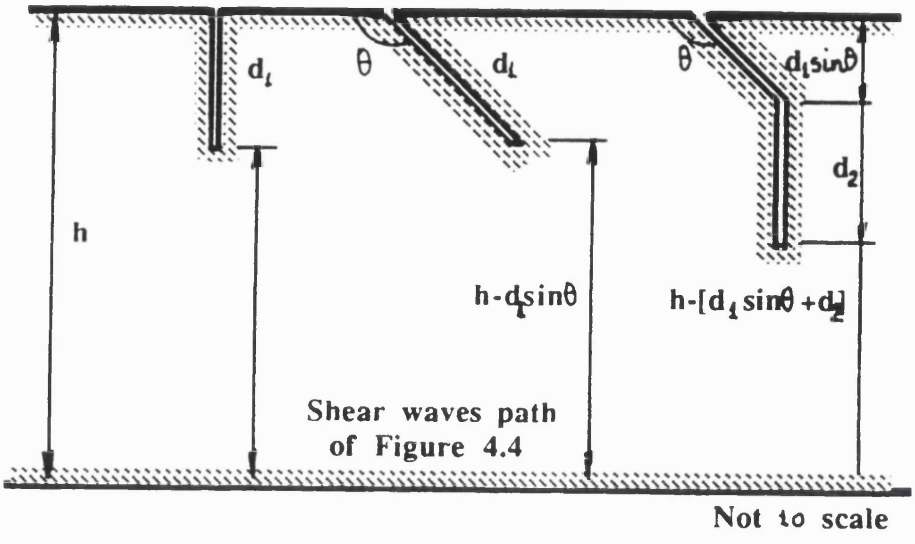

Figure 7.19 Ray theory analysis depicting the paths of the mode-converted shear waves generated at a corner A and reflected at the lower surface

between the upper and lower corners A and B (ΔT=16 μs). If we compare a normal slot of length 'd' and an angled one with approximately the same length, where the depth is smaller 'dcosθ' (Figure 7.8) and the path of the faster shear waves is longer 'h-dcosθ', there is a further decrease in the transit time (ΔT=15 μs). However, this observation does not facilitate the exact quantitative discrimination between the two cases, especially for very small lengths, since the examination is usually performed by sending a complex of echoes by a broadband transducer. The isolation of the returning signals, which are due to the small wavefields that follow the above mentioned path is invariably difficult.

Regarding now the kinked cracks, we can assume that the Rayleigh waves travelling down the first crack face follow a path similar to that in Figure 7.19 namely they are mode-converted to shear waves, reflect at the back wall and mode-convert again to Rayleigh waves when they travel back to the crack tip. In a similar

way as in Equation 5.7, the transit time between the first echo from A and the back-wall echo, is:

$$\Delta T = 2\left(\frac{d_1}{c_R} + \frac{d_2}{c_R}\right) + 2\left(\frac{h - (d_1\cos\theta + d_2)}{c_T}\right) \qquad (7.2)$$

or, assuming for a moment that the angled part length d_1 is known:

$$d_2 = \frac{c_R(\Delta T\ c_T - 2h) - 2d_1(c_T - c_R\cos\theta)}{2(c_T - c_R)} \qquad (7.3)$$

Application of Equation 7.3 in the kinked cracks cases of Figure 7.19 did not yield satisfactory results (about 50 % discrepancy which was strongly dependent on the chosen values of the transverse velocities). This is due to the nature of Equation 7.3, which produces transit times for the "short" and the "long" kinked crack very close to each other (15.2μs and 15.7μs respectively).

It seems that it must be added to the condition of application of the time-of-flight technique the prerequisite that the wavelength be smaller than the angled part. This is normally not easily attainable, especially for very small cracks such as these formed in fretting fatigue situations. Indeed, when the wavelength is in the order of the angled part length, the pulse sees this entire part at the same time and no discernible time differences occur. In this middle to low frequency regime, a surface grazing compression pulse is also formed, which generates its own Rayleigh and shear wavefields, compromising a single interpretation of the scattered wavefield for angled cracks. Another major limitation for kinked cracks is that the back wall echo is in any case a complex of several echoes, due to the additional shear waves generation at the angled corners of the crack. The returning Rayleigh waves from the crack tip are difficult to separate from the waves that are due to other features of the crack, since the arrival time of each mode-converted shear wave varies according to the where it was initially generated.

However, the main finding from the Equations of the type of 7.1 and 7.3 is

that the crack length is proportionate to the time delay between first and back-wall echo complexes, on the grounds that the waves travel more time as shear waves in the bulk of the body. This is a conclusion that can help the detection of a crack more than the quantitative characterisation of a crack. If the crack becomes longer, then the slower Rayleigh waves propagate on its faces for a longer distance 'd' relatively to constant plate thickness 'h'. The time-domain signals confirm this observation, albeit quantitatively, due again to very small difference between the velocities and the rather high d_1/λ ratios, in terms of the angled part. This is indicated by the (small) difference between the transit time (ΔT=15.7 μs) for the 'long' kinked crack (Figure 7.12c) and for the angled crack (ΔT=15 μs) (Figure 7.8). A same indication can also be seen in Figure 7.17. If a time difference can be reliably measured, this observation indicates that the crack has developed away from the surface. The digital time-measuring facility of the modern oscilloscopes can help this discrimination.

7.7.3 Arrival times of the secondary waves

In this subsection the nature of the secondary reflected waves is investigated and possible explanation is sought. First, the disturbances 'S' of Figure 7.1 can be attributed to the shear waves generated at the bottom corner 'B' (Figure 6.3). Indeed the transit time for the first reflected pulse from 'A' is:

$$\Delta T_1 = \frac{2x}{c_R} \qquad (7.4)$$

(x is the transducer-corner distance), while the corresponding transit time for the shear waves generated at 'B' by the Rayleigh wave which travels down the vertical side 'AB' is:

$$\Delta T_2 = \frac{x}{c_R} + \frac{h}{c_R} + \frac{\sqrt{x^2+h^2}}{c_T} \qquad (7.5)$$

(h is the plate thickness). The resulting time difference between the arrival times of the Rayleigh waves complex 'A' and the shear waves 'S' is:

$$\Delta T = \Delta T_2 - \Delta T_1 = -\frac{x}{c_R} + \frac{\sqrt{x^2+h^2}}{c_T} \qquad (7.6)$$

The results are 9.2μs, 10μs and 11.1μs for transducer-corner distance of 40mm, 30mm and 20mm respectively, which are approximately in agreement with the position of the series of disturbances 'S' of Figure 7.1 (corresponding to 6.4mm, 7.0mm and 7.8mm in it).

Nevertheless, the 'high' value of pulse 'S' is not easily explained by this scenario, if a ray analysis analogous to that of Section 6.2 is carried out. Besides, the exact position of 'S' is somewhat closer to the first reflection than the value predicted above. In accordance with Munasinghe and Farnell (1973) and the numerical visualisations of Blake (1988), it would be tempting to attribute the high value of 'S' to the direct interaction of the tail of the incident Rayleigh wave with the vertical side 'AB' of the plate, which creates a Rayleigh wave travelling down to B and back to the transducer, after being mode-converted to shear wave through the bulk of the body. The path of the waves emanating by this interaction is slightly shorter than of those transmitted past the apex 'A', hence the faster arrival of the pulse 'S'. The authors state that the resulting amplitudes are quite significant causing enhancement of the pulse 'S'. When the corner is not 90°, the simultaneous interaction of the tail of the incident pulse with the whole of the corner is lost and no analogous phenomenon occurs.

Focusing now on the kinked cracks, it can be seen from the time-domain signals shown in Figure 7.11 that there are some additional waves seen as

disturbances between the main signal from the kinked cracks and the backwall echoes. These overshadow some of the signals from main features of the kinked cracks. As they seem to move when the transducer-target distance changes, their identification might help the determination of the optimum distance for the transducer relatively to the target.

A possible explanation for the origin of these waves could be that they are shear waves which are generated at the apexes of the angled part of the kinked crack. Their wavefront is reflected and eventually directed back towards the transducer, propagating through the bulk of the specimen. Its ensuing spreading can be inferred from the ray model of Figure 7.20. When it reaches the transducer at the surface, the time that has elapsed after the initial transmission of the pulse will be:

$$\Delta T_2 = \frac{x}{c_R} + \frac{R}{c_T} \qquad (7.7)$$

where the wavefront radius, according to the preceding description is approximately

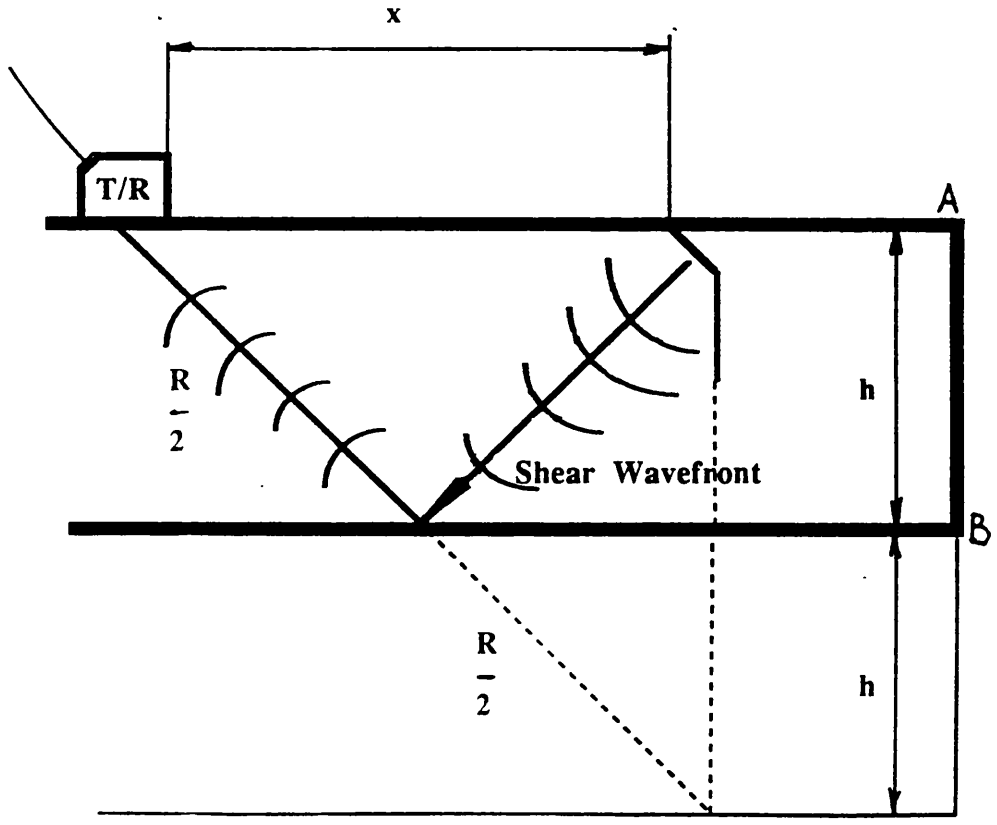

Figure 7.20 Ray theory depicting the wave arrival time of the secondary waves

given by the expression:

$$R = \sqrt{x^2+(2h)^2} \tag{7.8}$$

x is the distance transducer-slot and h is the distance between second angle and back-wall, which is taken as roughly equal to the block thickness.

The remarkable property of these back reflected shear waves is manifested by the observation that they seem to get closer to the first reflected pulse A as the distance transducer-target increases. This is due to their faster velocity relatively to that of the Rayleigh waves. Working out the arithmetic for the time difference $\Delta T=\Delta T_2-\Delta T_1$, the values of ΔT for the geometry in question will be 9.4, 7.5 and 6.1 μs for distances 20, 30 and 40 mm respectively, which are in agreement with the position of the additional pulses seen in Figure 7.11. Of course these "disturbances" are rather extended, since in fact they are not generated at a single point. As a short comment, this observation presents another feature that needs attention, because the distance of the transducer from the target must be adjusted in such a way so that no other reflections interfere with the Rayleigh waves reflections from any feature of the kinked crack.

Note also how "cleaner" the signal is before the first complex "A" of reflected Rayleigh waves, when the transducer gets farther from the target, in all the time traces (Figures 7.11). Apparently, when the transducer-target distance increases, the faster surface-skimming longitudinal waves have more time to separate.

7.8 Practical implications for a Rayleigh wave characterisation method

7.8.1 Transducer wavelength selection

When ultrasonic inspection is used for the characterisation of kinked cracks, the first step is to optimise the inspection configuration and instrumentation, so as to achieve the best possible signal to noise ratio. Fracture mechanics analysis can provide the tools for predicting the order of magnitude of the expecting cracks and hence some indication for the choice of inspection wavelength. This is very important, bearing in mind that most of the energy of the Rayleigh wave is concentrated near the surface. Best results are obtained when the angled part is comparable or longer than the wavelength. The reflection coefficient in this case allows unequivocal interpretation of the total crack length, and additionally yields the type of the crack, namely whether it is kinked or not. Time-of-flight considerations can also yield the total length, provided there are wavelength portions shorter than both the angled and normal part, so that the returning signals do not overlap. On the other hand, as the inspection wavelength is becoming much longer than the angled part, the backscattered signal contains increasingly little, if any, information about the angled part. An experimental attempt with $d_1/\lambda \leq 0.25$ showed there is no influence of the angled part in either domain of study, that can efficiently be used for NDE purposes. The incident pulse ignores the angled part, but it can still provide quantitative information about the normal part. In this case, the inspection refers to a virtually normal slot, where the angled part acts as an surface abnormality.

The experimental study showed that the conditions of applicability of the time of flight and spectral methods are very similar. They both rely on a high frequency multiple scattering theory to interpret the data. For the time of flight analysis this translates into the requirement that the spatial extent of the pulse be small compared to the crack. The simplistic time-domain analysis in the experimental study substantiated this point. A small spatial extent implies a large bandwidth transducer,

which must allow at least one complete cycle of oscillation in the high frequency spectra in order to size to defect. Only in this case can the crack tip return be discernible and cause modulation to the spectrum. If there is more than one cycle then the periods can be averaged to increase the accuracy of the sizing (Figures 7.13).The anticipated physical length of the crack also affects the testing. In general, high testing frequencies should be avoided when the surface of the fretted specimens is very rough and the wavelengths are of the order of the size of the surface asperities.

The masking of some important reflections from features of the crack by the secondary waves arrivals also needs attention. It might compromise both the time of flight analysis and the selection of the truncated signal for the frequency analysis. The problem is not an elementary one and has to do with many aspects of the transducer construction and angle, materials matching, plate dimensions etc, but the discussion of the previous section can provide some hints for the more simple case of the ray paths for higher frequencies. Moreover, multiple measurements by coupling the transducer in different positions relatively to the cracks can help the identification of the different returning signals. Also, the back wall echoes do provide some qualitative indications in terms of the crack propagation, although the multiple generating sources in kinked cracks makes the quantitative evaluation of the returning complexes difficult.

7.8.2 Condition of the surface

Victorov (1967) examines the effect of the surface condition and machining on the Rayleigh waves attenuation. It is shown that attenuation depends very significantly on the method of finishing and on the surface films. The present laboratory study involves parameters which are controllable to some extend, whereas in real cases the influence of debris in the crack as well as of crack closure, residual stresses, the possible 3-D nature of many cracks etc cannot easily be accounted for.

The ideal conditions for the absence of Rayleigh waves attenuation cannot be determined analytically, apart from trivial cases. For the simplest form of surface irregularity, the sinusoidal corrugation, a parameter $\Lambda=\lambda_R/(1\pm c_R/c_L)$ should be greater than some Λ_{max} ($12.740\lambda_T$ for aluminium, $4.895\lambda_T$ for steel), otherwise much of the energy of the incident pulse leaks away into scattered transverse waves (Viktorov (1967)). An examination of a sawtooth surface condition, by using a perturbation theory can be found in Auld (1973)

The possible curvature of the crack corners poses a more complex problem. For "sharp" knee corners the "second" high pulse (Figures 7.11-12) determines the knee position for kinked cracks with a distinct knee angle. It can be expected that for radius of curvature 'r' at the knee point, such that $r/\lambda \geq 1.5$ the Rayleigh wave will follow the contour until it is reflected at the crack tip (Viktorov (1967); the value refers to a 90° rounded wedge). This case can easier be treated by a simplistic time of flight measurement, since the crack tip arrival remains unaffected by the knee corner. In terms of a spectral method based on the Rayleigh waves reflection, the curvature can significantly affect the reflected wavefield, causing new resonances and destroying the high frequency oscillations which would otherwise occur (Blake and Bond (1992)).

Erroneous results can also be obtained due to the phenomenon of crack closure, especially when the stamp presses onto the fretted surface during testing. Clark *et al* (1987) have examined the effect of crack closure on the reliability of NDE predictions. They found that although most NDE techniques were fairly reliable for small negative loads, the reliability of length sizing reduces with increasing negative loads, until a point of no-detection is reached. This is due to the contact of the crack faces, which contributes a larger amount to the wave transmitted through the crack and thereby reduces the reflected energy. These changes will reduce the detectability and lead to the crack size estimates that are too small. The problem of crack closure detection is very important for the interpretation of fatigue data and

needs further investigation, because it influences strongly the capability for accurate life predictions. For this reason, it has recently received much interest and is still under scrutiny (Rehbein *et al* (1990)). Finally, note that the presence of fluids or corrosion products between the crack faces results in overestimate of the crack depth (Doyle and Scala (1990)).

7.8.3 Orientation of the crack

One of the main criticisms of the simple time of flight and spectroscopic techniques is that they invariably give information about the length of the crack and give no details about their orientation and width. A full characterisation of the crack may have been possible with multi probe methods (Silk (1976), Coffey (1980)), if panoramic access to the crack is possible. Bearing in mind the greater experimental problems of the pitch-catch methods, it seems sensible that the spectral reflected Rayleigh wavefield can be more appropriate.

The findings of this study showed that the shape of the reflection coefficients spectra contains some information about crack orientation. Especially for the high frequency regime and according to the discussion in Section 6.2, the reflection is characterised by the term R_α which depends on the angle. The orientation of the slot (inclined or normal to the surface) can be deduced from the fact that the reflection from a normal crack is akin to that from a 90° wedge (Reflection coefficient≈0.35-40) and unquestionably much stronger than that from the inclined and kinked slots (Reflection coefficient≈0.10-0.15). These reflection refer to rather high frequencies ($d/\lambda \geq 2$-3), since in the low frequency region ($d/\lambda < 0.5$) there is little structure, the reflection coefficient increases linearly with wavenumber and the amount of information obtainable is limited (Visscher (1986)).

This ultrasonics analysis dealt only with a 135° initial angle. An illustration

of the dependence of the reflection coefficient from the angle of the slot is presented in Figure 7.21, compiled from data published by Gautessen (1985,1987) (spectral theory), Kinra and Vu (1986) (experimental results) and Blake and Bond (1990a-b) (finite differences/finite elements). It can be mentioned that as the internal angle increases from 90° to 180°, the amplitude of the reflected Rayleigh waves first increases up to the 105° corner and then decreases monotonically to zero, as it must do because the Rayleigh waves remain unscattered on the half-space (the 180° wedge). These variations could be used to evaluate the orientation of the angled part. The time domain signal from the first angle can be truncated, its magnitude can be determined and eventually compared with Figure 7.21 to yield the crack inclination. Of course it is supposed that the wavelengths are smaller or of the same size as the angled part.

The reflection is generally stronger for acute angled slots (Kinra and Vu (1986) and Figure 7.21). A plausible scenario for the intensification of the reflected wavefield for acute angles is that the smaller the angle, the more possible is for the strong body waves scattered at the leading crack face to mode-convert into Rayleigh waves and superimpose onto the directly reflected Rayleigh waves. Thus the transmitted pulse gets weaker and the reflected pulse gets stronger. On the other hand, the body waves reflected from the leading face of an obtuse angled slot are generally weaker and aim towards the interior of the half-space (Figure 7.18) namely away from the surface and thus their contribution to the reflected surface waves dwindles. Therefore, the above analysis indicates that the reflection coefficient is a very strong discriminator between an acute slot and its obtuse complementary slot.

The experimental investigation also showed that the examination from the acute angle (45°) side did not aid the length measurements, because the waves scattered past the knee point were much weaker than the stronger arrivals from the first corner and they could not induce any modulations. A strong modulation is therefore a basic requirement for the employed spectral technique for length

measurement. Because the spectral modulations depend on the reflection and transmission coefficients of the corners of a surface feature (Section 6.2) and these coefficients depend strongly on the angle (Figure 7.21), the effect of crack orientation on spectral modulation needs to be established.

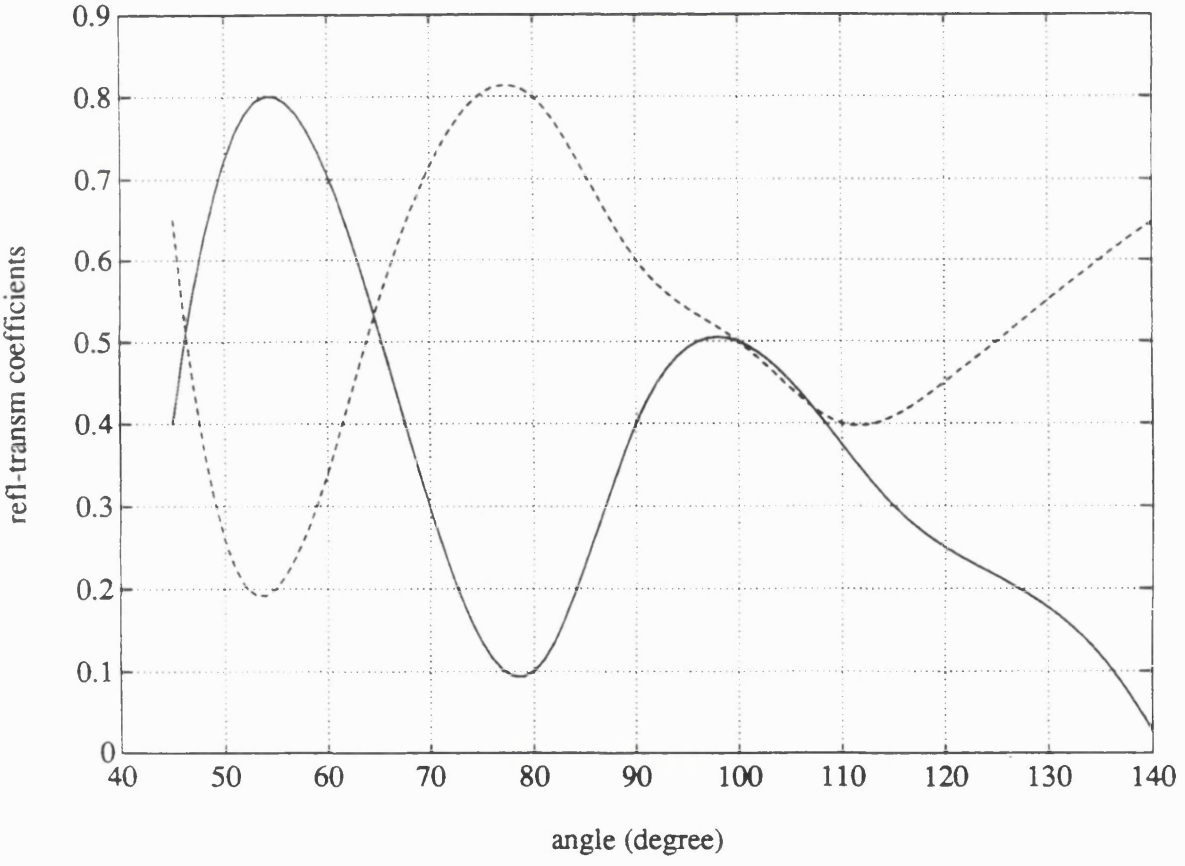

Figure 7.21 Reflection and transmission coefficients for corners in aluminium (ν=0.33-0.34) (data from Gautessen (1987))

For this purpose, consider Equation 6.8, which gives the backscattered wave for a crack. It can be supposed that, at least for the high frequency spectral analysis, the theoretical values of R_α and T_α from Figure 7.21 can be used to examine how the backscattered amplitude depends on the crack angle on the incident wave side. If the influence of the leading order terms of Equation 6.8 is considered, it is obvious that the strength of the modulations depends on the relative value of the second term $T^2_\alpha R_t$ over the value of the first term R_α (R_t=0.1). Clearly, the amplitude of the modulations is very small for angles 55°-60° and 110°, where the reflection coefficient is high and the transmission coefficient is low and hence the method is least suitable for these angles. By the same token, the method is better applied for 135° than for 45° slanted cracks. For kinked cracks the above analysis becomes very complicated, but it can still assumed that the fourth order term of Equation 6.10 which includes the slot tip influence R_t affects the leading terms in a similar way. This conjecture is at least partly supported by the experimental measurements for 135°, where the modulations due to the slot tip are superposed on a spectral reflection coefficient akin to that of a 135° slot. The conclusion is that the sensitivity of the spectral technique varies markedly with crack angle, but a quantitative evaluation is possible, at least for high frequencies.

8. CONCLUSIONS AND SUGGESTIONS FOR FURTHER WORK

8.1 Summary of the results

The results reported in this thesis allow conclusions to be drawn about the characterisation of fretting fatigue cracks, when these cracks are still in the first stage of their propagation. Fretting fatigue cracks appearing in standard specimens in materials evaluation programmes were considered. The cracks are modelled as kinked surface slots which remain open during their examination with a Rayleigh waves ultrasonics characterisation method. A stress and fracture mechanics analysis was first conducted, in order to study the parameters that affect the shape of these cracks as well as to obtain an estimation of the anticipated order of size of the kinked cracks, so that a suitable range of transducer frequencies can be chosen.

In the fracture mechanics part of this study, contact pressure and tangential stress distributions can be obtained by stress analysis for given contact conditions. The stress analysis showed the local influence of the fretting phenomenon. The combined action of the frictional and the normal pressure cause the emergence of cracks which are initially at an angle to the surface and develop under the fretting pads. Although in practice the microstructure of the material plays a significant role, according to the present theoretical model the possible points of crack initiation were found to be located just under the edges of the fretting pads.

The method of continuous dislocations was then employed with an aim of determining the angled cracks SIFs in a typical fretting fatigue situation. A new

mathematical model was formulated and a numerical scheme was developed for the case of normally and tangentially half-space, which emulates the fretting specimen, in the presence of a crack. The comparison of this method with the more popular finite elements method demonstrated the superiority of the present method in terms of speed and computer space, at least for the present configuration. The continuous dislocations method requires no meshing of the crack model; the numerical analysis of the model is faster and it can been carried out even on a small computer. The method can also be easily adapted for most crack tip singularities, so is suitable for the study of both edge and buried cracks. Next, the stability and accuracy properties of the numerical scheme were analyzed and the convergence properties of the solution were demonstrated.It was found that for "shallow" crack angles ($\leq 30°$ under the pads) the resulting matrices were small for simple crack geometries and convergence occurs relatively fast. The model was further extended to the case when the specimen and the fretting pad are of different material.

New SIFs results for fretting crack for various lengths, angles and friction coefficient have been determined, based on the understanding that the general requirements for the applicability of the LEFM hold true. The mode-I SIFs were found to be negative under the pads. This indicates a crack closure phenomenon which seems to alleviate the influence of the bulk fatigue stress and can lead to crack arrest, if the bulk tensile stress cannot on its own sustain the crack propagation. It was also found, however, that the tangential stress, which is due to the friction, can make the SIFs positive especially for small cracks and therefore suppression of friction is in general desirable. The critical crack size in fretting fatigue was estimated by comparing the calculated results of the SIFs with the threshold SIF in terms of both crack length and SIFs ratio R. The fatigue analysis showed that fretting generally reduces the critical defect size. The influence of the normal pressure was estimated and it was found that increase in normal pressure may be beneficial for the component life under fretting conditions. The influence of the materials of the fretting pad and the specimen was also investigated. It was concluded that a simpler

model with uniform distribution of fretting tractions, can adequately describe the fretting fatigue configuration, in most cases. For the solution of the model, the uncoupling of the crack and contact models gave good results and reduced the calculation time.

The general conclusion, substantiated by experimental data from the literature, is that fretting fatigue may best be assessed by a method based on fracture mechanics, rather by simply relating fretting fatigue strength to relative slip range. Some problems may be introduced by the short length of the cracks involved, and therefore care must be taken as regards the validity of fracture mechanics calculations for short cracks.

In the second part of this study an ultrasonics testing method using Rayleigh waves was examined. The aim was to demonstrate the possibility of characterising fretting fatigue cracks in terms of their length and stage of their growth, so that they can complement the fracture mechanics study with crack length data. The kinked crack propagation was modelled by a series of 2-D slots in aluminium alloy plates, whose initial angle was chosen to be 135° (or 45° under the pads). First, a spectral ray analysis was conducted in order to determine the amplitudes of the returning signals from the crack for high frequencies. A ultrasonics spectroscopy system was next described. By employing this system, Rayleigh waves pulses were directed towards model slots and their interaction with the slots was analyzed in both the time and frequency domain. The reflection coefficients for kinked cracks for the case when the testing wavelengths are of the same size scale as the angled part, were determined. The results were compared with data from the literature, where these were available. It was found that simply comparing the amplitude of the scattered wavefield with those from reference features is vulnerable to the large errors which plague ultrasonic experiments. Nevertheless, measuring the spacing of the extremities in the reflection coefficient and connecting them with the total crack length through a simple relationship does provide a means of quantitative characterisation of the

crack length.

The simplistic time-of-flight technique was found to be quite straightforward for the crack characterisation, if some *ad hoc* data for the crack length are known, so that the suitable range of testing frequencies are used. As regards the reflection coefficient of a kinked crack, this can be expressed in terms of the ratio d_1/λ, which gives the relation between the angled part length 'd_1' and the wavelength 'λ'. For values of $d_1/\lambda \geq 2\text{-}3$, namely for high frequencies, the pulse increasingly sees the kinked slot as if it were a angled slot. The echo resulting from the interaction of the incident pulse with the knee was evident in all measurements and its amplitude agreed well with that predicted by a spectral technique. Its position can provide enough data for the measurement of the angled part length, in the time domain. Truncating the portion of the signal reflected from the first corner and studying it in the frequency domain can yield information about the crack orientation. On the other end, when long wavelengths are used for the testing, the incident pulse barely recognises the angled part of a kinked slot. The behaviour of the kinked slot is there akin to that for a slot which is normal to the surface. This case is applicable for minute cracks when the attenuation due to surface asperities does not allow the testing with higher frequencies. Inspection with frequencies in the region between these two limits facilitates the cracks evaluation through the use of spectral analysis.

A correctly selected position for coupling of the transducer relatively to the slot is also necessary, so that the secondary signals do not interfere with the main backscattered signal. Careful interpretation of the secondary echoes which emerge in a tested plate is necessary, as they can mask reflections from important features of the crack. For this reason, the coupling of the transducer at various distances from the slot may be considered. The examination by the pitch-catch method or from the other side of the crack, whenever possible, is not advisable, since the important echoes are too tiny for unequivocal interpretation.

8.2 Suggestions for further work

Further experimental research is needed for the characterization of the frictional force which affects the fretting fatigue for different frictional waveforms (Rooke and Edwards (1987)) as well as on the history of loading during the loading and unloading phases (Sheppard *et al* (1986)). Supplementary studies are also required for the investigation of the limits of the SIF approach to the fretting fatigue. The crack tip plasticity effects for small cracks and the increase of the calculated SIF due to them must be included in this quest. Plastic fracture mechanics can be employed for very small cracks.

The mathematical crack-contact problem is of extreme interest. Its solution in more complex configurations can be facilitated by the powerful numerical methods currently available. The continuous dislocations method which was employed in the first part of this work can be extended to treat various combinations of materials and distributions of the frictional traction. It has also been demonstrated elsewhere that this method can successfully deal with partially closed cracks and open kinked cracks (Li Yinghzi and Hills (1990)). Its extension for partially closed kinked cracks (Hills and Nowell (1989)) which are subjected to normal and tangential loading should be quite straightforward. As the transition from an angled crack to a perpendicular one is sometimes smooth and there may be no distinct knee point, an analysis of an arc-shaped crack (as in Xiaping and Comninou (1990)) encountered in fretting fatigue should also be pursued.

The short cracks initiation and characterisation have drawn considerable interest in recent years, as their role in microvoid coalescence and crack formation is realised (de los Rios and Miller (1986)). The effects of the mixed mode loading on the crack growth thresholds have been also considered (Pook (1985)). As these factors influence the fretting fatigue crack growth, more sophisticated models need

to be incorporated in the fretting fatigue studies. The classical phenomena of the fretting as a tribology and wear problem, which affect the initial formation of cracks were beyond the scope of this work, but obviously need exploration.

In terms of the Rayleigh waves scattering, numerical models can be employed for the study of the kinked cracks. These can consider different ratios of d_1/λ (angled part length over the wavelength). The numerical models can easily be adapted to deal with curved geometries (Blake and Bond (1992)), namely the cases where the kinked geometry is smoother, with no distinct knee point. They can also be combined with energy models and ray theory, so that the interaction of a Rayleigh wave pulse with a plate, instead of a half-space, can be investigated (as in Bond and Taylor (1991)). The ensuing numerical visualizations will give not only a better understanding of the phenomenon, but they will also direct the investigation in the selection of the proper position of the transducers to avoid the spurious reverberations.

Experimental and theoretical work must be extended to measure the phase change of the scattered Rayleigh waves for a slot. The effect of Poisson's ratio on the reflection and transmission coefficients and on the phase angle should be considered. The available results in the literature to date (for example Gautessen (1987)), seem to be incomplete and have large discrepancies between them.

The crack closure phenomena are of paramount importance, and should be dealt with (Buck *et al* (1990)). A NDE measurement capable of determining the effective crack depth during partial crack closure would be important, since it could determine important quantities such as the residual stress, crack closure stress and time dependent stress relaxation, which seem to modify the various expressions of the Paris'-type equations. A study of the reliability of the inspection for these complicated scatterers would also be interesting.

Finally, the stress field and SIFs in a kinked crack could be theoretically

calculated by using ultrasonics theory. This can be carried out either for $d/\lambda \leq 0.01$ (in the long wavelength limit by using quasistatic approximation, Resch *et al* (1979)) or for $d/\lambda > 1$ (ray theory, Achenbach *et al* (1982)), which would provide another source of information and check for the fracture mechanics parameters.

The ultimate objective of every NDE method is to find the location, length and orientation of the crack from the scattered field, so that accurate failure predictions can be made. We are far from achieving this goal, even though some properties of the scattered field can be used for the so-called inversion problem. The problem itself is intellectually challenging. As an epilogue, it is worth quoting Pao (1983) who reviewed the theory of elastic waves propagation and scattering for the 50th anniversary issue of the *Journal of Applied Mechanics-Transactions of the ASME*: "Looking ahead a little further, we believe the inverse problems will be a good topic for a review article in the centennial volume of the *J. Appl. Mech.*"

APPENDIX

Stress Field in the neighbourhood of a dislocation

The problem of defining the stress field induced by a dislocation in the neighbourhood of an elastic inclusion with different elastic properties from the dislocation itself, has been solved by Dundurs *et al* (1964,1965). Using the coordinates of Figure A1 and employing the subscripts 1 and 2 for reference to the regions indicated, the Airy stress functions for a Burgers vector normal to the interface are:

$$\xi_{2N} = \frac{G_1 b_x}{\pi(\kappa_1+1)}[-(2-A-B)r_1 logr_1 \sin\theta_1+(B-A)(r_1\theta_1\cos\theta_1+2c\theta_1)] \qquad (A.1)$$

$$\xi_{1N} = \frac{G_1 b_x}{\pi(\kappa_1+1)}[-2r_1 logr_1 \sin\theta_1+(B+A)r_2 logr_2 \sin\theta_2+$$

$$+(B-A)r_2\theta_2\cos\theta_2-2Ac(\sin 2\theta_2-2c\frac{\sin\theta_2}{r_2})]$$

For a Burgers parallel to the interface the Airy stress functions are:

$$\xi_{1P} = \frac{G_1 b_y}{\pi(\kappa_1+1)}[2r_1 logr_1 \sin\theta_1-(B+A)r_2 logr_2 \sin\theta_2+$$

$$+(B-A)r_2\theta_2\cos\theta_2+2Ac(2logr_2-cos2\theta_2+2c\frac{\cos\theta_2}{r_2})] \qquad (A.3)$$

$$\xi_{2P} = \frac{G_1 b_y}{\pi(\kappa_1+1)}[-(2-A-B)r_1 logr_1 \sin\theta_1-(B-A)(r_1\theta_1\cos\theta_1+2clogr_1)] \qquad (A.4)$$

where G is the shear modulus, ν is the Poisson's ratio and:

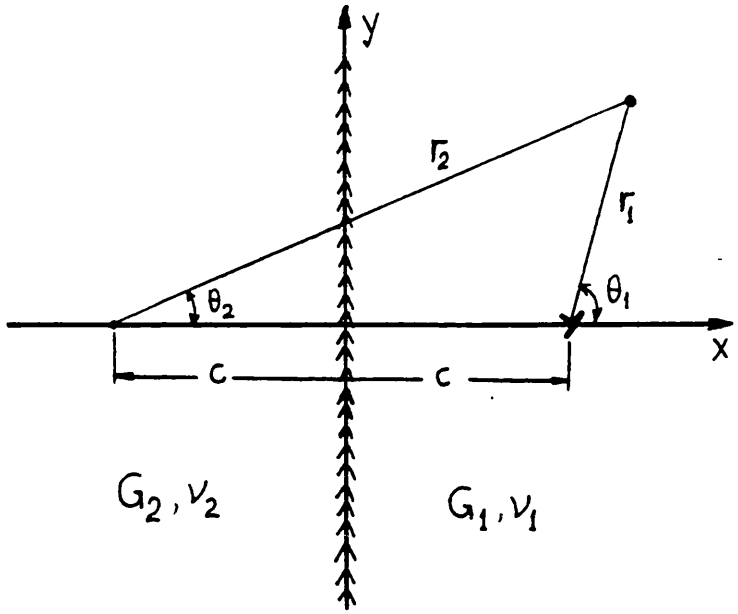

Figure A.1 Edge dislocation near a bimetallic interface (after Dundurs et al (1964))

$$A = (1-\Gamma) / (1+\Gamma\kappa_1), \qquad B = (\kappa_2-\Gamma\kappa_1) / (\kappa_2+\Gamma) \qquad (A.5)$$

with $\Gamma = G_2/G_1$, $\kappa=3-4\nu$ for plane strain and $\kappa=(3-\nu)/(1+\nu)$ for plane stress.

Obviously, in our case $\Gamma=1$, $A=B=0$ and $\kappa_1=\kappa_2$ since we do not deal with two different materials. The desired stress components are simply the derivatives of the Airy stress function:

$$\sigma_{xx}=\frac{\partial^2\xi}{\partial y^2}, \quad \sigma_{xy}=-\frac{\partial^2\xi}{\partial x\partial y}, \quad \sigma_{yy}=\frac{\partial^2\xi}{\partial x^2} \qquad (A.6)$$

Alternatively, the stresses can be calculated by making use of the Equations A.1-4 and the Appendix of a paper by Dundurs and Mura (1964), where they performed all the algebraic calculations. The results, taken from Nowell and Hills (1987) are:

$$G_{xxx} = y\left[\frac{-2}{r_1^2} - \frac{4(x-c)^2}{r_1^4} + \frac{2}{r_2^2} + \frac{4(x+c)^2}{r_2^4} - \frac{8c(x+c)}{r_2^4} + \frac{32(x+c)^3}{r_2^6} + \frac{8c^2}{r_2^4} - \frac{32c^2(x+c)^2}{r_2^6}\right] \quad \text{(A.7)}$$

$$G_{xyy} = y\left[\frac{-2}{r_1^2} + \frac{4(x-c)^2}{r_1^4} + \frac{2}{r_2^2} - \frac{4(x+c)^2}{r_2^4} + \frac{24c(x+c)}{r_2^4} - \frac{32(x+c)^3}{r_2^6} - \frac{8c^2}{r_2^4} + \frac{32c^2(x+c)^2}{r_2^6}\right] \quad \text{(A.8)}$$

$$G_{yxy} = y\left[\frac{-2}{r_1^2} + \frac{4(x-c)^2}{r_1^4} + \frac{2}{r_2^2} - \frac{4(x+c)^2}{r_2^4} - \frac{8c(x+c)}{r_2^4} + \frac{32(x+c)^3}{r_2^6} + \frac{8c^2}{r_2^4} - \frac{32c^2(x+c)^2}{r_2^6}\right] \quad \text{(A.9)}$$

$$G_{xxy} = \left[\frac{-2(x-c)}{r_1^2} + \frac{4(x-c)^3}{r_1^4} + \frac{2(x+c)}{r_2^2} - \frac{4(x+c)^2}{r_2^4} - \frac{4c}{r_2^4} + \frac{32(x+c)^2}{r_2^4} - \frac{32c(x+c)^4}{r_2^6} - \frac{24c^2(x+c)}{r_2^4} + \frac{32c^2(x+c)^3}{r_2^6}\right] \quad \text{(A.10)}$$

$$G_{yxx} = \left[\frac{-2(x-c)}{r_1^2} - \frac{4(x-c)^3}{r_1^4} + \frac{2(x+c)}{r_2^2} - \frac{4(x+c)^2}{r_2^4} - \frac{4c}{r_2^4} - \frac{16(x+c)^2}{r_2^4} + \frac{32c(x+c)^4}{r_2^6} + \frac{24c^2(x+c)}{r_2^4} - \frac{32c^2(x+c)^3}{r_2^6}\right] \quad \text{(A.11)}$$

$$G_{yyy} = \left[\frac{6(x-c)}{r_1^2} - \frac{4(x-c)^3}{r_1^4} - \frac{6(x+c)}{r_2^2} + \frac{4(x+c)^2}{r_2^4} - \frac{4c}{r_2^4} + \frac{32(x+c)^2}{r_2^4} - \frac{32c(x+c)^4}{r_2^6} - \frac{24c^2(x+c)}{r_2^4} + \frac{32c^2(x+c)^3}{r_2^6}\right] \quad \text{(A.12)}$$

where:

$$r_1^2 = (x-c)^2 + y^2$$
$$r_2^2 = (x+c)^2 + y^2 \qquad \text{(A.13)}$$

In the same paper by Dundurs *et al* the resulting displacements are given. We can find the gradients at the interface between two bodies by taking x=0 and $\theta_1=\theta_2$:

$$\frac{\partial u_x}{\partial y} = b_x \left[\frac{1}{\pi}\frac{2yc^2}{(y^2+c^2)^2}\right] + b_y \left[-\frac{c}{\pi}\frac{c^2-y^2}{(y^2+c^2)^2}\right] \qquad \text{(A.14)}$$

The expressions in brackets provide the two additional kernels K^{surf}_i, i=x and y in the case where the material properties of the system are taken into account.

REFERENCES

Abdel Mageed A.M. and Pandey R.K. (1990), "Fatigue Crack Closure in Kinked Cracks and Path of Crack Propagation", *Int. J. Fracture,* Vol. 44, pp. R39-R42

Abramowitz M. and Stegun I.A. (1965), *Handbook of Mathematical Functions,* Dover, (New York)

Achenbach J.D. and Gautesen A.K. (1978) " A Ray Theory for Elastodynamic Stress Intensity Factors", *J. Appl. Mechanics,* Vol. 45, pp. 123-129

Achenbach J.D., Gautesen A.K. and Mendelsohn D.A. (1980) "Ray Analysis of Surface-Wave interaction with and Edge Crack", *IEEE Trans. Sonics Ultras.,* Vol. SU-27, No.3 ,pp. 124-129

Achenbach J.D., Gautesen A.K. and McMaken H.(1982), *Ray Methods for Waves in Elastic Solids* ,Pittman UK, (London)

Achenbach J.D. (1990), "From Ultrasonics to Failure Prevention", *Proc. IUTAM Symp. on Elastic wave propag. and Ultrasonic Evaluation,* ed. S.K. Datta, J.D. Achenbach, Y.S. Rajapakse, Elsevier, (Amsterdam)

Atkins A.G. and Mai Y.W. (1985), *Elastic and Plastic Fracture: Metals, Polymers, Ceramics, Composites, Biological Materials",* Ellis Norwood Ltd, London

Auld B.A. (1973), *Acoustic fields and waves in solids,* J. Wiley and Sons, New York

Auld B.A. (1979), "General Electromagnetic Reciprocity Relations applied to the calculation of elastic wave scattering coefficient", *Wave Motion,* Vol. 1, pp. 3-10

Blake R.J. (1988) "Numerical Models for Rayleigh Wave Scattering from Surface Features", Ph.D. Thesis, University of London.

Blake R.J. and Bond L.J. (1990a) "A general model for Rayleigh Wave- surface feature scattering problems", in *Review of Progress in Quantitative Nondestructive Evaluation*, Vol. 9A, D.O Thomson and D.E Chimenti, Eds, Plenum Press, (New York and London), pp. 77-84

Blake R.J. and Bond L.J. (1990b), "Rayleigh Waves Scattering from surface Features: Wedges and down steps",*Ultrasonics*, Vol. 28, pp. 214-228

Blake R.J. and Bond L.J. (1992), "Rayleigh Wave Scattering from 3-D Hemispherical Depressions and Surface Slots", in *Review of Progress in Quantitative Nondestructive Evaluation*, Vol. 11, D.O Thomson and D.E Chimenti, Eds, Plenum Press, (New York and London)

Blom A.F., Hedlund A., Zhao W., Fathulla A., Weiss B. and Stickler R. (1986), "Short fatigue crack growth behaviour in Al 2024 and Al 7475", in *The Behaviour of Short Fatigue Cracks,* EGF Pub.1, K.J. Miller and E.R. de los Rios, Eds, Mechanical Engineering Publications, London, pp. 37-66

Bond L.J.(1978),"Surface Cracks in metals and their characterisation using Rayleigh Waves", PhD Thesis, The City University, London , UK

Bond L.J.,(1979), "A computer model of the interaction of acoustic surface waves with discontinuities", *Ultrasonics,* Vol. 17, pp. 71-77

Bond L.J., Punjani M. and Saffari N. (1984a) "Review of some recent advances in quantitative ultrasonic NDT", *IEE Proc.,* Part A, Vol 131, pp. 265-274

Bond L.J. and Saffari N.(1984b) "Mode conversion ultrasonics testing",*Research*

Techniques in NDT, Vol.7, Ed. Sharpe R.S. ,Academic Press, (New York and London), pp. 145-189

Bond L.J. and Taylor J. (1991), "Interaction of Rayleigh waves with a rib attached to a plate", *Ultrasonics,* Vol. 29 , pp. 451-458

Bray D.E. and Stanley R.K. (1989), *Nondestructive Evaluation, A Tool for Design, Manufacturing and Service,* McGraw-Hill Book Company, New York.

Broek D. (1974), *Elementary Fracture Mechanics*, Noordhoff, (Leiden)

Brook D. and Wynne R.J. (1988), *Signal Processing*, Edward Arnold, (London)

Buck O., Thomson R.B., Rehbein D.K. and VanWyk L. (1990), "Acoustic wave interaction with partially closed cracks", *Proc. IUTAM Symp. 1989*, Ed. S.K. Datta *et al*, Elsevier, (Amsterdam)

Chaloner C.A. and Bond L.J. (1987), "Investigation of the 1-D inverse Bond technique", *IEE Proc.*, Vol. 134, Pt. A, No. 3, pp. 257-265

Clark R, Dover W.D. and Bond L.J. (1987), "The effect of crack closure on the reliability of NDT predictions of crack size", *NDT Int,* Vol. 20, No. 5, pp. 269-275

Coffey J.M. ((1980), "Ultrasonic measurement of Crack Dimensions in Laboratory Specimens", in *The measurement of crack length and shape during fracture and fatigue,* Beevers C.J, Ed., Engineering Materials Advisory Services Ltd, (Cradley Heath, Warley, U.K), pp. 345-385

Comninou Maria (1976) "Stress Singularity at a Sharp Edge in Contact Problems with Friction",*ZAMP*, Vol. 27,pp.493-499

Cooper J.A., Dewhurst R.J. and Palmer S.B. (1986), "Characterization of surface-breaking defects in metals with the use of laser-generated ultrasound", *Phil. Trans. R. Soc. Lond.*, A 320, pp. 319-328

Datta S.K. and Shah A.H. (1987), "Ultrasonic Scattering by planar and non-planar cracks", in *Review of Progress in Quantitative Nondestructive Evaluation*, Vol. 6A, D.O Thomson and D.E Chimenti, Eds, Plenum Press, (New York and London), pp. 69-78

Davies S.J. and Palmer S.B. (1991), "Laser-generated Rayleigh wave interactions with surface-breaking defects", in *Review of Progress in Quantitative Nondestructive Evaluation,* Vol. 10A, D.O Thomson and D.E Chimenti, Eds, Plenum Press, (New York and London), pp. 121-128

de Los Rios E.R., Mohammed H.J. and Miller K. J. (1985) "A micro-mechanics analysis for short fatigue crack growth", *Int. J. Eng. Matls and Struct.*, Vol. 8, pp. 49-64.

Dewynne J.N., Hills D.A. and Nowell D. (1992), "The opening displacement of Surface-breaking Plane Cracks "*J. Strain Analysis,* in press

DiLeonardo G.(1979), "Fracture toughness characterization of materials under multiaxial loading", *Int.J.Fracture*, Vol.15, No.6, pp. 537-552

Doyle P.A. and Scala C.M. (1978), "Crack Depth Measurement by Ultrasonics: a Review", *Ultrasonics*, Vol. 16, pp. 164-170

Doyle P. A. (1986) "Depth Measurement for Cracks in Corners Using Ultrasonics Rayleigh Waves", *J. NDE*, 5,pp. 179-187

Doyle P.A. and Scala C.M. (1987)"Depth measurements for corner cracks Using Rayleigh wave spectrum modulation" ,*Proceedings Ultrasonics Int. 87* , Butterworths, (Oxford), pp. 407-412

Doyle P.A. and Scala C.M. (1990),"Depth measurements for corner cracks of arbitrary angle using Rayleigh waves", *Ultrasonics*, Vol. 28, No. 2, pp. 77-82

Dundurs J. and Mura T.(1963) "Interaction between an edge dislocation and a circular inclusion", *J. Mech.Phys.Solids*,Vol. 12, pp.177-189

Dundurs J. and Sendeckyj G.P.(1964) "Behaviour of an edge dislocation near a bimetallic interface",*J.Appl.Phys.*, Vol.36, pp. 3353-3354

Dundurs J. and Lee M.S. (1972) "Sharp concentrations at a sharp edge in contact problems",*J. Elasticity*, Vol. 2, pp. 109-112

Edwards P.R., Ryman R.J. and Cook R.(1977) "Fracture Mechanics Prediction of Fretting Fatigue",*Proc. 9th ICAF Symposium*, (Darmstadt), pp. 255-262

Edwards P.R. and Cook R. (1978a) "Fracture Mechanics Prediction of Fretting Fatigue under Constant and Variable Loading", *Proc. 11th ICAF Symposium*, pp 505-517

Edwards P.R. and Cook R. (1978b) "Frictional Force Measurements on Fretted specimens", *RAE Technical Report 78059*, RAE Farnborough.

Edwards P.R. (1981) "The application of fracture mechanics to fretting fatigue", in *Fretting Fatigue*, (Edited by Waterhouse R.B.),Applied Science Pub. Ltd., (Barking, Essex), pp. 67-97

Endo K. , Goto H. and Nakamura T. (1973) "Fretting Fatigue Strength of Several Materials Combinations", *Bull. JSME*, Vol.16, No. 92, pp.143-150

Endo K., Goto H. and Fukunaga T.(1974) "Behaviors of Frictional Force in Fretting Fatigue", *Bull. JSME*, Vol.17, No. 108, pp.647-654

Endo K. and Goto H. (1976) "Initiation and Propagation of fretting fatigue cracks", *Wear*,Vol. 38, pp.311-324

Ensminger D, (1973), *Ultrasonics,* M. Dekker, Inc, (New York)

Erdogan F. and Sih G.C.(1963), "On the Crack Extension in Plates Under Plane Loading and Transverse Shear", *J. Basic Engineering, Trans. ASME*, Vol.85, pp.519-527

Erdogan F. and Gupta G.D. (1972) "On the Numerical Solution of Singular Integral Equations", *Quart. Appl. Math*, No. 1, pp.525-534

Erdogan F., Gupta G.D. and Cook T.S.(1973) "Numerical Solution of Singular Integral Equations " in *Methods of Analysis and Solutions of Crack Problems*, (Edited by G.C.Sih), Noordhoff, (Leyden), pp. 368-425

Erdogan F. and Arin K. (1975), "A half plane and a strip with an arbitrarily located crack", *Int.J.Fracture*, Vol. 11, No.2, pp. 191-204

Erdogan F. (1978), "Mixed Boundary-Value problems in Mechanics", in *Mechanics Today*, Ed. S.Nemat-Nasser, Vol. 4, pp.1-86, Pergamon Press, (Oxford)

Eringen A. (1974), *Elastodynamics,* Vol. II, Academic Press, (New York)

ESDU Data Item 67012 (1967), Engineering Sciences Data Unit, London

Ewalds H. L. and Wanhill R.J.L. (1984), *Fracture Mechanics*, Arnolds, (Delft and London)

Fitting D.W. and Adler L. (1981), *Ultrasonic spectral analysis for nondestructive evaluation,* Plenum Press, (New York)

Forsyth P.J.E. (1981) "Occurences of Fretting Fatigue in Practice", in *Fretting Fatigue* (Edited by Waterhouse R.B.), Applied Science, (Barking, Essex), pp. 99-126

Freund L.B. (1971), "The Oblique Reflection of a Rayleigh wave from a Crack Tip", *Int. J. Solid Struct.*, Vol. 7, pp. 1199

Frost N.E., Marsh K.J. and Pook L.P. (1974), *Metal Fatigue*, Clarendon Press, (Oxford)

Gautesen A.K. (1985), Scattering of a Rayleigh wave by an Elastic Quarter Space", *J. Appl. Mechanics*, Vol. 52, pp.664-668

Gautesen A.K. (1987), "Scattering of a Rayleigh wave by an Elastic Wedge", *Wave Motion*, Vol. 9, pp. 51-57

Gdoutos E. E. and Theocaris P.S. (1975) "Stress Concentrations at the Apex of a Plane Indenter Acting on an Elastic Half Plane", *J.Applied Mechanics*, Trans. ASME, Series E, Vol. 42, pp.688-692

Gdoutos E.E. (1984), *Problems of mixed mode crack propagation*, in Eng. Applications of Fract. Mech., Editor Sih, G.C., Martinus Nijhof Publishers, (The Hague)

Georgiou G.A. and Bond L.J.(1987) "Quantitavive studies in ultrasonic wave-defect interaction", *Ultrasonics*, Vol. 25, pp.328-333

Glass N.E., Loudon R. and Maradudin A.A. (1981), "Propagation of Rayleigh Surface waves across a large amplitude grating", *Phys. Rev.,B*, Vol. 24, pp. 6843-6861

Graaf K. (1975), *Wave Motion in Elastic Solids*, Clarendon Press, Oxford 1975

Gupta G.D.and Erdogan F.(1974) "The problem of edge cracks in an Infinite Strip", *J. Appl. Mechanics*, December 1974,pp.1001-1006

Harker A.H. (1988), *Elastic waves in solids with applications to nondestructive testing of pipelines*, British Gas plc in association with Adam Hilger (Bristol)

Hasebe N. and Inohara S. (1980) "Stress Analysis of a Semi-Infinite Plate with an Oblique Edge Crack", *Ing. Arch.*,Vol. 49, pp.51-62

Hattori T, Nakamura M, Sakata H and Watanabe T. (1988), "Fretting Fatigue Analysis Using Fracture Mechanics", *JSME Int.J.*, Series 1, Vol. 31, No. 1, pp. 100-107

Hills D.A., Sackfield A. and Uzel A. (1984) "The Green's function for a slant edge crack', *Engineering Fracture Mech*, Vol. 20, No. 2., pp. 245-253

Hills D.A. and Comninou Maria (1985a) "A normally loaded half-plane with an edge crack", *Int. J. Solids Structures*, Vol.21, No. 4, pp.399-410

Hills D.A. and Comninou Maria (1985b) "An analysis of fretting fatigue cracks during loading phase", *Int. J. Solids Structures*, Vol.21, No. 7, pp.721-730

Hills D.A., Nowell D. and O'Connor J.J. (1988) "On the Mechanics of Fretting Fatigue", *Wear*, Vol. 125,pp.129-146

Hills D.A. and Nowell D. (1989),"Stress Intensity Calibrations for Closed Cracks", *J. Strain Analysis*, Vol. 24, No. 1, pp. 37-43

Hirano K., Kobayashi H., Nakazawa H. and Hayashi A. (1987), "Monitoring of surface fatigue crack growth and crack tip closure behaviour by the ultrasonic method", in *Role of Fracture Mechanics in Modern Technology,* G.C. Sih, H. Nisitani and T. Isihara, Eds, Elsevier Science Publishers (North Holland), pp. 723-733

Hirao M., Fukuoka H. and Miura Y. (1982), "Scattering of Rayleigh surface waves by edge cracks: Numerical simulation and experiment", *J. Acoust. Soc. Am.*, Vol. 72, No. 2, pp. 602-606

Hua Gao, Brown M.W. and Miller K.J.(1982) "Mixed mode fatigue thresholds", *Fatigue Engineering Materials Structures*, Vol. 5, No.1, pp.1-17

Hudgell R.J., Morgan L.L. and Lumb R.F. (1974), "Non-destructive measurement of the depth of the depth of surface breaking cracks using ultrasonic Rayleigh waves", *Brit.J.NDT*, Vol. 16, pp. 144-149

Hudson J.A. and Knopoff L. (1964), "Transmission and Reflection of Surface Waves at a Corner etc", *J. Geoph. Res.*, Vol. 69, pp. 281-289

Irwin G.R. and Paris P.C. (1971), "Fundamental aspects of Crack Growth and Fracture", in *Fracture*, ed. Liebowitz H., Ch. 1, Vol. III, Academic Press

Johnson K.L.(1985), *Contact Mechanics*, Cambridge Univ. Press

Khadem R. and O'Connor J.J. (1969), "Adhesive or frictionless compression of an elastic rectangle between two identical elastic half-spaces", *Int J.Engng Sci.*, Vol. 7, pp. 153-168

Kino G.S. (1978), "The application of reciprocity theory to scattering of acoustic waves by flaws", *J. Appl. Phys.*, Vol. 49, No. 6, pp. 3190-3199

Kino G.S. (1987), *Acoustic Waves-Devices, Imaging and Analog Signal Processing*, Prentice-Hall, (New Jersey)

Kinra V. and Vu B.(1985) "Diffraction of Rayleigh Waves in half-space I.Normal edge cracks", *J. Acoust. Soc. Am.*, 77, pp.1425-1430

Kinra V. and Vu B.(1986) "Diffraction of Rayleigh Waves in half-space II. Inclined edge cracks", *J. Acoust. Soc. Am.*, 79(6), pp. 1688-1692

Knott J.F. (1973), "*Fundamentals of Fracture Mechanics*", Butterworths, London

Krautkrämer J. and Krautkrämer H, (1983), *Ultrasonic Testing of Materials*, Springer-Verlag, (Berlin, Heidelberg and New York)

Krenk Steen (1975) "On the elastic strip with an internal crack", *Int. J. Solids Structures*, Vol. 11, pp. 693-708

Krenk S.,(1975) "On the Use of the Interpolation Polynomial for Solutions of Singular Integral Equations", *Q. appl. Maths*, Vol. 32, pp.479-484

Kundu T and Mal A.K. (1981),"Diffraction of Elastic Waves by a Surface crack on a Plate,", *J. App.Mechanics*, Vol. 48, pp.570-576

Lewis D. and Dally J.W. (1970), "Photoelastic Analysis of Rayleigh Wave Propagation in Wedges", *J. Geophys. Rev.*, Vol. 75, pp. 3387-3398

Lindley T.C. and Nix K.J. (1985), "The role of fretting in the initiation and early growth of fatigue cracks in turbo-generator materials", in *Multiaxial Fatigue, ASTM STP 853*, K.J. Miller and E.R. de los Rios, Eds, American Society for Testing and Materials, Philadelphia, pp. 340-360

Li Yinghi and D.A.Hills (1990), "Stress Intensity Factors Solutions for Kinked Surface Cracks", *J. Strain Analysis*, Vol. 25, No. 1, pp. 21-27

Lokhov V.P.(1989)" Examination of the diffraction of a Rayleigh wave at the crack edge.", *Soviet J. NDT*, Vol. 25, No. 3, pp. 189-196

Luong W.C., Keer L.M. and Achenbach J.D.(1975), "Elastodynamic Stress Intensity Factors of a crack near an Interface",*Int J Solids Struct.*, Vol 11, pp. 919-915

Mendelson D.A., Achenbach J.D. and Keer L.M. (1980), "Scattering of elastic waves by a surface-breaking crack",*Wave Motion,* 2, pp.277-292

Miller K.J. (1986), "An Introduction", in *The behaviour of short fatigue cracks,* EGF Pub.1 (Miller K.J. and de los Rios E.R., eds), Mechanical Engineering Publications, London, pp. 1-3

Miller K.J. (1989), "Short Fatigue Cracks", in *Advances in fatigue Science and Technology,* pp. 3-22, ed. C. Moura Branco and L.Guerra Rosa: Proceed. of the NATO Advanced Study Institute, Kluwer Academic

Momoi T.(1985), "Scattering of Rayleigh waves in an elastic three-quarter space", *J. Phys. Earth,* Vol. 33, pp. 323-343

Morgan L.L. (1974), "The spectroscopic determination of surface topography using acoustic surface waves", *Acoustica,* Vol. 30, pp. 222-228

Munasinghe M. and Farnell G.W. (1973), "Finite difference analysis of Rayleigh wave scattering at vertical discontinuities", *J. Geoph. Res.*, Vol. 78, pp. 2454-2466

Murakami Y, Khuri-Yakub B.T., Kino G.S., Richardson J.M. and Evans A.G. (1978), "An application of Wiener filtering to non-destructive evaluation", *Appl. Phys. Lett.,* Vol. 33, No. 8, pp. 685-687

Murakami Y. (chief editor) (1985) *Stress Intensity Factors Handbook,* Vol. I and II, Pergamon Press

Muskhelishvili N.I. (1953), *Singular Integral Equations,* P.Noordhoff Ltd., Groningen, Holland

Mutoh Y., Tanaka K. and Kondoh M. (1989), "Fretting Fatigue in SUP9 Spring Steel Under Random Loading", *JSME International Journal,* Series I, Vol. 32, No. 2, pp. 274-281

NAG (1990), The Numerical Algorithms Group Ltd, NAG Central Office, Mayfield House, 256 Banbury Road, Oxford OX2 7DE, U.K.

Neal S.P., Speckman P.L. and Enright M.A. (1992), "Error analysis and ultrasonic scattering amplitude estimation using the Wiener filter with limited prior information",in *Review of Progress in Quantitative Nondestructive Evaluation,* Vol. 11, D.O Thomson and D.E Chimenti, Eds, Plenum Press, (New York and London), (in press)

Nichols D.J and Martin J.W. (1991), "A comparison of small fatigue crack growth,

low cycle fatigue and long fatigue crack growth in Al-Li alloys", *Fatigue Fract. Engineering Mater. Struct.*, Vol. 14, No. 2-3, pp. 185-192

Nied H.F. and Erdogan F. (1981) "A cracked beam or plate transversely loaded by stamp", *Int.J.Solids Structures,* Vol. 15, pp. 951-965

Nishioka K. and Hirakawa K. (1969) "Fundamental Investigations of Fretting Fatigue", *Bull.JSME*, Vol.12 (various parts)

Nix K.J. and Lindley T.C. (1985) "The application of Fracture Mechanics to Fretting Fatigue", *Fatigue Fract. Engineering Mater. Stuct.*, Vol.8, No. 2, pp. 143-160

Nix K.J. and Lindley T.C. (1988) "The influence of relative slip range and contact material on the fretting fatigue properties of 3.5NiCrMoV rotor steel", *Wear*, Vol.125, pp.147-162

Norriss T.H. (1985), "The role of NDT in relation to damage-tolerant aircraft design", *Brit.J.NDT*, pp. 345-350

Nowell D. and Hills D.A. (1987a), "Open Cracks at or near Free Edges", *J. Strain Analysis*, Vol. 22, No. 3 ,pp. 177-185

Nowell D. and Hills D.A. (1987b), "Mechanics of Fretting Fatigue Tests", *Int.J.Mech.Sci.*, Vol.29, No.5, pp.355-365

Nowell D. and Hills D.A. (1990), "Crack initiation criteria in fretting fatigue", *Wear*, Vol. 136, pp. 329-343

Otsuka A. (1991), "Mode II Fatigue under Compression Stress Field- a simplified

model for fatigue crack growth in rolling contact fatigue", International Conference on "*Mixed-Mode Fracture and Fatigue*", MMFF91, 15-17 July 1991, Vienna, Austria

Pao Yih-Hsing and Mow Chao-Chow (1973), *Diffraction of Elastic waves and Dynamic Stress Concentrations*", The Rand Corporation, Russak, N.Y.

Pao Yih-Hsing (1983), "Elastic Waves in Solids", *J Appl Mechanics*, Vol. 50, pp.1152-1164

Papoulis A. (1977), *Signal Analysis*, McGraw Hill

Paris P. and Erdogan F. (1963), "A critical analysis of crack propagation laws", *J. Basic Engineering, Trans. ASME*, Vol. 85, pp. 528-534

Peterson R.E. (1974), *Stress Concentration Factors*, John Wiley and Sons, New York

Pook L.P. (1971), "The effect of crack angle on fracture toughness", *Engineering Fract Mech*, Vol. 3, pp. 205-218

Pook L.P. (1975), "Analysis and application of fatigue crack growth data", *J. Strain Analysis*, Vol. 10, No. 4, pp. 242-250

Pook L.P. (1976), "Various aspects of the fatigue damage threshold in mild steel", *Proc. SEE Conference "Fatigue Testing and Design"*, London

Pook L.P.(1985), "A failure mechanism map for mixed mode I and II fatigue crack growth thresholds", *Int. J. Fracture*, Vol. 28, pp. R21-R23

Pook L.P. (1989), "The Significance of Mode I Branch Cracks for Mixed Mode

Fatigue Crack Growth Threshold Behaviour", *Biaxial and Multiaxial Fatigue*, EGF3, pp. 247-263, ed. Brown and Miller, Mech.Eng.Public., London

Portz K., Stegeman G.I. and Maradudin A.A. (1981), "Raleigh wave reflection at plate edges", *Appl. Phys. Lett.*, Vol. 38, No. 11, pp. 856-858

Rehbein D.K., Thompson R.B and Buck O. (1990), "Fatigue Crack Characterization by Ultrasonic Inspection", *J. Test. Eval.*, Vol.18, No. 6, pp. 421-429

Resch M.T., Khuri-Yakub B.T.,Kino G.S. and Shyne J.C. (1979), "The Acoustic Measurement of Stress Intensity Factors", *Appl. Phys. Lett.*, Vol. 34, pp. 182-184

Resch M.T., Shyne J.C., Kino G.S. and Nelson D.V. (1982), "Long Wavelength Rayleigh Wave Scattering from Microscopic Surface Fatigue Cracks", in *Review of Progress in Quantitative Nondestructive Evaluation*, Vol. 1, D.O Thomson and D.E Chimenti, Eds, Plenum Press, (New York and London), pp. 573-578

Rolfe S.T. and Barsom J.M. (1977), *Fracture and Fatigue Control in Structures*, Prentice-Hall Inc., Englewood Cliffs, New Jersey

Rooke D.P. and Jones D.A. (1977) "Stress Intensity Factors in Fretting Fatigue", *RAE Technical Report 77181*, RAE Farnborough and (1979),in *J.Strain Analysis*", Vol.14, No. 1, pp.1-6

Rooke D.P. and Edwards P.R. (1987) "Wave forms in fretting fatigue", *RAE Technical Report 87032*, RAE Farnborough

SAE, Fatigue Design Handbook, (1988), 2nd Edition, R.C.Rice, Chief Editor, published by the Society of Automotive Engineers, Inc., 400 Commonwealth Drive, Warrendale PA, 15096-0001

Saffari N. and Bond L.J. (1987a), "Body to Rayleigh Wave Mode-Conversion at Steps and Slots", *J. Non-Destr. Eval.*, Vol. 6, No. 1

Saffari N., Bond L.J., Dewhurst R.J., McKie A.D.W. and Palmer S.B. (1987b) "Rayleigh wave interaction with discontinuities: a numerical and an experimental study", *Proc. Ultr. Int. '87*, pp. 153-158, Butterworth

Saka M., Schneider E., and Holler P. (1989), "A new approach to detect and size closed cracks by ultrasonics", *Res. Nondestr. Eval.*, Vol. 1, No. 2, pp. 65-75

Sato K. ,Fujii H. and Kodama S. (1986) "Crack Propagation Behaviour in Fretting Fatigue", *Wear*, Vol.107, pp.245-262

Sato K. (1988), "Damage formation during fretting fatigue", *Wear*, Vol. 125, pp. 163-174

Scott P.M. and Thorpe T.W. (1981) "A critical review of crack tip stress intensity factors in semi-elliptical cracks", *Fatigue Engn Mater. Struct*, Vol. 4, pp. 291-309

Scruby C.B., Dewhurst R.J., Hutchins D.A. and Palmer S.B. (1982), "Laser Generation of Ultrasound in Metals", in *Research Techniques in non-destructive testing*, (Sharpe R.S. ed.), Vol. 5, pp. 281-327, Academic Press, New York

Sheppard S.D., Hills D.A. and Barber J.R. (1986) "An analysis of Fretting Cracks,II. Loading and Reloading Phases", *Int.J.Solids Structures*, Vol. 22, No. 4, pp. 387-396

Sih G.C. and Barthelemy B.M. (1980) "Mixed Mode Fatigue Crack Predictions", *Engineering Fract Mech*, Vol. 13, pp .439-459

Silk M.G. (1977) in *Research Techniques in NDT*, Vol. 2, ed. R.S.Sharpe, Academic Press, (Leyden)

Som A (1991),"*The Ultrasonic Characterisation of Solid-State Bonds*", Ph.D Thesis, University of London

Swift T. (1983), "Verification of methods for damage tolerance evaluation of aircraft structures to FAA requirements", *Proceedings 12th ICAF Symposium*, (Toulouse, France), pp. 1.1/1-1.1/87

Taylor D. (1986), "Fatigue of short cracks: the limitations of fracture mechanics", in *The Behaviour of Short Fatigue Cracks*, EGF Pub.1, K.J. Miller and E.R. de los Rios, Eds, Mechanical Engineering Publications, London, pp. 479-490

Theocaris P.S. and Ioakimidis N.I. (1977), "Numerical Integration Methods for the Solution of Singular Integral Equations", *Quart. Applied Mathematics*, Vol.35, pp.173-183

Singh G.P. and Singh A. (1981), "A technique for notch depth determination using pulse-echo Rayleigh waves", *Mat. Eval.*, Vol.39, pp. 1232-1236

Stepanishen P.R. (1981), "Pulsed transmit/receive response of ultrasonic piezoelectric transducers",*J. Acoust. Soc. Am.*,Vol. 69,No. 6,pp. 1815-1827

Stone D.E.W. (1987), "The Reliability of Inspection Techniques for Military Aircraft", *NDT, Proc. 4th Eur. Conf.*, ed J.M. Farley and R.W. Nichols, Vol. 2, pp. 819-831, Pergamon, London

Stroud A. H. and Secrest D., (1966), *Gaussian Quadrature Formulas*, Prentice Hall,

New York

Tanaka K. and Mura T. (1981a), "A Dislocation Model for Fatigue Crack Initiation", *J. Appl. Mechanics,* Vol.48, pp.97-103

Tanaka K., Nakai Y. and Yamashita M. (1981b), "Fatigue Growth Thresholds of Small Cracks", *Int. J. Fracture,* Vol.17, No. 3, p.519

Tanaka K., Mutoh Y., Sakoda S. and Leadbeater G. (1985), "Fretting Fatigue in 0.55C Spring Steel and 0.45C Carbon Steel", *Fatigue Fract. Engineering Mater. Struct.*, Vol. 8, No. 2, pp. 129-142

Thomson R.B. (1983), "Quantitative Ultrasonic Nondestructive Evaluation Methods", *J. Appl. Mechanics,* Vol. 50, pp. 1191-1201

Timoshenko S.P. and Goodier J.N. (1970), *Theory of Elasticity*, McGraw- Hill, (New York)

Titman B.R. and Buck O. (1980), "Fatigue Lifetime Prediction with the Aid of SAW NDE", *J. NDE*, Vol. 1,No.2, pp. 123-136

Tittmann B.R., Buck O., Ahlberg L., DeBilly M, Cohen-Tenoudji F.,Jungman A. and Quentin G. (1980), "Surface wave scattering from elliptical cracks for failure prevention", *J. Appl. Phys.*, Vol. 51, No. 1, pp.142-150

Tsamasfyros G. and Theocaris P.S. (1982), "A Reccurence Formula for the Direct Solution of Singular Integral Equations", *Computer Methods in Applied Mechanics and Engineering*, Vol.31, pp. 79-89

Urick, R.J. (1973), *Principles of Underwater ultrasound*, McGraw Hill, New York

Victorov I.A. (1967), *Rayleigh Waves and Lamb Waves-Physical Theory and Application*, Plenum Press, (New York)

Visscher W.M., (1986),"Scattering of elastic waves by small surface breaking or subsurface cracks in 3-D", in *Review of Progress in Quantitative Nondestructive Evaluation,* Vol. 5, D.O Thomson and D.E Chimenti, Eds, Plenum Press, (New York and London), pp. 43-52

Vu B.Q. and Kinra V.K. (1981), "Diffraction of Rayleigh waves in a Half-Space", *Rep. CUMER-81-7*, Univ. of Colorado at Boulder, CO.

Wanhill, R.J.H. (1986), "Short Cracks in Aerospace Structures", in *The Behaviour of Short Fatigue Cracks,* EGF Pub.1, K.J. Miller and E.R. de los Rios, Eds, Mechanical Engineering Publications, London, pp. 27-36

Waterhouse R.B. (1981) *Fretting Fatigue* ,Appl. Sci. Pub. Ltd., (Barking, Essex)

Weston-Bartholomew W. (1981a), "Using Ultrasonic surface waves to predict fatigue failure (The corner reflector method), *Int Advances in NDT*, Vol. 7, pp. 31-55

Weston-Bartholomew W. (1981b), "A possible method of detecting incipient creep in engineering materials" *Int Advances in NDT,* Vol. 7, pp. 57-89

Wharton M.H., Waterhouse R.B., Hirakawa K. and Nisioka K. (1973) "The effect of different contact materials on the fretting fatigue strength of an aluminium alloy", *Wear*, Vol. 26, pp. 253-260

Williams M.L. (1952) "Stress Singularities Resulting From Various Boundary Conditions in Angular Corners of Plates in Extension", *J. Appl. Mechanics*, pp. 526-528

Williams J.G. (1984), *Fracture of Polymers,* Arnold, (London)

Wright G.P. and O'Connor J.J. (1971) "Finite Element Analysis of Alternating Axial Loading of an Elastic Plate Pressed between two Elastic Rectangular Blocks with Finite Friction", *Int.J.Engineering.Sci.*, Vol.9, pp.555-570

Xiaping Lu and Maria Comninou (1989), "The sinusoidal crack", *Engineering Fracture Mechanics*, Vol. 34, No. 3, pp.649-656

Yew C.H., Chen K.G. and Wang D.L. (1984), "An experimental study of interaction between surface waves and a surface breaking crack", *J. Acoust. Soc. Am.*, Vol. 75, No. 1, pp. 189-196

Yu B.Y.(1982), "A discussion on the mixed mode J-integral fracture criterion", *Engineering Fract. Mechanics,* Vol. 16, p. 16

Zachary L.W., Burger C.P., Schmerr L.W. and Singh A.,(1979), "Surface-Crack Characterisation by use of Dynamic Photoelasticity Spectroscopy", *SESA Spring Meeting,* May 20-25, San Francisco, California

Zhang Ch. and Achenbach J.D. (1988) "Scattering of body Waves by an inclined surface-breaking crack", *Ultrasonics,* Vol. 26, pp.132-138 (1987)

ADDENDUM

Hanson M.T. and Keer L.M. (1989), "Stress analysis and contact problems for an elastic quarter-plane", Q.J. Mech. appl. Math., Vol. 42, Pt.3, pp.363-383

Yahsi O.S. and Demir Y. (1989), "Cracked Strip Problem Subjected to Nonsymmetric Transverse Loading by a Stamp", in Localised Damage, computer aided assessement; A.Aliabadi and B.Brebbia, Eds, Vol.1, pp. 247-264, Springer Verlag (Berlin and New York)